N° d'ordre :

الجمهورية الجزائرية الديمقراطية الشعبية

République Algérienne Démocratique et Populaire

وزارة التعليم العالي والبحث العلمي

Ministère de L'enseignement Supérieur et de La Recherche Scientifique

جامعة عين تموشنت بلحاج بوشعيب

Universite Ain Témouchent-Belhadj Bouchaib

Faculté: des Sciences et Technologie
Departement: Science de la Matière
Laboratoire: Catalyse et Synthèse en Chimie Organique " LCSCO "
Laboratoire: Chimie Appliquée " LAC "

THESE

Présentée pour l'obtention du diplôme de **DOCTORAT**
Domaine: Science de la Matière
Filière: Chimie
Spécialité: Chimie organique et Macromoléculaire

Par: Melle Benzenine Djamila

Intitulé

Nouvelles stratégies de synthèse des composés polycycliques

Soutenue publiquement, le 29/10/2025, devant le jury composé de:

Nom & Prénoms	Grade	Qualité	Etablissement de rattachement
Mr Bousalem Samain	Pr	Président	Université d'Ain Temouchent
Mme KibouZahira	Pr	Rapporteur	Université d'Ain Temouchent
Mme Bailiche Zohra	Pr	Examinateur	Université d'Ain Témouchent
Mme BousalahNouria	Pr	Examinateur	Université de Tlemcen
Melle Belhadj Fatima	MCA	Examinateur	Université Oran 1
Mr ChoukchouBraham Noureddine	Pr	Invité	Université de Tlemcen

Année Universitaire : 2025/2026

Order Number:

الجمهورية الجزائرية الديمقراطية الشعبية

Democratic and Popular Algerian Republic

وزارة التعليم العالي والبحث العلمي

Ministry of Higher Education and Scientific Research

جامعة عين تموشنت بلحاج بوشعيب

Ain Témouche University-Belhadj Bouchaib

Faculty of Science and Technology
Department of Materials Science
Laboratory of Catalysis and Synthesis in Organic Chemistry "LCSCO"
Laboratory of Applied Chemistry "LAC"

THESIS

Presented for the **DOCTORAL** Degree
Domain: Matter Science
Field: Chemistry
Specialty: Organic Chemistry and Macromolecular
By: Miss. Benzenine Djamila

Titled

New Synthetic Strategies for Polycyclic Compounds

Publicly defended on 10/29/2025, in front of the jury composed of:

Last Name & First Name	Grade	Role	Affiliated Institution
Mr. Bousalem Samain	Professor	President	University of Ain Temouchent
Mrs. Kibou Zahira	Professor	Supervisor	University of Ain Temouchent
Mrs. Bailiche Zohra	Professor	Examiner	University of Ain Temouchent
Mrs. Bousalah Nouria	Professor	Examiner	University of Tlemcen
Miss.Belhadj Fatima	MCA	Examiner	University of Oran 1
Mr. Choukchou BrahamNoureddine	Professor	Guest	University of Tlemcen

Academic Year: 2025/2026

DEDICATION

To GOD ALMIGHTY, the source of all wisdom and strength,
for guiding me every step of the way.

To my beloved parents, whose unconditional love, prayers, and sacrifices
have been the foundation of my journey.

To my brothers and sisters, and their children,
for their constant support and affection.

To my entire family, for always standing by me with kindness and
encouragement.

To my dear friends, for their presence, understanding, and words of
motivation.

And to all those who lent a helping hand, whether near or far:
your support has left a lasting mark on this achievement.

ACKNOWLEDGEMENTS

First and foremost, I extend my sincere gratitude to the Laboratory of Applied Chemistry at the Faculty of Science and Technology, University of Ain Témouchent, under the direction of Professor Smain BOUSALEM, for his warm and welcoming environment.

This thesis was carried out within the Laboratory of Catalysis and Synthesis in Organic Chemistry (LCSCO) at the University of Abou Bakr Belkaid Tlemcen. I would like to express my sincere thanks to Professor Noureddine CHOUKCHOU-BRAHAM, former director of the laboratory, and to Professor Chewki ZIANI-CHERIF, the current director, for giving me the opportunity to be part of the LCSCO team.

I would like to express my heartfelt thanks to my thesis supervisor Professor Zahira KIBOU, University of Belhadj Bouchaib Ain Témouchent for her unwavering guidance, insightful advice, and the trust she placed in me throughout this research journey.

I also wish to thank the distinguished members of the thesis jury:

- *Professor Smain BOUSALEM (University of Ain Témouchent), Jury President*
- *Professor Zohra BAILICHE (University of Ain Témouchent), Examiner*
- *Professor Nouria BOUSALAH, spouse of MERAD (University of Tlemcen), Examiner*
- *Miss Fatima BELHADJ (University Oran 1 Ahmed Ben Bella), Examiner*
- *Professor Noureddine CHOUKCHOU-BRAHAM (University of Tlemcen), Guest Examiner*

My profound appreciation goes to the many collaborators who contributed to this work:

- *Professor Chewki ZIANI-CHERIF and Dr. Mohammed BENABDALLAH, University of Tlemcen, for the time they devoted to the NMR analyses.*
- *Professor Amina BERRICHI, University of Ain Témouchent, for synthesizing the heterogeneous catalysts based on gold nanoparticles used in this study.*

- *Professor Esma CHOUKCHOU-BRAHAM, Director of the Toxicology Laboratory at the Faculty of Medicine, University of Tlemcen, for hosting me in her laboratory for the corrosion studies.*
- *Professor Tarik ATTAR, Higher School of Applied Sciences in Tlemcen, for his constructive scientific advice*
- *Dr. Abbes BENCHADLI, for his valuable training and assistance with the calculations.*

I am also grateful to:

- *Professor Ismail DAOUD, University of Biskra, for his assistance in molecular modeling*
- *Dr. Nadia ASSAOUI, University of Tlemcen, for her contributions to the antimicrobial evaluations.*

My warmest thanks go to Dr. Julio SEIJAS, Director of the Organic Chemistry Laboratory at the University of Santiago de Compostela in Lugo (Spain), for carrying out the MS and NMR analyses, as well as to the analytical teams in Lugo and Santiago, and to the Scientific and Technical Research Center in Physico-Chemical Analyses (CRAPC), for their valuable technical support.

I would also like to acknowledge the invaluable help of the technical staff of the LCSCO laboratory, particularly Mrs Fatima Zahra MOKRI and the postdoctoral researchers.

I owe special thanks to my family, whose encouragement and faith in me have been my greatest motivation in achieving both academic and personal milestones.

Summary

ABBREVIATIONS

Abbreviation

%: Percent

Δm: The weight loss

°C: Degrees Celsius

2-PyO-(2Cl, 2,4-diCl): 4-(2-Chlorophenyl)-6-(2,4-dichlorophenyl)-2-oxo-1,2-dihydropyridine-3-carbonitrile

2-PyO-(2Cl, 2-Naph): 4-(2-Chlorophenyl)-6-(naphthalen-2-yl)-2-oxo-1,2-dihydropyridine-3-carbonitrile

2-PyO-(2Cl, 3,4-diMe): 4-(2-Chlorophenyl)-6-(3,4-dimethylphenyl)-2-oxo-1,2-dihydropyridine-3-carbonitrile

2-PyO-(2Cl, 4F): 4-(2-Chlorophenyl)-6-(4-fluorophenyl)-2-oxo-1,2-dihydropyridine-3-carbonitrile

2-PyO-(2Cl, 4Me): 4-(2-Chlorophenyl)-6-(p-tolyl)-2-oxo-1,2-dihydropyridine-3-carbonitrile

2-PyO-(2Cl, 4OMe): 4-(2-Chlorophenyl)-6-(4-methoxyphenyl)-2-oxo-1,2-dihydropyridine-3-carbonitrile

2-PyO-(4F, 2,4-diCl): 6-(2,4-Dichlorophenyl)-4-(4-fluorophenyl)-2-oxo-1,2-dihydropyridine-3-carbonitrile

2-PyO-(4F, 2-Naph): 4-(4-Fluorophenyl)-6-(naphthalen-2-yl)-2-oxo-1,2-dihydropyridine-3-carbonitrile

2-PyO-(4F, 3,4-diMe): 6-(3,4-Dimethylphenyl)-4-(4-fluorophenyl)-2-oxo-1,2-dihydropyridine-3-carbonitrile

2-PyO-(4F, 4F): 4,6-Bis(4-fluorophenyl)-2-oxo-1,2-dihydropyridine-3-carbonitrile

2-PyO-(4F, 4Me): 4-(4-Fluorophenyl)-6-(p-tolyl)-2-oxo-1,2-dihydropyridine-3-carbonitrile

2-PyO-(4F, 4OMe): 4-(4-Fluorophenyl)-6-(4-methoxyphenyl)-2-oxo-1,2-dihydropyridine-3-carbonitrile

2-PyO-(H, 2-Naph): 6-(Naphthalen-2-yl)-2-oxo-4-phenyl-1,2-dihydropyridine-3-carbonitrile

2-PyO-(H, 4F): 6-(4-Fluorophenyl)-2-oxo-4-phenyl-1,2-dihydropyridine-3-carbonitrile

2-PyO: 2-Pyridones

A: Arrhenius constant

ADME: Absorption, Distribution, Metabolism, and Excretion

Al_2O_3: Basic alumina

Alk: Alkenes

Alk-2,4-diCl: Ethyl 3-(2,4-dichlorophenyl)-2-cyanoacrylate

Alk-2Cl: Ethyl 3-(2-chlorophenyl)-2-cyanoacrylate

Alk-3Cl: Ethyl 3-(3-chlorophenyl)-2-cyanoacrylate

Alk-4Cl: Ethyl 3-(4-chlorophenyl)-2-cyanoacrylate

Alk-4F: Ethyl 2-cyano-3-(4-fluorophenyl)acrylate

Alk-H: Ethyl 2-cyano-3-phenylacrylate

APTS: para-toluenesulfonic acid

ATCC: American Type Culture Collection

BBB: Blood–Brain Barrier

Br-2OMe: 2-Bromo-1-(2-methoxyphenyl)ethanone

Br-4F: 2-Bromo-1-(4-fluorophenyl)ethanone

Br-4Me: 2-Bromo-1-(p-tolyl)ethanone

Br-4OMe: 2-Bromo-1-(4-methoxyphenyl)ethanone

Br-H: 2-Bromo-1-phenylethanone

BSA: Bovine Serum Albumin

CFU: Colony-Forming Units

C_{inb}: Concentration of the corrosion inhibitor

COSY: Correlation Spectroscopy

d: Doublet

DAPI: 4′,6-Diamidino-2-phenylindole

DMSO-d_6: Deuterated Dimethyl Sulfoxide

DNA: Deoxyribonucleic Acid

DS: Discovery Studio

E_a: Activation energy

EtOH: Ethanol

FT-IR: Fourier Transform Infrared Spectroscopy

G: Gram

H: Hour

H_2SO_4: Sulfuric acid

H-bond: Hydrogen bond

HCl: Hydrochloric acid

HMBC: Heteronuclear Multiple Bond Correlation

HNO_3: Nitric acid

HPLC: High-Performance Liquid Chromatography

HSQC: Heteronuclear Single Quantum Coherence

Hz: Hertz

IC_{50}: Half-maximal Inhibitory Concentration

IE%: Inhibitory efficiency

IMTh: Imidazo[2,1-b]thiazole

IMTh-2Naph: 6-(Naphthalen-2-yl)imidazo[2,1-b]thiazole

IMTh-2OMe: 6-(2-Methoxyphenyl)imidazo[2,1-b]thiazole

IMTh-3OMe: 6-(3-Methoxyphenyl)imidazo[2,1-b]thiazole

IMTh-4Cl: 6-(4-Chlorophenyl)imidazo[2,1-b]thiazole

IMTh-4F: 6-(4-Fluorophenyl)imidazo[2,1-b]thiazole

IMTh-4Me: 6-(p-Tolyl)imidazo[2,1-b]thiazolle

IMTh-4OMe: 6-(4-Methoxyphenyl)imidazo[2,1-b]thiazole

IMTh-H: 6-Phenylimidazo[2,1-b]thiazole

IP: Imidazo[1,2-a]pyridine

IP-2Naph: 2-(2-naphtylphenyl)imidazo[1,2-a]pyrimidine

IP-2OMe: 2-(2-methoxyphenyl)imidazo[1,2-a]pyridine

IP-3,4diMe: 2-(3,4-dimethylhenyl)imidazo[1,2-a]pyridine

IP-3Br: 2-(3-bromophenyl)imidazo[1,2-a]pyridine

IP-3OMe: 2-(3-methoxyphenyl)imidazo[1,2-a]pyridiine

IP-4Br: 2-(4-bromophenyl)imidazo[1,2-a]pyridine

IP-4Cl: 2-(4-chlorophenyl)imidazo[1,2-a]pyridine

IP-4F: 2-(4-fluorophenyl)imidazo[1,2-a]pyridine

IP-4Me: 2-(4-methylphenyl)imidazo[1,2-a]pyridine

IP-4OMe: 2-(4-methoxyphenyl)imidazo[1,2-a]pyridine

IP-H: 2-Phenylimidazo[1,2-a]pyridine

IPM: Imidazo[1,2-a]pyrimidine

IPM-2Naph: 2-(2-naphtylphenyl)imidazo[1,2-a]pyrimidine

IPM-2OMe: 2-(2-methoxyphenyl)imidazo[1,2-a]pyrimidine

IPM-3,4diMe: 2-(3,4-dimethylhenyl)imidazo[1,2-a]pyrimidine

IPM-3Br: 2-(3-bromophenyl)imidazo[1,2-a]pyrimidine

IPM-3OMe: 2-(3-methoxyphenyl)imidazo[1,2-a]pyrimidine

IPM-4Br: 2-(4-bromophenyl)imidazo[1,2-a]pyrimidine

IPM-4Cl: 2-(4-chlorophenyl)imidazo[1,2-a]pyrimidine

IPM-4F: 2-(4-fluorophenyl)imidazo[1,2-a]pyrimidine

IPM-4Me: 2-(4-methylphenyl)imidazo[1,2-a]pyrimidine

IPM-4OMe: 2-(4-methoxyphenyl)imidazo[1,2-a]pyrimidine

IPM-H: 2-Phenylimidazo[1,2-a]pyrimidine

IPMs: Imidazo[1,2-a]pyrimidines

IR: Infrared Spectroscopy

IR: Infrared spectroscopy

J: joul

K: the adsorption constant

K_{ads}: the adsorption constant.

kcal/mol: Kilocalories per mole

m: Multiplet

MBC: Minimum Bactericidal Concentration

mg: Milligram

MHA: Müeller-Hinton-Agar

MIC: Minimum Inhibitory Concentration

min: Minute

mL: Milliliter

mmol: Millimole

MOE: Molecular Operating Environment

mp: Melting point

MS m/z: Mass Spectrometry

MW: Microwave

NBS: N-Bromosuccinimide

NMR: Nuclear Magnetic Resonance

PBS: Phosphate Buffered Saline

PDB: Protein Data Bank

ppm: Parts per million

PTSA: p-Toluenesulfonic Acid

$R = 8.314\ J.mol^{-1}.K^{-1}$

R^2: correlation coefficients

RMSD: Root-Mean-Square Deviation

RT: Room Temperature

s: Singlet

S: The surface of the metal part (cm^2)

SAR: Structure–Activity Relationship

sec: Second

T: Temperature (K)

t: The measurement time

t: Triplet

TCBS: Thiosulfate-Citrate-Bile-Salts-Sucrose

TLC: Thin Layer Chromatography

TMS: Tetramethylsilane

UV: Ultraviolet

UV-Vis: Ultraviolet–Visible Spectroscopy

v/cm^{-1}: Wavenumber

W_{corr}: Corrosion rate

W_{inb}: Corrosion rates in the presence of the inhibitor

XRD: X-Ray Diffraction

YPGA: Yeast, Peptone-Glucose-Agar

ΔG_{ads}: The standard free energy of adsorption

ΔH_{ads}: The standard enthalpy of adsorption and

$\Delta S_{ads:}$ The standard entropy of adsorption

θ : The recovery rate values

µg/mL : Micrograms per milliliter

GENERAL INTRODUCTION

- **Introduction**

Organic chemistry remains at the forefront of innovation in the synthesis of complex molecular structures with potential therapeutic and industrial applications. Heterocycles are among the most fundamental molecular architectures in organic chemistry, representing over half of all known organic compounds. Their presence in natural products, pharmaceuticals, agrochemicals, and functional materials highlights their undeniable importance in multiple scientific and industrial fields.

Among them, nitrogen-based heterocycles, such as imidazopyridines, imidazopyrimidines, imidazothiazoles, and 2-pyridones, have drawn intense interest due to their wide spectrum of biological activities, including anticancer, antimicrobial, anti-inflammatory, and antioxidant properties. This has led to sustained efforts in the development of novel synthetic methodologies and functionalized analogues with enhanced bioavailability, target selectivity, and minimal toxicity.

- **Presentation of the subject**

Building on this context, the present work is devoted to the design, synthesis, and application of four families of nitrogen-containing heterocycles: imidazo[1,2-a]pyridines, imidazo[1,2-a]pyrimidines, imidazo[2,1-b]thiazoles, and 2-pyridones. These frameworks were selected for their high pharmacological relevance and their structural adaptability, which make them excellent candidates for therapeutic development and materials science. The research aimed to explore both innovative synthetic approaches aligned with green chemistry principles and preliminary evaluations of their potential in corrosion inhibition, antimicrobial activity, and molecular modeling.

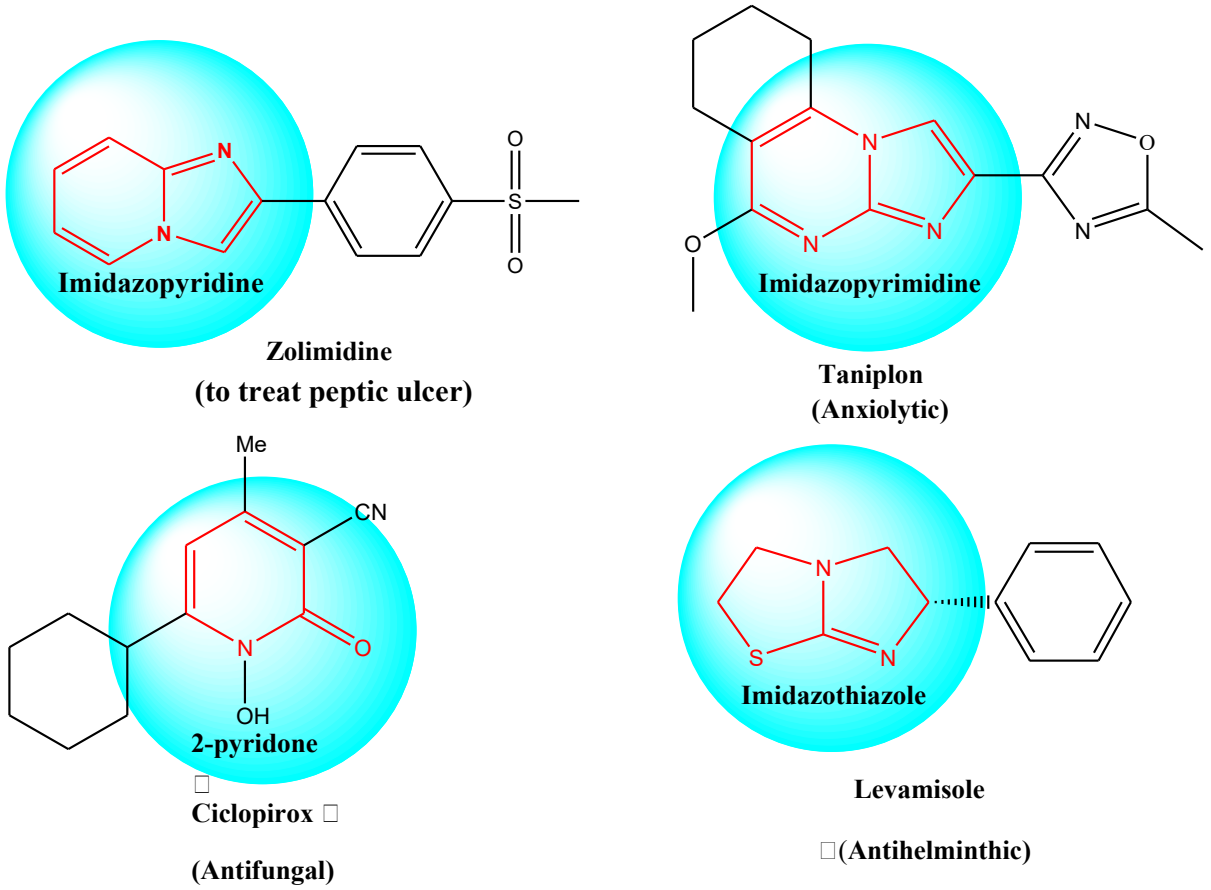

Figure 1: Structures and Activities of Commercial Drugs Containing Imidazopyridine, Imidazopyrimidine, Imidazothiazole, and 2-Pyridone Moieties

In this context, the present work focuses on the synthesis and application of four distinct heterocyclic families:

- Imidazo[1,2-a]pyridines (**IPs**)
- Imidazo[1,2-a]pyrimidines (**IPMs**)
- Imidazo[2,1-b]thiazoles (**IMThs**)
- 2-Pyridone derivatives (**2-PyOs**)

The originality of this research lies not only in the diversity of synthesized structures, but also in the strategic choice of eco-compatible and efficient reaction conditions. Particular attention has been given to:

- the use of green solvents such as ethanol and water,
- heterogeneous catalysis (e.g. Au/TiO_2, Al_2O_3),
- microwave and ultrasound-assisted reactions, promoting faster kinetics, higher yields, and reduced environmental impact.

This dissertation is divided into two major parts:

- **Part A: Synthesis Strategies**

This section is devoted to the development and optimization of synthetic approaches for the target heterocycles.

- Chapter 1 describes the preparation of imidazo-fused heterocycles (**IPs**, **IPMs**, and **IMThs**), obtained via the condensation of 2-aminoheterocycles (2-aminopyridine, 2-aminopyrimidine, or 2-aminothiazole) with bromoarylketones. These brominated intermediates were first synthesized by the bromination of aryl ketones using N-bromosuccinimide (NBS), in the presence of an acid catalyst in chloroform.

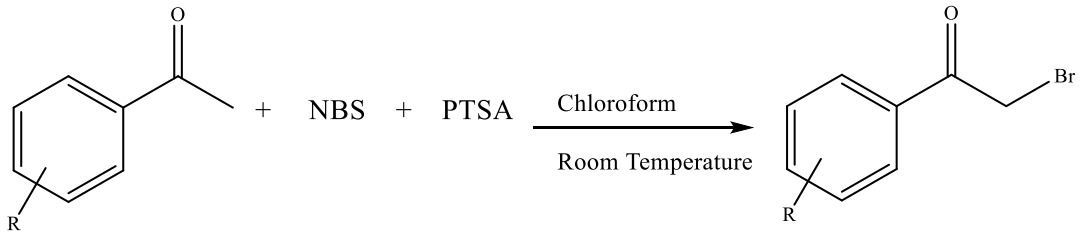

Scheme 1: Schematic route of bromoarylketone synthesis

This key step provided access to a versatile series of bromoketones, which were then employed in the formation of the imidazo-heterocycles under three different conditions: classical heating, heterogeneous catalysts, and microwave-assisted protocols.

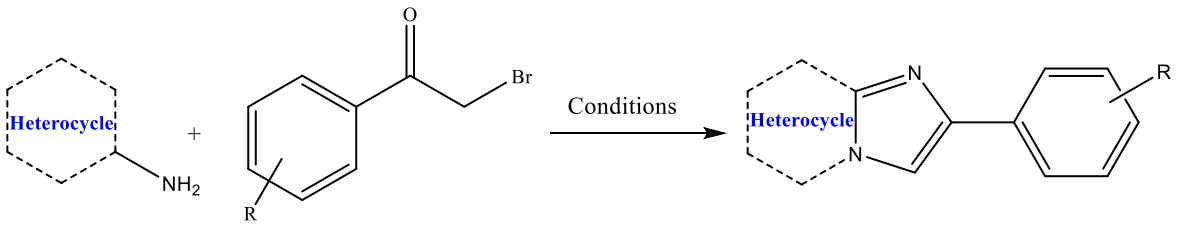

Scheme 2: General synthetic pathways of **IPs**, **IPMs**, and **IMThs** under different conditions (classic, catalytic, microwave).

- Chapter 2 focuses on the multicomponent synthesis of 2-pyridone derivatives. The synthetic strategy involved two stages:

    1. The preparation of alkene intermediates by condensation of aldehydes with active methylene compounds under basic conditions.

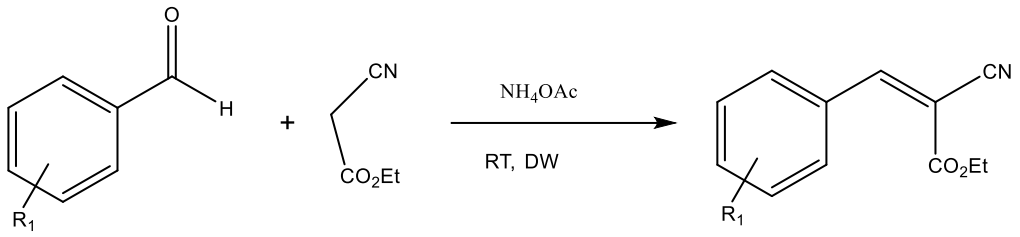

Scheme 3: Synthesis of alkenes

    2. A subsequent reaction of the preformed alkenes with aromatic ketones and ammonium acetate, leading to the formation of functionalized 2-pyridone derivatives.

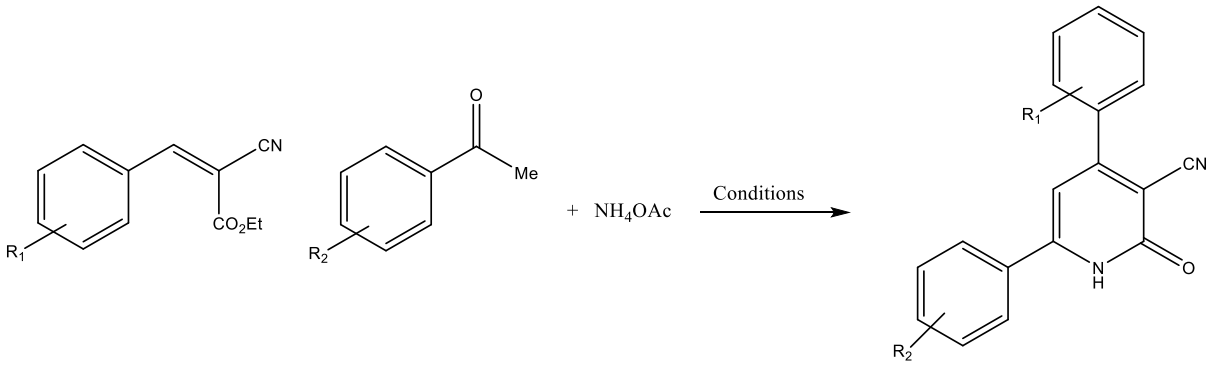

Scheme 4: Multicomponent synthesis of 2-pyridones

Two methods were employed for the synthesis:

- Conventional heating in ethanol at 80 °C,
- Ultrasound-assisted synthesis to accelerate the reaction and improve efficiency.

- Part B: Applications

This section explores the practical applications of the synthesized compounds through three major axes:

❖ Chapter 1: Corrosion Inhibition Studies

This chapter is devoted to the investigation of the corrosion inhibition properties of selected imidazo[1,2-a]pyridine (**IP**) and imidazo[1,2-a]pyrimidine (**IPM**) derivatives on mild steel in acidic medium. The choice of these heterocyclic compounds is motivated by their structural features, which make them suitable candidates for interactions with metallic surfaces. In this context, their potential as corrosion inhibitors was examined in a controlled environment using 1 M hydrochloric acid.

To evaluate the inhibitory performance of the synthesized molecules, the gravimetric method was employed. This technique, which involves monitoring the weight loss of metal specimens exposed to corrosive media, was selected for its simplicity, reliability, and relevance for comparative studies. It provides a direct measure of corrosion rates in the presence and absence of inhibitors and allows the assessment of the influence of several operational parameters.

Within this framework, the study considers the effect of inhibitor concentration, temperature, and immersion time in order to establish trends that can guide the understanding of inhibitor behavior under different conditions. Although detailed interpretations and numerical values are presented in the corresponding chapter, this introductory section highlights the methodological approach adopted to explore how **IP** and **IPM** derivatives interact with metallic substrates. Thermodynamic parameters associated with the corrosion process, such as activation energy and changes in enthalpy and entropy, were also examined to provide additional insight into the general nature of the interaction between the inhibitors and the metal surface.

Overall, this chapter introduces the experimental foundations and scientific rationale behind the corrosion studies conducted in this work, outlining the methodologies, conditions, and analytical tools used to examine the inhibition potential of the synthesized heterocycles

.

❖ Chapter 2: Biological Activity Evaluation

This chapter focuses on the antimicrobial evaluation of selected synthesized **IP** and **IPM** derivatives. These classes of heterocycles are widely recognized for their pharmacological potential, and the objective of this work was to investigate their *in vitro* antimicrobial activity against a representative panel of microbial strains.

The biological screening was performed using the agar well diffusion method, a standard microbiological technique commonly employed to assess the antimicrobial capacity of chemical compounds. The study included both Gram-positive and Gram-negative bacterial strains, as well as yeast strains, in order to provide an overview of the potential spectrum of activity of the synthesized molecules.

To complement this qualitative evaluation, the minimum inhibitory concentration (MIC) and the minimum bactericidal concentration (MBC) were determined for the most active derivatives. These parameters provide quantitative information on the inhibitory, bactericidal, and fungicidal effects of the tested compounds, allowing a clearer comparison of their antimicrobial performance.

In this section, the focus is on the methods used to evaluate the biological properties of the synthesized **IP** and **IPM** derivatives. The detailed results, structure–activity relationships, and the individual performance of each compound are presented and discussed in the corresponding chapter.

❖ Chapter 3: Molecular Docking Studies

This chapter presents a computational study designed to complement the experimental biological investigations through molecular docking simulations. The aim was to explore how the synthesized **IP** and **IPM** derivatives can interact with selected biological targets, particularly proteins involved in bacterial activity.

Docking simulations were performed using appropriate protein structures obtained from the Protein Data Bank (PDB), allowing the identification of potential interactions such as hydrogen bonding and π–π stacking that may contribute to biological activity.

In addition to docking, the drug-likeness of the compounds was evaluated using basic physicochemical criteria, and their ADME-Tox profiles (Absorption, Distribution, Metabolism, Excretion, and Toxicity) were predicted to assess their suitability as potential therapeutic agents.

This study integrates synthetic chemistry with computational approaches to provide molecular insights that support the investigation of bioactive and potentially therapeutic heterocyclic compounds.

The thesis concludes with an Experimental Part that outlines the detailed procedures and characterization methods applied during the synthesis and evaluation of the studied compounds.

CHAPTER 1: SYNTHESIS OF IMIDAZO-HETEROCYCLES

1. Introduction to imidazoheterocycles

Heterocycles are representative of a large class of organic substances, and are of great interst, mainly because of the involvement-of heterocyclic scaffolds in the core framework of numerous medications [1–5]. Among these, nitrogen-containing heterocyclic compounds play a pivotal role in drug discovery. The development of efficient protocols for the synthesis of highly active therapeutic agents incorporating azaheterocycles with biological activities is an essential research topic [6–15]. Fused imidazole ring systems are widespread in natural products and demonstrate diverse biological and pharmaceutical activities. The imidazole ring is notably found as a key structural element in several natural compounds, such as histamine, histidine, and nucleic acids [16].

2. Imidazoheterocycles: Classification and Biological Interest

Imidazoheterocycles are a subclass of fused nitrogen-containing heterocycles where an imidazole ring is fused to other heterocyclic systems such as pyridine, pyrimidine, or thiazole [17–19]. According to the nature of the second ring, they are classified into imidazo[1,2-a]pyridines, imidazo[1,2-a]pyrimidines , and imidazo[2,1-b]thiazoles (Figure 1).

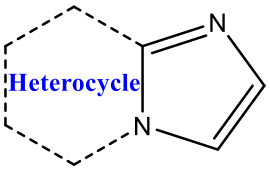

Figure 1: General structure of imidazoheterocycles

In this chapter, we focus on three types: imidazo[1,2-a]pyridines (**IPs**), imidazo[1,2-a]pyrimidines (**IPMs**), and imidazo[2,1-b]thiazoles (**IMThs**). These systems have been reported in the literature as key scaffolds in bioactive molecules, with each class showing distinct pharmacological profiles [20–22]. (Figure 2)

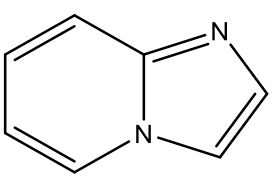

Imidazo[1,2-a]pyridine **(IP)**

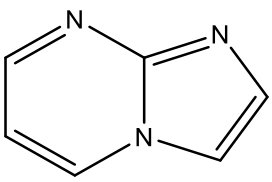

Imidazo[1,2-a]pyrimidine **(IPM)**

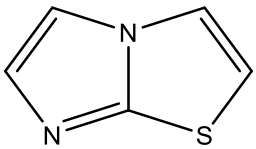

Imidazo[2,1-b]thiazole **(IMTh)**

Figure 2: Core chemical structures of **IPs**, **IMPs** and **IMThs**

3. Literature Survey on the Synthesis of Imidazoheterocycles

3.1. Imidazo[1,2-a]pyridines (IPs)

3.1.1. Biological properties of IPs

Imidazo[1,2-a]pyridines exhibit a wide range of biological activities such as antimitotic [23], antiviral [24], anticancer [25], antidiabetic [26], anti-inflammatory [27], antifungal [28], antibacterial [29], anxiolytic [30], antiprotozoal [31], and antipyretic [32]. Importantly, compounds containing the imidazo[1,2-a]pyridine moiety represent the key structure of many marketed drugs, including Zolpidem [33], Zolimidine [34], Alpidem [35], GSK812397 [36], Saripidem [37], Necopidem [38], Olprinone [39], Miroprofen [40], and Minodronic acid [41] (Figure 3). All these bioactivities make the imidazo[1,2-a]pyridine scaffold particularly attractive for chemists due to its excellent pharmaceutical and medicinal applications and its use in advanced organic chemistry [42].

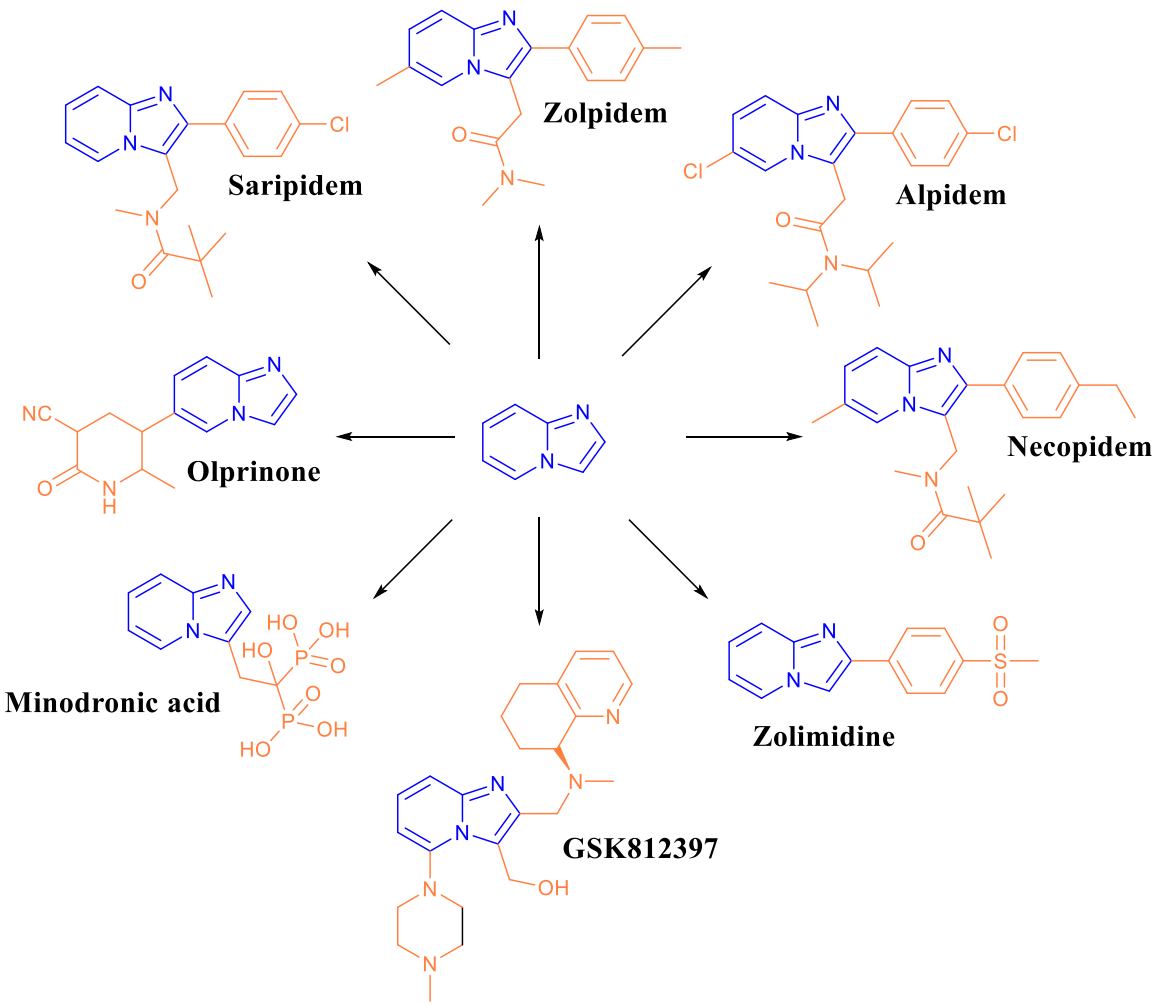

Figure 3: Marketed drugs featuring the imidazo[1,2-a]pyridine core.

3.1.2. Described syntheses of IPs

Given the growing interest in imidazo[1,2-a]pyridines as key building blocks in medicinal chemistry, various synthetic routes have been explored and optimized. These methods vary in terms of reaction conditions, starting materials, and overall efficiency. We present here some of the reported studies on the main synthetic approaches used to synthesize imidazo[1,2-a]pyridines frameworks.

An efficient and practical one-pot ultrasound-assisted protocol for synthesizing substituted imidazo[1,2-a]pyridine derivatives was developed by Paengphua et al. using [BMIM]PF_6 as a catalyst in 2018 (Scheme 1). This procedure tolerates a broad range of substrates, including various acetophenones and 2-aminopyridines. This protocol offers milder conditions, easier purification, better efficiency, and reduced reaction times compared to conventional heating. The combination of ionic liquids and sonication boosts reaction efficiency and ensures operational simplicity. [43]

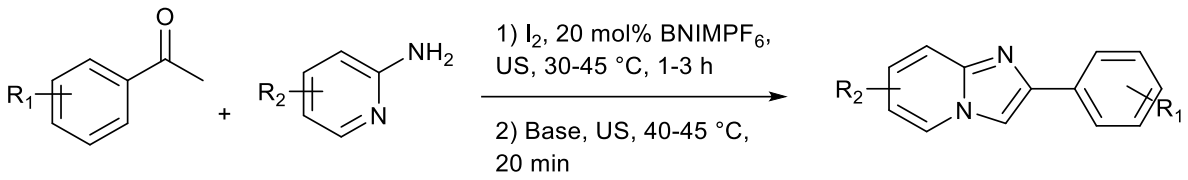

Scheme 1: Synthesis of Paengphua

Li et al. developed a practical synthetic strategy for the generating N-aryl-substituted imidazo[1,2-a]pyridine-3-carboxamide derivatives with promising biological activity in 2020 (Scheme 2). The route begins with the cyclization of 2-aminopyridines and β-ketoesters subjected to microwave irradiation in ethanol at 120 °C. This key condensation step yields ethyl imidazo[1,2-a]pyridine-3-carboxylates as valuable intermediates. These intermediates were then functionalized with different substituted anilines to yield the target compounds. The strategy offers versatility and high efficiency in producing biological screening [44].

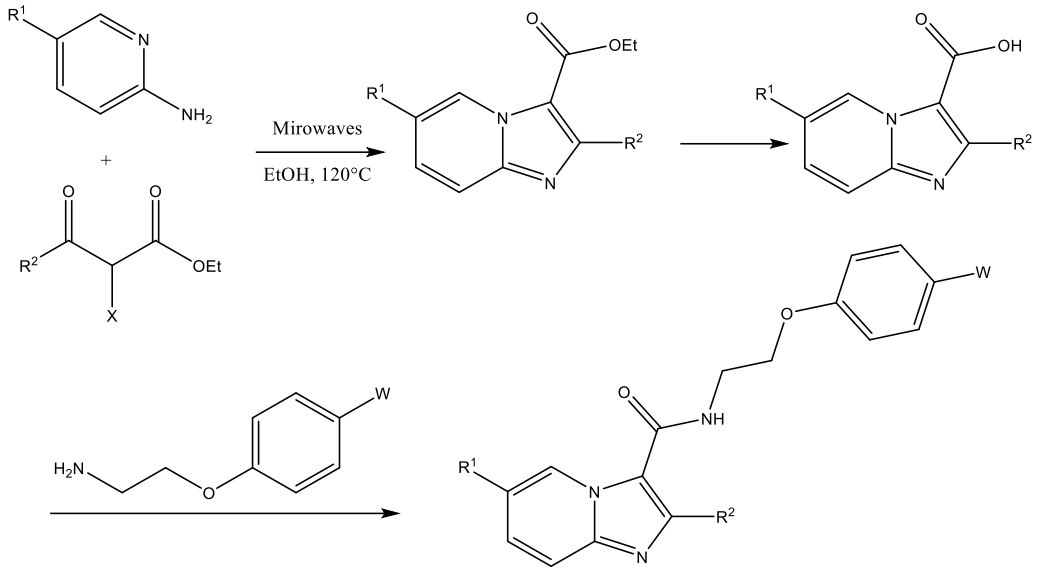

Scheme 2: Synthesis of Li

In 2021, Butera et al. prepared a series of imidazo[1,2-a]pyridines via a microwave assisted multicomponent reaction (Scheme 3). Their synthetic approach involved reacting phenyl-based isocyanides with biphenyl-2-aminopyridines and aldehydes in a DCM/MeOH solvent system catalyzed by scandium triflate [$Sc(OTf)_3$]. The Boc protecting group was then removed with HCl to afford the target heterocycles. This protocol offered high yields, structural diversity, and rapid synthesis [45].

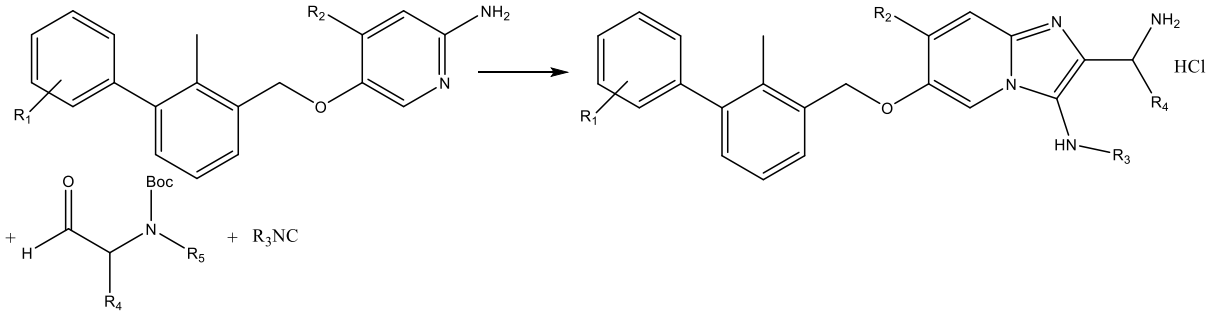

Scheme 3: Synthesis of Butera

In 2022, Stahlberger et al. prepared 3-aminoimidazo[1,2-a]pyridines linked to a [2.2]paracyclophane framework by a multicomponent reaction (Scheme 4). The condensation of 4-formyl-PCP, 2-aminopyridine, and diverse isocyanides in a mixture of MeOH/DCM at ambient temperature proceeded smoothly in the presence of either perchloric acetic acid or glacial acid, which exhibited comparable catalytic efficiency. Both aliphatic and aromatic isocyanides were well tolerated, affording the desired products in high yields [46].

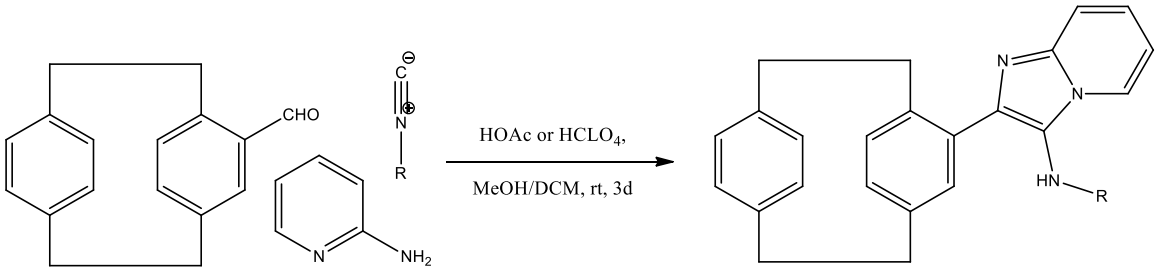

Scheme 4: Synthesis of Stahlberger

Jiang et al. reported a green synthesis of imidazo[1,2-a]pyridines via a one-pot, three-component reaction of terminal alkynes, 2-aminopyridines, and aldehydes in 2024 (Scheme 5). The synthesis was catalyzed by a new nanocatalyst, $CuCl_2$ supported on Fe_3O_4 nanoparticles functionalized with 1,10-phenanthroline-5,6-diol (Fe_3O_4@Diol/Phen-$CuCl_2$). This system was performed in PEG as an environmentally friendly medium. The procedure stands out for its high yield, eco-friendly compatibility, short reaction time, and catalyst reusability, making it a sustainable and practical strategy for the preparation of imidazo[1,2-a]pyridine derivatives [47].

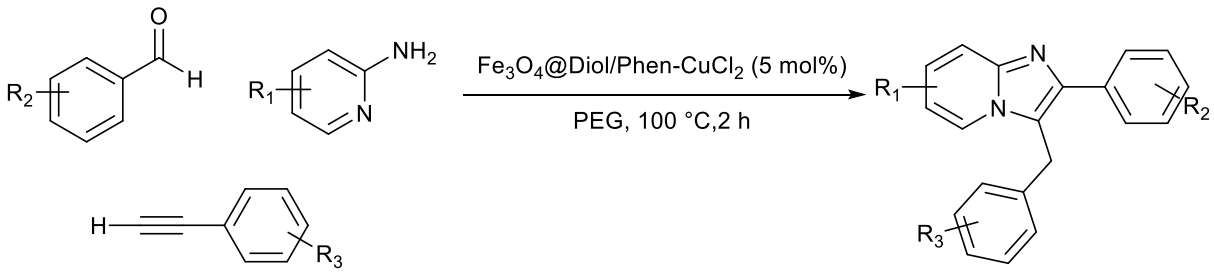

Scheme 5: Synthesis of Jiang

In 2025, Armendariz-Barrientos et al. developed a novel procedure for the synthesis of hybrid coumarin-3-yl-imidazo[1,2-a]pyridine derivatives (Scheme 6). The reaction was carried out by mixing brominated coumarins with 2-aminopyridine in the presence of sodium bicarbonate in acetonitrile for one hour. This mixture underwent microwave irradiation at 140◦C for one hour. The main advantages of this protocol are mild reaction conditions, high yields, and brief reaction time [48].

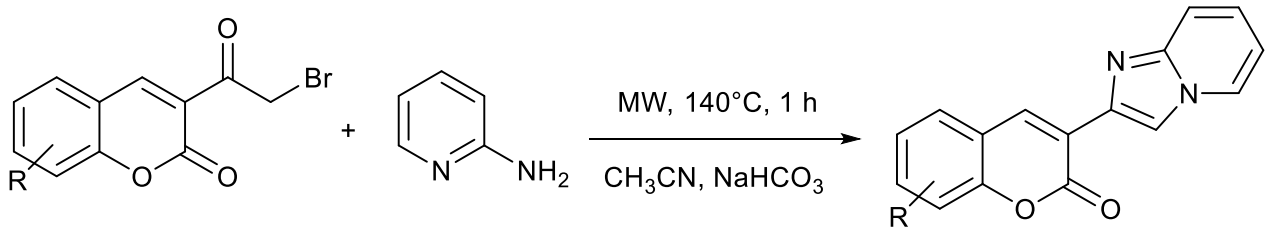

Scheme 6: Synthesis of Armendariz-Barrientos

3.1.3. Our syntheses of imidazo[1,2-a]pyridines

Synthesis of arylbromoketones

The synthesis of all our imidazo-heterocycles began with bromoacetophenones, which acted as key intermediates for the cyclization with 2-aminopyridine, 2-aminopyrimidine, or 2-aminothiazole, to afford the corresponding imidazo[1,2-a]pyridines, imidazo[1,2-a]pyrimidines, and imidazo[2,1-b]thiazoles.

Bromoacetophenones serve as important intermediates in heterocyclic synthesis [49–52]. To obtain these bromoarylketones, the corresponding arylketones were brominated using N-bromosuccinimide (NBS) in chloroform as the reaction medium, with p-toluenesulfonic acid (PTSA) as a catalyst (Scheme 7).

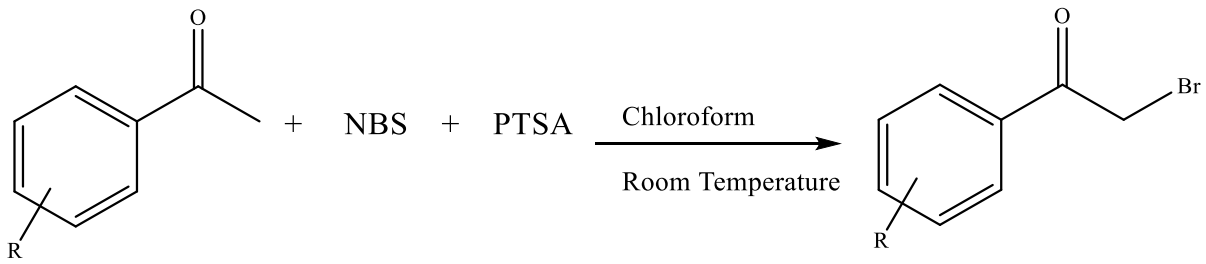

Scheme 7: Synthesis of arylbromoketones

The obtained results are presented in Table 1.

Table 1: Synthesized aryl bromoketones and their corresponding yield

Entry	R_1	Abbreviation	Structure	Yield (%)
1	H	Br-H	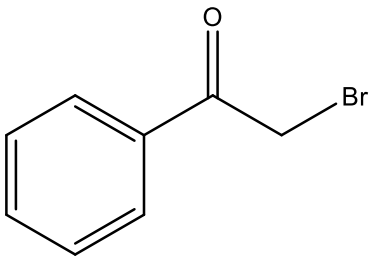	60
2	2-OMe	Br-2OMe	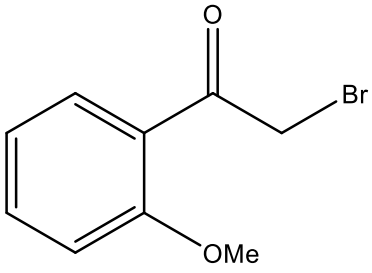	81

3	3-OMe	Br-3OMe	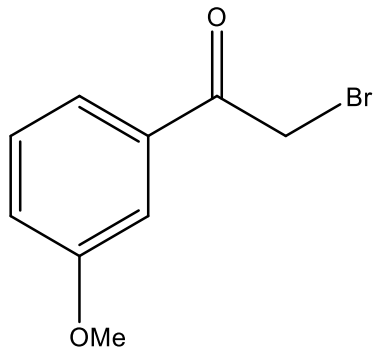	67
4	4-OMe	Br-4OMe	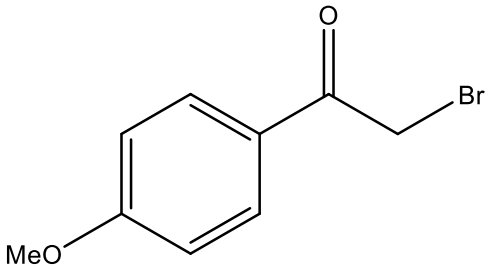	71
5	4-Me	Br-4Me	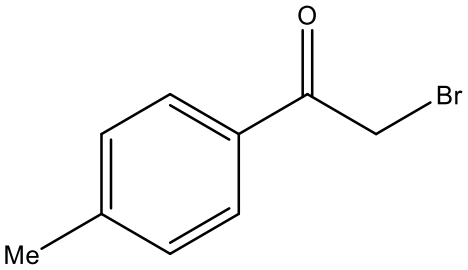	50
6	3,4-diMe	Br-3,4-diMe	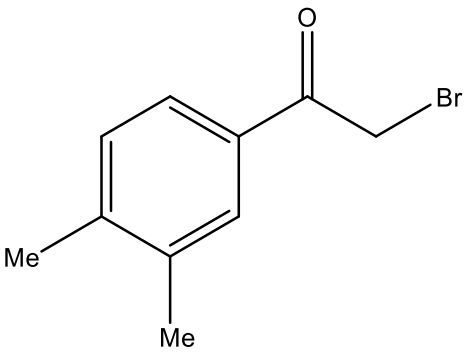	52
7	Naph	Br-Naph	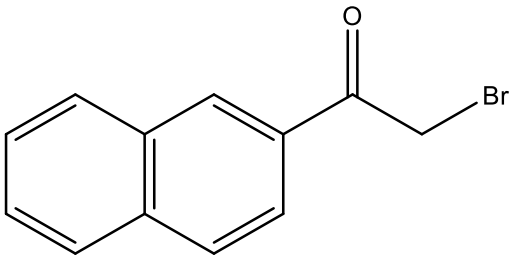	65

8	3-Br	Br-3Br	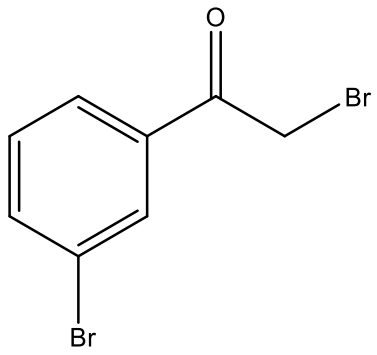	88
9	4-Br	Br-4Br	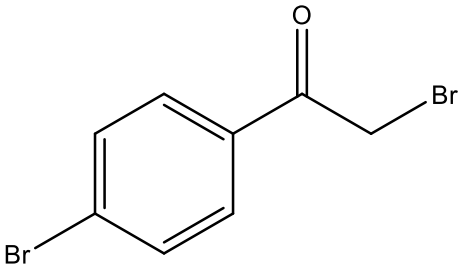	91
10	4-F	Br-4F	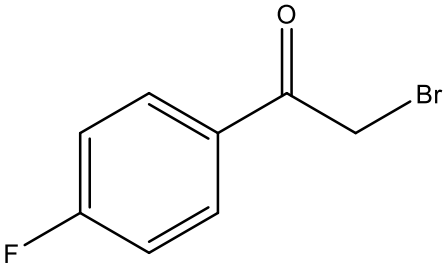	87

As shown in Table 1, the bromination reactions proceeded smoothly, affording the desired products in moderate to excellent yields, depending on the nature of the substituents on the aromatic ring.

We then synthesized imidazo[1,2-a]pyridine derivatives by reacting 2-aminopyridine with bromoacetophenones under reflux in ethanol, both in the absence and presence of 4% Au/TiO_2 as a catalyst (with the catalyst prepared according to Berrichi et al. [53]) (Scheme 8).

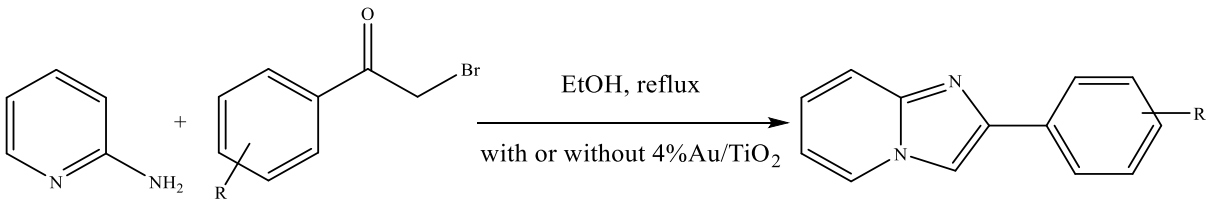

Scheme 8: Synthesis of imidazo[1,2-a]pyridine derivetives

The following table summarizes all the prepared imidazo[1,2-a]pyridines.

Table 2: Structures, and yields of the synthesized imidazo[1,2-a]pyridine derivatives.

Entry	Abbreviation	R	Structure	Yield (%)
1	**IP-H**	H	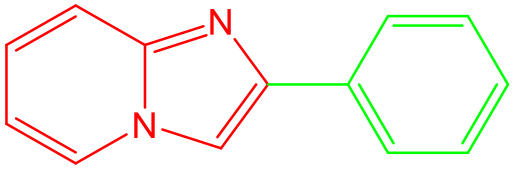	47[a]; 82[b]
2	**IP-3Br**	3Br	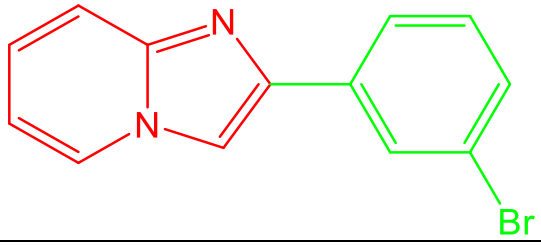	40[a]; 50[b]
3	**IP-4Br**	4Br	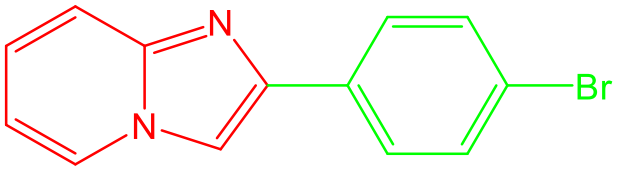	57[a]; 96[b]
4	**IP-4Me**	4Me	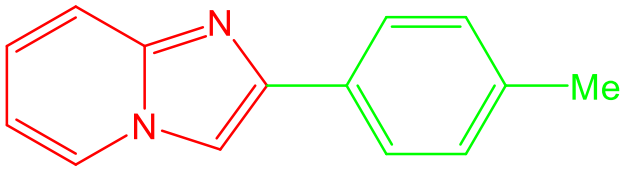	39[a]; 66[b]
5	**IP-2OMe**	2OMe	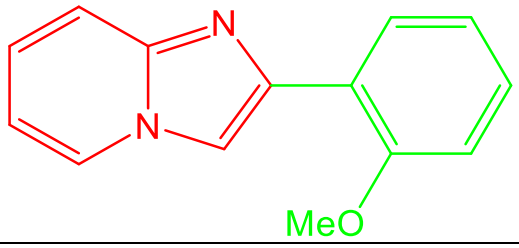	33[a]; 68[b]
6	**IP-3OMe**	3OMe	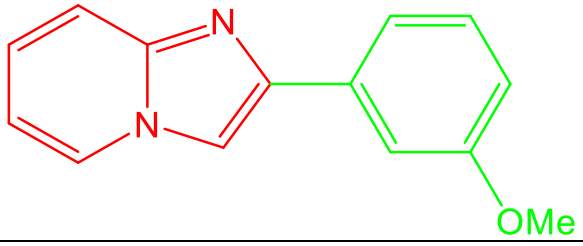	47[a]; 84[b]
7	**IP-4OMe**	4OMe	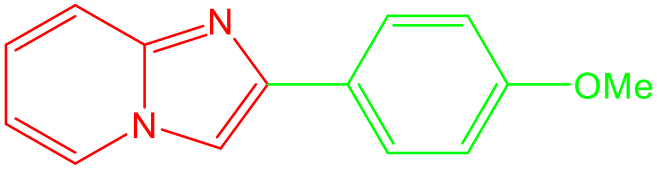	49[a]; 92[b]
8	**IP-4F**	4F	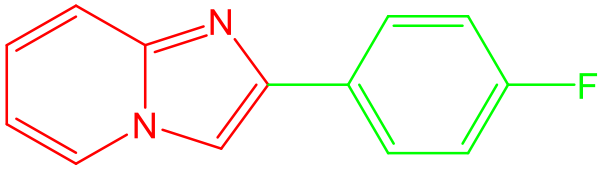	53[a]; 89[b]

9	**IP-4Cl**	4Cl	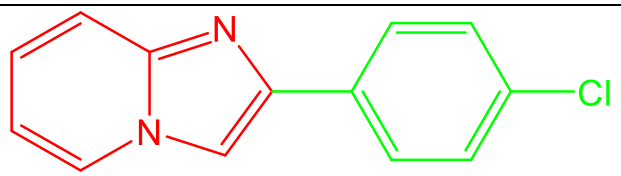	46[a]; 83[b]
10	**IP-2Naph**	2Naph	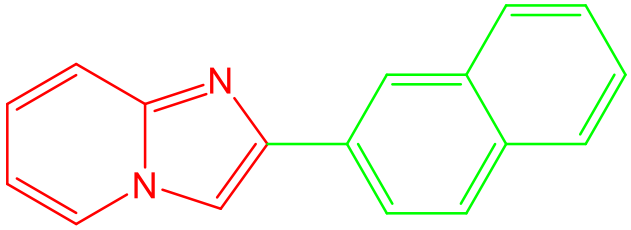	41[a]; 85[b]
11	**IP-3,4-diMe**	3,4-diMe	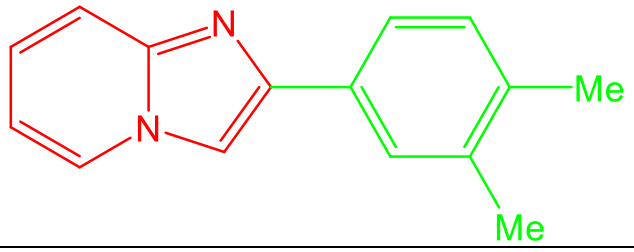	33[a]; 60[b]

a) EtOH, Reflux, 3-4h.
b) 4% Au/TiO_2, EtOH, Reflux, 1-2h.

Table 2 summarizes the synthesized imidazo[1,2-a]pyridine derivatives with various aryl or arylalkyl substituents at the R position. Each compound is identified by an abbreviation (e.g., **IP-H**, **IP-3Br**, etc.), and the corresponding structures are provided alongside their yields obtained under two different reaction conditions:

- **a)** Conventional heating in refluxing EtOH (3–4 h)
- **b)** Catalysis synthesis using 4% Au/TiO_2 (10% w/w) in EtOH under reflux (1–2 h)

The overall reaction efficiency was found to be strongly influenced by both the synthetic approach and the nature of the substituent.

- The yields obtained under catalytic conditions (b) are consistently higher than those obtained using classical thermal conditions (a), highlighting the remarkable catalytic activity 4%Au/TiO_2 in promoting the cyclization.
- The best yield under condition (b) is recorded for **IP-4Br** (96%), followed by **IP-4OMe** (92%) and **IP-4F** (89%).
- In contrast, substrates like **IP-2Naph** (85%), **IP-3OMe** (84%), **IP-4Cl** (83%) and **IP-H** (82%) provided comparatively lower yields under both conditions.
- The lowest yields under classical conditions (a) were recorded for **IP-3,4-diMe** (33%), **IP-2OMe** (32%), **IP-4Me** (39%), and **IP-3Br** (40%) whereas significant improvements were observed when using the 4%Au/TiO_2 method.

Overall, this table clearly demonstrates the synthetic efficiency and versatility of the catalytic route, especially when mediated by 4% Au/TiO_2, providing an effective approach to access structurally diverse imidazo[1,2-a]pyridines in high yields and shorter reaction times.

3.2. Imidazo[1,2-a]pyrimidines (IPMs)

3.2.1. Biological properties of IPMs

As aromatic heterocyclic systems, imidazo[1,2-a]pyrimidines exhibit a wide range of pharmacological properties due to their significant therapeutic potential [54]. The imidazo[1,2-a]pyrimidine scaffold is of great interest in medicinal chemistry because it displays diverse physiological activities, including antioxidant [55], anti-inflammatory [56], anxiolytic [57], anticonvulsant [58], benzodiazepine receptor agonist [59], calcium channel blockers [60], antitubercular [61], anticancer [62], antimalarial [63], antiviral [64], antimicrobial [65], and antifungal [66] effects. Moreover, imidazo[1,2-*a*]pyrimidines constitute the core structure of several marketed drugs and commercially available compound libraries, such as divaplon, fasiplon, and taniplon (Figure 4) [21]. This widespread presence may be attributed to their distinctive physicochemical properties and structural similarity to natural substrates such as purines [67]. Due to their close structural analogy to purine heterocycles and the presence of a guanidine-like functionality, imidazo[1,2-a]pyrimidines can interact with diverse biological targets, leading to multiple biological effects. However, further detailed investigations remain necessary to fully assess their biological potential and therapeutic scope, particularly in the field of antimicrobial research [65].

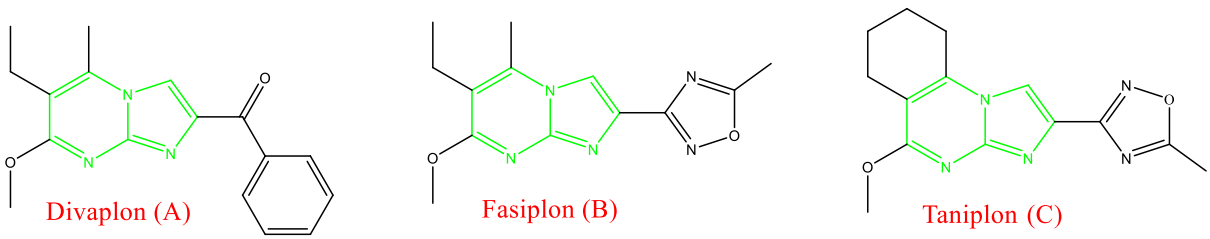

Figure 4: Pharmacologically active drugs holding imidazo[1,2-*a*]pyrimidine scaffolds

3.2.2. Described syntheses of IPMs

Over the past years, imidazo[1,2-a]pyrimidines have emerged as important scaffolds in many pharmacologically active compounds. Numerous synthetic methods have been developed and documented. In the following part, we present a review of some reported syntheses described in the literature.

Gómez-García et al. reported in 2018 the synthesis of a set of 3-benzoyl imidazo[1,2-a]pyrimidines from N-heteroarylformamidines using an accessible and efficient method, achieving high yields (Scheme 9). The objective of their work was develop a protocol free from microwave irradiation or conventional heating. The target molecules were prepared from N,N-dimethyl-N-pyrimidilformamidine, obtained in full yield through condensation, under reflux conditions, of 2-aminopyrimidine and an excess of N,N-dimethylformamide dimethyl acetal. The synthetic pathway employed is a variant of their previous work. The resulting intermediates were treated at room temperature with various phenacyl bromides under inert atmosphere to give the final products, the 3-benzoyl derivatives, after three hours in synthetically useful yields.[67]

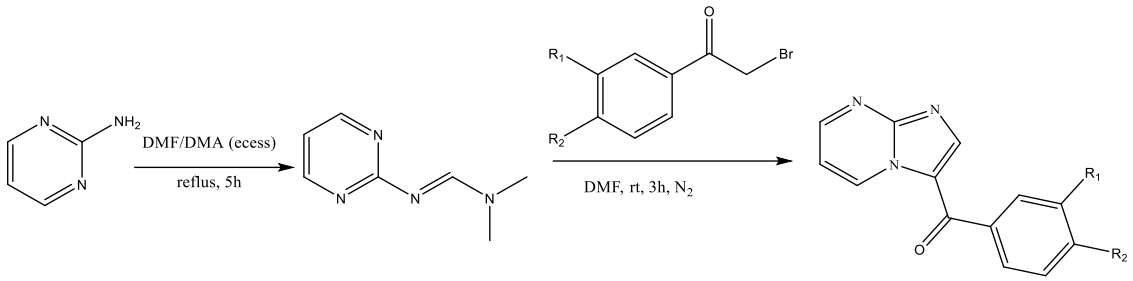

Scheme 9: Synthesis of Gómez-García

Güngör in 2020 prepared new imidazo[1,2-a]pyrimidine derived Schiff bases through an imine formation reaction by conventional heating and microwave irradiation methods (Scheme 10). The reactions were performed in refluxing toluene with magnesium sulfate ($MgSO_4$) as the drying agent. Under conventional conditions, the final products required reaction times of 10-36 h with moderate to good yields, while they were synthesized in only 45-120 min with better yields under microwave irradiation. These findings highlight the performance of microwave irradiation as an environmentally friendly, efficient and sustainable method [68].

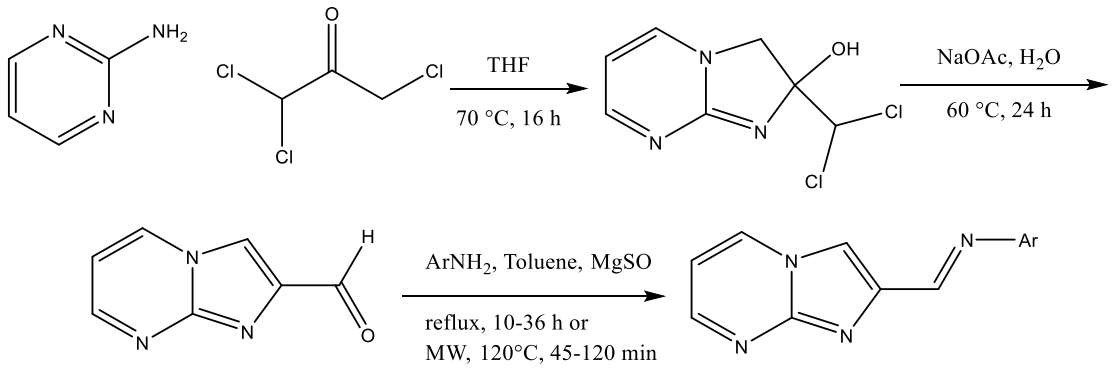

Scheme 10: Synthesis of Güngör

In 2021, Rehan et al. reported the synthesis of a new set of 2-aryl-3-(pyrimidine-2-ylamino)imidazo[1,2-a]pyrimidine derivatives via one-pot reaction of 2-aminopyrimidine and aromatic ketones (Scheme 11). These reactions were carried out under the influence of iodine and DMSO. The mixture of acetophenone and I_2 in DMSO was heated for 6 hours under reflux at 100 °C, followed by the addition of 2-aminopyrimidine under additional heating for 2 hours. The desired heterocycles were acquired in good yields [55].

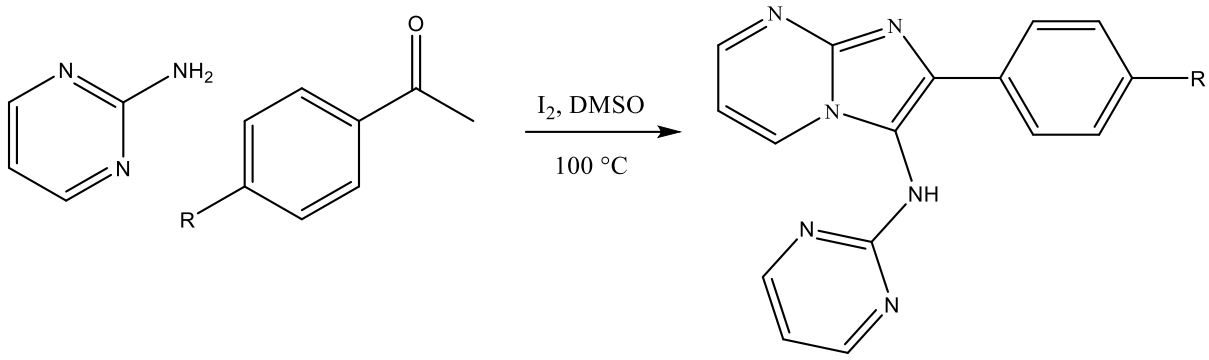

Scheme 11: Synthesis of Rehan

In 2023, Azzouzi et al. prepared a new series of imidazo[1,2-a]pyrimidine-linked Schiff base derivatives via an efficient and simple synthetic procedure that adheres to the key principles of green chemistry, making it appropriate to industrial-scale production (Scheme 12). The first step was a condensation between 2-bromo-1-phenylethan-1-one and 2-aminopyrimidine in acetone overnight at ambient temperature. The resulting 2-phenylimidazo[1,2-a]pyrimidine was then subjected to a sequence of reactions to afford the corresponding imidazo[1,2-a]pyrimidine Schiff base derivatives in good to excellent yields [64].

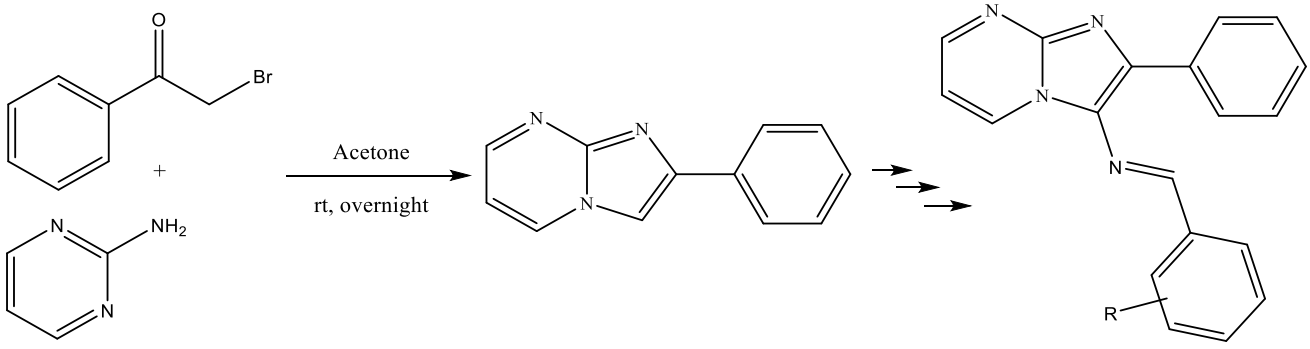

Scheme 12: Synthesis of Azzouzi

In 2025, Aggrawal et al. described an eco-friendly and facile method for regioselective preparation of a set of imidazo [1,2-a]pyrimidine derivatives through multicomponent reaction of 2-aminopyrimidine, unsymmetrical β -diketones and N-bromosuccinimide in DCM (Scheme

13). The reaction occurs via generation of α-bromo-β-diketones *in situ*, followed by condensation with 2-aminopyrimidine without the use of any inorganic or organic catalyst. Their strategy offers many advantages like avoidance of toxic and metal-based catalysts, diverse substrate compatibility, high yields, operational simplicity, and easy work-up [69].

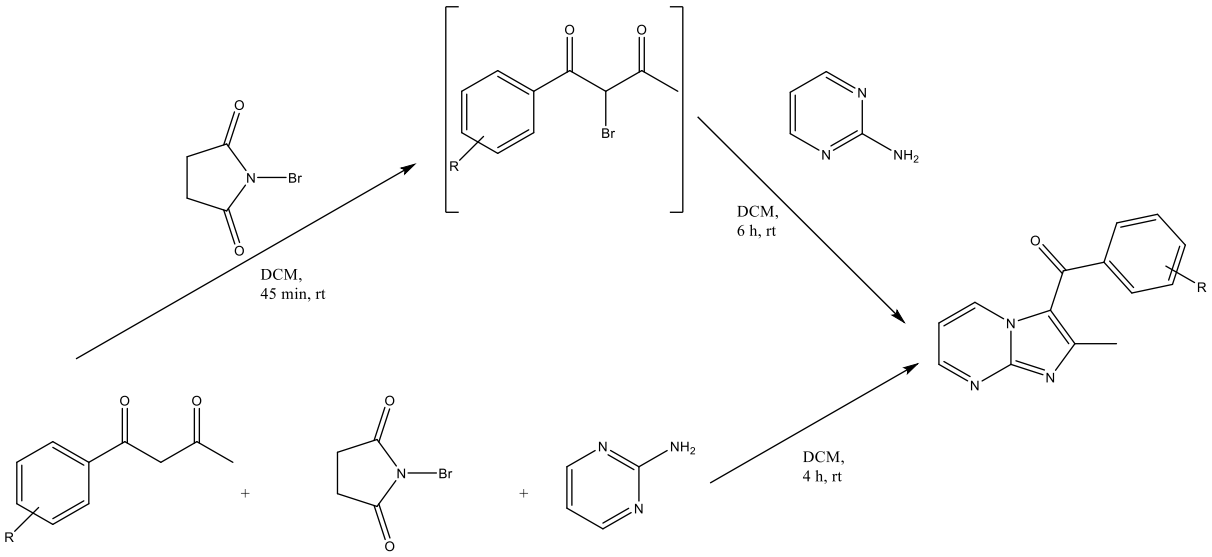

Scheme 13: Synthesis of Aggrawal

3.2.3. Our syntheses of imidazo[1,2-a]pyrimidines

The reaction between 2-aminopyrimidine and bromoacetophenones afforded imidazo[1,2-a]pyrimidine derivatives using different methodologies: standard ethanol reflux, ethanol reflux catalyzed by 1% Au/TiO_2 (with the catalyst prepared according to Berrichi et al. [53]), and microwave-assisted synthesis with Al_2O_3 under solvent-free conditions (Scheme 14).

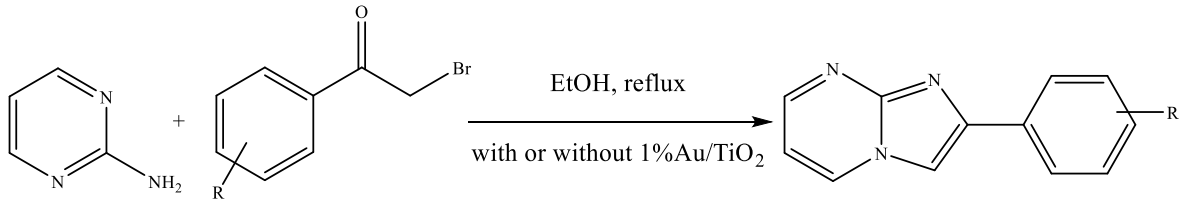

Scheme 14: Synthesis of imidazo[1,2-a]pyrimidines.

The ensuing table outlines all the synthesized imidazo[1,2-a]pyrimidine derivetives.

Table 3: Structures and yields of imidazo[1,2-a]pyrimidines obtained by different protocols.

Entry	Abbre-viation	R	Structure	Yield (%)
1	**IPM-H**	H	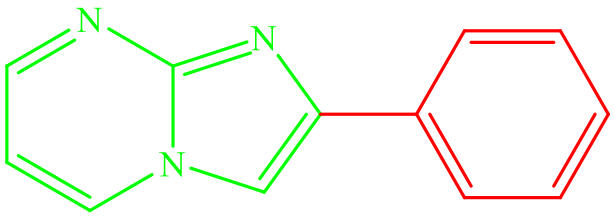	37[a]; 73[b]; 70 [c]
2	**IPM-3Br**	3Br	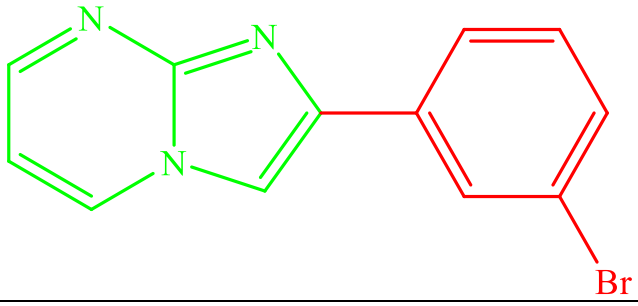	44[a]; 60[b]; 56 [c]
3	**IPM-4Br**	4Br	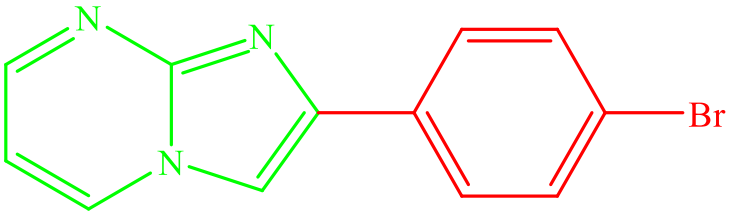	61[a]; 72[b]; 63[c]
4	**IPM-4Me**	4Me	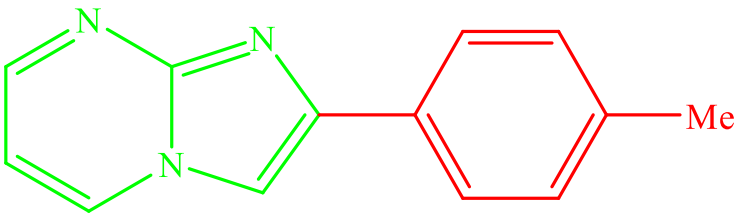	62[a]; 76[b]; 68[c]
5	**IPM-2OMe**	2OMe	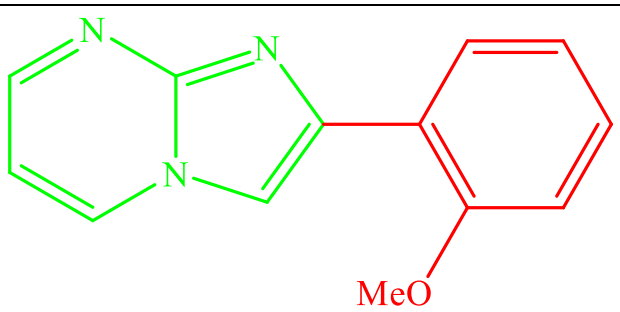	42[a]; 76[b]; 57[c]
6	**IPM-3OMe**	3OMe	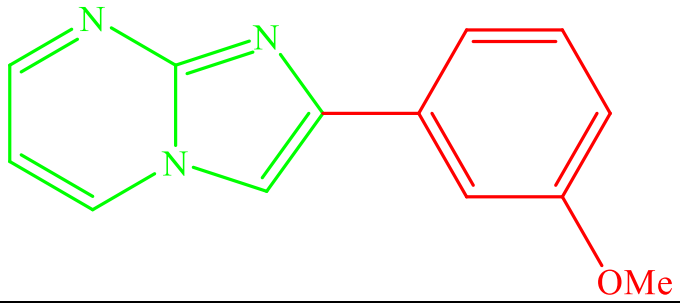	49[a]; 71[b]; 53[c]

7	**IPM-4OMe**	4OMe	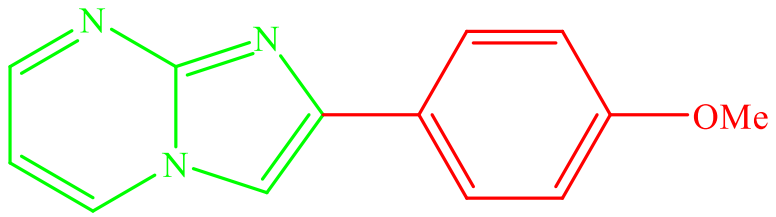	32[a]; 65[b]; 52[c]
8	**IPM-4F**	4F	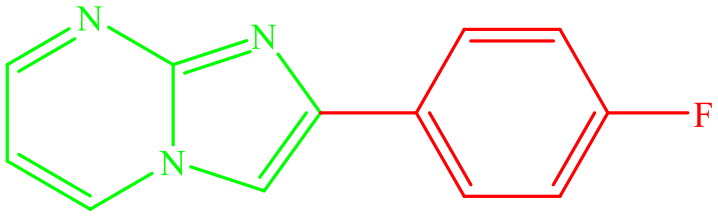	50[a]; 68[b]; 63[c]
9	**IPM-4Cl**	4Cl	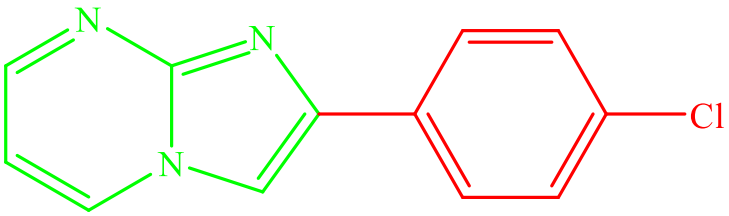	60[a]; 73[b]; 65[c]
10	**IPM-2Naph**	2Naph	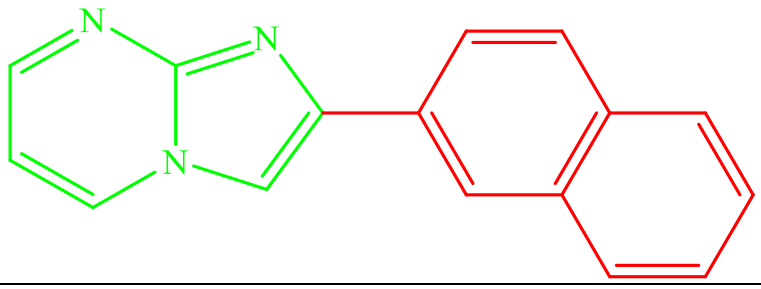	53[a]; 79[b]; 67[c]
11	**IPM-3,4-diMe**	3,4-diMe	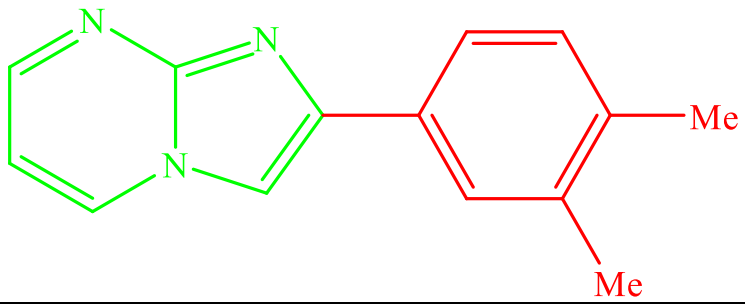	41[a]; 81[b]; 64[c]

- a) EtOH, Reflux, 5-6h.
- b) 1% Au/TiO_2, EtOH, Reflux, 2-3h.
- c) Al_2O_3 no solvent, MW, 90-300 sec

Table 3 presents the structures and yields of imidazo[1,2-a]pyrimidine derivatives prepared under three different synthetic protocols:

- Classical heating in ethanol (reflux, 5-6 h),
- Catalytic reflux in EtOH using 1% Au/TiO_2 (2–3 h),
- Microwave-assisted synthesis under solvent-free conditions using Al_2O_3 as a catalyst (90–300 seconds).

The recorded yields vary significantly based on the nature of the substituent (R) and the synthetic methodology employed.

- Catalysis with 1%Au/TiO_2 (condition b) led to the highest yields for all compounds, demonstrating its effectiveness as a green and efficient catalyst that significantly reduces reaction time while e while enhancing yield.
- The best performance under this condition was observed for **IPM-3,4-diMe** and **IPM-2Naph**, with yields of 81% and 79%, respectively. Both **IPM-4Me** and **IPM-2OMe** also afforded yields of 76% under the same condition.
- **IPM-4Cl** and **IPM-4Br** exhibited excellent reactivity under all three protocols.
- For **IPM-4OMe** and **IPM-H** notable changes in yields were observed, increasing from 32% (a) to 65% (c), and from 37% (a) to 73% (c) respectively, when moving from the conventional (a) to the microwave (c) conditions.
- The microwave-assisted protocol thus proved highly effective, especially for the non-substituted compound (**IPM-H**), providing rapid access to the desired products with good yields.
- In contrast, classical heating gave lower yields and required longer reaction times.
- The lowest yields were obtained for **IPM-4OMe** (32%) and **IPM-H** (37%) under classical conditions, while substantial improvements were achieved using the 1%Au/TiO_2 and microwave methodologies.

Overall, this comparison highlights the clear advantages of modern green techniques, particularly heterogeneous catalysis and microwave irradiation, which provide higher efficiency, shorter reaction times, and cleaner synthetic processes in the preparation of imidazo[1,2-a]pyrimidines.

3.3. Imidazo[1,2-a]pyrimidines (IMThs)

3.3.1. Biological properties of IMThs

Recently, much attention has been directed toward the chemistry and biological potential of fused heterocyclic systems due to their wide range of physiological activities. Among the nitrogen- and sulfur-containing heterocycles, imidazo[2,1-b]thiazole derivatives hold particular importance because of their diverse pharmacological properties. These compounds have been reported in the literature to exhibit antibacterial, antitubercular, antifungal, antitumor, antiviral,

analgesic, anti-inflammatory, antihypertensive, cardiotonic, diuretic, herbicidal, and insecticidal activities. Levamisole (Figure 5), an imidazo[2,1-b]thiazole compound, is widely used as an antihelminthic agent in livestock [70]. In view of their biological significance, we became interested in the synthesis of new imidazo[2,1-b]thiazole derivatives.

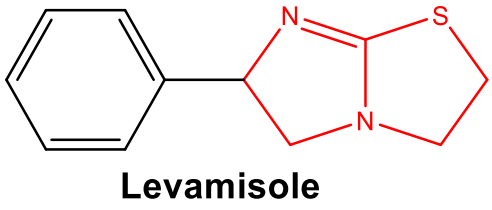

Figure 5: Molecular structure of Levamisole based on the imidazo[2,1-b]thiazole backbone

3.3.2 Described syntheses of IMThs

The presence of the imidazo[2,1-b]thiazole scaffold in therapeutic agents, combined with its structural versatility and broad pharmacological potential, underscores the importance of developing efficient synthetic strategies to access this valuable framework in medicinal chemistry.

In 2019, Abdel-Maksoud et al. developed and reported a novel library of imidazo[2,1-b]thiazole derivatives (Scheme 15). The target compounds were obtained through a multi-step synthetic sequence. The first step involved the condensation and cyclization of 2-aminothiazole with 2-bromo-1-(3-fluorophenyl)ethan-1-one under reflux conditions in absolute ethanol, affording the corresponding imidazo[2,1-b]thiazole intermediate. This intermediate was then subjected to further chemical transformations to yield the desired products in good yields [71].

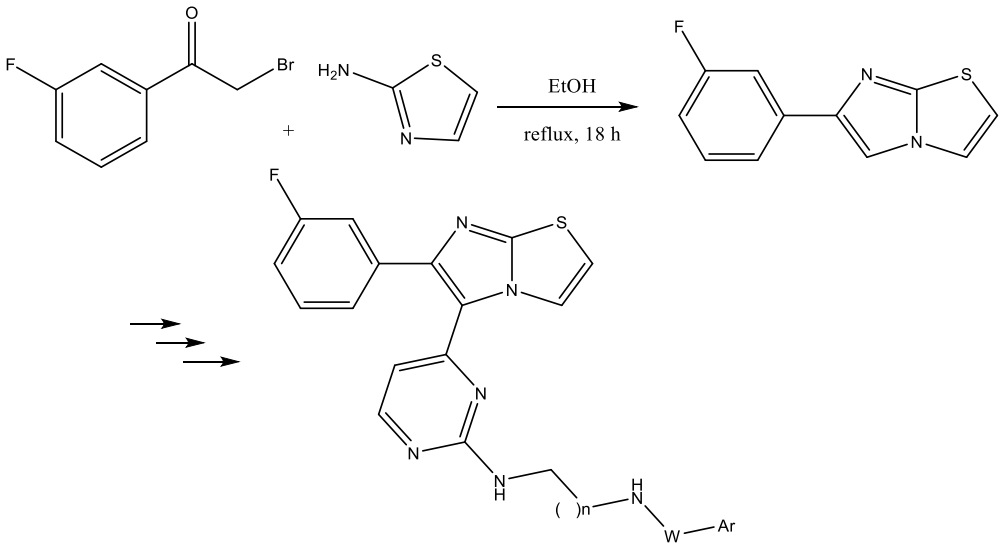

Scheme 15: Synthesis of Abdedel-Maksoud

In 2020, Consty et al. reported the design and synthesis of a Schiff base fluorescent sensor, namely (Z)-N'-(3-ethoxy-2-hydroxybenzylidene)imidazo[2,1-b]thiazole-6-carbohydrazide (Scheme 16). The synthetic route began with the preparation of imidazo[2,1-b]thiazole-6-carboxylate, obtained by reacting ethyl 3-bromo-2-oxopropanoate with 2-aminothiazole in a THF/ethanol mixture at room temperature for 20 hours, followed by reflux heating for 4 hours. The resulting product was then treated with hydrazine in ethanol at ambient temperature overnight, affording imidazo[2,1-b]thiazole-6-carbohydrazide. This intermediate was subsequently condensed with 3-ethoxy-2-hydroxybenzaldehyde under stirring at room temperature for 12 hours in ethanol, yielding the target Schiff base compound with a 53.9% yield [72].

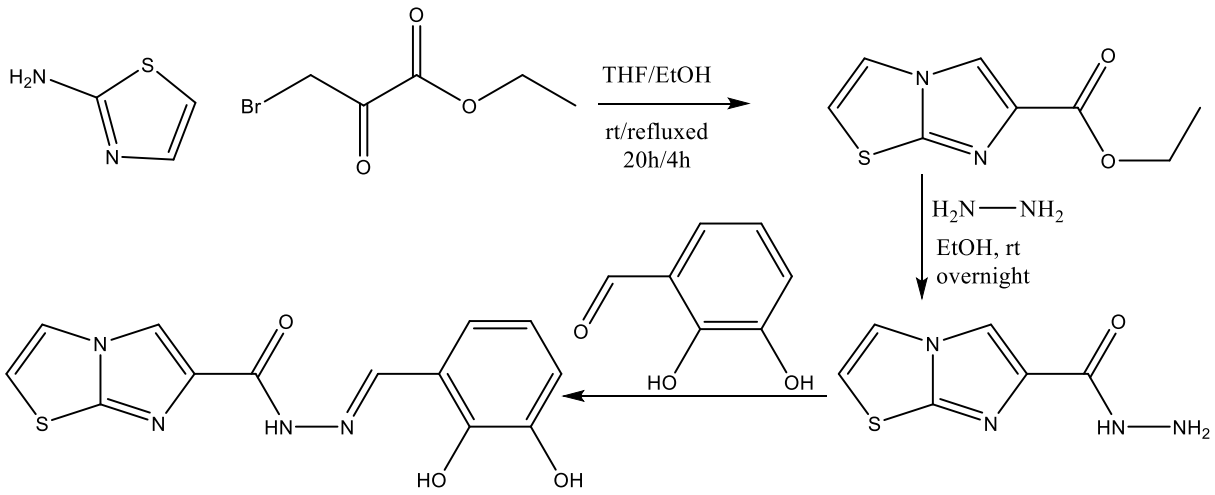

Scheme 16: Synthesis of Consty

In 2021, Gadekar et al. [73] reported the design and synthesis of a series of saturated 2,3-dihydroimidazo[2,1-b]thiazole derivatives (Scheme 17). The compound 6-(3-nitrophenyl)-2,3-dihydroimidazo[2,1-b]thiazole was obtained in good yield by reacting 4,5-dihydrothiazol-2-amine and potassium carbonate with 2-bromo-1-(3-nitrophenyl)ethanone in anhydrous DMF at 90 °C for 2 hours. Subsequently, a mixture of the resulting 6-(3-nitrophenyl)-2,3-dihydroimidazo[2,1-b]thiazole and acetic anhydride was treated with $AlCl_3$ and heated at 130 °C for 72 hours, affording 1-(6-(3-nitrophenyl)-2,3-dihydroimidazo[2,1-b]thiazol-5-yl)ethanone. This intermediate was then subjected to further transformations to yield the final derivatives.

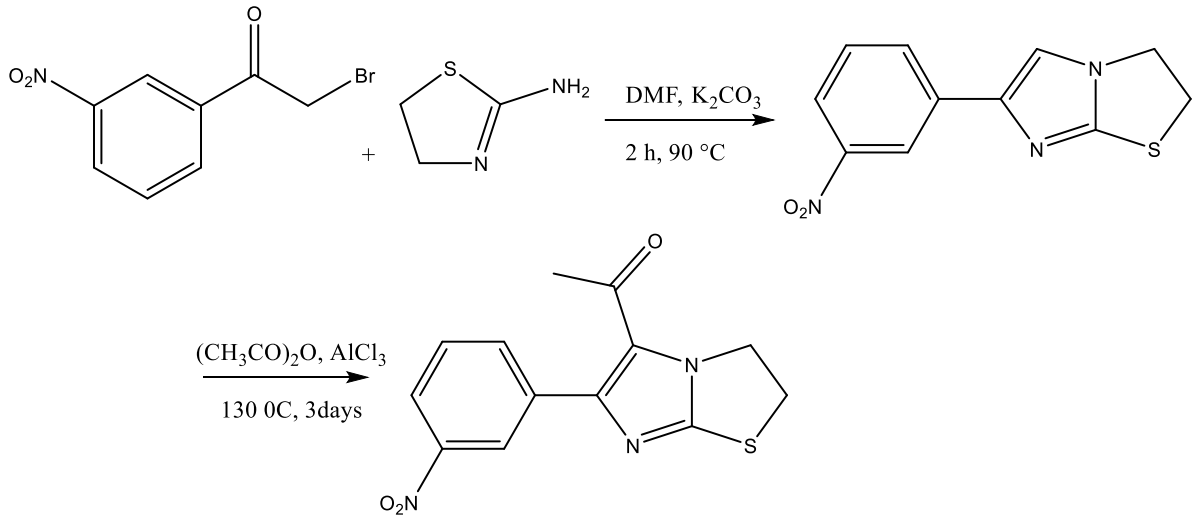

Scheme 17: Synthesis of Gadekar

In 2022, Chitti et al. [74] developed an efficient synthetic route for the preparation of (4-(2-(4-substituted phenyl/aliphatic group-1H-1,2,3-triazol-1-yl)ethyl)piperazin-1-yl)(6-methylimidazo[2,1-b]thiazol-5-yl)methanone derivatives through a straightforward strategy combining various 1,2,3-triazole analogues and piperazine with imidazo[2,1-b]thiazoles (Scheme 18). They first synthesized ethyl 6-methylimidazo[2,1-b]thiazole-5-carboxylate in 80% yield by refluxing ethyl 2-chloroacetoacetate with 2-aminothiazole in 1,4-dioxane for 24 hours. The resulting intermediate was then subjected to a sequence of reactions to yield the desired imidazo[2,1-b]thiazole–triazole–piperazine hybrids.

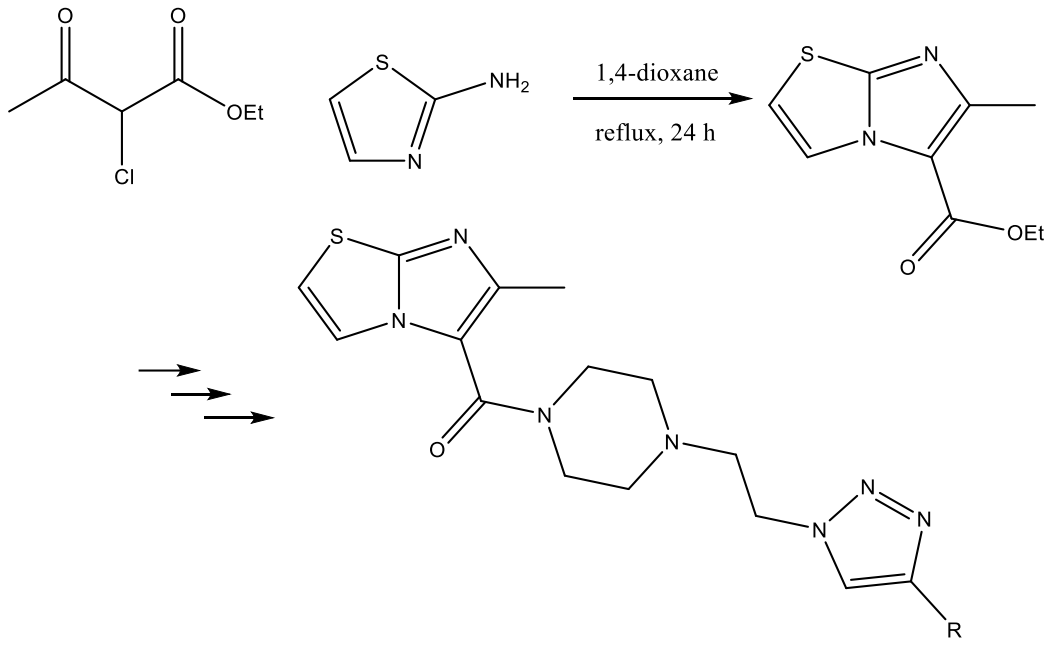

Scheme 18: Synthesis of Chitii

In 2023, Calderón-Rangel et al. [75] reported the synthesis of bis-heterocycles incorporating the imidazo[2,1-b]thiazole scaffold linked to a chromone moiety via a multicomponent reaction conducted under catalyst-free conditions. In this method, 2-aminothiazole and various isocyanides were added to a solution of 4-oxo-4H-chromene-3-carbaldehyde in anhydrous toluene (Scheme 19). The reaction mixture was heated at 100 °C for 30 minutes, affording the desired products in good yields.

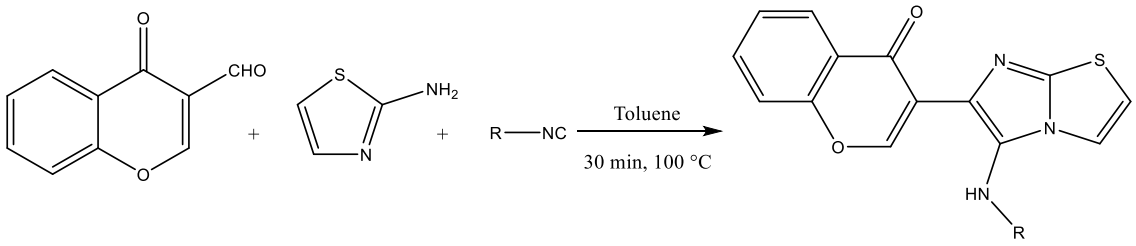

Scheme 19: Synthesis of Calderón-Rangel

3.3.3. Our syntheses of imidazo[2,1-b]thiazoles

Imidazo[2,1-b]thiazoles were synthesized by reacting 2-aminothiazole with bromoacetophenones in ethanol under reflux, either in the absence or presence of Al_2O_3 (Scheme 20).

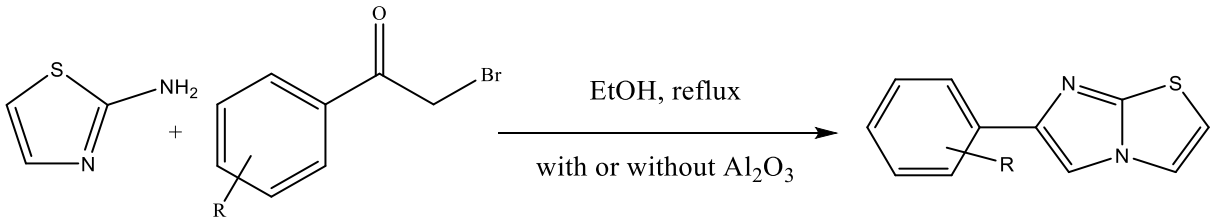

Scheme 20: Synthesis of imidazo[2,1-b]thiazole derivatives.

The following table summarizes all the obtained imidazo[2,1-b]thiazole derivatives along with their corresponding yields.

Table 4: Structures, and yields of the prepared imidazo[2,1-b]thiazoles.

Entry	Abbreviation	R	Structure	Yield (%)
1	IMTh-H	C_6H_5	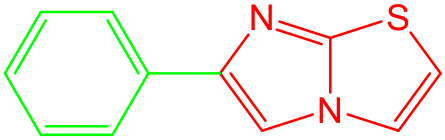	67 [a]; 80 [b]
2	IMTh-4Me	4-MeC_6H_4	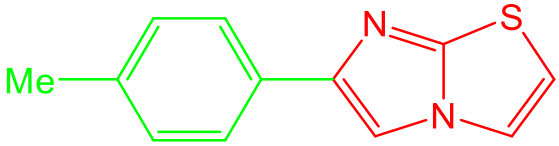	76 [a]; 91 [b]

3	IMTh-2Naph	2-naphtyl	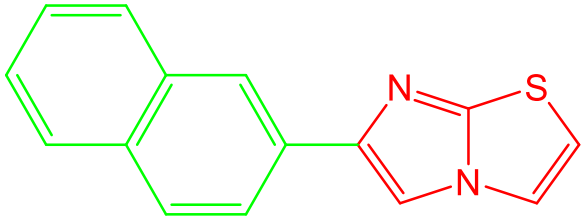	72 [a]; 79 [b]
4	IMTh-2OMe	2-$MeOC_6H_4$	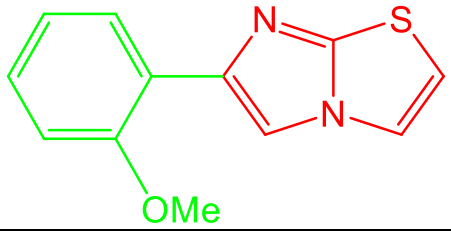	62 [a]; 66 [b]
5	IMTh -3OMe	3-$MeOC_6H_4$	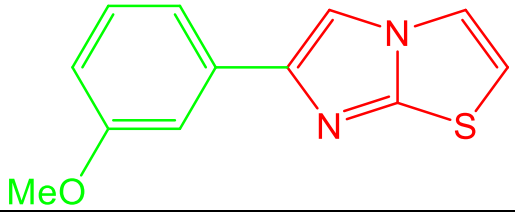	82 [a]; 93 [b]
6	IMTh-4OMe	4-$MeOC_6H_4$	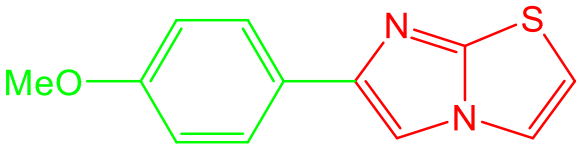	80 [a]; 88 [b]
7	IMTh -4Cl	4-ClC_6H_4	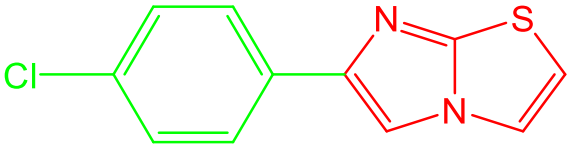	83 [a]; 93 [b]
8	IMTh-4F	4-FC_6H_4	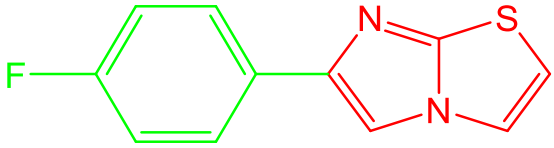	50 [a]; 87 [b]

- a) EtOH, Reflux, 8-12h.
- b) Al_2O_3, EtOH, Reflux, 6-8h.

Table 4 provides an overview of the structures and isolated yields of the synthesized imidazo[2,1-b]thiazole derivatives (IMTh-1 to IMTh-8), obtained under two different sets of conditions:

(a) Conventional reflux in ethanol (8–12 h), and

(b) Reflux in ethanol in the presence of Al_2O_3 (6–8 h).

- The introduction of Al_2O_3 as a heterogeneous catalyst (condition b) markedly enhanced the yields for most derivatives compared to the conventional method (condition a), confirming its catalytic efficiency and environmentally friendly character.

- The highest yields were obtained for **IMTh-4Cl** and **IMTh-3OMe**, which afforded 83% and 82% under condition (a), respectively, and both increased to an excellent 93% under condition (b).
- **IMTh-4Me** also demonstrated excellent reactivity under both protocols, yielding 76% under conventional conditions (a) and 91% under Al_2O_3 catalysis (b).
- A significant yield improvement is noted for **IMTh-4F**, increasing from 50% (a) to 87% (b), indicating that the Al_2O_3-catalyzed route effectively overcomes the deactivating effects of fluorine.
- Even in the case of the unsubstituted compound **IMTh-H**, a notable increase was observed, from 67% to 80%, confirming the beneficial influence of the catalytic system.
- Derivative bearing a 2-naphthyl group (**IMTh-2Naph**) maintained good to excellent yields across both methods (72%/79%).

Generally, the data clearly demonstrate that the Al_2O_3-mediated protocol not only reduces the reaction time but also improves the efficiency across a broad range of substrates. This approach is particularly attractive from a green chemistry perspective due to the use of a recyclable solid support and ethanol as an environmentally benign solvent. The results affirm the robustness and general applicability of the method for the synthesis of imidazo[2,1-b]thiazole derivatives.

4. Conclusion

In this chapter, a series of imidazo-based heterocycles, including imidazo[1,2-a]pyridines, imidazo[1,2-a]pyrimidines, and imidazo[2,1-b]thiazoles, were successfully synthesized using various catalytic and environmentally benign approaches. The comparative analysis of these synthetic protocols demonstrates the significant impact of reaction conditions and catalysts on both yield and efficiency. In particular, the use of heterogeneous catalysts such as Au/TiO_2 and Al_2O_3, as well as microwave-assisted techniques, provided notable improvements in reaction times and product yields. The influence of substituents on the aryl ring was also evident in all synthesized frameworks. These results confirm the versatility and efficiency of the developed methodologies, which are not only synthetically robust but also align with the principles of green chemistry. Overall, this study contributes to advancing sustainable synthetic strategies for constructing valuable heterocyclic scaffolds with potential biological relevance.

References

1. Talbi, S.; Dib, M.; Bouissane, L.; Abderrafia, H.; Rabi, S.; Khouili, M. Recent Progress in the Synthesis of Heterocycles Based on 1,3-Diketones. *Curr. Org. Synth.* **2021**, *19*, 220–245, doi:10.2174/1570179418666211011141428.

2. Das, A.; Banik, B.K. Sustainable Reactions in the Synthesis of Heterocycles. *Curr. Organocatalysis* **2022**, *9*, 3–3, doi:10.2174/2213337209012203281645 23.

3. Ma, X.-L.; Wang, Y.-H.; Shen, J.-H.; Hu, Y. Progress in the Synthesis of Heterocyclic Compounds Catalyzed by Lipases. *Pharm. Front.* **2021**, *03*, e87–e97, doi:10.1055/s-0041-1736233.

4. Maheshwari, K.K.; Bandyopadhyay, D. Heterocycles in the Treatment of Neglected Tropical Diseases. *Curr. Med. Chem.* **2020**, *28*, 472–495, doi:10.2174/0929867327666200219141652.

5. Ali, I.; Lone, M.; Al-Othman, Z.; Al-Warthan, A.; Sanagi, M. Heterocyclic Scaffolds: Centrality in Anticancer Drug Development. *Curr. Drug Targets* **2015**, *16*, 711–734, doi:10.2174/1389450116666150309115922.

6. Kumari, S.; Maddeboina, K.; Bachu, R.D.; Boddu, S.H.S.; Trippier, P.C.; Tiwari, A.K. Pivotal Role of Nitrogen Heterocycles in Alzheimer's Disease Drug Discovery. *Drug Discov. Today* **2022**, *27*, 103322, doi:10.1016/j.drudis.2022.07.007.

7. Benzenine, D.; Kibou, Z.; Berrichi, A.; Bachir, R.; Choukchou-Braham, N. New Synthesis of Imidazo[1,2-a]Pyrimidines Catalyzed Using Gold Nanoparticles. In Proceedings of the ECSOC-25; MDPI: Basel Switzerland, November 14 2021; Vol. 8, p. 110.

8. Belhadj, F.; Kibou, Z.; Cheikh, N.; Choukchou-Braham, N.; Villemin, D. Convenient Access to New 4-Substituted Aminopyrido[2,3-d]Pyrimidine Derivatives. *Tetrahedron Lett.* **2015**, *56*, 5999–6002, doi:10.1016/j.tetlet.2015.09.042.

9. Kibou, Z.; Villemin, D.; Lohier, J.F.; Cheikh, N.; Bar, N.; Choukchou-Braham, N. Easy Solventless Synthesis of New Mono and Bis Amino-5H-Chromeno [3,4-c] Pyridin-5-One Derivatives. *Tetrahedron* **2016**, *72*, 1653–1661, doi:10.1016/j.tet.2016.01.063.

10. Kibou, Z.; Cheikh, N.; Choukchou-Braham, N.; Mostefa-kara, B.; Benabdellah, M.; Villemin, D. New Methodology for the Synthesis of 2-Pyridones Using Basic Al2O3 as

Catalyst. *J. Mater. Environ. Sci.* **2011**, *2*, 293–298.

11. Belhadj, F.; Kibou, Z.; Benabdallah, M.; Aissaoui, M.; Rahmoun, M.N.; Villemin, D.; Choukchou-Braham, N. Synthesis and Biological Evaluation of New Chromenes and Chromeno[2,3-d] Pyrimidines. *South African J. Chem.* **2021**, *75*, 150–155, doi:10.17159/0379-4350/2021/v75a18.

12. Kibou, Z.; Aissaoui, N.; Daoud, I.; Seijas, J.A.; Vázquez-Tato, M.P.; Klouche-Kheli, N.; Choukchou-Braham, N. Efficient Synthesis of 2-Aminopyridine Derivatives: Antibacterial Activity Assessment and Molecular Docking Studies. *Molecules* **2022**, *27*, 3439, doi:10.3390/molecules27113439.

13. Medjdoub, A.; Belhadj, F.; Saidi Merzouk, A.; Baba Hamed, Y.; Kibou, Z.; Choukchou-Braham, N.; Merzouk, H. In Vitro Peripheral Blood Mononuclear Cell Proliferation, Cytokine Secretion and Oxidative Stress Modulation by Pyrido[2,3-d] Pyrimidines. *Chem. Pap.* **2020**, *74*, 903–913, doi:10.1007/s11696-019-00924-5.

14. Baba-Ahmed, I.; Kibou, Z.; Daoud, I.; Belhadj, F.; Belarbi, L.; Daich, A.; Choukchou-Braham, N. Synthesis, Molecular Docking and ADME-TOX Studies of New Tacrine Analogs as Promising for Alzheimer's Disease Therapy. *Curr. Org. Chem.* **2022**, *26*, 1218–1233, doi:10.2174/1385272826666220914114544.

15. Missoum, H.; Datoussaid, Y.; Choukchou-braham, N. Synthesis of Heterocycle via Vilsmeier-Haack Reaction. *Molecules* **2020**, *1*, 8101, doi:10.3390/ECSOC-24-08101.

16. Tripathi, P.; Malviya, A. Imidazole Scaffold: A Review of Synthetic Strategies and Therapeutic Action. *Biomed. Pharmacol. J.* **2023**, *16*, 1159–1168, doi:10.13005/bpj/2696.

17. Volpi, G.; Laurenti, E.; Rabezzana, R. Imidazopyridine Family: Versatile and Promising Heterocyclic Skeletons for Different Applications. *Molecules* **2024**, *29*, doi:10.3390/molecules29112668.

18. Karaaslan, C.; Doganc, F.; Alp, M.; Koc, A.; Karabay, A.Z.; Göker, H. Regioselective N-Alkylation of Some Imidazole-Containing Heterocycles and Their in Vitro Anticancer Evaluation. *J. Mol. Struct.* **2020**, *1205*, 1–13, doi:10.1016/j.molstruc.2019.127673.

19. Fascio, M.L.; Errea, M.I.; D'Accorso, N.B. Imidazothiazole and Related Heterocyclic Systems. Synthesis, Chemical and Biological Properties. *Eur. J. Med. Chem.* **2015**, *90*,

666–683, doi:10.1016/j.ejmech.2014.12.012.

20. Ma, C.H.; Chen, M.; Feng, Z.W.; Zhang, Y.; Wang, J.; Jiang, Y.Q.; Yu, B. Functionalization of Imidazo[1,2-a]Pyridinesviaradical Reactions. *New J. Chem.* **2021**, *45*, 9302–9314, doi:10.1039/d1nj00704a.

21. Mantipally, M.; Gangireddy, M.R.; Gundla, R.; Badavath, V.N.; Mandha, S.R.; Maddipati, V.C. Rational Design, Molecular Docking and Synthesis of Novel Homopiperazine Linked Imidazo[1,2-a]Pyrimidine Derivatives as Potent Cytotoxic and Antimicrobial Agents. *Bioorganic Med. Chem. Lett.* **2019**, *29*, 2248–2253, doi:10.1016/j.bmcl.2019.06.031.

22. Zhao, T.; Yang, Y.; Yang, J.; Cui, Y.; Cao, Z.; Zuo, D.; Zhai, X. Harmine-Inspired Design and Synthesis of Benzo[d]Imidazo[2,1-b]Thiazole Derivatives Bearing 1,3,4-Oxadiazole Moiety as Potential Tumor Suppressors. *Bioorganic Med. Chem.* **2021**, *46*, 116367, doi:10.1016/j.bmc.2021.116367.

23. An, W.; Wang, W.; Yu, T.; Zhang, Y.; Miao, Z.; Meng, T.; Shen, J. Discovery of Novel 2-Phenyl-Imidazo[1,2-a]Pyridine Analogues Targeting Tubulin Polymerization as Antiproliferative Agents. *Eur. J. Med. Chem.* **2016**, *112*, 367–372, doi:10.1016/j.ejmech.2016.02.004.

24. Rajitha, G.; Ravibabu, V.; Ramesh, G.; Rajitha, B. Synthesis and Antimicrobial Activity of Novel Imidazo[1,2-a]Pyridinopyrimidine-2,4,6(1H,3H,5H)-Triones and Thioxopyrimidine-4,6(1H,5H)Diones. *Res. Chem. Intermed.* **2016**, *42*, 1989–1998, doi:10.1007/s11164-015-2130-2.

25. Dahan-Farkas, N.; Langley, C.; Rousseau, A.L.; Yadav, D.B.; Davids, H.; De Koning, C.B. 6-Substituted Imidazo[1,2-a]Pyridines: Synthesis and Biological Activity against Colon Cancer Cell Lines HT-29 and Caco-2. *Eur. J. Med. Chem.* **2011**, *46*, 4573–4583, doi:10.1016/j.ejmech.2011.07.036.

26. Shaabani, A.; Nosrati, H.; Seyyedhamzeh, M. Cellulose@Fe2O3 Nanoparticle Composites: Magnetically Recyclable Nanocatalyst for the Synthesis of 3-Aminoimidazo[1,2-a]Pyridines. *Res. Chem. Intermed.* **2015**, *41*, 3719–3727, doi:10.1007/s11164-013-1484-6.

27. Sigalapalli, D.K.; Kiranmai, G.; Parimala Devi, G.; Tokala, R.; Sana, S.; Tripura, C.; Jadhav, G.S.; Kadagathur, M.; Shankaraiah, N.; Nagesh, N.; et al. Synthesis and

Biological Evaluation of Novel Imidazo[1,2-a]Pyridine-Oxadiazole Hybrids as Anti-Proliferative Agents: Study of Microtubule Polymerization Inhibition and DNA Binding. *Bioorganic Med. Chem.* **2021**, *43*, 116277, doi:10.1016/j.bmc.2021.116277.

28. Etivand, N.; Khalafy, J.; Poursattar Marjani, A. Facile, One-Pot, Four-Component Synthesis of a New Series of Imidazo[1,2-a]Pyridines in Presence of TPAB in EtOH under Reflux Conditions. *Res. Chem. Intermed.* **2019**, *45*, 3379–3394, doi:10.1007/s11164-019-03797-1.

29. Swami, S.; Agarwala, A.; Shrivastava, R. Indium Triflate Promoted One-Pot Multicomponent Synthesis of Structurally Diverse 3-Amino-Imidazo[1,2-a]Pyridines. *Mol. Divers.* **2017**, *21*, 81–88, doi:10.1007/s11030-016-9699-2.

30. Bhavya, K.; Mantipally, M.; Roy, S.; Arora, L.; Badavath, V.N.; Gangireddy, M.; Dasgupta, S.; Gundla, R.; Pal, D. Novel Imidazo[1,2-a]Pyridine Derivatives Induce Apoptosis and Cell Cycle Arrest in Non-Small Cell Lung Cancer by Activating NADPH Oxidase Mediated Oxidative Stress. *Life Sci.* **2022**, *294*, 120334, doi:10.1016/j.lfs.2022.120334.

31. Chen, G.; Li, B.; Hu, B.; Zhang, X.; Fan, X. FeCl3-Catalyzed C-3 Functionalization of Imidazo[1,2-a]Pyridines with Diazoacetonitrile under Oxidant- and Ligand-Free Conditions. *Tetrahedron Lett.* **2020**, *61*, 151774, doi:10.1016/j.tetlet.2020.151774.

32. Bagdi, A.K.; Santra, S.; Monir, K.; Hajra, A. Synthesis of Imidazo[1,2-a]Pyridines: A Decade Update. *Chem. Commun.* **2015**, *51*, 1555–1575, doi:10.1039/c4cc08495k.

33. Salamatmanesh, A.; Heydari, A. Magnetic Nanostructure-Anchored Mixed-Donor Ligand System Based on Carboxamide and N-Heterocyclic Thiones: An Efficient Support of CuI Catalyst for Synthesis of Imidazo[1,2-a]Pyridines in Eutectic Medium. *Appl. Catal. A Gen.* **2021**, *624*, 118306, doi:10.1016/j.apcata.2021.118306.

34. Katrun, P.; Kuhakarn, C. K 2 S 2 O 8 -Mediated Halogenation of 2-Arylimidazo[1,2-a]Pyridines Using Sodium Halides as the Halogen Sources. *Tetrahedron Lett.* **2019**, *60*, 989–993, doi:10.1016/j.tetlet.2019.03.008.

35. Cao, H.; Liu, X.; Zhao, L.; Cen, J.; Lin, J.; Zhu, Q.; Fu, M. One-Pot Regiospecific Synthesis of Imidazo[1,2- a]Pyridines: A Novel, Metal-Free, Three-Component Reaction for the Formation of C–N, C–O, and C–S Bonds. *Org. Lett.* **2014**, *16*, 146–149, doi:10.1021/ol4031414.

36. Luan, N.; Liu, Z.; Han, S.; Shen, L.; Li, J.; Zou, D.; Wu, Y.; Wu, Y. PhI(OAc)2-Mediated Oxidative C[Sbnd]H Sulfoximination of Imidazopyridines under Mild Conditions. *Tetrahedron Lett.* **2020**, *61*, 151362, doi:10.1016/j.tetlet.2019.151362.

37. Huang, Q.; Dong, H.; Li, B.; Hu, W.; Wang, Y. Rhodium Catalyzed Direct C3-Ethoxycarbonylmethylation of Imidazo[1,2-a]Pyridines with Ethyl Diazoacetate. *Tetrahedron* **2020**, *76*, 130998, doi:10.1016/j.tet.2020.130998.

38. Cao, H.; Liu, X.; Liao, J.; Huang, J.; Qiu, H.; Chen, Q.; Chen, Y. Transition Metal-Mediated C=O and C=C Bond-Forming Reactions: A Regioselective Strategy for the Synthesis of Imidazo[1,2- A]Pyridines and Imidazo[1,2- A]Pyrazines. *J. Org. Chem.* **2014**, *79*, 11209–11214, doi:10.1021/jo501671x.

39. Azizi, S.; Shadjou, N.; Soleymani, J. CuI/Fe3O4 NPs@Biimidazole IL-KCC-1 as a Leach Proof Nanocatalyst for the Synthesis of Imidazo[1,2-a]Pyridines in Aqueous Medium. *Appl. Organomet. Chem.* **2021**, *35*, 1–13, doi:10.1002/aoc.6031.

40. Tashrifi, Z.; Mohammadi-Khanaposhtani, M.; Larijani, B.; Mahdavi, M. C3-Functionalization of Imidazo[1,2-a]Pyridines. *European J. Org. Chem.* **2020**, *2020*, 269–284, doi:10.1002/ejoc.201901491.

41. Tran, R.Q.; Jacoby, S.A.; Roberts, K.E.; Swann, W.A.; Harris, N.W.; Dinh, L.P.; Denison, E.L.; Yet, L. Synthesis of 3-Aryl-2-Phosphinoimidazo[1,2-: A] Pyridine Ligands for Use in Palladium-Catalyzed Cross-Coupling Reactions. *RSC Adv.* **2019**, *9*, 17778–17782, doi:10.1039/c9ra02200g.

42. Hussain, N.; Gogoi, P.; Das, M.R.; Sengupta, P.; Fedorov, V.E.; Asanov, I.P.; Kozlova, M.N.; Artemkina, S.B. Development of Novel Efficient 2D Nanocomposite Catalyst towards the Three-Component Coupling Reaction for the Synthesis of Imidazo[1,2-a]Pyridines. *Appl. Catal. A Gen.* **2017**, *542*, 368–379, doi:10.1016/j.apcata.2017.05.033.

43. Paengphua, P.; Chancharunee, S. Facile Synthesis of Imidazo[1,2-a]Pyridines Promoted by Room-Temperature Ionic Liquids under Ultrasound Irradiation. *Monatshefte fur Chemie* **2018**, *149*, 1835–1840, doi:10.1007/s00706-018-2238-3.

44. Li, L.; Wang, A.; Wang, B.; Liu, M.; Lv, K.; Tao, Z.; Ma, C.; Ma, X.; Han, B.; Wang, A.; et al. N-(2-Phenoxy)Ethyl Imidazo[1,2-a]Pyridine-3-Carboxamides Containing Various Amine Moieties: Design, Synthesis and Antitubercular Activity. *Chinese Chem. Lett.* **2020**, *31*, 409–412, doi:10.1016/j.cclet.2019.07.038.

45. Butera, R.; Ważyńska, M.; Magiera-Mularz, K.; Plewka, J.; Musielak, B.; Surmiak, E.; Sala, D.; Kitel, R.; De Bruyn, M.; Nijman, H.W.; et al. Design, Synthesis, and Biological Evaluation of Imidazopyridines as PD-1/PD-L1 Antagonists. *ACS Med. Chem. Lett.* **2021**, *12*, 768–773, doi:10.1021/acsmedchemlett.1c00033.

46. Stahlberger, M.; Schwarz, N.; Zippel, C.; Hohmann, J.; Nieger, M.; Hassan, Z.; Bräse, S. Diversity-Oriented Synthesis of [2.2]Paracyclophane-Derived Fused Imidazo[1,2-a]Heterocycles by Groebke-Blackburn-Bienaymé Reaction: Accessing Cyclophanyl Imidazole Ligands Library. *Chem. - A Eur. J.* **2022**, *28*, 1–7, doi:10.1002/chem.202103511.

47. Jiang, S. Copper (II) Complex Supported on Magnetic Nanoparticles as a Novel Nanocatalyst for the Synthesis of Imidazo[1,2-a]Pyridines. *Mol. Divers.* **2024**, *28*, 3859–3877, doi:10.1007/s11030-023-10781-w.

48. Armendariz-Barrientos, K.; Pérez, L.A.; Lagunas-Rivera, S.; Alcaraz-Contreras, Y.; García-Revilla, M.A.; Prado-Garcia, H.; García-Becerra, R.; Vazquez, M.A. Novel N-Quaternary Coumarin-3-Yl-Imidazo[1,2-a]Pyridines as Fluorescent Hybrids: Their Synthesis and Biological Evaluation in Cancer Cells. *Results Chem.* **2025**, *13*, doi:10.1016/j.rechem.2024.101959.

49. Vekariya, R.; Panchal, S.; Patel, K.; Patel, H. Solvent and Catalyst Free, Regioselective .α-Bromination of Aralkyl Ketones Using N-Bromosuccinimide (NBS) Under Microwave Irradiation: An Efficient Protocol. *Curr. Microw. Chem.* **2015**, *2*, 61–68, doi:10.2174/2213335602011502121115O6.

50. Adhikari, M. V.; Samant, S.D. Sonochemical Bromination of Acetophenones Using P-Toluenesulfonic Acid-N-Bromosuccinimide. *Ultrason. Sonochem.* **2002**, *9*, 107–111, doi:10.1016/S1350-4177(01)00108-0.

51. Pravst, I.; Zupan, M.; Stavber, S. Halogenation of Ketones with N-Halosuccinimides under Solvent-Free Reaction Conditions. *Tetrahedron* **2008**, *64*, 5191–5199, doi:10.1016/j.tet.2008.03.048.

52. Grjol, B.; Jereb, M. Reactivity of Substrates with Multiple Competitive Reactive Sites toward NBS under Neat Reaction Conditions Promoted by Visible Light. *Chem. Pap.* **2021**, *75*, 5235–5248, doi:10.1007/s11696-021-01711-x.

53. Berrichi, A.; Bachir, R.; Bedrane, S.; Choukchou-Braham, N.; Belkacemi, K.

Heterogeneous Bimetallic Au–Co Nanoparticles as New Efficient Catalysts for the Three-Component Coupling Reactions of Amines, Alkynes and CH2Cl2. *Res. Chem. Intermed.* **2019**, *45*, 3481–3495, doi:10.1007/s11164-019-03803-6.

54. Rawat, M.; Rawat, D.S. Copper Oxide Nanoparticle Catalysed Synthesis of Imidazo[1,2-a]Pyrimidine Derivatives, Their Optical Properties and Selective Fluorescent Sensor towards Zinc Ion. *Tetrahedron Lett.* **2018**, *59*, 2341–2346, doi:10.1016/j.tetlet.2018.05.005.

55. Rehan, T.A.; Al-Lami, N.; Alanee, R.S. Anti-Cancer and Antioxidant Activities of Some New Synthesized 3-Secondary Amine Derivatives Bearing Imidazo [1,2-A] Pyrimidine. *Eurasian Chem. Commun.* **2021**, *3*, 339–351, doi:10.22034/ecc.2021.277531.1151.

56. Shang, L. Le; Feng, Y.; Gao, X.L.; Chen, Z.R.; Xia, Y.; Jin, W.W.; Liu, C.J. DMAP-Catalyzed C—N Bond Formation for Diverse Synthesis of Imidazo[1,2-a]Pyrimidine and Pyrimido[1,2-a]Benzimidazole Derivatives. *Chinese J. Chem.* **2020**, *38*, 1595–1599, doi:10.1002/cjoc.202000214.

57. Güngör, T. Microwave Assisted, Sequential Two-Step, One-Pot Synthesis of Novel Imidazo[1,2-a] Pyrimidine Containing Tri/Tetrasubstituted Imidazole Derivatives. *Turkish J. Chem.* **2021**, *45*, 219–230, doi:10.3906/KIM-2009-40.

58. Goel, R.; Luxami, V.; Paul, K. Synthetic Approaches and Functionalizations of Imidazo[1,2-a]Pyrimidines: An Overview of the Decade. *RSC Adv.* **2015**, *5*, 81608–81637, doi:10.1039/c5ra14795f.

59. Kobak, R.Z.U.; Akkurt, B. Formation and Uses of Imidazo[1,2-a]Pyrimidines and Related Compounds: A Review Comprising Years 2000-2021. *J. Turkish Chem. Soc. Sect. A Chem.* **2022**, *9*, 1335–1386, doi:10.18596/jotcsa.1110922.

60. Atif, H.Y.S.; Wagare, D.S.; Ahmed, A.Z.; Durrani, A.N. Ultrasound Promoted One-Pot Synthesis of 2-Arylimidazo[1,2-a]Pyrimidines in Glycerol. *Rasayan J. Chem.* **2021**, *14*, 2645–2651, doi:10.31788/RJC.2021.1446502.

61. Aeluri, R.; Alla, M.; Polepalli, S.; Jain, N. *Synthesis and Antiproliferative Activity of Imidazo[1,2-a]Pyrimidine Mannich Bases*; Elsevier Ltd, 2015; Vol. 100; ISBN 2014151784.

62. Annareddygari, S.; Kasireddy, V.; Reddy, J. Synthesis of Novel Amide-Functionalized

Imidazo[1,2-a]Pyrimidin-5(1H)-Ones and Their Biological Evaluation as Anticancer Agents. *Russ. J. Org. Chem.* **2022**, *58*, 412–418, doi:10.1134/S1070428022030216.

63. Ravindar, L.; Hasbullah, S.A.; Rakesh, K.P.; Hassan, N.I. Pyrazole and Pyrazoline Derivatives as Antimalarial Agents: A Key Review. *Eur. J. Pharm. Sci.* **2023**, *183*, 106365, doi:10.1016/j.ejps.2022.106365.

64. Azzouzi, M.; Ouafi, Z. El; Azougagh, O.; Daoudi, W.; Ghazal, H.; Barkany, S. El; Abderrazak, R.; Mazières, S.; Aatiaoui, A. El; Oussaid, A. Design, Synthesis, and Computational Studies of Novel Imidazo[1,2-a]Pyrimidine Derivatives as Potential Dual Inhibitors of HACE2 and Spike Protein for Blocking SARS-CoV-2 Cell Entry. *J. Mol. Struct.* **2023**, *1285*, 135525, doi:10.1016/j.molstruc.2023.135525.

65. Ramírez-Trinidad, Á.; Carrillo-Jaimes, K.; Rivera-Chávez, J.A.; Hernández-Vázquez, E. Synthesis and Cytotoxic/Antimicrobial Screening of 2-Alkenylimidazo[1,2-a]Pyrimidines. *Med. Chem. Res.* **2023**, *32*, 144–157, doi:10.1007/s00044-022-02997-6.

66. Güngör, T. One Pot, Multicomponent Protocol for the Synthesis of Novel Imidazo[1,2-a]Pyrimidine-Based Pyran Analogs: A Potential Biological Scaffold. *Monatshefte fur Chemie* **2020**, *151*, 781–789, doi:10.1007/s00706-020-02601-w.

67. Gómez-García, O.; Andrade-Pavón, D.; Campos-Aldrete, E.; Ballinas-Indilí, R.; Méndez-Tenorio, A.; Villa-Tanaca, L.; Álvarez-Toledano, C. Synthesis, Molecular Docking, and Antimycotic Evaluation of Some 3-Acyl Imidazo[1,2-a]Pyrimidines. *Molecules* **2018**, *23*, 1–17, doi:10.3390/molecules23030599.

68. GÜNGÖR, T. Preparation of Novel Imidazo[1,2-a]Pyrimidine Derived Schiff Bases at Conventional and Microwave Heating Conditions. *Balıkesir Üniversitesi Fen Bilim. Enstitüsü Derg.* **2020**, *22*, 428–438, doi:10.25092/baunfbed.707673.

69. Aggarwal, R.; Sharma, M.; Sumran, G.; Kumar, P. Multicomponent Catalyst-Free Regioselective Synthesis and Binding Studies of 3-Aroyl-2-Methylimidazo[1,2- a]Pyrimidines with BSA Using Biophysical and Computational Techniques. *RSC Adv.* **2025**, *15*, 15999–16014, doi:10.1039/D5RA01795E.

70. Solomon, N.; Hayes, J. Levamisole: A High Performance Cutting Agent. *Acad. Forensic Pathol.* **2017**, *7*, 469–476, doi:10.23907/2017.039.

71. Abdel-Maksoud, M.S.; Ammar, U.M.; Oh, C.H. Anticancer Profile of Newly Synthesized BRAF Inhibitors Possess 5-(Pyrimidin-4-Yl)Imidazo[2,1-b]Thiazole Scaffold. *Bioorganic Med. Chem.* **2019**, *27*, 2041–2051, doi:10.1016/j.bmc.2019.03.062.

72. Consty, Z.A.; Zhang, Y.; Xu, Y. A Simple Sensor Based on Imidazo[2,1-b]Thiazole for Recognition and Differentiation of Al3+, F− and PPi. *J. Photochem. Photobiol. A Chem.* **2020**, *397*, 112578, doi:10.1016/j.jphotochem.2020.112578.

73. Gadekar, P.K.; Urunkar, G.; Roychowdhury, A.; Sharma, R.; Bose, J.; Khanna, S.; Damre, A.; Sarveswari, S. Design, Synthesis and Biological Evaluation of 2,3-Dihydroimidazo[2,1-b]Thiazoles as Dual EGFR and IGF1R Inhibitors. *Bioorg. Chem.* **2021**, *115*, 105151, doi:10.1016/j.bioorg.2021.105151.

74. Chitti, S.; Van Calster, K.; Cappoen, D.; Nandikolla, A.; Khetmalis, Y.M.; Cos, P.; Kumar, B.K.; Murugesan, S.; Gowri Chandra Sekhar, K.V. Design, Synthesis and Biological Evaluation of Benzo-[d]-Imidazo-[2,1-b]-Thiazole and Imidazo-[2,1-b]-Thiazole Carboxamide Triazole Derivatives as Antimycobacterial Agents. *RSC Adv.* **2022**, *12*, 22385–22401, doi:10.1039/d2ra03318f.

75. Calderón-Rangel, D.; Pérez, K.A.G.; Díaz, A.C.; Gámez-Montaño, R. One-Pot Synthesis of Imidazo[2,1-b]Thiazole via Groebke–Blackburn–Bienaymé Reaction under Free Catalyts. In Proceedings of the ECSOC 2023; MDPI: Basel Switzerland, November 15 2023; p. 103.

CHAPTER 2: SYNTHESIS OF 2-PYRIDONES

1. Introduction

Heterocycles, which account for more than 50% of all known organic molecules, are among the most crucial compounds for humans and biological systems. They form a significant class of natural products and are highly relevant due to their biological importance [1]. Therefore, the synthesis of heterocyclic compounds containing therapeutic molecules for humans is a primary objective in organic synthesis and medicinal chemistry [2]. Among them, 2-pyridones (**2-PyO),** also known as 2-Hydroxypyridines [3], are widespread nitrogen-based heterocycles found in both natural and synthetic compounds [4]**.** They have garnered the attention of many researchers in the past few years because of their prevalence in various natural products [5].

2. Biological properties of 2-pyridones

2-Pyridones are essential in the pharmaceutical fields and also serve as fundamental building blocks for bioactive substances and natural products [6]. They have shown numerous biological and pharmacological activities [7], including antioxidant [8], neuroprotective [9], antifungal [10], cardiotonic [11], anti-inflammatory [12], antipyretic[13], and anticancer [14] properties. Figure 1 illustrates four examples of natural products based on 2-pyridone, namely: recinin with antibacterial and insecticidal properties, fischerine with neuroprotective effects, pyridomacrolidine and sambutoxin, both of which demonstrate anticancer activities. These bioactivities have been recognized over the past two decades [15].

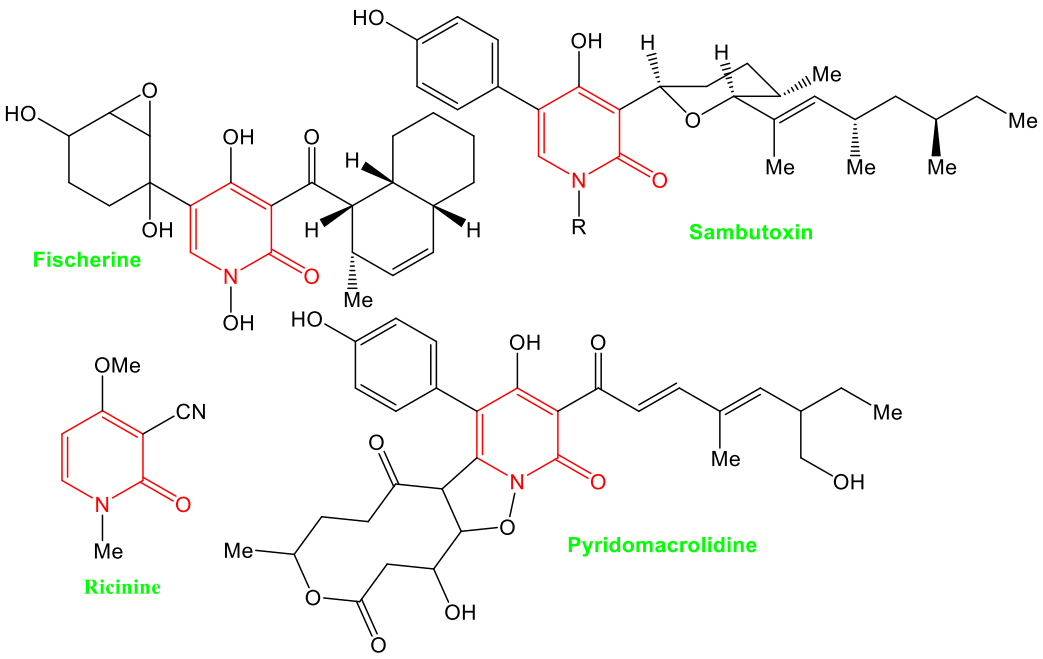

Figure 1: Bioactivities of some 2-pyridones.

Examples of marketed 2-pyridone drugs are shown in Figure 2. Ciclopirox [16] is used as an antifungal agent, whereas milrinone [17] and amrinone [18] are employed in the treatment of heart failure.

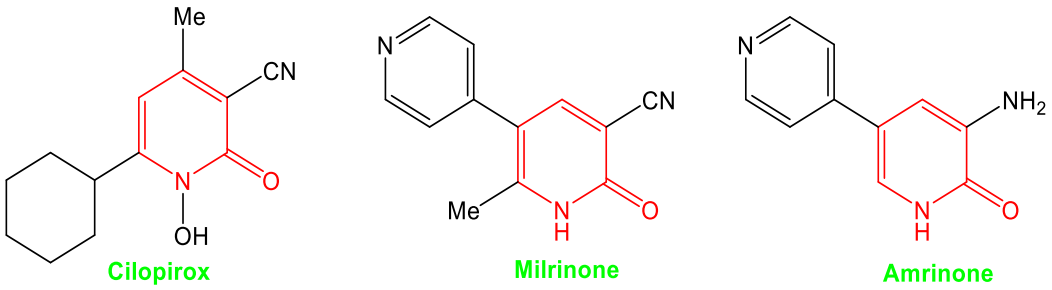

Figure 2: Example of some 2-pyridone drugs

3. Described syntheses of 2-pyridones

In 2011, Kibou et al. accomplished a practical and simple preparation of 2-pyridones via the three-component one-pot reaction catalyzed by Al_2O_3 (Scheme 1). The reaction was carried out under solvent-free conditions, affording the expected compounds in excellent yields. With a reduced reaction time, the method provided the 2-pyridones from enaminones with easy procedure and simple purification [19].

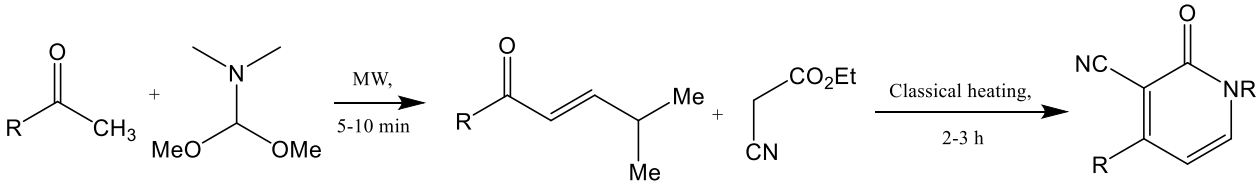

Scheme 1: Synthesis of Kibou

In 2022, Ibrahim et al. prepared a series of chalcones by the condensation of benzyloxy acetophenone with varied aldehydes in 10% aqueous NaOH and ethanol (Scheme 2). The resulting chalcones were reacted with cyanoacetamide using piperidine as a catalyst for 6 h under reflux in ethanol, affording the corresponding 2-pyridone-3-carbonitrile compounds in high yields [20].

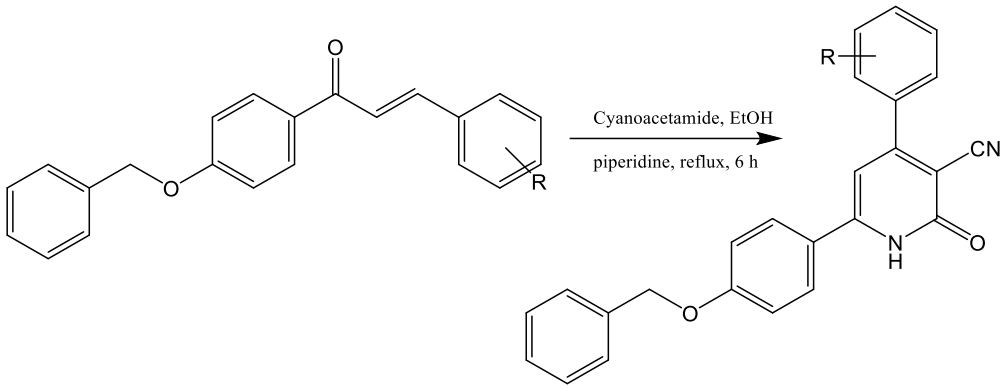

Scheme 2: Synthesis of Ibrahim

Over the same year, Anizadeh et al. reported the synthesis of novel 2-pyridone derivatives fused with 1,2,3-triazole moiety, catalyzed by [Fe_3O_4@SiO_2@$(CH_2)_3$-urea-dithiocarbamic acid] under solvent-free conditions (Scheme 3). The heterocycles were synthesized by reacting aromatic aldehydes, a triazole derivative, ethyl cyanoacetate, ammonium acetate and prepared catalyst at 110 °C for 15-40 minutes as monitored by TLC. Mild reaction conditions, high yields, low catalyst loading, and short reaction times are the main advantages of the described method [21].

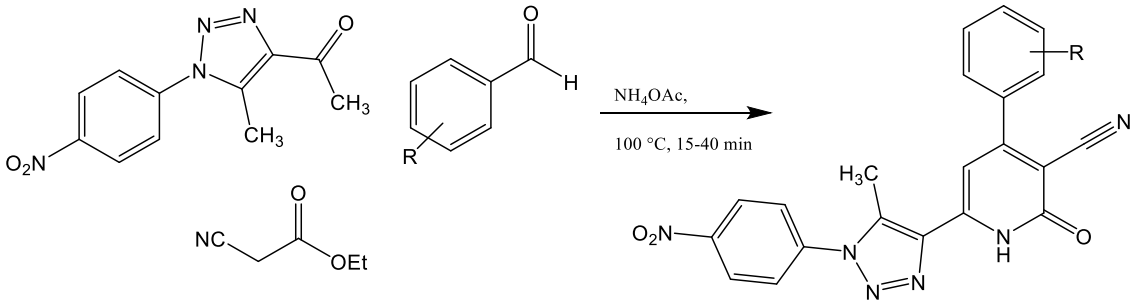

Scheme 3: Synthesis of Anizadeh

In 2023, Chen et al. successfully developed a synthesis of new class of 2-pyridones via an acid-catalyzed reaction involving 5-aryl-1,3-dioxan-5-ol, (S)-2,4-dioxo-4-(2-(1-oxo-3-propan-2-yl)hydrazineyl)butan-1-ylium derivatives and *N*-bromosuccinimide **(**Scheme 4). The reaction mixture was heated at 80 °C for 4 hours in 1,4-dioxane to afford the target 2-pyridones in moderate to excellent yields. Simple operation, broad functional groups tolerance, and a wide substrate scope are the main advantages for the described method [22].

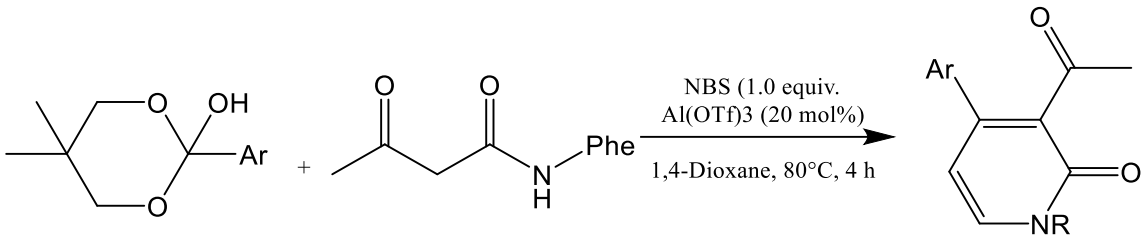

Scheme 4: Synthesis of Chen

In same year (2023), Das et al. [11] reported the synthesis of two series of functionalized *N*-amino-3-cyano-2-pyridone derivatives. They combined cyanoacetohydrazide, aldehydes and malononitrile (for the first series of compounds), or ethyl cyanoacetate (for the second series) in PEG-200 as a green solvent. The reaction mixture was heated at 100 °C for 6 hours with malononitrile or 8 hours with ethyl cyanoacetate (Scheme 5). Mild reaction conditions, short time reaction, high yields, the use of an eco-friendly biodegradable solvent in the absence of additional catalysts, simple starting materials and facile work up are the main advantages of this strategy [11].

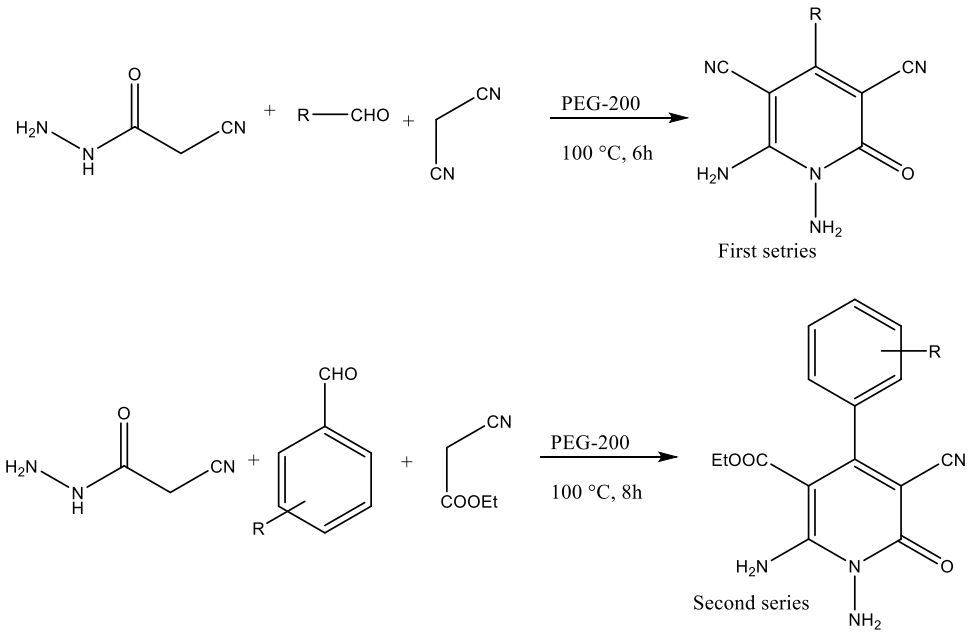

Scheme 5: Synthesis of Das

In 2024, Tang et al. [23] reported an efficient and straightforward method for the preparation of a series of 51 different 3-cyano-2-pyridone derivatives (Scheme 6). Various prop-2-yn-1-ones were reacted with 2-cyano-N-alkylatedacetamide and K_2CO_3 in 1,4-dioxane for 8 hours at 100 ◦C affording the desired 2-pyridone in high yields. The advantagesof this method include its wide functional group tolerance, metal-free process, mild conditions, and simple operation.

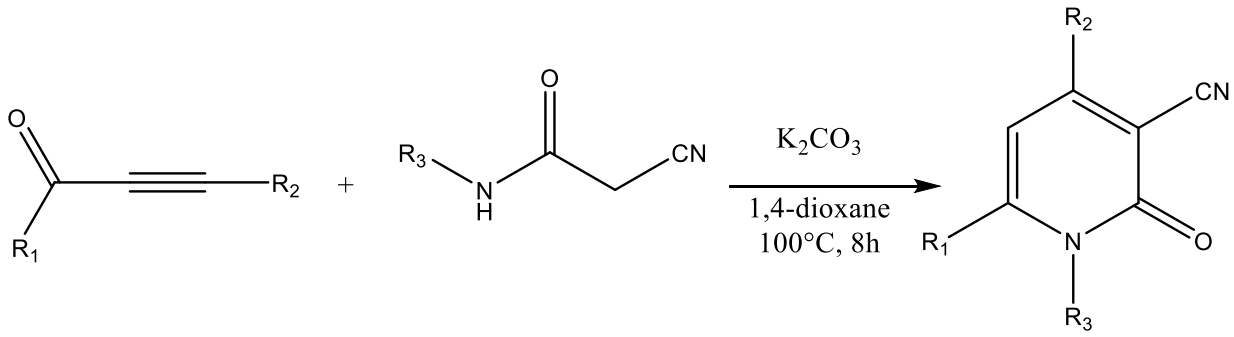

Scheme 6: Synthesis Tang

4. Synthesis of 2-pyridones

Due to the importance of 2-pyridone derivatives, numerous methods for their synthesis have been developed and reported in the literature [24]. Among these, multicomponent reactions (MCRs) have gained significant attention in organic synthesis owing to their advantages, such as short reaction times, high yields, and easy product isolation [25].

Motivated by these advantages, we sought to develop a greener synthetic route. Herein, we report a novel one-pot synthesis of 4,6-diaryl-3-cyano-2-pyridone derivatives using two approaches: the first involves conventional heating, and the second employs ultrasound-assisted synthesis, both carried out under identical conditions. This efficient procedure is based on a three-component reaction involving alkenes, ketones, and ammonium acetate (Scheme 7).

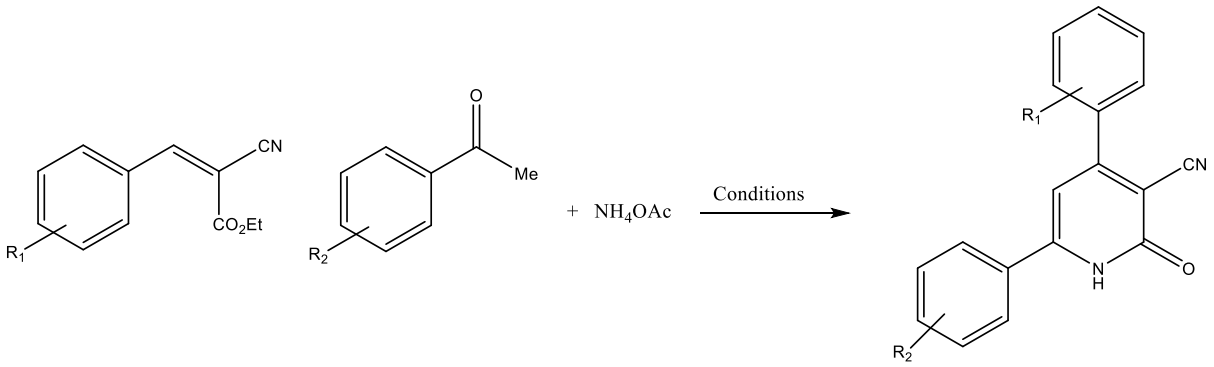

Scheme 7: Multicomponent synthesis of 2-pyridone derivatives

4. a. Synthesis of Alkenes (Alks)

Alkenes are well-known key intermediates in the synthesis of heterocycles [26–30]. In our study, they were used as precursors for the preparation of 2-pyridone derivatives. The alkenes (Alks) were prepared via the condensation of aromatic aldehydes with ethyl 2-

cyanoacetate in the presence of ammonium acetate (NH_4OAc), using distilled water (DW) as the solvent at room temperature (RT) and stirred overnight (Scheme 8).

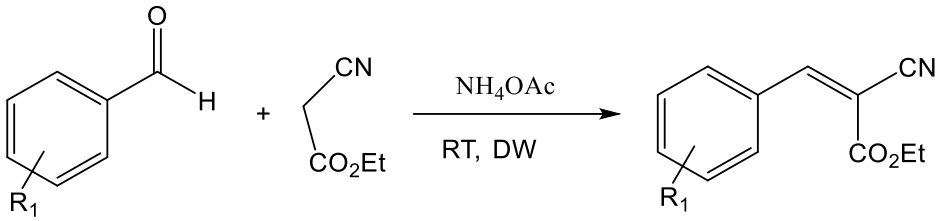

Scheme 8: Synthesis of alkenes

The obtained results for the preparation of alkenes are grouped in Table 1.

Table 1: Various synthesized alkenes

Entry	R_1	Abbreviation	Structure	Yield (%)
1	H	Alk-H	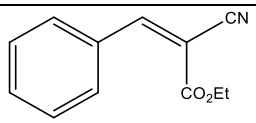	82
2	2-Cl	Alk-2Cl	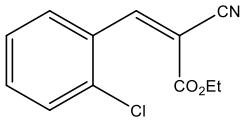	90
3	3-Cl	Alk-3Cl	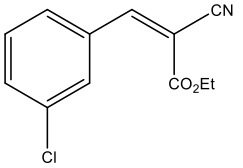	81
4	2,4-diCl	Alk-2,4diCl	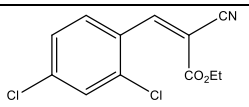	80
5	4-Cl	Alk-4Cl	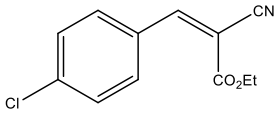	86
6	4-F	Alk-4F	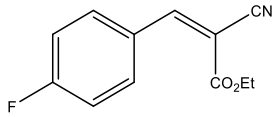	92

The resulting alkenes were obtained in high yields, which were influenced by the varying reactivity of malononitrile with different benzaldehyde derivatives.

4.b. Our syntheses of 2-pyridones

The target products were synthesized by reacting the previously prepared alkenes with aryl-ketone derivatives and ammonium acetate in ethanol. The reactions were performed either under conventional reflux conditions (method a) or using ultrasonic irradiation (method b), as illustrated in Scheme 9.

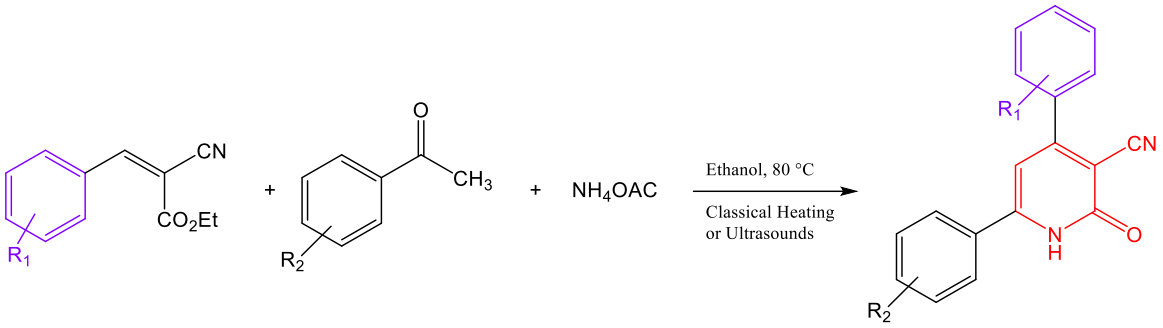

Scheme 9: Synthesis of 2-pyridone derivatives under classical heating or ultrasonic conditions

Figures 3, 4, and 5 show the different 2-pyridones prepared from Alk-2Cl, Alk-4F, and Alk-H respectively.

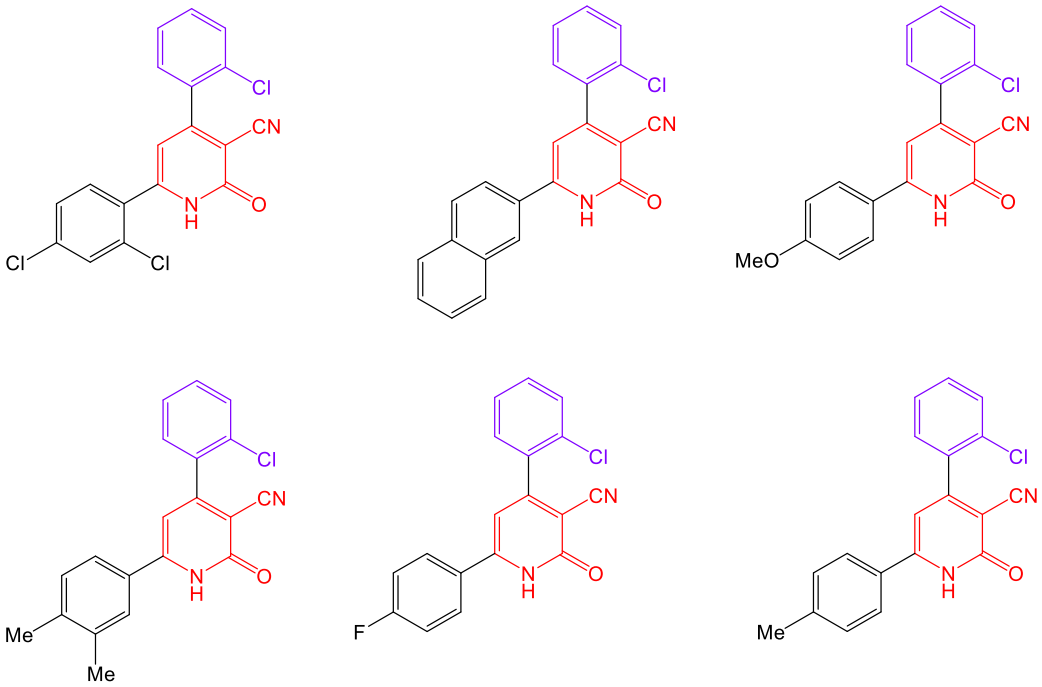

Figure 3: 2-pyridones synthesized from the alkene Alk-2Cl.

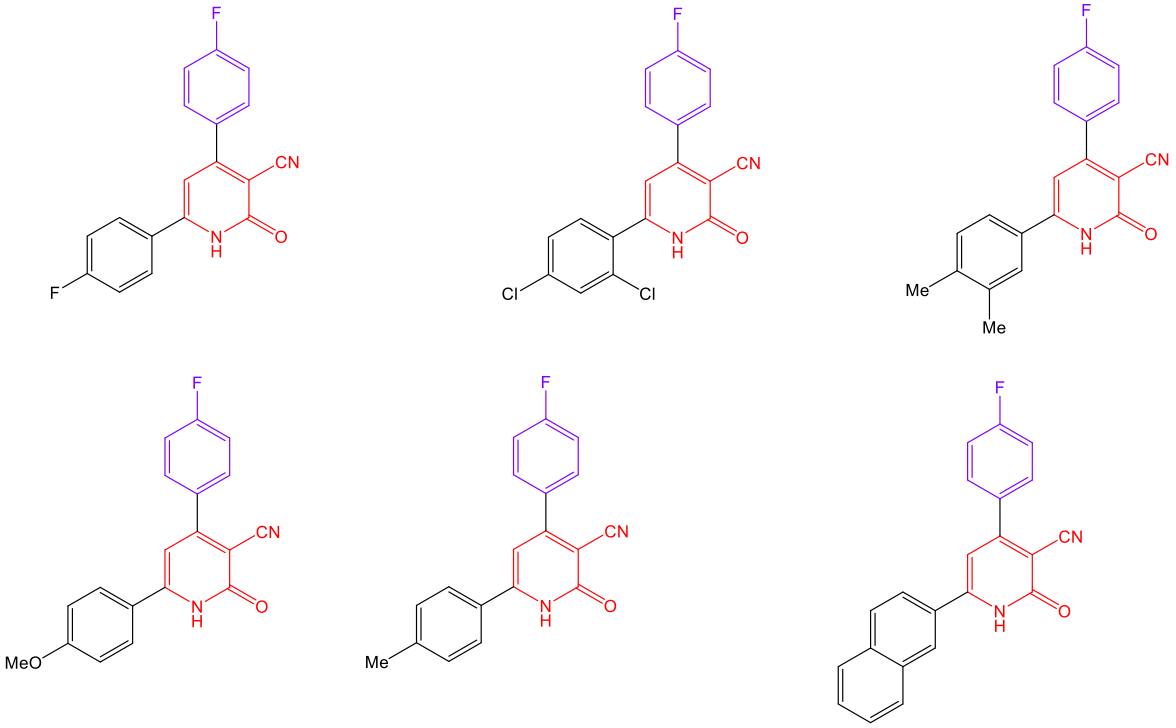

Figure 4: 2-pyridones synthesized from the alkene Alk-4F.

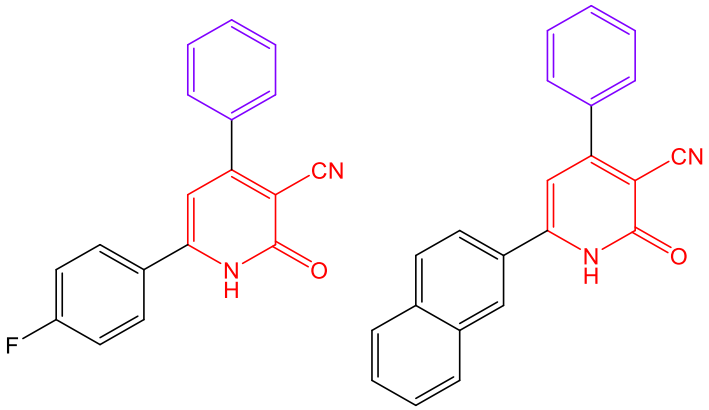

Figure 5: 2-pyridones synthesized from the alkene Alk-H.

Table 2 summarizes all the prepared 2-pyridones under classical and ultrasound conditions.

Table 2: Synthesized 4,6-diaryl-3-cyano-2-pyridone derivatives obtained via classical and ultrasound-assisted methods.

Entry	Abbreviation	R_1	R_2	Structure	Yield (%)
1	**2-PyO-(2-Cl, 4F)**	2-Cl	4F	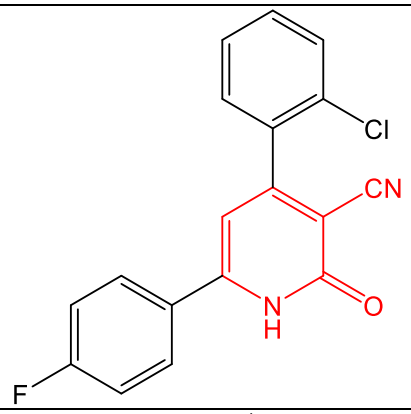	30 [a]; 90 [b]
2	**2-PyO-(2Cl, 2.4-diCl)**	2-Cl	2,4-Cl_2	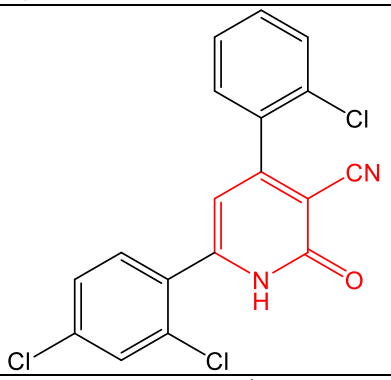	38 [a];85 [b]
3	**2-PyO-(2Cl, 2Naph)**	2-Cl	2-naphtyl	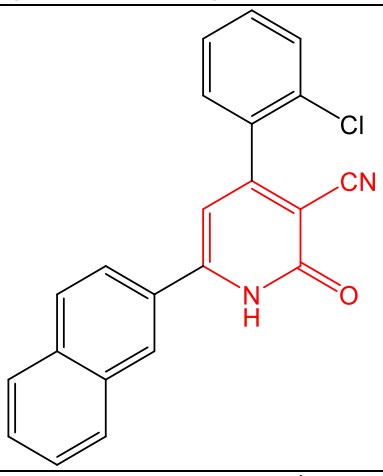	20 [a]; 36 [b]
4	**2-PyO-(2Cl, 4OMe)**	2-Cl	4-OMe	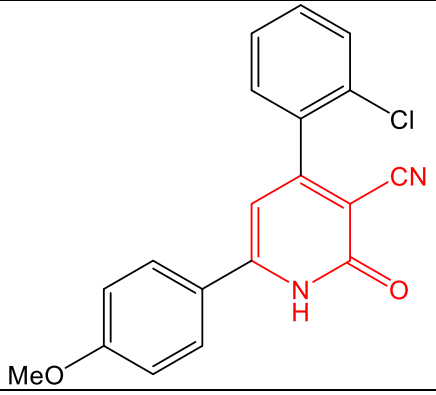	12 [a]; 46 [b]

5	**2-PyO-(2Cl, 4Me)**	2-Cl	4-Me	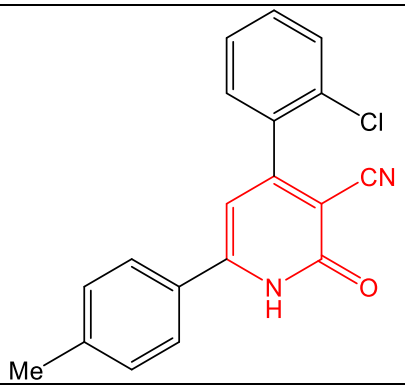	17 [a]; 41 [b]
6	**2-PyO-(2Cl, 3.4diMe)**	2-Cl	3,4-Me_2	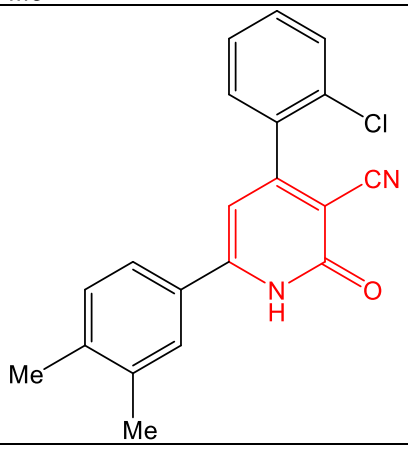	91 [b]
7	**PyO-(4F, 4F)**	4F	4F	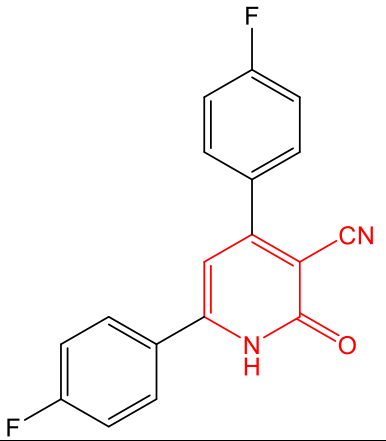	70 [a]; 83 [b]
8	**2-PyO-(4F, 2.4-diCl)**	4F	2,4-Cl_2	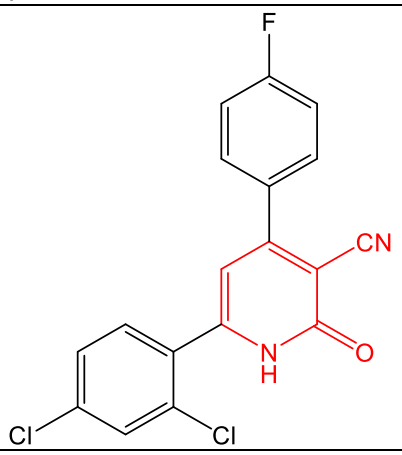	79 [a]; 90 [b]

9	**2-PyO-(4F, 2-Naph)**	4F	2-naphtyl	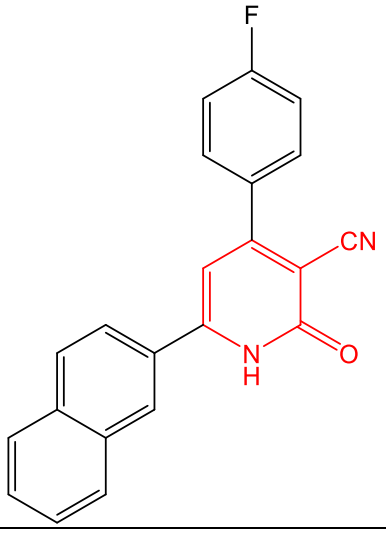	80 [a]; 81 [b]
10	**2-PyO-(4F, 4OMe)**	4F	4-OMe	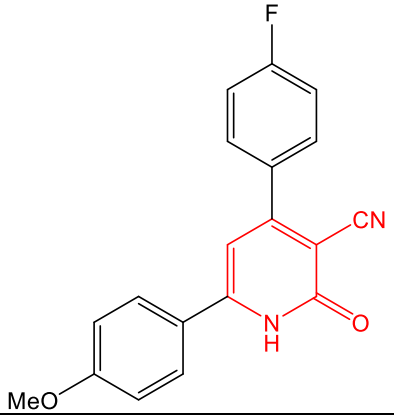	12 [a]; 35 [b]
11	**2-PyO-(4F, 4Me)**	4F	4-Me	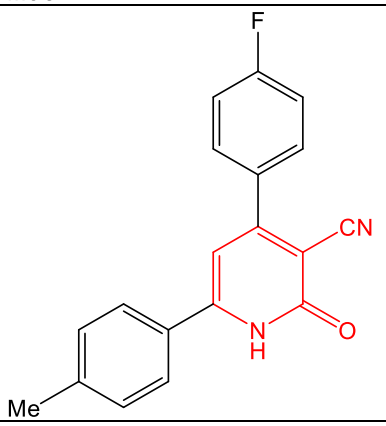	22 [a]; 62 [b]
12	**2-PyO-(4F, 3.4-diMe)**	4F	3,4-Me_2	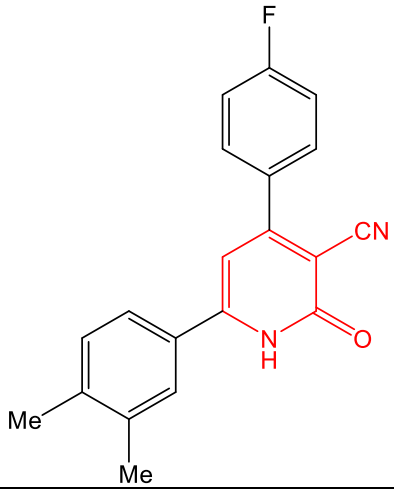	47 [a]; 60 [b]

13	**2-PyO-(H, 4F)**	H	4-F	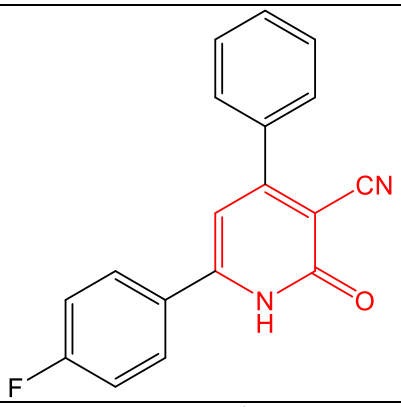	89 [b]
14	**2-PyO-(H, 2-Naph)**	H	2-naphtyl	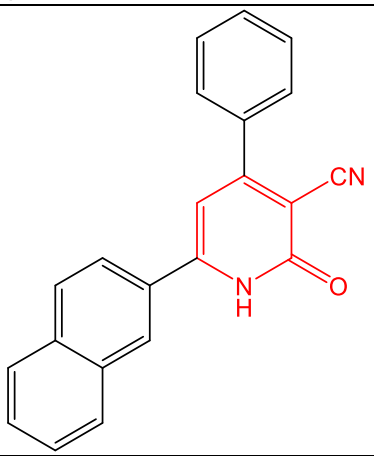	59 [b]

- a: classical heating, EtOH, 80°C, 10h.
- b: ultrasound-assisted synthesis, EtOH, 80°C, 3-6h.

The table above summarizes the synthesis of 2-pyridone derivatives using two different reaction methods. Both procedures are conducted in ethanol at 80 °C, but differed in reaction time. The results show that:

- yields obtained through ultrasonication method are consistently higher than those from the conventional one, with increases up to nearly fourfold (entry 4) and threefold (entries 1, 10, and 11).
- Reaction time is reduced by more than half (3–6 hours vs. 10 hours).
- Ultrasonication allows achieving high to excellent yields, even when the improvement is modest in some cases
- Overall, ultrasonication markedly enhances the reaction efficiency and yields for nearly all entries.

5. Conclusion

In this chapter, we have demonstrated that our multicomponent synthesis of 2-pyridone derivatives under ultrasound cavitation, a novel approach developed in our laboratory, proceeds

smoothly and efficiently, yielding new derivatives of diverse structures within a significantly shorter time and with higher yields compared to the classical method. With a limited set of starting materials, we were able to produce a substantial number of products in a relatively short period.

The application of ultrasound-assisted synthesis in preparing 2-pyridones offered remarkable advantages over standard technique. While the conventional approach is effective, ultrasonication emerged as a more robust alternative, providing higher yields and shorter times. It is particularly suitable for reactions that afford low yields under classical conditions. Moreover, this method aligns with the principles of green chemistry by minimizing the use of harsh solvents and reducing energy consumption, thus representing a more sustainable alternative to traditional methods.

The synthesis of such compounds opens promising prospects for the future production of various 2-pyridone derivatives with broad potential applications.

References

1. Buntrock, R.E. Review of Heterocyclic Chemistry , 5th Edition . *J. Chem. Educ.* **2012**, *89*, 1349–1350, doi:10.1021/ed300616t.

2. Pawełczyk, A.; Sowa-Kasprzak, K.; Olender, D.; Zaprutko, L. Molecular Consortia-Various Structural and Synthetic Concepts for More Effective Therapeutics Synthesis. *Int. J. Mol. Sci.* **2018**, *19*, 1–19, doi:10.3390/ijms19041104.

3. Hejazi, S.A.; Osman, O.I.; Alyoubi, A.O.; Aziz, S.G.; Hilal, R.H. The Thermodynamic and Kinetic Properties of 2-Hydroxypyridine/2-Pyridone Tautomerization: A Theoretical and Computational Revisit. *Int. J. Mol. Sci.* **2016**, *17*, doi:10.3390/ijms17111893.

4. Jessen, H.J.; Gademann, K. 4-Hydroxy-2-Pyridone Alkaloids: Structures and Synthetic Approaches. *Nat. Prod. Rep.* **2010**, *27*, 1168–1185, doi:10.1039/b911516c.

5. Biswas, A.; Maity, S.; Pan, S.; Samanta, R. Transition Metal-Catalysed Direct C−H Bond Functionalizations of 2-Pyridone Beyond C3-Selectivity. *Chem. - An Asian J.* **2020**, *15*, 2092–2109, doi:10.1002/asia.202000506.

6. Amer, M.M.K.; Aziz, M.A.; Shehab, W.S.; Abdellattif, M.H.; Mouneir, S.M. Recent

Advances in Chemistry and Pharmacological Aspects of 2-Pyridone Scaffolds. *J. Saudi Chem. Soc.* **2021**, *25*, 101259, doi:10.1016/j.jscs.2021.101259.

7. Dowarah, J.; Hazarika, B.; Sran, B.S.; Khiangte, D.; Singh, V.P. Design, Synthesis, Structural Investigation and Binding Study of 2-Pyridone-Based Pharmaceutical Precursor with DNA. *J. Mol. Struct.* **2023**, *1282*, doi:10.1016/j.molstruc.2023.135182.

8. Saleem, F.; Khan, K.M.; Ullah, N.; Özil, M.; Baltaş, N.; Hameed, S.; Salar, U.; Wadood, A.; Rehman, A.U.; Kumar, M.; et al. Bioevaluation of Synthetic Pyridones as Dual Inhibitors of α-Amylase and α-Glucosidase Enzymes and Potential Antioxidants. *Arch. Pharm. (Weinheim).* **2023**, *356*, doi:10.1002/ardp.202200400.

9. Lunić, T.; Lađarević, J.; Mandić, M.; Veruševski, V.; Nedeljković, B.B.; Mijin, D.; Božić, B. Antioxidant and Neuroprotective Activities of Selected 2-Pyridones: In Vitro and in Silico Study. *J. Mol. Struct.* **2022**, *1256*, doi:10.1016/j.molstruc.2022.132546.

10. Cruz, R.; Wuest, W.M. Beyond Ergosterol: Strategies for Combatting Antifungal Resistance in Aspergillus Fumigatus and Candida Auris. *Tetrahedron* **2023**, *133*, 133268, doi:10.1016/j.tet.2023.133268.

11. Das, S.; Paul, S.; Mitra, B.; Pariyar, G.C.; Ghosh, P. PEG-200: A Versatile Green Solvent Assisted Catalyst-Free One-Pot Three-Component Synthesis of Functionalised N-Amino-3-Cyano-2-Pyridone. *Results Chem.* **2023**, *5*, 100871, doi:10.1016/j.rechem.2023.100871.

12. Hurtado-Rodríguez, D.; Salinas-Torres, A.; Rojas, H.; Becerra, D.; Castillo, J.C. Bioactive 2-Pyridone-Containing Heterocycle Syntheses Using Multicomponent Reactions. *RSC Adv.* **2022**, *12*, 34965–34983, doi:10.1039/d2ra07056a.

13. Lalhruaizela; Patel, D.; Marak, B.N.; Dowarah, J.; Sran, B.S.; Yadav, U.C.S.; Singh, V.P. Supramolecular Architectures in Dihydropyridones: Synthesis, Crystal Structure, Hirshfeld Analysis, Cytotoxicity and in Silico Studies. *J. Mol. Struct.* **2022**, *1250*, 131671, doi:10.1016/j.molstruc.2021.131671.

14. Jiang, W.; Wang, X.; Shu, C.; Hou, Q.; Yang, K.; Wu, X. Design, Synthesis, and Evaluation of Novel Pyridone Derivatives as Potent BRD4 Inhibitors for the Potential Treatment of Prostate Cancer. *Bioorg. Chem.* **2022**, *119*, 105575, doi:10.1016/j.bioorg.2021.105575.

15. Sangwan, S.; Yadav, N.; Kumar, R.; Chauhan, S.; Dhanda, V.; Walia, P.; Duhan, A. A Score Years' Update in the Synthesis and Biological Evaluation of Medicinally Important 2-Pyridones. *Eur. J. Med. Chem.* **2022**, *232*, 114199, doi:10.1016/j.ejmech.2022.114199.

16. Mucha, P.; Borkowski, B.; Erkiert-polguj, A. Ciclopirox and Ciclopirox Olamine : Antifungal Agents in Dermatology with Expanding Therapeutic Potential. **2024**, 1–13.

17. Ribka, A.; Tarigan, T.; Sianturi, T.G. Efficacy and Safety of Milrinone in Treating Heart Failure Induced by Severe Pneumonia in Children with Congenital Heart Disease : A Systematic Review. **2024**, *01*, 34–50.

18. Zemljic, G.; Poglajen, G.; Frljak, S.; Cerar, A.; Okrajsek, R.; Sebestjen, M.; Knezevic, I.; Vrtovec, B. Renal Response to Levosimendan in Advanced Chronic Heart Failure Patients Listed for Heart Transplantation Predicts Early Postoperative Renal Function Course. *J. Cardiovasc. Dev. Dis.* 2025, *12*.

19. Kibou, Z.; Cheikh, N.; Choukchou-Braham, N.; Mostefa-kara, B.; Benabdellah, M.; Villemin, D. New Methodology for the Synthesis of 2-Pyridones Using Basic Al2O3 as Catalyst. *J. Mater. Environ. Sci.* **2011**, *2*, 293–298.

20. Ibrahim, M.H.; Harras, M.F.; Mostafa, S.K.; Mohyeldin, S.M.; Al kamaly, O.; Altwaijry, N.; Sabour, R. Development of Novel Cyanopyridines as PIM-1 Kinase Inhibitors with Potent Anti-Prostate Cancer Activity: Synthesis, Biological Evaluation, Nanoparticles Formulation and Molecular Dynamics Simulation. *Bioorg. Chem.* **2022**, *129*, 106122, doi:10.1016/j.bioorg.2022.106122.

21. Anizadeh, M.R.; Zolfigol, M.A.; Torabi, M.; Yarie, M.; Notash, B. Urea-Dithiocarbamic Acid Functionalized Magnetic Nanoparticles Modified with Ch-Cl: Catalytic Application for the Synthesis of Novel Hybrid Pyridones via Cooperative Geminal-Vinylogous Anomeric-Based Oxidation. *J. Mol. Liq.* **2022**, *364*, 120016, doi:10.1016/j.molliq.2022.120016.

22. Chen, S.; Zhang, T.; Xu, Z.; You, B.; Li, M.; Gu, Y. A Lewis Acid-Catalyzed Tandem Reaction Enabling 2-Arylglycerol Derivative as Versatile 1,3-Biselectrophiles for the Synthesis of 4H-Chromenes and 2-Pyridinones. *Chinese Chem. Lett.* **2023**, 108130, doi:10.1016/j.cclet.2023.108130.

23. Tang, Y.; Wu, N.; Xu, J.; Zhang, X.; Li, Y.; Wang, X. Metal-Free Cascade Formation of

C–C and C–N Bond for the Construction of 3-Cyano-2-Pyridones with Insecticidal Properties. *Molecules* **2024**, *29*, doi:10.3390/molecules29122792.

24. Torres, M.; Gil, S.; Parra, M. New Synthetic Methods to 2-Pyridone Rings. *Curr. Org. Chem.* **2005**, *9*, 1757–1779, doi:10.2174/138527205774610886.

25. Hosseini, H.; Bayat, M. An Efficient and Ecofriendly Synthesis of Highly Functionalized Pyridones: Via a One-Pot Three-Component Reaction. *RSC Adv.* **2018**, *8*, 27131–27143, doi:10.1039/c8ra05690k.

26. Wei, L.; Shen, C.; Hu, Y.Z.; Tao, H.Y.; Wang, C.J. Enantioselective Synthesis of Multi-Nitrogen-Containing Heterocycles Using Azoalkenes as Key Intermediates. *Chem. Commun.* **2019**, *55*, 6672–6684, doi:10.1039/c9cc02371b.

27. Appaturi, J.N.; Ratti, R.; Phoon, B.L.; Batagarawa, S.M.; Din, I.U.; Selvaraj, M.; Ramalingam, R.J. A Review of the Recent Progress on Heterogeneous Catalysts for Knoevenagel Condensation. *Dalt. Trans.* **2021**, *50*, 4445–4469, doi:10.1039/d1dt00456e.

28. Gawande, M.B.; Jayaram, R. V. A Novel Catalyst for the Knoevenagel Condensation of Aldehydes with Malononitrile and Ethyl Cyanoacetate under Solvent Free Conditions. *Catal. Commun.* **2006**, *7*, 931–935, doi:10.1016/j.catcom.2006.03.008.

29. Zhao, S.; Fan, Y.; Wang, Z.; Qiao, Y.; Jia, X. Knoevenagel Reaction Promoted by Functional Ionic Liquids with Primary and Tertiary Amines. *Green Chem. Lett. Rev.* **2024**, *17*, 1–14, doi:10.1080/17518253.2024.2337743.

30. Merugu, S.K.; Bollikolla, H.B. Improved Knoevenagel Condensation Protocol for the Synthesis of Cyanoacrylates and Their Anticancer Activity. *J. Mex. Chem. Soc.* **2023**, *67*, 60–69, doi:10.29356/jmcs.v67i1.1835.

CHAPTER 3: APPLICATIONS

CHAPTER 3: A-CORROSION INHIBITION STUDY

A- Corrosion Inhibition Study

I. Introduction and bibliographic study

Mild steel, a form of low-carbon steel, is commonly used as a construction material in a wide range of industries due to its excellent mechanical properties and relatively low cost [1]. It is widely preferred for its cost-effectiveness and availability and is frequently employed in the oil industry for the production of tanks, pipes, and reservoirs [2]. Acidic solutions are increasingly utilized across various industrial sectors, with key applications such as descaling, industrial cleaning, pickling, and the acidification of oil wells [3]. Commonly used acids include hydrochloric acid (HCl), nitric acid (HNO_3), and sulfuric acid (H_2SO_4) [4]. Despite its numerous technological applications, mild steel's use is limited by its low resistance to acidic corrosion [5].

Over the past five decades, metal corrosion has generated growing interest in sectors such as construction, energy, ... It is estimated that about one-third of steel is lost due to corrosion, leading to significant global economic losses [6]. Metal corrosion is an age-old challenge, dating back to the early discovery of metals. It is defined as the gradual deterioration of the properties of metals and materials due to chemical or electrochemical reactions with their atmospheric environment [7]. Additionally, it impacts society by affecting the health and safety of people working in industries and those living nearby [8]. Although the corrosion of metals and their alloys in service is an inevitable phenomenon, it can be controlled [9].

Being used primarily to remove corrosion products and oxides from surfaces without altering the metal itself, it is highly recommended to incorporate inhibitors into these solutions [2]. Protecting steel from corrosion extends the lifespan of equipment while limiting the release of toxic metals into the environment [10]. In industry, anticorrosive agents are commonly used in acidic media to prevent or reduce the corrosion rates of metallic materials [11].

Organic and inorganic compounds are commonly used as anticorrosive agents. However, it is important to mention that most inorganic products are environmentally unfriendly and toxic. Due to stringent environmental regulations and increasing ecological awareness, their use as corrosion inhibitors is now significantly limited [12]. An effective and practical solution to this issue is the use of organic and synthetic type corrosion inhibitors, due to their ease of synthesis, excellent inhibitory effect, and advantageous economic impacts. Generally, heterocyclic compounds containing large electronegative atoms (such as N, O, and

S), conjugated double bonds, and polar functional groups are the most effective corrosion inhibitors [13], [14]. Many organic heterocycles, such as piperidine, piperazine, imidazole, pyridine, and pyrimidine, are reported among the most powerful acid corrosion inhibitors [15], [16].

a. Examples of organic inhibitors

Two fused heterocyclic compounds, 2-phenylquinazolin-4(3H)-one (PQO) and 2-phenyl-4H-benzo[d]oxazin-4-one (POO), were examined by Hemapriya et al. to determine their capabilities to control the corrosion of mild steel in a 1M H_2SO_4 solution, using gravimetric and electrochemical methods (Scheme 1). Both inhibitors showed excellent results in preventing corrosion, with their effectiveness increasing with concentration and decreasing with rising temperature. The order of inhibitor effectiveness is as follows: PQO > POO. Gravimetric measurements showed a correspondence with the thermodynamic and kinetic models of Langmuir, displaying correlation coefficients close to unity. The data suggest a physisorption mechanism based on the values of E_a and $DG°_{ads}$ [8].

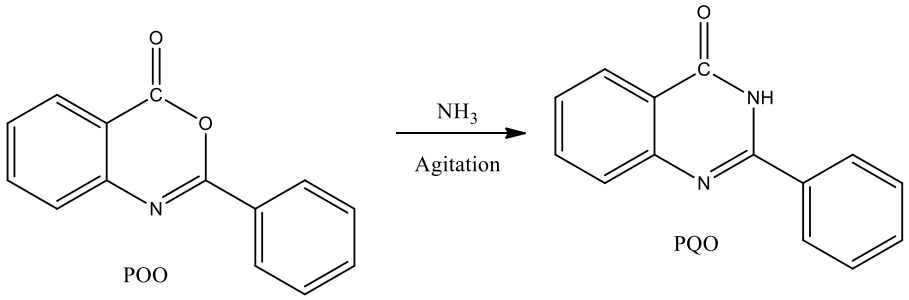

Scheme 1: Inhibitor structures by Hemapriya.

Ech-chihbi et al. synthesized 2-phenylimidazo[1,2-a]pyrimidine-3-carboxaldehyde and studied its corrosion-inhibiting effect on carbon steel (C steel) in a 1 M HCl solution (Scheme 2). Experiments were conducted using impedance spectroscopy techniques, weight loss measurements, and potentiodynamic polarization. The results indicated that the corrosion rate is directly proportional to the increase in inhibitor concentration. Studies revealed that this compound is of the mixed type and obeys the Langmuir isotherm model [17].

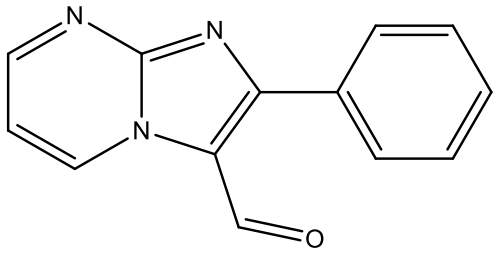

Scheme 2: Inhibitor structures by Ech-chihbi.

Four new bis-coumarins were synthesized and studied to inhibit the corrosion of carbon steel in 0.5 M H_2SO_4 using electrochemical methods by Abd El-Raouf et al. (Scheme 3). The tested products were found to be effective, exhibiting mixed-type anticorrosive action. It is noteworthy that their corrosion inhibition activities increased with the elevation of their concentrations and the measurement temperature. The coumarins studied showed chemical adsorption on the surface of the steel and obeyed the Langmuir adsorption isotherm [10].

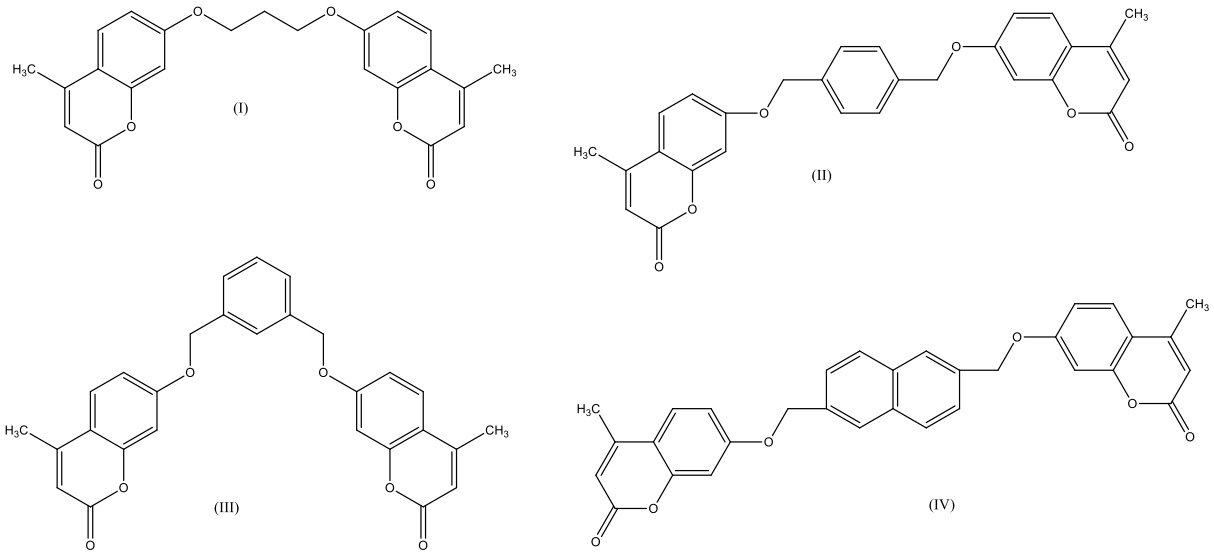

Scheme 3: Inhibitor structures by Abd El-Raouf.

Zhang et al. studied the inhibitory activity of three pyrido[1,2-a]benzimidazoles for the corrosion of mild steel in an HCl solution using gravimetric and electrochemical methods (Scheme 4). The heterocycles in question exhibited excellent anticorrosive activities, achieving 98.96% inhibition efficiency at an optimal concentration of 0.25 mmol/L. The results obtained revealed that these compounds are considered mixed-type, and their adsorption mode follows the Langmuir isotherm type [5].

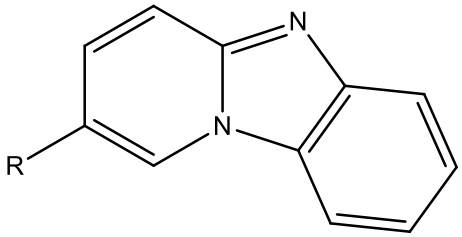

TBIP : R = CF_3
BIP: R = H
MBIP : R = CH_3

Scheme 4: Inhibitor structures by Zhang.

El Aatiaoui et al. synthesized a series of Schiff bases based on an imidazo[1,2-a]pyridine scaffold, namely (E)-N-(2-phenylimidazo[1,2-a]pyridin-3-yl)-1-(1H-pyrrol-2-yl)methanimine (IMP1), (E)-N-(2-phenylimidazo[1,2-a]pyridin-3-yl)-1-(thiophen-2-yl)methanimine (IMP2), and (E)-1-(5-nitrothiophen-2-yl)-N-(2-phenylimidazo[1,2-a]pyridin-3-yl)methanimine (IMP3) (Scheme 5). The inhibitory capacity of these compounds on the corrosion of mild steel was evaluated in hydrochloric solution using weight loss and electrochemical methods. The results obtained reveal that the inhibition efficiency is directly proportional to the increase in inhibitor concentration and inversely proportional to the rise in temperature, and that these compounds follow the Langmuir isotherm model and are of the physisorption type [18].

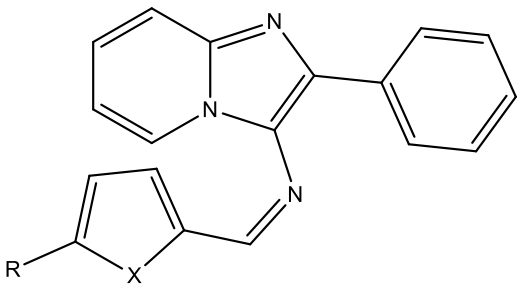

IMP_1 : X = N; R = H
IMP_2 : X = S; R = H
IMP_3 : X = S; R = NO_2

Scheme 5: Inhibitor structures by El Aatiaoui.

Idelfitri et al. synthesized an acid thiosemicarbazone derivative of Meldrum named 2,2-dimethyl-5-(4-nitrobenzylidene)-1,3-dioxane-4,6-dione bis(4-ethyl-3-thiosemicarbazone) (4NMATSC) and tested it as an anticorrosive in an HCl solution using weight loss techniques and mapping analysis. The 4NMATSC under study proved to be a good corrosion inhibitor by forming a protective layer through adsorption on the surface of mild steel (Scheme 6). The

corrosion inhibition efficiency increased with the rising concentrations of the inhibitor, reaching 68.88% at the highest concentration of 5 ppm [19].

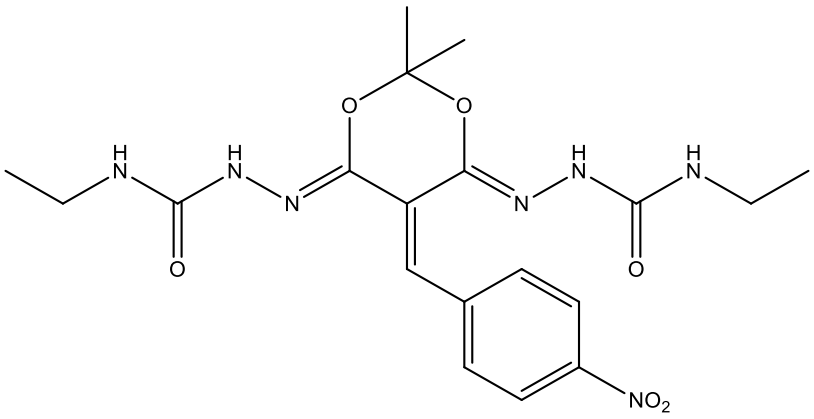

Scheme 6: Inhibitor structures by Idelfitri.

El Mouden et al. studied the anticorrosive effect of two compounds on C38 steel in acidic environments of 1.0 M HCl, namely (1-Allyl-6-nitro-1H-indazole (1a) and 1-Ethyl-5-nitro-1H-benzimidazole-2-thiol (2b)) (Scheme 7). The inhibitory efficiency of 1a and 2b was investigated using methods such as electrochemical, gravimetric, and electrochemical impedance spectroscopy. The experimental results showed that both products successfully inhibited the corrosion of the steel, with a maximum IE (%) value of 97.5% corresponding to T = 298 K for 2b. Additionally, the inhibition efficiency IE decreased with increasing temperature, the behavior of the inhibitor is of mixed nature, and the adsorption isotherm is consistent with the Langmuir isotherm [20].

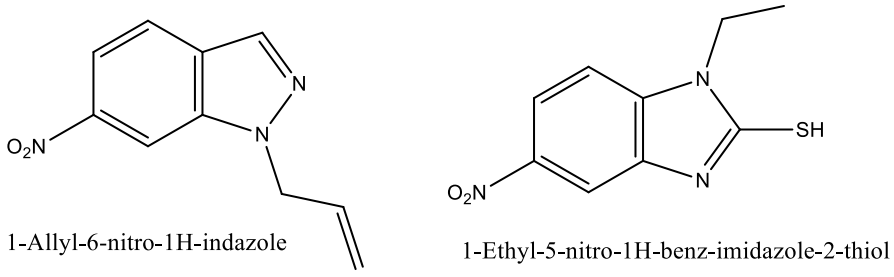

Scheme 7: Inhibitor structures by El Mouden.

b. Mechanism of inhibition of organic inhibitors

Organic corrosion inhibitors are organic compounds that have polar groups containing N, O, and/or S atoms, or heterocycles with conjugated double bonds, or polar functional groups [21]. Their effectiveness mainly depends on their ability to adsorb onto the metallic surface by

replacing the water molecules adsorbed at the corrosion interface [10]. Consequently, the film formed by these molecules adsorbs onto the metal surface, generating a passive layer that inhibits the electrochemical reactions that drive corrosion progression [3].

Under optimal dosing of the anticorrosive, the attraction between the inhibitor and the metal is predominant. In contrast, once this dosage is exceeded, the repulsion between the inhibitor molecules becomes stronger. The nature of the organic inhibitor, the characteristics of the metal, and the working conditions, such as acid concentration and immersion temperature, significantly influence this behavior [22], [23]. The nature of adsorption manifests according to the specific type of interaction between the steel surface and the molecules. If it involves a transfer of electron pairs to the unoccupied "d" orbital of the steel, forming coordination bonds, it is referred to as chemisorption (chemical adsorption). Conversely, if this interaction is primarily electrostatic, it is called physisorption (physical adsorption) [24]. The following table summarizes the main properties of chemisorption and physisorption [25].

Table **1:** Comparison between chemisorption and physisorption [25].

Chemisorption	**Physisorption**
- The force of attraction is the chemical bonding force	- The attractive force is Van der Waal forces
- It is irreversible	- It is reversible
- Formation of mono-molecular layers	-Formation of multi-molecular layers
- Heat adsorption is high	-Heat adsorption is low
- Activation energy is required	-Activation energy is not required
- It takes place at high temperature	- It occurs at low temperature.

c. Objective of the study

The objective of this study is to measure the effectiveness of corrosion inhibitors for mild steel in a normal HCl solution at different concentrations, temperatures, and immersion times. Two families of compounds are examined: the 2-arylimidazo[1,2-a]pyridines and the 2-arylimidazo[1,2-a]pyrimidines using the gravimetric method (weight loss).

II. Experimental method

a. Material

i. Organic inhibitors

The arylimidazopyridine/pyrimidine compounds were synthesized in the Laboratory of Catalysis and Synthesis in Organic Chemistry (LCSCO) in Tlemcen according to the procedure reported in the materials and methods section.

- 2-Arylimidazo[1,2-a]pyridines :

1. 2-phenylimidazo[1,2-a]pyridine (**IP-H**)
2. 2-(4-fluorophenyl)imidazo[1,2-a]pyridine (**IP-F**)
3. 2-(4-chlorophenyl)imidazo[1,2-a]pyridine (**IP-Cl**)
4. 2-(4-bromophenyl)imidazo[1,2-a]pyrimidine (**IP-Br**)

- 2-Arylimidazo[1,2-a]pyrimidines:

1. 2-phenyimidazo[1,2-a]pyrimidine (**IPM-H**)
2. 2-(4-fluorophenyl)imidazo[1,2-a]pyrimidine (**IPM-F**)
3. 2-(4-chlorophenyl)imidazo[1,2-a]pyrimidine (**IPM-Cl**)
4. 2-(4-bromophenyl)imidazo[1,2-a]pyrimidine (**IPM-Br**)

Table 2 presents the chemical structures of the compounds studied. The gravimetric method was used in this study. The thermodynamic parameters were determined and discussed, as well as the adsorption mechanism of the inhibitors. Additionally, a comparison between the two families of compounds was made.

Table 2: Chemical structures, names, and abbreviations of the organic compounds studied.

Abbreviation	Chemical structure
IP-H	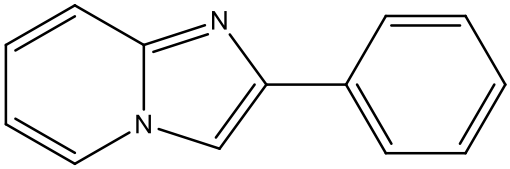
IP-F	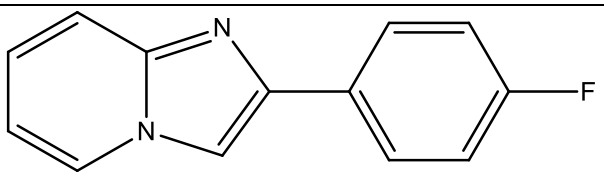

IP-Cl	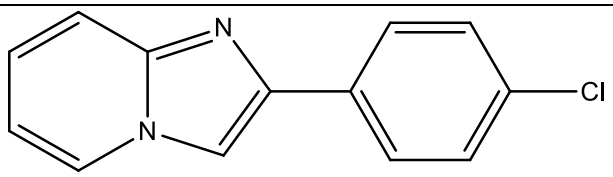
IP-Br	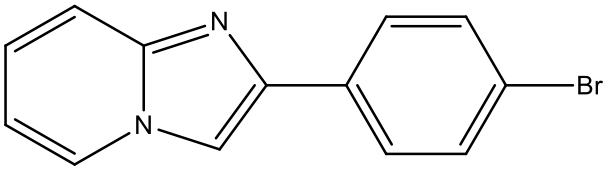
IPM-H	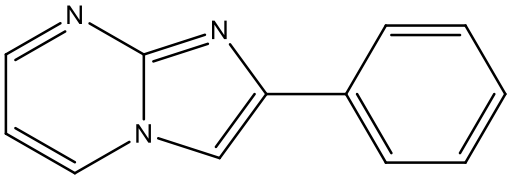
IPM-F	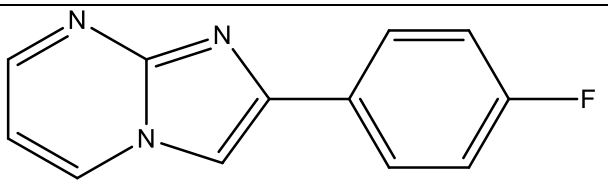
IPM-Cl	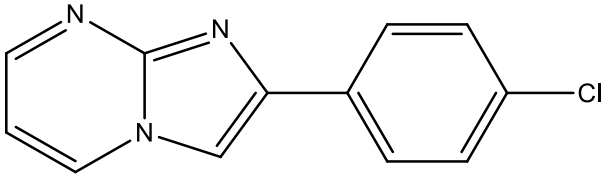
IPM-Br	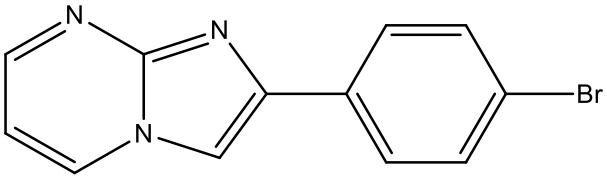

ii. Mild Steel Sample

The material used is mild steel, which is commonly used for the production of castings. Its chemical composition is shown in Table 3.

Table 3: Chemical Composition of Mild Steel.

Elements	Percentage (%)
Carbon (C)	0.06
Manganese (Mn)	0.073
Phosphorus (P)	0.010
Sulfur (S)	0.005
Silicon (Si)	0.02
Aluminium (Al)	0.044
Titanium (Ti)	0.04
Iron (Fe)	Balance

iii. Test solutions

Analytical 37% hydrochloric acid (HCl) was diluted with distilled water to obtain a 1M HCl solution (the blank or inhibitor solution). The heterocycles were added to the acid at concentrations of 5×10^{-5} M, 7.5×10^{-5} M, 10^{-4} M, 2.5×10^{-4} M, and 5×10^{-4} M to form the test solutions.

b. Experimental procedure

The mild steel sheets were mechanically cut into nearly equal-sized coupons. These coupons were ground with sandpaper of various grits, ranging from 80 to 1200 successively. The dimensions of the coupons were measured using a caliper to calculate the surface area of each piece. They were weighed using an analytical balance before each test.

Then, the metal pieces were degreased with acetone and distilled water, dried using a hair dryer, and immersed in the acid solution with or without a known inhibitor at a precise concentration. To maintain the desired temperature, the coupons were placed in a water bath for a specified time according to the tests. They were weighed again after drying to calculate the weight loss. Parallel duplicate experiments were conducted to determine the average corrosion rate.

c. Gravimetric method

This method has the advantage of its simplicity for implementation and does not require significant equipment. Its principle is based on measuring the weight loss Δm experienced by a sample with a surface area S, in a corrosive solution maintained at a constant temperature, during the immersion time t [26].

The corrosion rate (W_{corr}) is evaluated by the following equation [27] :

$$\boldsymbol{Wcorr = \frac{\Delta m}{St}} \quad \boldsymbol{(g.h^{-1}.cm^{-2})} \ldots\ldots\ldots\ldots\ldots\ldots \boldsymbol{(I)}$$

With:
Δm: the weight loss (g)

t: the measurement time (hour)

S: the surface area of the metal part (cm^2)

The inhibitory efficiency (IE%) of organic products was calculated by measuring the corrosion rates in the absence and presence of the inhibitor, noted respectively as (W_{corr}) and (W_{inb}).
The inhibition efficiency was determined using the following equation [28]:

$$\mathbf{EI} = \frac{Wcorr - Winb}{Wcorr} * \mathbf{100} \ldots\ldots\ldots\ldots\ldots\ldots \mathbf{(II)}$$

III. Results and Discussion

Mild steel corrosion was determined by the gravimetric method (weight loss) using two families of heterocyclic compounds, namely:

- Imidazo[1,2-a]pyridines and
- Imidazo[1,2-a]pyrimidines.

Different parameters were studied, such as the effect of concentration, temperature, and immersion time followed by a thermodynamic study.

A. Inhibition of mild steel corrosion by imidazo[1,2-a]pyridines (IP)

The imidazo[1,2-a]pyridines are known as excellent inhibitors of metal corrosion [29]. The objective of this part is to study the effect of imidazo[1,2-a]pyridines (**IP-H, IP-F, IP-Cl**, and **IP-Br**) on the corrosion of mild steel in a molar medium of HCl. The influence of the concentration of the aforementioned imidazo[1,2-a]pyridines, immersion time, and temperature has been studied. Thus, calculations were carried out to characterize the nature of the adsorption, and a thermodynamic study was conducted to discuss this process.

a. Effect of IP-H concentration

The concentration of corrosion inhibitors plays a crucial role in their effectiveness: a dose that is too low in inhibitor is insufficient to protect the metal, while an excessive concentration may not provide any additional benefit. It is therefore essential to properly adjust the optimal concentration for effective protection against corrosion [30].

To study the effect of concentration on the inhibitor 2-phenylimidazo[1,2-a]pyridine (**IP-H**) as a corrosion-inhibiting agent, we immersed mild steel pieces in a molar solution of HCl at different concentrations (7.5×10^{-5}, 10^{-4}, 2.5×10^{-4}, and 5×10^{-4} mol/L) in a thermostatic bath for five hours. The same operation was repeated at different temperatures (298, 308, 318, 328, and 338 K).

The following table shows the experimental results of the variation of the inhibiting efficiency (IE) of **IP-H** as a function of concentration and temperature.

Table 4: Evolution of the inhibiting efficiency for different concentrations of **IP-H**

IE (%)					
T(K) / C (mol. L^{-1})	298	308	318	328	338
$7,5 \times 10^{-5}$	53,77	59,06	65,04	70,83	75,80
10^{-4}	58,98	63,21	69,82	74,76	80,15
$2,5 \times 10^{-4}$	65.90	71,81	76,31	81,90	86,96
5×10^{-4}	72,67	78,48	83,05	88,45	93,48

Figure 1 shows the evolution of the inhibiting power of **IP-H** as a function of concentration and temperature in a normal HCl solution after 5 hours of immersion. This figure visualizes the impact of the inhibitor concentration on its inhibiting effect after a 5-hour immersion period.

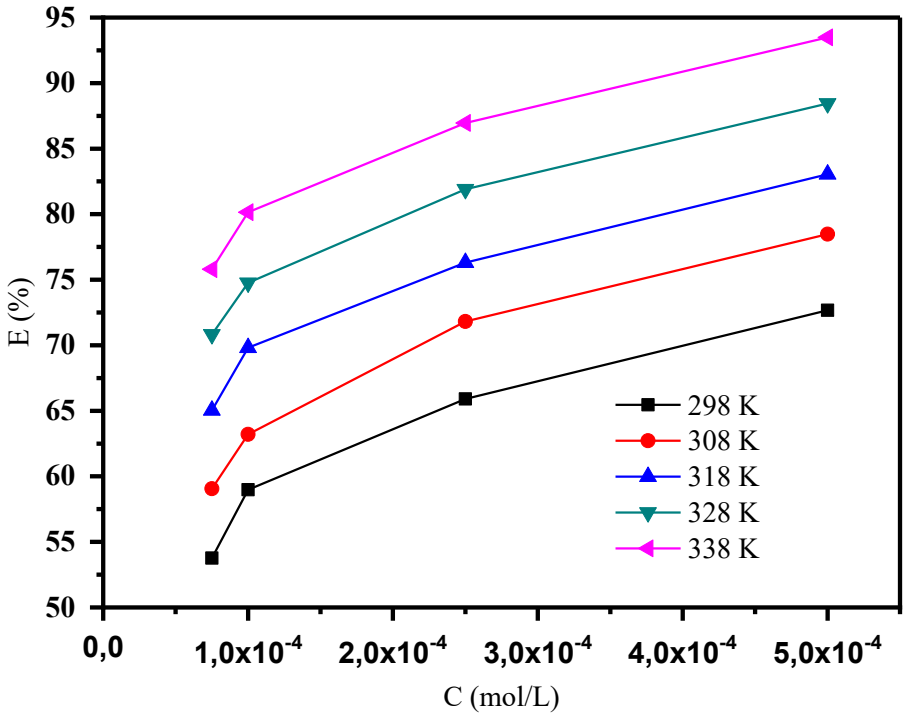

Figure 1: Variation of **IP-H** inhibitor efficacy as a function of concentration

From Figure 1, we note that the inhibiting efficiency is proportional to the concentration of **IP-H**. Furthermore, the curves indicate that temperature influences this efficiency; the higher the temperature, the greater the inhibiting efficiency.

The highest inhibition efficiency was obtained for a concentration of 5 x 10^{-4} M, reaching 93.48% at 338 K. Thus, the optimal concentration is determined. The results show that as both concentration and temperature increase, the protection improves; in other words, the steel surface is covered.

b. Effect of IP-H temperature

The effect of temperature on the inhibition mechanism of mild steel in the presence of **IP-H** is demonstrated in Figure 2. The corrosion inhibition efficiency shows an increasing trend with rising temperature.

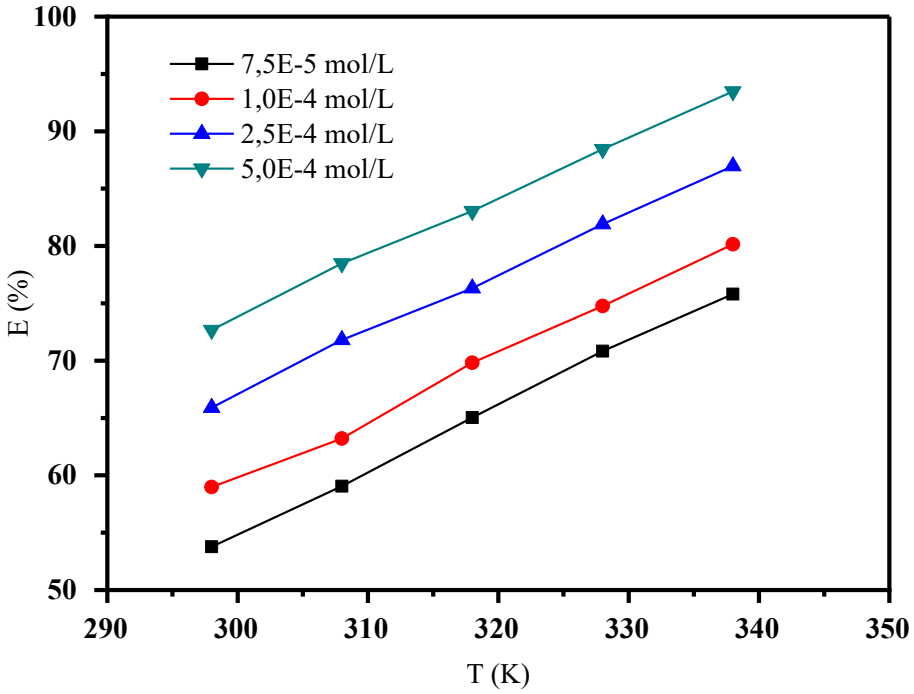

Figure 2: Impact of temperature on the efficacy of the **IP-H** inhibitor

The following table represents the variation in the corrosion rate (W_{corr}) of the corrosive solution with and without the inhibitor, 2-phenylimidazo[1,2-a]pyridine (**IP-H**), on mild steel, varying the temperature and concentrations over 5 hours.

Table 5: Influence of temperature on the variation in corrosion rate for different concentrations of the inhibitor (**IP-H**).

W_{corr} (mg/h.cm^2)					
T(K) / **C (mol. L^{-1})**	**298**	**308**	**318**	**328**	**338**
Blank (HCl)	1,43 x10^{-4}	5,20x10^{-4}	1,06 x10^{-3}	1,88 x10^{-3}	4,37 x10^{-3}
7,5 x 10^{-5}	6,61x10^{-5}	1,12x10^{-4}	3,70x10^{-4}	5,48x10^{-4}	1,05x10^{-3}
10^{-4}	5,86x10^{-5}	1,91x10^{-4}	2,78x10^{-4}	4,21x10^{-4}	8,67x10^{-4}
2,5 x 10^{-4}	4,87x10^{-5}	1,46x10^{-4}	2,08x10^{-4}	3,40x10^{-4}	5,69x10^{-4}
5 x 10^{-4}	5,22x10^{-5}	8,50x10^{-5}	1,41x10^{-4}	2,17 x10^{-4}	2,84x10^{-4}

Figure 3 shows the evolution of the corrosion rate of the product **IP-H** as a function of concentration and temperature. The corrosion rate decreases with increasing concentration and increases with rising temperature.

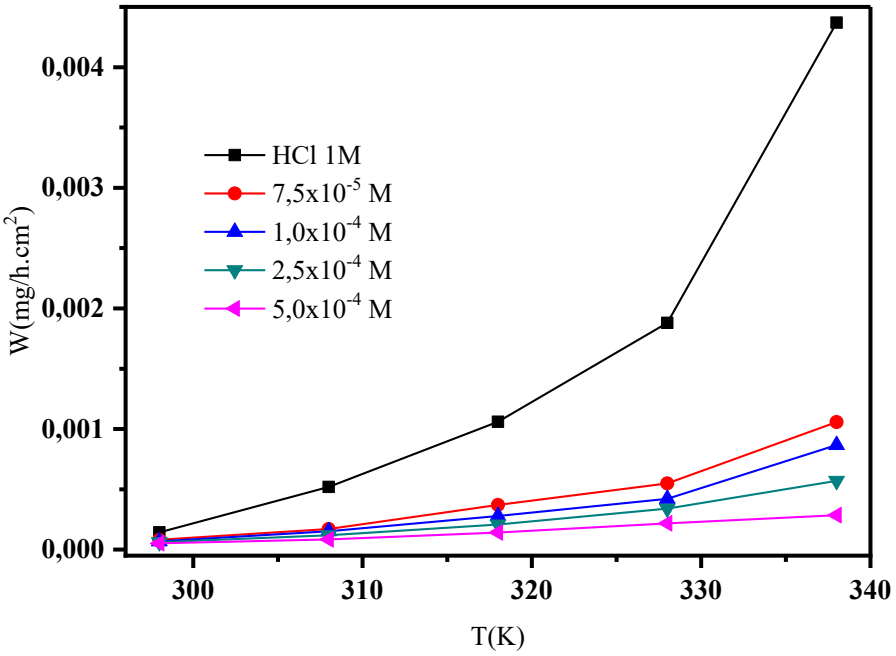

Figure 3: Effect of temperature and concentration on corrosion rate of **IP-H** inhibitor

c. Effect of immersion time of imidazo[1,2-a]pyridines

To determine the optimal immersion time for the four derivatives of imidazo[1,2-a]pyridine (**IP-H, IP-F, IP-Cl,** and **IP-Br**), gravimetric measurements were performed on mild steel in a corrosive environment of 1M HCl while keeping the temperature (308 K) and concentration (5 x 10^{-4} M) constant. The experiment was conducted by varying the immersion time (1, 2, 3, 4, 5, 6, and 24 hours).

Table 6: Variation of the inhibitory efficiency as a function of the immersion time of imidazo[1,2-a]pyridines (**IP-H, IP-F, IP-Cl,** and **IP-Br**)

	IE (%)						
t (h) / **Inhibitor**	**1**	**2**	**3**	**4**	**5**	**6**	**24**
IP-H	72,72	82,49	91,26	91,82	94,48	93,13	87,60

IP-F	82,54	84,53	92,73	92,95	96,06	93,33	90,58
IP-Cl	83,21	85,43	92,89	93,92	96,21	94,38	94,02
IP-Br	85,09	87,55	93,55	94,50	97,51	96,53	93,59

Figure 4 shows the influence of immersion time on the inhibitory efficiency of 2-arylimidazo[1,2-a]pyridines (**IP-H, IP-F, IP-Cl,** and **IP-Br**). The results reveal that the anticorrosive power increases with the increase in immersion time in the four corrosion inhibitor solutions, reaching its maximum at 5 hours. Subsequently, a slight decrease in inhibitory efficiency is observed over time.

Furthermore, it is noted that the inhibitory efficiency of the brominated derivative (**IP-Br**) is higher than that of the chlorinated derivative (**IP-Cl**), followed by the fluorinated derivative (**IP-F**), and finally by the unsubstituted product (**IP-H**). In other words, the anticorrosive power of the compounds follows the descending sequence: **IP-Br** > **IP-Cl** > **IP-F** > **IP-H**, demonstrating that the presence of a bromine substituent significantly enhances the inhibitory power.

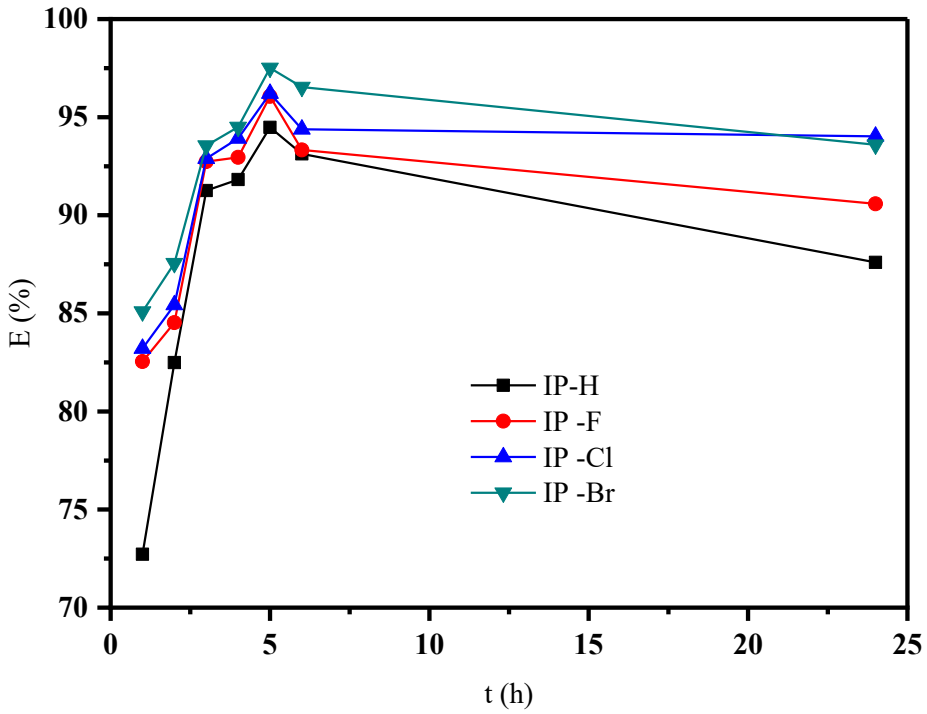

Figure 4: Influence of immersion time on the variation in the inhibitory efficacy of inhibitors (**IP-H, IP-F, IP-Cl,** and **IP-Br**).

These results imply that the inhibitors act by adsorption onto the metal, forming a barrier layer between the mild steel and the corrosive solution. Therefore, in order to confirm the adsorption of 2-phenylimidazo[1,2-a]pyridine on the surface of the steel, we performed further calculations to provide essential information about the interaction between the inhibitor and the metal surface.

d. Adsorption isotherm

The effectiveness of organic products in inhibiting corrosion largely depends on their adsorption capability on metal surfaces. Therefore, it is crucial to evaluate this relationship in order to deepen the research on corrosion inhibitors. It is noteworthy that the adsorption mechanism of corrosion inhibitors can be understood through the study of the adsorption isotherm as well as the adsorption behavior of the corrosion inhibitors [31].

The empirical evaluation of the most suitable adsorption isotherm with surface coverage data is important in order to exploit the corrosion rate measurements for calculating the thermodynamic parameters associated with the adsorption of the corrosion inhibitor.

The main models considered are the Temkin [32], El-Awady [33], Freundlich [34], and Langmuir [35] isotherms. The latter describes how a corrosion inhibitor adsorbs onto the metal surface by forming a single, uniform layer. It helps analyze how the inhibitory effectiveness of a compound manifests on the surface of a metal and the distribution of a corrosion inhibitor on a metal [36]. The Langmuir isotherm can be described by the relationship (III) [18]:

$$\frac{\theta}{1-\theta} = Kads.Cinb \ldots\ldots\ldots\ldots\ldots\ldots \textbf{(III)}$$

To determine θ (the degree of surface coverage), it was assumed [37] that the inhibitory effectiveness is primarily caused by the blockage of the adsorbed species, hence the use of equation (III). This parameter, in the 1M hydrochloric acid solution at different inhibitor concentrations, was evaluated from gravimetric measurements at 298–338 K and graphically analyzed to match the most appropriate adsorption isotherm.

$$\theta = \frac{IE}{100} \ldots\ldots\ldots\ldots\ldots\ldots \textbf{(IV)}$$

Using the inhibitory effectiveness (IE) calculated from the gravimetric method, we calculated θ from relation (IV). From equation (III), we can derive equation (V) in order to find other more in-depth parameters. The curves of C_{inb}/θ as a function of C_{inb} for the temperatures: 298, 308, 318, 328, and 338 K form a straight plot (Figure 6) with a slope close to unity, indicating that the studied product **IP-H** follows the Langmuir adsorption isotherm, according to equation (V):

$$\frac{Cinb}{\theta} = \frac{1}{Kads} + Cinb \ldots\ldots\ldots\ldots\ldots\ldots \textbf{(V)}$$

With:

$\mathbf{C_{inb}}$: the concentration of **IP-H**

$\mathbf{K_{ads}}$: the adsorption constant.

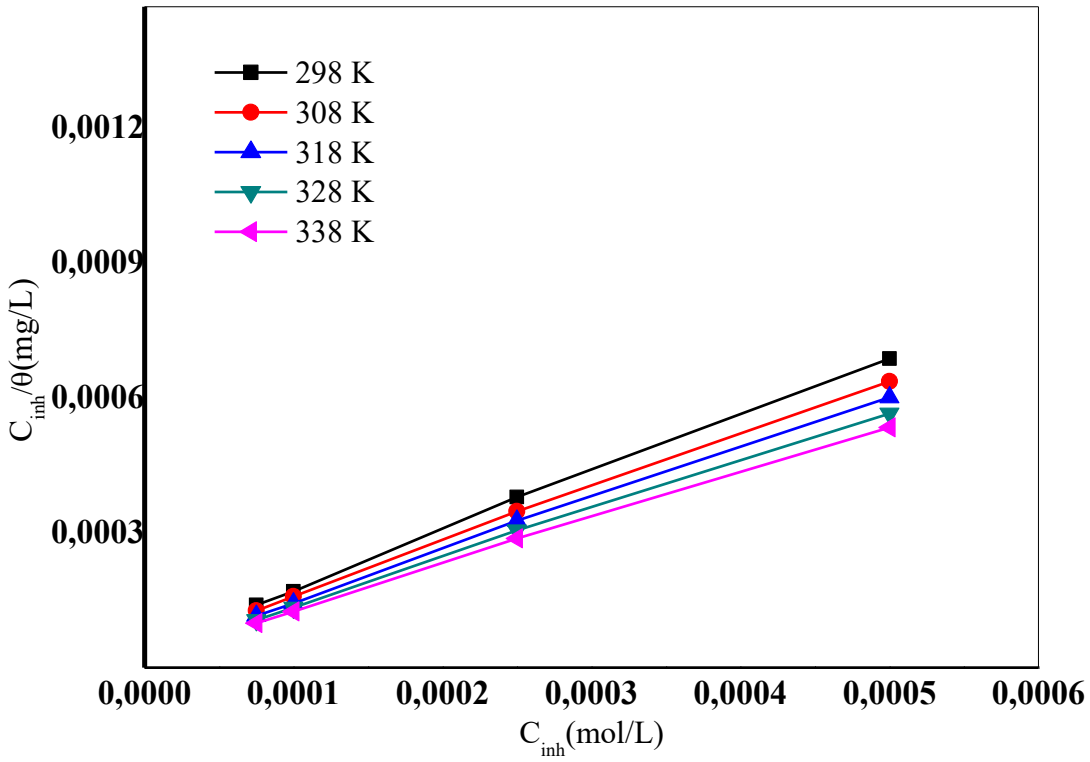

Figure 6: Adsorption isotherm of **IP-H** inhibitor on mild steel in 1N HCl at different temperatures

We were thus able to deduce the values of the adsorption constant K from equation (V) and the values of the standard free energy of adsorption (ΔG_{ads}) from relation (VI):

$$K = \frac{1}{55,5} exp\left(\frac{\Delta Gads}{RT}\right) \ldots\ldots\ldots\ldots\ldots\ldots \textbf{(VI)}$$

Where the value 55.5 represents the concentration of water in solution (mol/L) [11]. The values of the standard enthalpy of adsorption and the standard entropy of adsorption (ΔH_{ads} and ΔS_{ads}, respectively) can be deduced using equation (VII), which is known from Gibbs Helmholtz [38]:

$$\Delta G_{ads} = \Delta H_{ads} - T\Delta S_{ads} \ldots\ldots\ldots\ldots\ldots\ldots \textbf{(VII)}$$

The following table lists the values of K_{ads}, ΔH_{ads}, ΔS_{ads} and ΔG_{ads}.

Table 7: Thermodynamic parameters for the adsorption of **IP-H** on mild steel at [298-338] K in 1M HCl.

T (K)	R^2	K_{ads}	ΔH_{ads}(kj/mol)	ΔS_{ads}	ΔG_{ads} (KJ/mol)
298	0,99872	22465,95285	25,01284	0,20063	-34,77
308	0,99921	25033,92096		0,19881	-36,21
318	0,99891	31678,65176		0,19821	-38,01
328	0,99917	36474,11979		0,19698	-39,59
338	0,99925	41622,26958		0,19583	-41,17

The recovery rate values, θ, are plotted. For the **IP-H** inhibitor, the C_{inh}/θ curve as a function of concentration shows a linear trend, with correlation coefficients (R^2) close to 1. This demonstrates that the Langmuir isotherm is obeyed for the adsorption on the mild steel surface.

To determine the nature of the adsorption from the values of the adsorption energy (ΔG_{ads}), studies [39] have shown that when it is negative, it indicates that the adsorption process is spontaneous and that the film formed by the adsorbed corrosion inhibitor product on the metal is stable. Generally, if ΔGads is around 20 kJ/mol or less, it indicates physisorption, and if it is around 40 kJ/mol or more, it indicates chemisorption. In the first case, the adsorption is characterized by physical interactions such as Van der Waals forces (which are reversible and weak). In the second case, there is the formation of irreversible and stronger chemical bonds, such as coordination or covalent bonds between the corrosion inhibitor and the metal [40]. The calculated values of ΔG_{ads} range from -34.77 to -41.17. The calculated ΔG_{ads} values of **IP-H** are approximately −40 kJ/mol. This suggests electron transfer or sharing takes place between the metal surface and the anticorrosive molecules, leading to bond formation. Therefore, this is classified as chemisorption.

e. Thermodynamic parameters of IP-H corrosion

The Arrhenius equation is frequently used [41][42][43] to model the effect of temperature on the corrosion rate, showing that this rate is a linear function of the inverse of the temperature (1/T).

$$Ln(Wcorr) = \frac{-E_a}{RT} + LnA \quad \text{..... (IV)}$$ so:

$$\mathbf{Ln\left(\frac{Wcorr}{T}\right) = \frac{-\Delta H}{RT} + LnA \text{..... (V)}}$$

With:

W_{corr}: corrosion rate

E_a: activation energy (kJ. mol^{-1})

T: temperature (K)

A: Arrhenius constant

R = 8.314 $J.mol^{-1}.K^{-1}$

Plots depicting the variation of the logarithm of the corrosion rate (LnW) as a function of the inverse of temperature (1/T) are used to determine the pre-exponential factor (A) and activation energies (E_a) (Figure 7).

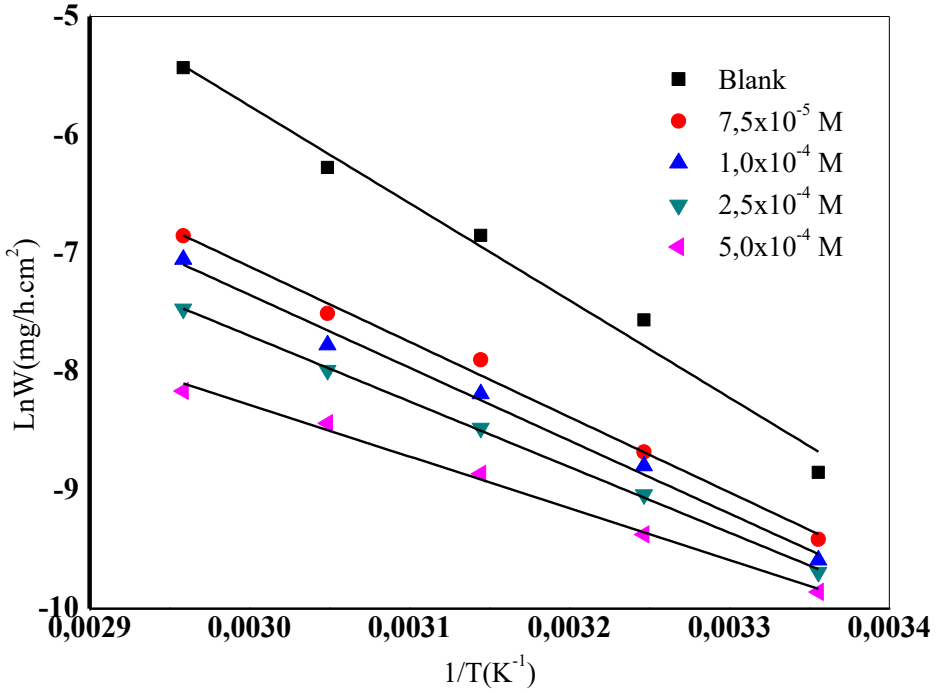

Figure 7: Arrhenius plots of the dissolution of mild steel at different concentrations in the presence and absence of **IP-H** in a normal HCl solution.

Figure 8 illustrates the variation of Ln (W_{corr}/T) as a function of 1/T for the acid alone (blank) and for the different concentrations of the inhibitor **IP-H**.

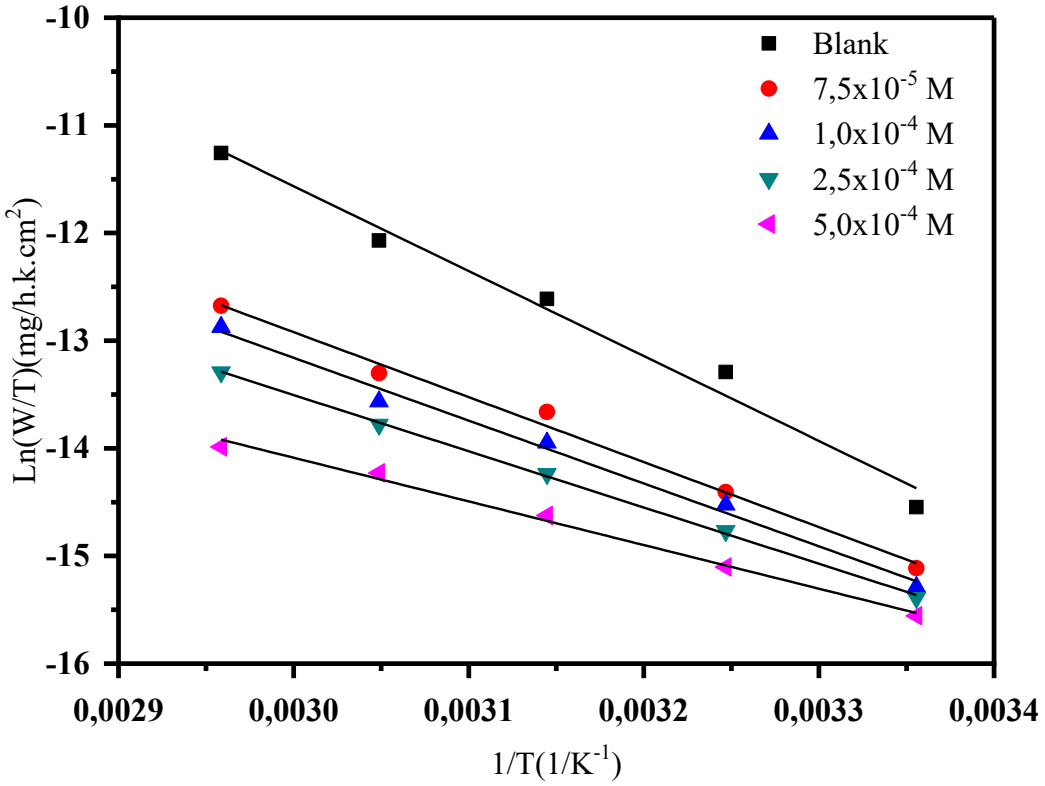

Figure 8: Trends of Ln (Wcorr/T) as a function of 1/T in the presence and absence of **IP-H**

Thermodynamic parameters such as activation energy (E_a), activation enthalpy (ΔH_a), and activation entropy (ΔS_a) were thus derived from the Arrhenius equation (Table 8). All plots display correlation coefficients (R^2) of 0.98 or higher, at different concentrations of **IP-H**. The slope of the obtained corresponds to $\Delta H/RT$, and the value of the y-intercept corresponds to LnA. From these plots, we were able to determine the values of ΔH and ΔS [44]. Table 8 summarizes the results obtained from these plots.

This indicates that the corrosion of mild steel in a normal HCl solution follows the kinetic model. The relationship between the inhibition efficiency (IE) of an anticorrosive agent and the temperature (T) can be interpreted in three ways [45]:

- IE increases with increasing T, with E_a (solution with inhibitor) < E_a (solution without inhibitor);
- IE remains constant with T, with E_a (solution with inhibitor) = E_a (solution without inhibitor);

- IE decreases with increasing T, with E_a (solution with inhibitor) > E_a (solution without inhibitor)

Based on the slope calculations from the obtained plots, it is observed that:

- E_a (solution with inhibitor) < E_a (solution without inhibitor), indicating that **IP-H** is effective in reducing corrosion.
- The inhibition efficiency (IE) increases with higher concentration and temperature in the presence of **IP-H**, demonstrating its strong efficacy at elevated temperature and concentrations, which is characteristic of effective inhibitors.

These types of bonds can withstand corrosion at high temperatures, suggesting chemisorption with the formation of a chemical adsorption film on the surface of mild steel.

Table 8 shows the following results:

- The parameter ΔS for the reaction involving the dissolution of mild steel in 1M hydrochloric acid solution with the presence of **IP-H** is lower than that of the solution without the inhibitor. This indicates that the presence of this inhibitor acts on the reaction dynamics, potentially suggesting reduced corrosion rates.
- All values of enthalpies (ΔH_a) are positive, reflecting the endothermic nature of the corrosion process of mild steel.
- We note that the difference between E_a and ΔH (E_a-ΔH) vary in the same way with all the concentrations, verifying the thermodynamic relationship between E_a and ΔH [18]:

$$\mathbf{E_a - \Delta H = RT = cste}$$

Table 8: Evolution of activation energy (E_a), activation enthalpy (ΔH_a), and activation entropy (ΔS_a) as functions of temperature and concentration, both with and without **IP-H.**

	R^2	E_a (KJ)	R^2	ΔH (KJ)	E_a-ΔH	ΔS	ΔGK (J/mol)
Blank	0,97978	68,21	0,978	65,58	2,63	-96,94	28,95
$7,5x10^{-5}$	0,99118	52,82	0,99013	50,18	2,63	-154,39	47,60
10^{-4}	0,98997	51,17	0,98883	48,53	2,63	-161,33	51,35
$2,5x10^{-4}$	0,99906	46,06	0,99889	43,43	2,63	-179,52	58,92
$5x10^{-4}$	0,99234	36,35	0,99085	33,72	2,63	-213,49	72,19

II. Inhibition of mild steel corrosion by imidazo[1,2-a]pyrimidines (IPM)

In this section, we studied the inhibitory effect of imidazo[1,2-a]pyrimidines (**IPM**) on mild steel corrosion using the weight loss method, similar to our approach with previous inhibitors, imidazo[1,2-a]pyridines (**IP**). This method allowed us to quantify the weight loss of the mild steel samples, providing insights into the effectiveness of **IPM** under various conditions, including temperature, concentration and immersion time. Recognized as effective corrosion inhibitors for mild steel [46], the imidazo[1,2-a]pyrimidines were examined in normal hydrochloric acid, with a detailed thermodynamic study presented to discuss the adsorption process.

a. Effect of IPM concentration

To investigate the effect of concentration on the 2-phenylimidazo[1,2-a]pyrimidine (**IPM-H**) as a corrosion inhibitor, we immersed mild steel specimens in a normal hydrochloric acid solution at varying concentrations (7.5×10^{-5}, 10^{-4}, 2.5×10^{-4}, and 5×10^{-4} mol/L) within a thermostatic bath for five hours. This procedure was repeated across different temperatures (298, 308, 318, 328, and 338 K).

The table **9** presents the experimental data on the inhibiting efficiency (IE) of **IPM-H**, analyzed as a function of concentration and temperature.

Table **9**: Variation of inhibiting efficiency across different concentrations of **IPM-H.**

IE (%)					
T(K) / **C (mol.L^{-1})**	**298**	**308**	**318**	**328**	**338**
7,5 x 10^{-5}	53,73	76,43	85,06	85,32	85,88
10^{-4}	57,65	77,87	85,42	85,92	86,25
2,5 x 10^{-4}	64,70	85,16	89,14	90,63	91,23

5 x 10^{-4}	68,19	87,02	90,79	92,02	93,98

The following figure illustrates the inhibiting effectiveness of **IPM-H** as a function of concentration and temperature in a 1M HCl solution. This figure highlights the influence of inhibitor concentration on its corrosion-inhibiting performance over the 5 hours immersion period.

Figure 9: Variation of the effectiveness of the **IPM-H** inhibitor as a function of its concentration after a 5-hour immersion in a 1M HCl solution.

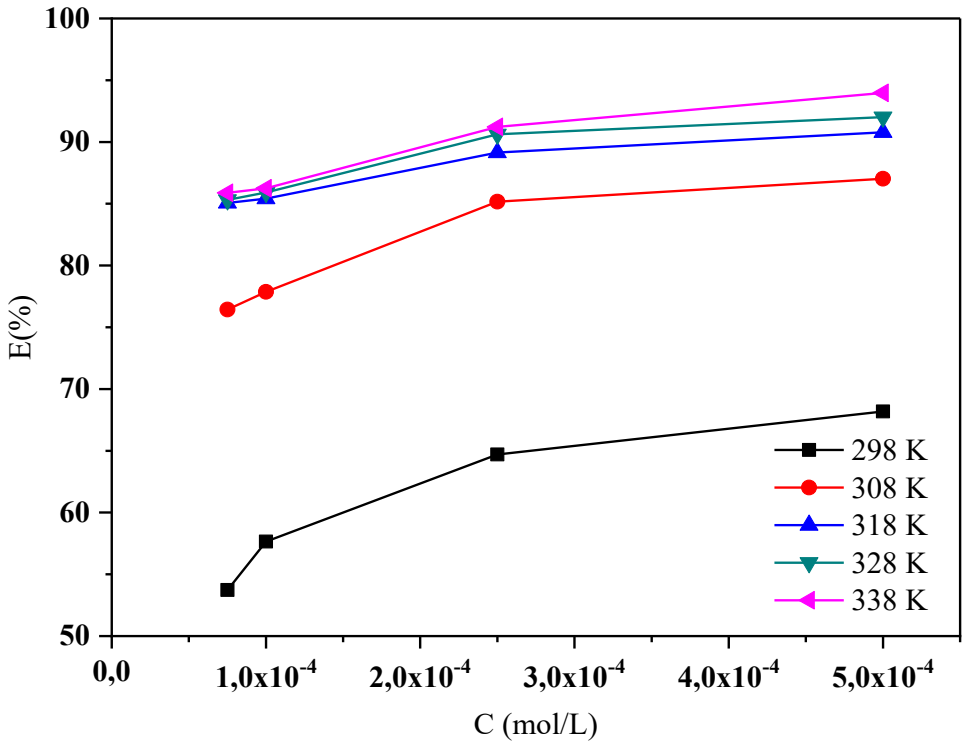

From Figure 9, it is observed that the inhibition efficiency increases with the concentration of **IPM-H**. Additionally, the curves suggest that temperature also affects this efficiency, with higher temperatures leading to enhanced inhibition.

The maximum inhibition efficiency was achieved at a concentration of 5 x 10^{-4} M, reaching 93.98% at 338 K, indicating the optimal concentration. These results demonstrate that as both concentration and temperature increase, protective coverage on the steel surface improves.

b. Effect of IPM-H temperature

Figure 10 illustrates the effect of temperature on the inhibition mechanism of mild steel in the presence of **IPM-H.** The inhibition efficiency displays an increasing trend as the temperature rises.

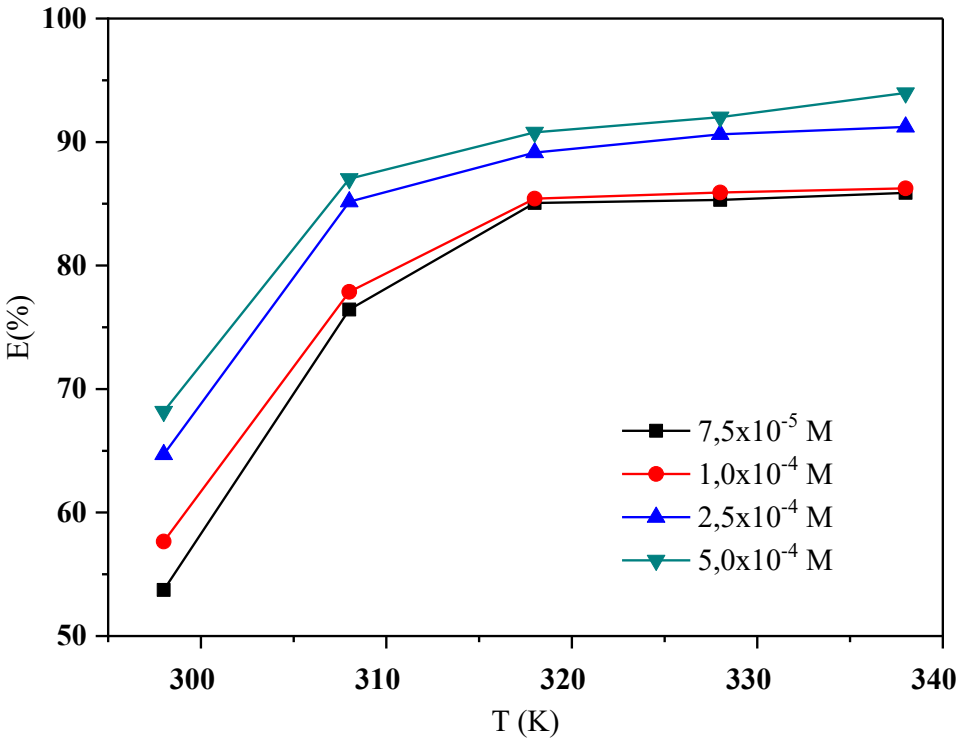

Figure 10: Effect of temperature on the efficacy of the **IPM-H** Inhibitor.

The table 10 shows the changes in the corrosion rate (W_{corr}) of the corrosive solution, both with and without the inhibitor, 2-phenylimidazo[1,2-a]pyrimidine (**IPM-H**), on mild steel. Measurements were taken over 5 hours, with varying temperatures and concentrations of the inhibitor.

Table 10: Influence of temperature on the corrosion rate variation across different concentrations of **IPM-H.**

W_{corr} (mg/h.cm²)					
T(K) / C (mol. L⁻¹)	298	308	318	328	338
7,5 x 10⁻⁵	6,63368E-5	6,07168E-5	5,06093E-5	4,56057E-5	6,63368E-5
10⁻⁴	1,22564E-4	1,15076E-4	7,7168E-5	6,7496E-5	1,22564E-4
2,5 x 10⁻⁴	1,58364E-4	1,54548E-4	1,15116E-4	9,7626E-5	1,58364E-4
5 x 10⁻⁴	2,75984E-4	2,64704E-4	1,76156E-4	1,50024E-4	2,75984E-4

The following figure illustrates the variation in the corrosion rate of **IPM-H** as a function of its concentration and temperature. The corrosion rate decreases with increasing concentration but increases as the temperature rises.

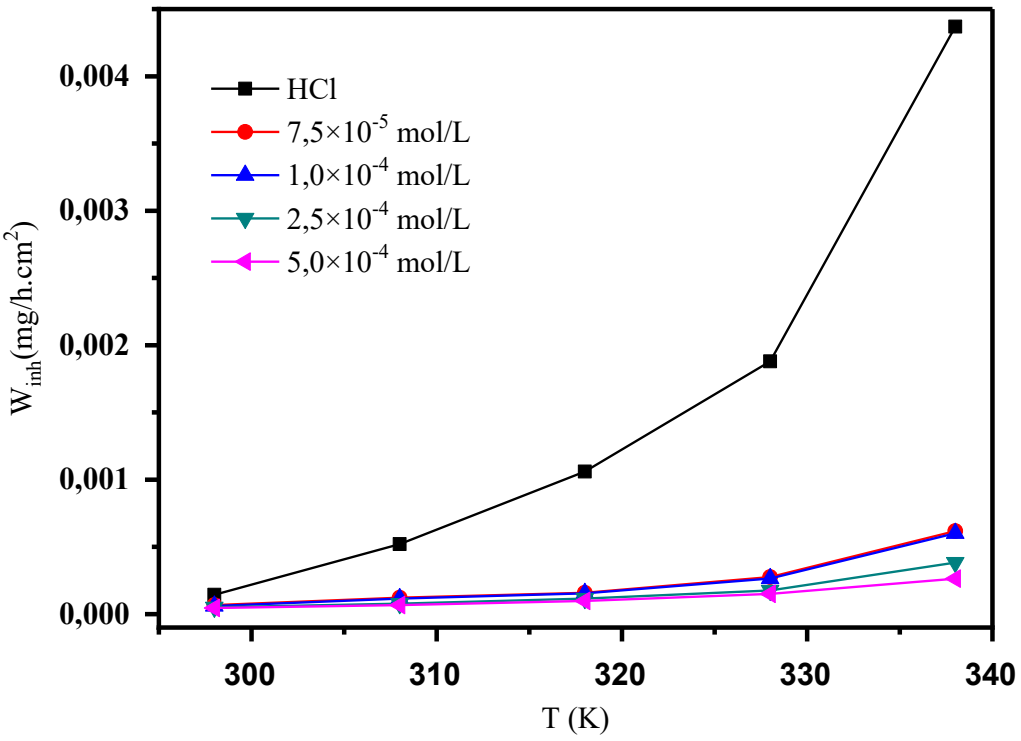

Figure 11: Impact of concentration and temperature on the corrosion rate of the **IPM-H** Inhibitor.

c. Effect of immersion time of imidazo[1,2-a]pyrimidines

To identify the optimal immersion time for the four imidazo[1,2-a]pyrimidine derivatives (**IPM-H, IPM-F, IPM-Cl,** and **IPM-Br**), weight loss analysis was conducted on mild steel in a molar solution of HCl corrosive medium. The temperature (308 K) and concentration (5 x 10^{-4} M) were maintained constant, while the immersion time was varied across intervals of 1, 2, 3, 4, 5, 6, and 24 hours.

Table 11: Inhibitory efficiency of imidazo[1,2-a]pyrimidine derivatives (**IPM-H, IPM-F, IPM-Cl,** and **IPM-Br**) at different immersion times.

	IE (%)						
t (h) / Inhibitor	1	2	3	4	5	6	24
IPM-F	74,98	76,16	81,08	87,08	93,09	93,01	91,3
IPM-H	84,12	84,64	85,12	91,93	94,27	92,5	90,63
IPM-Br	86,7	87,2	88,32	92,03	95,79	96,55	92,51
IPM-Cl	87,68	88.37	89.10	90,05	93,14	96,09	93,23

Figure 12 illustrates how immersion time affects the inhibitory efficiency of 2-arylimidazo[1,2-a]pyrimidine derivatives (**IPM-H, IPM-F, IPM-Cl,** and **IPM-Br**). The findings indicate that the anticorrosive effectiveness improves with longer immersion times in all four corrosion inhibitor solutions, peaking at 5 hours. After this point, a slight decline in inhibitory efficiency is noted over time.

Additionally, it is observed that the anticorrosive activity of the chlorinated derivative (**IPM-Cl**) surpasses that of the brominated derivative (**IPM-Br**), followed by the unsubstituted product (**IPM-H**), and finally the fluorinated derivative (**IPM-F**). In simpler terms, the inhibitory efficiency of the compounds decreases in the following order: **IPM-Cl** > **IPM-Br** >

IPM-H > **IPM-F**, indicating that the presence of a chlorine substituent significantly enhances the inhibitory power.

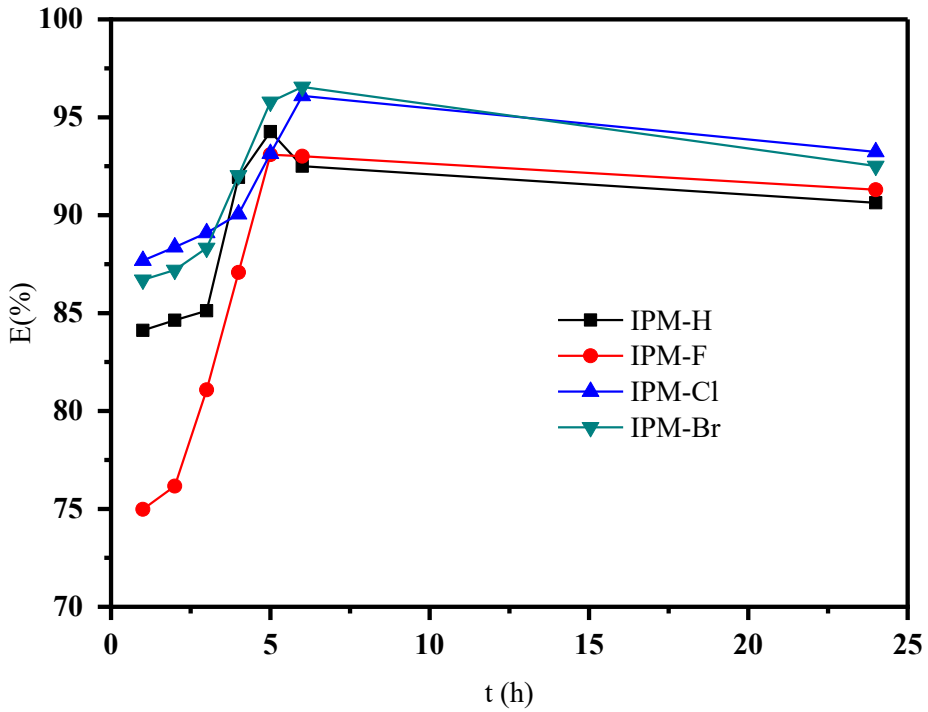

Figure 12: Impact of immersion time on the changes in anticorrosive potency efficacy of inhibitors (**IPM-H, IPM-F, IPM-Cl,** and **IPM-Br**).

These results suggest that the inhibitors function through adsorption onto the metal surface, generating a barrier layer that separates the mild steel from the corrosive solution. To validate the adsorption of imidazo[1,2-a]pyrimidines on the steel surface, we conducted additional calculations to gather critical information regarding the interaction between the inhibitor and the metal.

d. Adsorption isotherm

Evaluating the most appropriate adsorption isotherm using surface coverage data is crucial for leveraging corrosion rate measurements to calculate the thermodynamic parameters related to the adsorption of the corrosion inhibitor. The degree of surface coverage (θ) was evaluated from gravimetric measurements at 298–338 K in the normal HCl solution at different inhibitor concentrations and graphically analyzed to match the most appropriate adsorption isotherm.

The curves of C_{inb}/θ plotted against C_{inb} at temperatures of 298, 308, 318, 328, and 338 K yield a linear graph (Figure 13) with a slope approximately equal to one, suggesting that the studied product, **IPM-H**, adheres to the Langmuir adsorption isotherm.

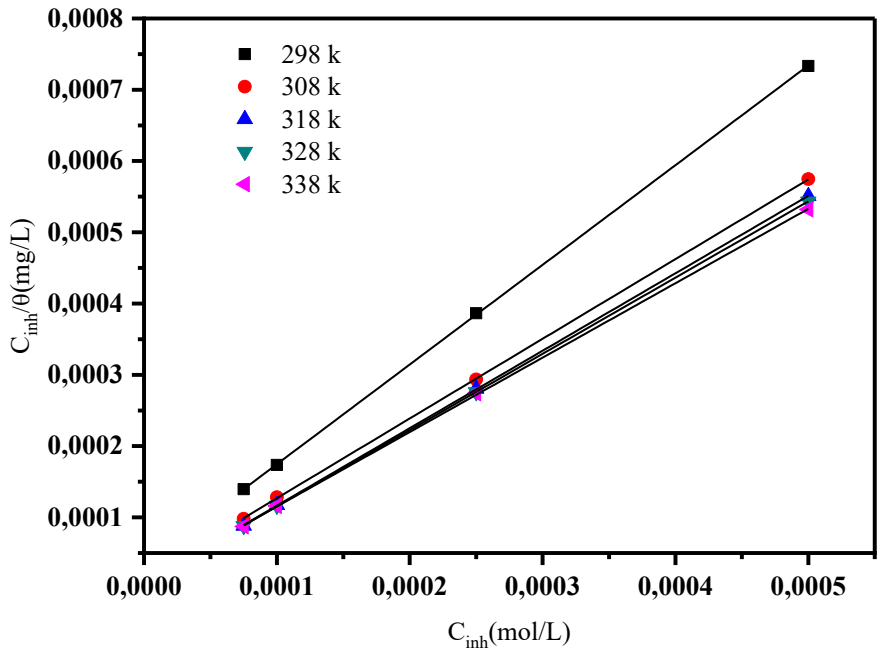

Figure 13: Isotherm of **IPM-H** adsorption on mild steel in 1M hydrochloric acid solution at different temperature conditions

We were thus able to deduce the values of the adsorption constant K and the values of the standard free energy of adsorption (ΔG_{ads}).

As a result, we were able to determine the values of the adsorption constant K and the standard free energy of adsorption (ΔG_{ads}).

Table 13: Thermodynamic parameters for the adsorption of **IPM-H** on mild steel at temperatures ranging from 298 to 338 K in 1N HCl.

T (K)	R^2	K_{ads}	ΔH_{ads}(kj/mol)	ΔS_{ads}	ΔG_{ads} (KJ/mol)
298	0,99996	28748,2589	-104,90597	-0,23329	-35,38646
308	0,99996	66411,10032		-0,2149	-38,71797
318	0,99997	128148,01016		-0,19872	-41,71291
328	0,99998	117822,21446		-0,18936	-42,79554
338	0,99989	91900,34243		-0,18196	-43,40205

The values of the recovery rate, θ, have been plotted. For the **IPM-H** inhibitor, the C_{inh}/θ curve against concentration exhibits a linear relationship, with R^2 (correlation coefficients) approximately equal to unity. This indicates that the Langmuir isotherm is followed for the adsorption on the mild steel surface.

The computed ΔG_{ads} values for **IPM-H** are nearly −40 kJ/mol. This indicates that electron sharing or transfer occurs between the anticorrosive molecules and the metal surface, resulting in bond formation. Consequently, this process is categorized as chemisorption.

e. Thermodynamic parameters of IPM-H corrosion

Graphs showing the variation in the logarithm of the corrosion rate (LnW) against the inverse of temperature (1/T) are utilized to evaluate the pre-exponential factor (A) and activation energies (E_a) (Figure 14).

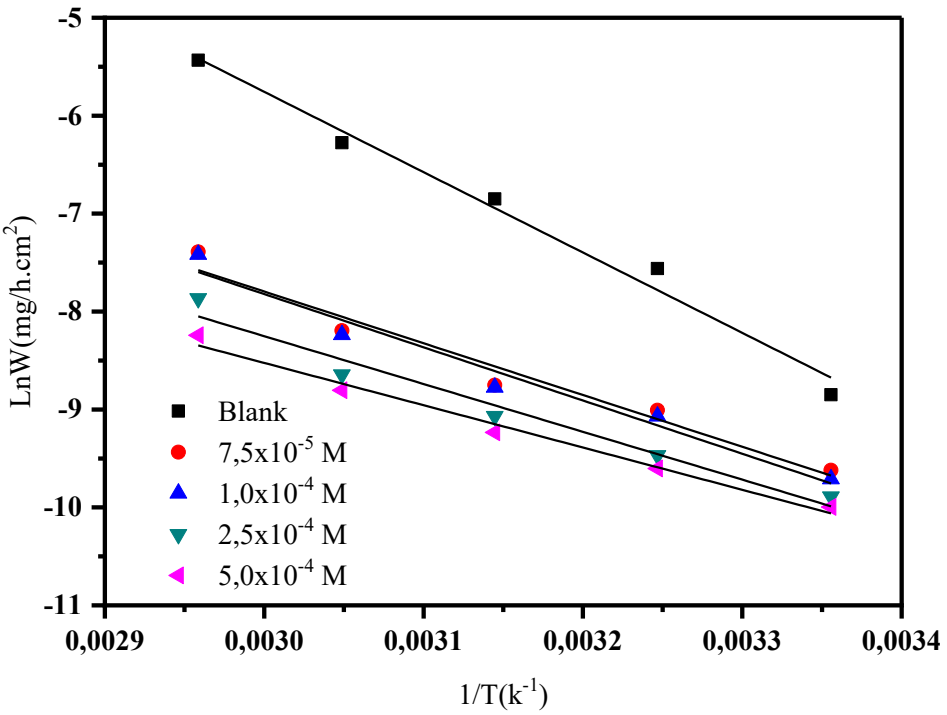

Figure 14: Arrhenius diagrams for mild steel in normal HCl solution in the absence and presence of **IPM-H** at different temperatures and concentrations.

Figure 15 shows the variation of Ln (W_{corr}/T) plotted against 1/T for the solution without inhibitor (blank) and for the various concentrations of the **IPM-H** inhibitor.

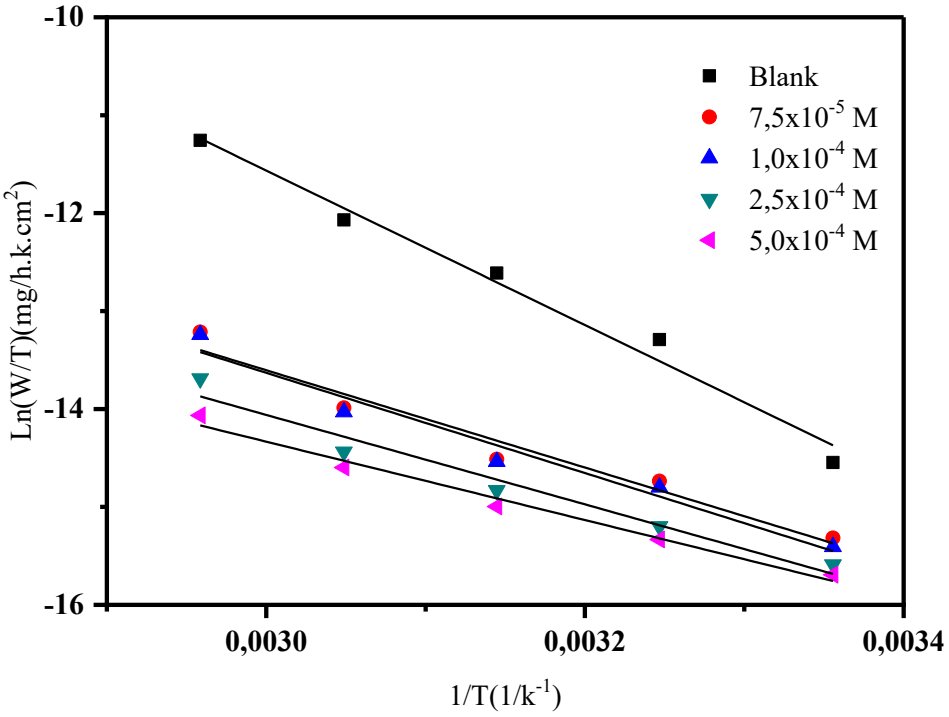

Figure 15: Variations of Ln (Wcorr/T) plotted against of 1/T with and without the presence of **IPM-H**.

Thermodynamic parameters, including activation entropy (ΔS_a), activation enthalpy (ΔH_a), and, activation energy (E_a), were derived from the Arrhenius equation (Table 14). All plots show correlation coefficients (R^2) close to unity across different concentrations of **IPM-H**. The slope of each plot represents $\Delta H/RT$, while the y-intercept corresponds to LnA. These plots allowed us to evaluate the values of ΔS and ΔH, which are summarized in Table 14. This analysis suggests that the corrosion of mild steel in 1M hydrochloric solution adheres to the kinetic model

From the slope calculations derived from the obtained plots, the following observations can be made:

- E_a (solution with inhibitor) < E_a (solution without inhibitor), indicating that **IPM-H** effectively reduces corrosion.
- The inhibition efficiency (IE) rises with increased temperatures and concentrations when **IPM-H** is present, highlighting its strong effectiveness at elevated conditions, which is a hallmark of efficient inhibitors.

These kinds of bonds are capable of withstanding corrosion at elevated temperatures, indicating chemisorption accompanied by the development of a chemical adsorption layer on the mild steel surface.

Table 15 presents the following results:

- The ΔS parameter for the reaction including the dissolution of mild steel in a normal HCl solution with **IPM-H** is inferior to the solution of hydrochloric acid alone. This suggests that the presence of this molecule influences the reaction dynamics, possibly reflecting decreased corrosion rates.
- All enthalpy values (ΔH_a) are positive, demonstrating the endothermic nature of the deterioration mechanism for mild steel.
- It is observed that the difference value of (Ea - ΔH) shows a similar variation across all concentrations, confirming the thermodynamic relationship between ΔH and E_a.

Table 15: Changes in activation enthalpy (ΔH_a), activation energy (E_a), and activation entropy (ΔS_a) considering temperature and concentration, for both the presence and absence **IPM-H.**

	R^2	E_a (KJ)	R^2	ΔH (KJ)	E_a-ΔH	ΔS	ΔGK (J/mol)
Blank	0,97978	68,21	0,978	65,58	2,63609	-96,945	28,95527
$7,5x10^{-5}$	0,95209	43,94	0,94647	41,30	2,63609	-186,73	57,55485
10^{-4}	0,95856	45,17	0,95384	42,54	2,63609	-183,24	58,31433
$2,5x10^{-4}$	0,95654	40,59	0,95108	37,96	2,63609	-200,55	65,82082
$5x10^{-4}$	0,98068	35,90	0,97802	33,27	2,63609	-216,90	73,34567

IV. Conclusions

From all the results, it can be deduced that:

1. The totality of the examined imidazo-heterocycles has demonstrated remarkable potency in reducing the corrosion of mild steel in a normal hydrochloric acid solution. The inhibitory effectiveness of each tested compound was found to increase with the addition of higher amounts of imidazo[1,2-a]pyridines/pyrimidines to the corrosive system.

2. The potency of these molecules was observed even under high-temperature conditions and was evident after five hours of immersion.
3. From the inhibition efficiency (IE) of imidazo[1,2-a]pyridines (**IP**) and imidazo[1,2-a]pyrimidines (**IPM**), it is evident that these molecules form a film that adsorbs onto the alloy surface, generating a passive layer that prevents the electrochemical processes responsible for corrosion.
4. **IP** and **IPM** followed the Langmuir isotherm as indicated by the gravimetric results. The maximum inhibition was exhibited at 5 x 10^{-4} M, attaining 93.48% and 93,98 at 338 K for **IP-H** and **IPM-H,** respectively.
5. The immersion effect of our eight organic heterocycles, namely **IP-H, IP-F, IP-Cl, IP-Br, IPM-H, IPM-F, IPM-Cl,** and **IPM-Br** was studied by keeping the temperature at 308 K and the concentration at 5 x 10^{-4} M constant while changing the immersion time (1, 2, 3, 4, 5, 6, and 24 hours). It was observed that the anticorrosive activity of the total compounds in study increased with increasing time to attain its maximum at five hours. After this, a small reduce in anticorrosive power is observed over time.
6. In addition, inhibitory efficiency for imidazo[1,2-a]pyridine derivatives follows the deceasing pattern : **IP-Br** > **IP-Cl** > **IP-F** > **IP-H** implying that the presence of a bromine substituent significantly boosts the inhibitory power.
7. On the other hand, this order changes for the imidazo[1,2-a]pyrimidine compounds to **IPM-Cl** > **IPM-Br** > **IPM-H** > **IPM-F** suggesting that the inclusion of a chlorine substituent significantly augments the inhibitory capability.
8. The negative value of the adsorption energy (ΔG_{ads}) indicates that a spontaneous process occurs for **IP** and **IPM**, requiring a chemisorption mechanism.
9. The results of the thermodynamic parameters confirm the % IE findings from gravimetric measurements corroborating that **IP** and **IPM** are powerful corrosion inhibitors for mild steel in 1M HCl solutions.

References:

[1] M. Yadav, D. Behera, and S. Kumar, “Experimental and theoretical investigation on adsorption and corrosion inhibition properties of imidazopyridine derivatives on mild steel in hydrochloric acid solution,” *Surf. Interface Anal.*, vol. 46, no. 9, pp. 640–652, 2014, doi: 10.1002/sia.5641.

[2] A. Ghazoui *et al.*, “Inhibitive effect of imidazopyridine derivative towards corrosion of C38 steel

in hydrochloric acid solution," *Res. Chem. Intermed.*, vol. 39, no. 6, pp. 2369–2377, 2013, doi: 10.1007/s11164-012-0763-y.

[3] R. T. Loto, "Anti-corrosion performance of the synergistic properties of benzenecarbonitrile and 5-bromovanillin on 1018 carbon steel in HCl environment," *Sci. Reports 2017 71*, vol. 7, no. 1, pp. 1–10, Dec. 2017, doi: 10.1038/s41598-017-17867-0.

[4] M. Goyal, S. Kumar, I. Bahadur, C. Verma, and E. E. Ebenso, "Organic corrosion inhibitors for industrial cleaning of ferrous and non-ferrous metals in acidic solutions: A review," Apr. 2018. doi: 10.1016/j.molliq.2018.02.045.

[5] W. Zhang, H. J. Li, M. Wang, L. J. Wang, A. H. Zhang, and Y. C. Wu, "Highly effective inhibition of mild steel corrosion in HCl solution by using pyrido[1,2-a]benzimidazoles," *New J. Chem.*, vol. 43, no. 1, pp. 413–426, 2019, doi: 10.1039/C8NJ04028A.

[6] Z. Y. Liu, D. Wang, D. T. Li, and H. Q. Wang, "The inhibition efficiencies of some organic corrosion inhibitors of iron: An insight from density functional theory study," *Comput. Theor. Chem.*, vol. 1214, no. May, p. 113759, 2022, doi: 10.1016/j.comptc.2022.113759.

[7] P. B. Raja *et al.*, "Reviews on Corrosion Inhibitors: A Short View," *Chem. Eng. Commun.*, vol. 203, no. 9, pp. 1145–1156, 2016, doi: 10.1080/00986445.2016.1172485.

[8] V. Hemapriya, M. Prabakaran, K. Parameswari, S. Chitra, S. H. Kim, and I. M. Chung, "Dry and wet lab analysis on benzofused heterocyclic compounds as effective corrosion inhibitors for mild steel in acidic medium," *J. Ind. Eng. Chem.*, vol. 40, pp. 106–117, 2016, doi: 10.1016/j.jiec.2016.06.013.

[9] A. Peter, I. B. Obot, and S. K. Sharma, "Use of natural gums as green corrosion inhibitors: an overview," *Int. J. Ind. Chem.*, vol. 6, no. 3, pp. 153–164, 2015, doi: 10.1007/s40090-015-0040-1.

[10] M. Abd El-Raouf, E. A. Khamis, M. T. H. Abou Kana, and N. A. Negm, "Electrochemical and quantum chemical evaluation of new bis(coumarins) derivatives as corrosion inhibitors for carbon steel corrosion in 0.5 M H2SO4," *J. Mol. Liq.*, vol. 255, pp. 341–353, 2018, doi: 10.1016/j.molliq.2018.01.148.

[11] A. E. A. S. Fouda, S. E. H. Etaiw, and S. Sobhy, "Metal-organic frameworks based on heterocyclic ligands and some transition metals as effective carbon steel corrosion inhibitors in aqueous environment," *J. Mol. Liq.*, vol. 348, p. 118402, 2022, doi: 10.1016/j.molliq.2021.118402.

[12] G. Serdaroğlu and S. Kaya, "Organic and Inorganic Corrosion Inhibitors," *Org. Corros. Inhib. Synth. Charact. Mech. Appl.*, pp. 59–73, Nov. 2021, doi: 10.1002/9781119794516.CH4.

[13] L. O. Olasunkanmi, I. B. Obot, M. M. Kabanda, and E. E. Ebenso, "Some quinoxalin-6-yl derivatives as corrosion inhibitors for mild steel in hydrochloric acid: Experimental and theoretical studies," *J. Phys. Chem. C*, vol. 119, no. 28, pp. 16004–16019, 2015, doi: 10.1021/acs.jpcc.5b03285.

[14] H. Elmsellem *et al.*, "Quantum chemical studies and corrosion inhibitive properties of mild steel by some pyridine derivatives in 1 N HCL solution," *Port. Electrochim. Acta*, vol. 32, no. 2, pp. 77–108, 2014, doi: 10.4152/pea.201402077.

[15] K. Babić-Samardžija, K. F. Khaled, and N. Hackerman, "N -heterocyclic amines and derivatives as corrosion inhibitors for iron in perchloric acid," *Anti-Corrosion Methods Mater.*, vol. 52, no. 1, pp. 11–21, Feb. 2005, doi: 10.1108/00035590510574871.

[16] L. Tan, J. Li, and X. Zeng, "Revealing the Correlation between Molecular Structure and Corrosion Inhibition Characteristics of N-Heterocycles in Terms of Substituent Groups," *Materials (Basel).*, vol. 16, no. 6, 2023, doi: 10.3390/ma16062148.

[17] E. Ech-chihbi *et al.*, "Experimental and computational studies on the inhibition performance of the organic compound '2-phenylimidazo [1,2-a]pyrimidine-3-carbaldehyde' against the corrosion of carbon steel in 1.0 M HCl solution," *Surfaces and Interfaces*, vol. 9, pp. 206–217, 2017, doi: 10.1016/j.surfin.2017.09.012.

[18] A. EL AATIAOUI *et al.*, "Experimental and theoretical study of new Schiff bases based on imidazo(1,2-a)pyridine as corrosion inhibitor of mild steel in 1M HCl," *J. Mol. Struct.*, vol. 1226, 2021, doi: 10.1016/j.molstruc.2020.129372.

[19] N. I. F. Idelfitri, N. N. Dzulkifli, N. A. N. Ash'ari, S. Sapari, F. I. Abdul Razak, and N. H. Pungot, "Synthesis, characterisation and corrosion inhibitory study of Meldrum's acid Thiosemicarbazone: Weight Loss, SEM-EDX and DFT," *Inorg. Chem. Commun.*, vol. 150, no. September 2022, pp. 1–11, 2023, doi: 10.1016/j.inoche.2023.110485.

[20] O. Id El Mouden *et al.*, "Anti-corrosive properties of two new green heterocyclic azole derivatives on C38 steel in 1 M (HCl) medium, experimental and theoretical study," *Results Chem.*, vol. 5, no. November 2022, p. 100641, Jan. 2023, doi: 10.1016/j.rechem.2022.100641.

[21] A. zaid, S. Merdas, and M. Hayal, "Heterocyclic Compounds Containing N atoms as Corrosion Inhibitors: A review," *J. Biosci. Appl. Res.*, vol. 7, no. 2, pp. 93–103, 2021, doi: 10.21608/jbaar.2021.178505.

[22] R. C. da S. Lessa, "Synthetic Organic Molecules as Metallic Corrosion Inhibitors: General Aspects and Trends," *Organics*, vol. 4, no. 2, pp. 232–250, 2023, doi: 10.3390/org4020019.

[23] M. A. Quraishi, D. S. Chauhan, and V. S. Saji, "Heterocyclic biomolecules as green corrosion

inhibitors," *J. Mol. Liq.*, vol. 341, p. 117265, 2021, doi: 10.1016/j.molliq.2021.117265.

[24] D. S. Zinad *et al.*, "A new synthesized coumarin-derived schiff base as a corrosion inhibitor of mild steel surface in hcl medium: Gravimetric and dft studies," *Int. J. Corros. Scale Inhib.*, vol. 9, no. 1, pp. 228–243, 2020, doi: 10.17675/2305-6894-2020-9-1-14.

[25] S. Ayob *et al.*, "A Review on Adsorption of Heavy Metals from Wood-Industrial Wastewater by Oil Palm Waste," *J. Ecol. Eng.*, vol. 22, no. 3, pp. 249–265, Mar. 2021, doi: 10.12911/22998993/132854.

[26] A. D. Usman and L. N. Okoro, "A Review : Weight Loss Studies on the Corrosion Behavior of Some Metals in Various Media," vol. 4, no. 13, pp. 17–24, 2015.

[27] T. Attar, A. Benchadli, and E. Choukchou-Braham, "Corrosion inhibition of carbon steel in perchloric acid by potassium iodide," *Int. J. Adv. Chem.*, vol. 7, no. 1, pp. 35–41, May 2019, doi: 10.14419/ijac.v7i1.19651.

[28] E. Ech-chihbi *et al.*, "Effect of some imidazopyridine compounds on carbon steel corrosion in hydrochloric acid solution," *Der Pharma Chem.*, vol. 8, no. 13, pp. 214–230, 2016.

[29] R. Salim, E. Ech-chihbi, H. Oudda, F. El Hajjaji, M. Taleb, and S. Jodeh, "A Review on the Assessment of Imidazo[1,2-a]pyridines As Corrosion Inhibitor of Metals," *J. Bio- Tribo-Corrosion*, vol. 5, no. 1, p. 0, 2019, doi: 10.1007/s40735-018-0207-3.

[30] Y. Li, D. Wang, and L. Zhang, "Experimental and theoretical research on a new corrosion inhibitor for effective oil and gas acidification," *RSC Adv.*, vol. 9, no. 26464, pp. 26464–26475, 2019, doi: 10.1039/c9ra04638k.

[31] A. A. Al-Amiery, Y. K. A. -Majedy, A. A. H. Kadhum, and A. B. Mohamad, "New coumarin derivative as an eco-friendly inhibitor of corrosion of mild steel in acid medium," *Molecules*, vol. 20, no. 1, pp. 366–383, 2015, doi: 10.3390/molecules20010366.

[32] A. S. Fouda, F. I. El-dossoki, A. El-hossiany, and E. A. Sello, "Adsorption and Anticorrosion Behavior of Expired Meloxicam on Mild Steel in Hydrochloric Acid Solution," *Surf. Engeneering Appl. Electrochem.*, vol. 56, no. 4, pp. 491–500, 2020, doi: 10.3103/S1068375520040055.

[33] Z. Bensouda, E. Hassan, E. Assiri, M. Sfaira, M. Ebn, and T. Abdellah, "Extraction , Characterization and Anticorrosion Potential of an Essential Oil from Orange Zest as Eco - friendly Inhibitor for Mild Steel in Acidic Solution," *J. Bio- Tribo-Corrosion*, vol. 5, no. 84, pp. 1–20, 2019, doi: 10.1007/s40735-019-0276-y.

[34] M. Nasibi *et al.*, "Journal of Adhesion Science and Nanosized scale roughness and corrosion

protection of mild steel in hydrochloric acid solution and in the presence of Turmeric (Curcuma Longa) Extract as a green corrosion inhibitor : FTIR , polarization , EIS , SEM , EDS," *J. Adhes. Sci. Technol.*, vol. 28, no. December 2014, pp. 2001–2015, 2014, doi: 10.1080/01694243.2014.941053.

[35] B. Chugh, A. K. Singh, A. Chaouiki, R. Salghi, S. Thakur, and B. Pani, "Jo u rn Pr," *J. Mol. Liq.*, vol. 299, p. 112160, 2019, doi: 10.1016/j.molliq.2019.112160.

[36] R. Saadi, Z. Saadi, R. Fazaeli, and N. E. Fard, "Monolayer and multilayer adsorption isotherm models for sorption from aqueous media," *Korean J. Chem. Eng*, vol. 32, no. 5, pp. 787–799, 2015, doi: 10.1007/s11814-015-0053-7.

[37] T. Attar, A. Benchadli, B. Messaoudi, N. Benhadria, and E. Choukchou-Braham, "Experimental and theoretical studies of eosin Y dye as corrosion inhibitors for carbon steel in perchloric acid solution," *Bull. Chem. React. Eng. Catal.*, vol. 15, no. 2, pp. 454–464, 2020, doi: 10.9767/bcrec.15.2.7753.454-464.

[38] K. Parashar and R. K. Dubey, "THERMODYNAMIC STUDY OF GREEN CORROSION INHIBITOR ON MILD STEEL WITH AQUEOUS EXTRACT OF ZIZIPHUS JUJUBA STEM IN 1M HCL SOLUTION," vol. XLVI, no. 1, pp. 17–28, 2020.

[39] A. Al-amiery, T. A. Salman, K. F. Alazawi, L. M. Shaker, A. A. H. Kadhum, and M. S. Takriff, "Quantum chemical elucidation on corrosion inhibition efficiency of Schiff base : DFT investigations supported by weight loss and SEM techniques," *Int. J. Low-Carbon Technol.*, vol. 00, pp. 1–8, 2019, doi: 10.1093/ijlct/ctz074.

[40] S. Issaadi, T. Douadi, A. Zouaoui, S. Chafaa, M. A. Khan, and G. Bouet, "Novel thiophene symmetrical Schiff base compounds as corrosion inhibitor for mild steel in acidic media," *Corros. Sci.*, vol. 53, no. 4, pp. 1484–1488, 2011, doi: 10.1016/j.corsci.2011.01.022.

[41] K. Benchekroun *et al.*, "Inhibition de la corrosion du fer dans HCl 1 M . Part I . E ´ nol et du 2-aminophe ´ nyl disulfure 1 ' effet inhibiteur du 2-aminothiophe," pp. 153–159, 2002, doi: 10.1039/b105859m.

[42] B. Zerga *et al.*, "Adsorption and corrosion inhibition of some tripodal compounds for mild steel in molar hydrochloric acid medium , Adsorption and corrosion inhibition of some tripodal compounds for mild steel in molar hydrochloric acid medium," *Der Pharma Chem. Chem.*, vol. 4, no. 5, pp. 1887–1896, 2012.

[43] A. C. Mauro, B. D. Ribeiro, R. Garrett, and R. M. Borges, "Ziziphus joazeiro Stem Bark Extract as a Green Corrosion Inhibitor for Mild Steel in Acid Medium," *MDPI precesses*, vol. 9, no. 1323, pp. 0–22, 2021, doi: 10.3390/pr9081323.

[44] L. A. Al Juhaiman, "Polyvinyl pyrrolidone as a corrosion inhibitor for carbon steel in HCl," *Int. J. Electrochem. Sci.*, vol. 11, no. 3, pp. 2247–2262, 2016, doi: 10.1016/s1452-3981(23)16098-6.

[45] G. Giselle, O. Olivares-xometl, P. Arellanes-lozada, N. V Likhanova, I. V Lijanova, and J. Arriola-morales, "Temperature Effect on the Corrosion Inhibition of Carbon Steel by Polymeric Ionic Liquids in Acid Medium," *Int. J. Mol. Sci.*, vol. 24, no. 6291, pp. 1–29, 2023, doi: 10.3390/ijms24076291.

[46] K. Cao, W. Huang, X. Huang, and J. Pan, "Imidazo [1,2-a] Pyrimidine Derivatives as Effective Inhibitor of Mild Steel Corrosion in HCl Solution: Experimental and Theoretical Studies," *Front. Mater.*, vol. 9, no. March, pp. 1–16, 2022, doi: 10.3389/fmats.2022.843522.

CHAPTER 3: B-BIOLOGICAL STUDY

B- Biological Study

1. Introduction

Through the bibliographic study in chapter 1, we have indicated the critical place occupied by both imidazo[1,2-a]pyridines (**IPs**) and imidazo[1,2-a]pyrimidines (**IPMs**) in the search for bioactive molecules. These biological activities change principally based on the position and nature of the substituents on the heterocyclic framework. In this case, in our work, we seek to synthesize products and we aim to evaluate the antimicrobial inhibitory activities of all prepared imidazo[1,2-a]pyridine and imidazo[1,2-a]pyrimidine derivatives through *in vitro* studies.

2. Bibliographic Study

2.1. Introduction

Over the past several decades, many outbreaks have taken place worldwide, including bacterial, fungal, viral, and parasitic infections, which have become an increasing concern for personal health, causing great economic losses for hospitals [1,2]. Antimicrobial resistance has emerged as a critical issue in recent years ant it arises when bacteria, fungi, and viruses no longer respond successfully to drugs, complicating infection treatment, increasing the risk of disease spread, and potentially leading to death [3]. Consequently, substantial efforts have been devoted to developing synthetic methods for producing diverse antimicrobial compounds [4–6]. The increasing occurrence of these outbreaks, coupled with the escalation in antimicrobial resistance, has intensified the need for new and potent antimicrobial treatments. Therefore, it is important to develop new approaches and strategies to overcome the issue of increasing antimicrobial resistance [7]. The evaluation of the antimicrobial activity of all the products was evaluated using the well diffusion method.

2.2. Solid medium diffusion methods

In the existing studies, many methods have been used for the assessment of antimicrobial activity. We will note here the two most used protocols:

a. Diffusion method by disk method

The disk diffusion technique is based on applying test products of known concentration onto Whatman paper disks or filter paper. These disks are then placed on a solid culture medium in Petri dishes that have been pre-inoculated with a bacterial strain. The dishes are incubated under conditions suited to the microorganism being studied. As the agent diffuses, its concentration gradually decreases, forming a concentration gradient around the disks. After incubation, in case the substance on the disks exhibits antimicrobial activity against the targeted organism, a clear zone of growth inhibition will be visible around each disk [8].

b. Diffusion method by well or cylinder method

This technique enables radial diffusion of the tested products from a well measuring six to seven mm in diameter, resulting in a distinct and readily measurable inhibition zone. Specifically, the method involves creating a vertical circular well in the agar and adding a solution of the compounds at a known concentration. The solution diffuses radially, producing a circular inhibition zone on the agar surface, which has been pre-seeded with a bacterial suspension. After incubation, the diameters of the inhibition zones around the wells are measured. This technique, which we employed in our study, is effective for estimating antimicrobial potency, especially for compounds with strong diffusion in solid media [9].

2.3. Studied Micro-organisms

To provide a comprehensive view of the biological activity scope of our products, a diverse selection of microorganisms was chosen, including six pathogenic Gram-positive bacteria, four pathogenic Gram-negative bacteria and three pathogenic fungi. The strains used are as shown below:

2.3.a. Gram-positive Bacteria

- ***Staphylococcus aureus*** [10]: Commonly known as *Staphylococcus aureus* and regarded as the most pathogenic species within the *Staphylococcus* genus, , these bacteria are Gram-positive cocci (spherical bacteria).They can sometimes cause wound or skin infections (such as boils) and, more rarely, lead to bloodstream infections or pneumonia.
- ***Micrococcus luteus*** [11]: Gram-positive, saprophytic, spherical bacterium attributed to the *Micrococcaceae* family. An obligatory anaerobe, *M. luteus* is commonly found in water, air, soil and dust and is also constituent of the skin microbiome in mammals.

- ***Listeria monocytogenes*** [12]: This pathogenic bacterium is responsible for the infection listeriosis. It is a facultative anaerobe, able to survive without or with oxygen. Capable of growing and reproducing within host cells, it ranks among the most virulent foodborne pathogens. In high-risk individuals, 20-30% of foodborne listeriosis cases can be fatal.
- ***Bacillus cereus*** [13]: This Gram-positive, rod-shaped bacterium is commonly found in food, marine sponges, and soils. Its species name, *cereus*, meaning "waxy" in Latin, refers to the colony's appearance when grown on blood agar. Some strains are pathogenic to humans, causing foodborne illnesses because of their spore-forming nature, while others offer benefits as animal probiotics or display mutualistic relationships with certain plants. *B. cereus* can be either facultatively anaerobic or aerobic and, like other *Bacillus* species, has the ability to form resistant endospores.
- ***Enterococcus faecalis*** [14]: These Gram-positive, oval-shaped bacteria belong to the group D streptococcus family and are typically found in the intestines of healthy individuals, as well as in the throat and on the skin. While normally harmless, they can cause various infections, particularly in hospital settings, making them a common source of nosocomial infections.

2.3.b. Gram-negative Bacteria

- ***Escherichia coli*** [15]: Also known as *E. coli*, this bacterium is commonly found in the human intestine and is generally harmless, forming part of our natural gut flora. However, certain strains of *E. coli* can cause gastroenteritis or urinary tract infections, and some pathogenic strains primarily lead to infections affecting the digestive tract.
- ***Pseudomonas aeruginosa*** [16]: this Gram-negative bacterium belongs to the *Pseudomonaceae* family, and commonly found in plants, soils, and both marine and freshwater environments. It is often implicated in nosocomial infections and is pathogenic, capable of causing lung and eye infections, as well as infections from burns. Its resistance to many antibiotics and antiseptics contributes to its growing presence in hospital settings.
- ***Klebsiella pneumoniae*** [17]: This rod-shaped, non-motile, encapsulated bacterium is facultatively anaerobic and ferments lactose. On MacConkey agar, it appears as a mucoid lactose fermenter. While it is part of the normal flora in the mouth, skin, and intestines, it can cause severe damage to the lungs if aspirated, particularly affecting the alveoli and leading to the production of bloody, brownish, or yellow jelly-like sputum.

2.3.c. Yeasts

- ***Candida albicans*** [18,19]: It is an opportunistic fungal pathogen commonly found in the human gut flora, and is capable of surviving outside the human body. Present in the gastrointestinal tract and mouth of 40-60% of healthy adults, it typically exists as a commensal organism. However, under certain conditions, particularly in immunocompromised individuals, it can become pathogenic. This yeast is one of the few species of *Candida* responsible for causing candidiasis, an infection that results from its overgrowth. Several strains of this species are cataloged in the ATCC, and we have selected three of them for further study.

3. Materials and Methods

3.1. Methodologies for Evaluating Antimicrobial Activity

The antimicrobial activity of all synthesized imidazo[1,2-*a*]pyridines and imidazo[1,2-*a*]pyrimidines was screened *in vitro* by using the disk diffusion protocol as described by Nariya *et al.* [20] against 13 microorganisms, namely:

- six Gram-positive bacteria,
- four Gram-negative bacteria and
- three yeasts (Table 2).

Table 2: Microorganism strains and their corresponding American Type Culture Collection (ATCC) numbers.

<table>
<tr><th colspan="6">Gram-positive Bacteria</th></tr>
<tr><td>Staphylococcus aureus ATCC 25923</td><td>Micrococcus luteus ATCC 9341</td><td>Listeria monocytogenes ATCC 15313</td><td>Bacillus cereus ATCC 10876</td><td>Bacillus subtilis ATCC6633</td><td>Enterococcus faecalis ATCC29212</td></tr>
<tr><th colspan="6">Gram-negative Bacteria</th></tr>
<tr><td>Escherichia coli ATCC 25912</td><td>Pseudomonas aeruginosa ATCC 27853</td><td colspan="2">Klebsiella pneumoniae ATCC 700603</td><td colspan="2">Salmonella typhimurium ATCC 13311</td></tr>
<tr><th colspan="6">Yeasts</th></tr>
<tr><td colspan="2">Candida albicans ATCC 26790</td><td colspan="2">Candida albicans ATCC 10231</td><td colspan="2">Candida albicans IPP 444</td></tr>
</table>

The species were maintained on nutrient agar, with each species being activated, 24 hours prior, on the agar medium to performing the antibacterial and antifungal tests. In the following, we outline the *in vitro* methods used to evaluate the antimicrobial activity of all prepared **IPs** and **IPMs**.

3.2. Preparation of microbial suspensions and inoculation process

Microbial suspensions are prepared by transferring bacterial species from enrichment broths (TCBS) onto solid culture media. For bacterial strains, the inoculation is performed on MHA (Müeller-Hinton-Agar) medium, while for fungal strains, YPGA (Yeast, Peptone-Glucose-Agar) medium is used. The cultures are incubated for 24 hours at 37°C for bacterial strains and for 48 hours at 30°C for fungal strains. Once colonies are grown, a few isolated colonies are selected and transferred into physiological water, adjusting the turbidity to 0.5 McFarland standard, corresponding to a microbial density of approximately 5 x 106 colony forming units/mL for bacteria and to 5 x 105 colony forming units/mL for yeast measured at 620 nm. A portion of this suspension (10 µl) is then utilized to inoculate new Petri dishes, where different inoculation methods, such as swabbing or flooding, are applied to ensure even distribution.

For the swabbing method, a dry, sterile swab is immersed in the prepared bacterial suspension, then gently pressed against the walls of the container to remove excess liquid. The MHA medium in the Petri dish is inoculated by starting at the edge and moving the swab across the entire surface in a left-to-right motion. The dish is rotated 60° after each pass, repeating this procedure three more times to ensure full coverage. The Petri dishes are then left to air dry at room temperature for a few minutes with the lid securely in place. Ensuring a consistent agar thickness of precisely 4 mm across the dish surface is essential.

3.3.Well diffusion method

The MHA medium is poured into a Petri dish to a thickness of 8 mm. Following flood inoculation with an appropriate dilution (approximately 5 x 106 colony forming units/mL for bacteria and to 5 x 105 colony forming units/mL for yeast measured at 620 nm) of the test microorganism, adjusted according to the MacFarland scale, 6 mm diameter wells are created. Into each well, 50 mg/ml of the test compounds dissolved in DMSO are added. After a 45-minute pre-diffusion under the hood and at room temperature, the plates are incubated at 37°C for bacteria and yeast. Finally, the diameters of the inhibition zones are measured and recorded in millimeters.

3.4. Determination of the MIC

The Minimum Inhibitory Concentration (MIC) is the lowest concentration of an antibiotic (measured in µg/ml) that completely prevents bacterial growth. It is determined using an antibiogram, which helps assess the effectiveness of antibacterial agents *in vivo*. The MIC is calculated through standardized methods based on international guidelines, allowing for the comparison of bacterial species' sensitivity profiles. The bacterial inoculum, in liquid medium, is inoculated into Petri dishes or a series of tubes (macro-dilution method) containing varying concentrations of the antibiotic. After incubation, the Minimum Inhibitory Concentration is identified as the lowest concentration of antibiotic in which no visible bacterial growth occurs.

The active compounds were evaluated by determining their MIC on an ELISA plate, following the method described by Premsai Rai et al. [21], with slight modifications. Briefly, bacterial cultures were inoculated in Brain-Heart Infusion Broth (BHIB), and yeast cultures in Sabouraud Broth, and incubated at 37°C for 24 hours. The optical density was then adjusted to 5 x 106 colony-forming units (CFU)/mL for bacteria and 5 x 105 CFU/mL for yeast, measured at 620 nm.

Imidazo[1,2-a]pyridines

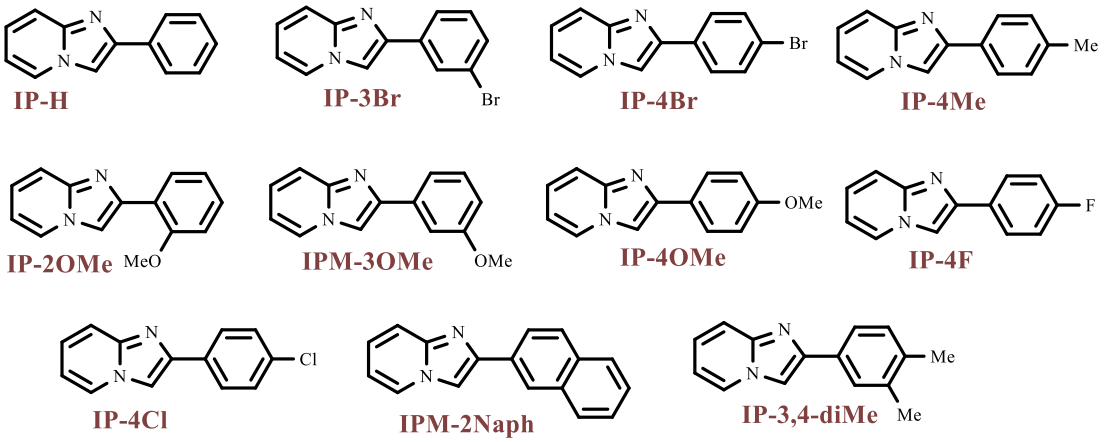

Imidazo[1,2-a]pyrimidines

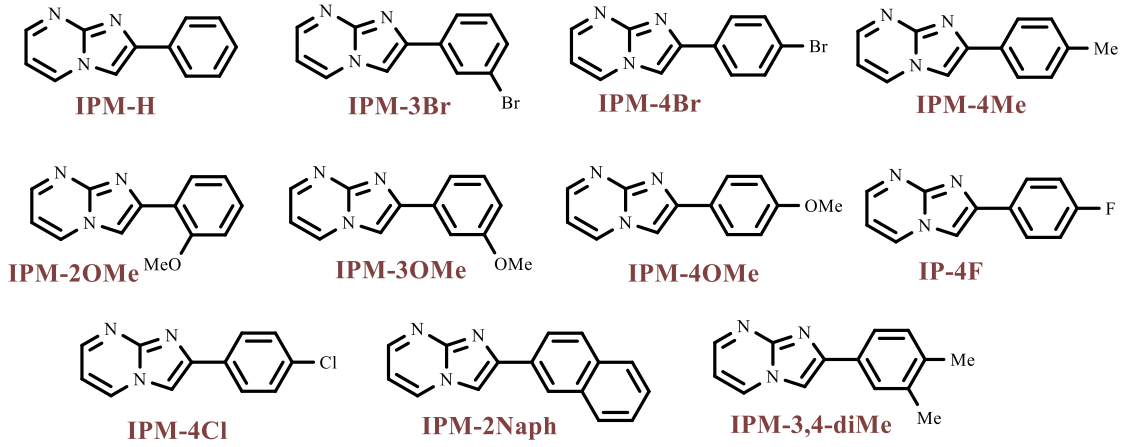

Scheme 1: Chemical structures of the heterocycles tested.

4. Results and Discussion

4.1. Imidazo[1,2-a]pyridine derivatives (IPs)

The antimicrobial activity of all tested **IPs** is mentioned in Table 3. Results indicate that compounds **IP-H, IP-3Br, IP-4Cl, IP-2Naph,** and **IP-3,4diMe** demonstrated significant activity against *C. albicans*, with inhibition zones ranging from 14±0.0 mm to 23.6±0.3 mm. Additionally, compounds **IP-H, IP-3Br, IP-2Naph,** and **IP-3,4diMe** exhibited moderate activity against *S. aureus, M. luteus, B. subtilis,* and *B. cereus*. However, only the **IP-3Br** compound showed a moderate activity against *E. coli* while none of the other compounds displayed activity against the Gram-negative bacteria, *E. faecalis*, or *L. monocytogenes*. Generally, Gram-positive bacteria appear to be more susceptible than Gram-negative bacteria,

likely due to differences in cell envelope structure. The Gram-positive cell wall, with its thick peptidoglycan layer, enables more effective penetration of active agents to target sites [22]. Structurally, it can be concluded that substituents with Br, Naph, Cl, and 3,4-diMe enhanced antimicrobial potency, while other substituents led to reduced activity.

The results presented in this chapter, including Tables 3 to 6, are taken from our published work in [23]

Table 3: Inhibition zones (in mm) of compounds **IPs** (concentration: 50 mg/mL of DMSO)

	Gram-positive Bacteria					
Products	***S. aureus***	***M. luteus***	***L. monocytogenes***	***E. faecalis***	***B. cereus***	***B. subtilis***
IP-H	**13.3±0.3**	**9.6±0.3**	/	**7.6±0.3**	**12.3±0.3**	**9.6±0.3**
IP-3Br	**11.6±0.3**	**10.3±0.3**	/	**7.6±0.3**	**12.6±0.3**	**14.3±0.3**
IP-4Br	/	/	/	/	/	/
IP-4Me	/	/	/	/	/	/
IP-2OMe	**6±0.6**	/	/	/	**7.3±0.3**	**6±0.6**
IP-3OMe	**6±0.6**	/	/	/	**10±0.6**	**6±0.6**
IP-4OMe	**6±0.6**	/	/	/	/	/
IP-4F	/	/	/	/	/	/
IP-4Cl	/	/	/	/	**9.3±0.3**	**6±0.6**
IP-2Naph	**17.3±0.3**	**19.6±0.3**	/	/	**12.6±0.3**	**11.6±0.3**
IP-3,4diMe	**10.6±0.3**	**15.3±0.3**	/	/	**10.6±0.3**	**11.3±0.3**

	Gram-negative Bacteria				Yeasts		
Products	***E. coli***	***K. pneumoniae***	***P. aeruginosa***	***S. typhymerium***	***C. albicans ATCC 26790***	***C. albicans ATCC 10231***	***C. albicans IPP 444***
IP-H	**7.3±0.3**	/	**7.6±0.3**	/	**21.6±0.3**	**19.6±0.3**	**23.6±0.3**
IP-3Br	**10.3±0.3**	/	**6.6±0.3**	/	**16.3±0.3**	**14±0.0**	**14±0.0**
IP-4Br	/	/	/	/	/	/	/
IP-4Me	/	/	/	/	**9±0.6**	/	**10±0.6**
IP-2OMe	/	/	/	/	/	/	/
IP-3OMe	/	/	/	/	/	/	/
IP-4OMe	/	/	/	/	/	/	/
IP-4F	/	/	/	/	/	/	**9.3±0.3**
IP-4Cl	/	/	/	/	**19.6±0.3**	/	**23±0.6**
IP-2Naph	/	/	/	/	**18.6±0.3**	**17.3±0.3**	**18.3±0.3**
IP-3,4diMe	/	/	/	/	**20.6±0.3**	**20.3±0.3**	**20.3±0.3**

The antimicrobial potency of compounds with an inhibitory zone of 12 mm or greater was further assessed by determining their Minimum Inhibitory Concentration (MIC) against sensitive microorganisms. A series of 10 serial dilutions were prepared from a concentration of 80 mg/mL, with each step halving the concentration of the stock solution. The results for the active compounds, summarized in Table 4, reveal MIC values ranging from 20 mg/mL to 0.625 mg/mL. Notably, compounds **IP-3,4DiMe** and **IP-3Br** showed strong activity against both *M. luteus* and *C. albicans*.

For some active imidazo[1,2-a]pyridines, the MBC values matched the MIC values, resulting in an MBC/MIC equal to 1, indicative of a bactericidal effect, in line with Payveld's findings [24]. Remarkably, the presence of a dimethyl group or a halogen, particularly Br, on the imidazo[1,2-a]pyridine rings increased activity.

Table 4: In-vitro MIC and MBC of active imidazo[1,2-a]pyridine derivatives.

Compounds	Antimicrobial threshold (mg/mL)	*S. aureus*	*M. luteus*	*B. cereus*	*B. subtilis*	*E. coli*	*C. albicans 26790*	*C. albicans 10231*	*C. albicans IPP 444*
IP-3Br	MIC	10	20	10	2.5	20	1.25	2.5	2.5
	MBC	20	20	10	5	20	2.5	1.25	2.5
IP-3,4diMe	MIC	10	2.5	10	10	/	0.625	0.625	0.625
	MBC	10	2.5	20	20	/	1.25	1.25	1.2
IP-4F	MIC	/	/	/	/	/	10	/	10
	MBC	/	/	/	/	/	10	/	20

4.2. Imidazo[1,2-a]pyrimidine derivatives (IPMs)

The antimicrobial potency of all tested IPMs is summarized in Table 4. The results demonstrate that compounds **IPM-H, IPM-4Br, IPM-4F, IPM-4OMe, IPM-2Naph,** and **IPM-3,4diMe** exhibited intense activity against *C. albicans* with inhibition zones ranging from 12.3±0,5 mm to 19.3±0,3 mm. Although compounds **IPM-4Br, IPM-2Naph,** and **IPM-3,4diMe** showed moderate activity against *S. aureus* and *M. luteus*, **IPM-4OMe** displayed excellent activity against *B. subtili*s (19.3±0,3 mm). Nevertheless, none of the compounds demonstrated activity against Gram-negative bacteria, *E. faecalis,* and *L. monocytogenes*. Generally, Gram-positive bacteria tend to be more sensitive than Gram-negative ones, likely due to differences in cell envelope composition. The Gram positive cell wall , which consists of a thick peptidoglycan layer, facilitates the penetration of active agents to their target sites [22]. Structurally, it can be concluded that para-directing substituents such as Br and OMe exhibited excellent antimicrobial potency; while, other substituents resulted in a decrease in activity.

Table 5: Inhibition zones of (in mm) of compounds **IPMs** (concentration: 50 mg/mL of DMSO)

	Gram-positive Bacteria					
Products	***S. aureus***	***M. luteus***	***L. monocytogenes***	***E. faecalis***	***B. cereus***	***B. subtilis***
IPM-H	**8.6±0.3**	**8.3±0.3**	/	/	/	**8.3±0.3**
IPM-3Br	**8.3±0.3**	/	/	/	/	/
IPM-4Br	**12.3±0.3**	**15.6±0.3**	/	/	**11±0.6**	**9.3±0.3**
IPM-4Me	/	/		/	/	/
IPM-2OMe	**8.6±0,3**	**9.6±0.3**		**7 ±0**	**7 ±0**	/
IPM-3OMe	**8.3±0.3**	**8±0.0**		/	**10.6±0.3**	**9.3±0.3**
IPM-4OMe	**12.6±0.3**	/	/	/	/	**19.3±0.3**
IPM-4F	**7.3±0.3**	/		/	**7 ±0.0**	**7±0.0**
IPM-4Cl	**8.6±0.3**	/	/	/	/	**7.6±0.3**
IPM-2Naph	**12.3±0.3**	**13.3±0.3**		/	**11.3±0.3**	**8.6±0.3**
IPM-3,4diMe	**10.6±0.3**	**9.3±0.3**		/	**12.3±0.3**	**9.3±0.3**

	Gram-negative Bacteria				Yeasts		
Products	***E. coli***	***K. pneumoniae***	***P. areuginosa***	***S. typhymerium***	***C. albicans ATCC 26790***	***C. albicans ATCC 10231***	***C. albicans IPP 444***
IPM-H	**8.6±0.3**	/	/	/	**9.6±0.3**	**15±1**	/
IPM-3Br	/	/	/	/	/	/	/
IPM-4Br	**6±0.0**	/	/	/	**13±0.57**	**18.3±0.6**	/
IPM-4Me	/	/	/	/	**8.6±0.3**	/	/
IPM-2OMe	/	/	/	/	/	/	/
IPM-3OMe	/	/	/	/	**10±0.5**	**11.6±0.3**	/
IPM-4OMe	/	/	/	/	**13±0.5**	**19.3±0.3**	/
IPM-4F	/	/	/	/	**14±0.57**	/	/
IPM-4Cl	/	/	/	/	/	/	/
IPM-2Naph	/	/	/	/	**15±0.3**	**12.3±0.5**	**14±0.5**
IPM-3,4diMe	/	/	/	/	**15.6±0.3**	**12.6±0.3**	**14.6±0.3**

The antimicrobial potency of active compounds, which exhibited an inhibitory zone of 12 mm or more, was evaluated against sensitive microorganisms to identify their MIC (Minimum Inhibitory Concentration). A series of ten serial dilutions was prepared from an initial concentration of 80 mg/m ml by reducing the stock solution in twofold steps. The outcomes for the active compounds are outlined in Table 6, which shows a range of MIC values between 20 mg/ml and 2.5 mg/ml. Compounds **IPM-4OMe, IPM-2Naph** and **IPM-3,4DiMe** demonstrated significant activity against *Candida albicans*, while compound **IPM-4OMe** showed efficacy against *B. subtilis*.

In the most active imidazo[1,2-a]pyrimidine compounds, MIC values were equivalent to MBC values, resulting in an MBC/MIC ratio of 1. This ratio of 1 indicates a bactericidal effect, consistent with the findings of Payveld [24].

Among the tested compounds, **IPM-2Naph** and **IPM-3,4diMe** exhibited the strongest antifungal activity, particularly against *Candida albicans* strains, with MIC values ranging from 2.5 to 5 mg/mL. The **IPM-4OMe** compound also demonstrated significant antibacterial activity against *B. subtilis* and moderate antifungal activity. In all active cases, the MBC values were equal to the MIC values, leading to an MBC/MIC ratio of 1, which indicates a bactericidal or fungicidal effect rather than a bacteriostatic one.

Overall, these results highlight the notable antimicrobial potential of the studied **IPM** derivatives, particularly against *C. albicans* and *B. subtilis*, confirming their relevance for further biological and computational investigations.

Table 6: In-vitro MIC and MBC of active 2-aryl-imidazo[1,2-a]pyrimidines.

Compounds	Antimicrobial threshold (mg/mL)	*S. aureus*	*M. luteus*	*B. cereus*	*B. subtilis*	*C. albicans 26790*	*C. albicans 10231*	*C. albicans IPP 444*
IPM-H	MIC	/	/	/	/	/	5	/
	MBC	/	/	/	/	/	10	/
IPM-4Br	MIC	/	/	/	/	5	5	/
	MBC	/	/	/	/	10	10	/
IPM-4OMe	MIC	5	/	/	2.5	5	2.5	/
	MBC	10	/	/	2.5	10	5	/
IPM-4F	MIC	/	/	/	/	5	/	/
	MBC	/	/	/	/	5	/	/
IPM-2Naph	MIC	10	5	/	/	2.5	5	5
	MBC	10	10	/	/	5	5	10
IPM-3,4diMe	MIC	/	/	20	/	2.5	5	2.5
	MBC	/	/	20	/	2.5	10	5

5. Conclusion

The analysis of antimicrobial activity reveals that specific imidazo[1,2-a]pyridine (**IPs**) and imidazo[1,2-a]pyrimidine derivatives (**IPMs**) demonstrated notable effectiveness against *Candida albicans* and certain Gram-positive bacteria, particularly *Staphylococcus aureus*, *Micrococcus luteus*, *Bacillus subtilis*, and *Bacillus cereus*. The tested compounds showed minimal to no activity against Gram-negative bacteria, which is likely due to the structural differences in bacterial cell envelopes. Compounds with bromine, naphthalene, chlorine, methoxy or dimethyl groups showed enhanced antimicrobial properties, while other substituents were less effective.

MIC values were established for compounds with inhibition zones of 12 mm or larger, with some compounds displaying bactericidal action as indicated by MBC/MIC ratios equal to 1. Structural modifications, such as the addition of halogens (particularly chlorine or bromine) or methyl groups in specific positions, significantly enhanced activity, particularly against *C. albicans* and Gram-positive strains. The findings suggest that the presence of specific substituents on the imidazo[1,2-a]pyridine and imidazo[1,2-a]pyrimidine frameworks play a critical role in determining antimicrobial potency, paving the way for potential therapeutic applications of these compounds. Notably, the results obtained with **IPM** derivatives were superior and encouraging, suggesting these compounds as promising candidates for further molecular docking studies.

References

1. Gómez-García, O.; Andrade-Pavón, D.; Campos-Aldrete, E.; Ballinas-Indilí, R.; Méndez-Tenorio, A.; Villa-Tanaca, L.; Álvarez-Toledano, C. Synthesis, Molecular Docking, and Antimycotic Evaluation of Some 3-Acyl Imidazo[1,2-a]Pyrimidines. *Molecules* **2018**, *23*, 1–17, doi:10.3390/molecules23030599.

2. Breijyeh, Z.; Karaman, R. Design and Synthesis of Novel Antimicrobial Agents. *Antibiotics* **2023**, *12*, 628, doi:10.3390/antibiotics12030628.

3. Rival, Y.; Grassy, G.; Taudou, A.; Ecalle, R. Antifungal Activity in Vitro of Some Imidazo[1,2-a]Pyrimidine Derivatives. *Eur. J. Med. Chem.* **1991**, *26*, 13–18, doi:10.1016/0223-5234(91)90208-5.

4. Mishra, N.P.; Mohapatra, S.; Sahoo, C.R.; Raiguru, B.P.; Nayak, S.; Jena, S.; Padhy, R.N. Design, One-Pot Synthesis, Molecular Docking Study, and Antibacterial Evaluation of Novel 2H-Chromene Based Imidazo[1,2-a]Pyridine Derivatives as Potent Peptide Deformylase Inhibitors. *J. Mol. Struct.* **2021**, *1246*, 131183, doi:10.1016/j.molstruc.2021.131183.

5. Devi, N.; Singh, D.; Rawal, R.K.; Bariwal, J.; Singh, V. Medicinal Attributes of Imidazo[1,2-. *Bentham Sci.* **2016**, *16*, 2963–2994.

6. Gürsoy, E.; Dincel, E.D.; Naesens, L.; Ulusoy Güzeldemirci, N. Design and Synthesis of Novel Imidazo[2,1-b]Thiazole Derivatives as Potent Antiviral and Antimycobacterial Agents. *Bioorg. Chem.* **2020**, *95*, 103496, doi:10.1016/j.bioorg.2019.103496.

7. Kowalska-Krochmal, B.; Dudek-Wicher, R. The Minimum Inhibitory Concentration of Antibiotics: Methods, Interpretation, Clinical Relevance. *Pathogens* **2021**, *10*, 165, doi:10.3390/pathogens10020165.

8. Felten, A.; Grandry, B.; Lagrange, P.H.; Casin, I. Evaluation of Three Techniques for Detection of Low-Level Methicillin-Resistant Staphylococcus Aureus (MRSA): A Disk Diffusion Method with Cefoxitin and Moxalactam, the Vitek 2 System, and the MRSA-Screen Latex Agglutination Test. *J. Clin. Microbiol.* **2002**, *40*, 2766–2771, doi:10.1128/JCM.40.8.2766-2771.2002.

9. Balouiri, M.; Sadiki, M.; Ibnsouda, S.K. Methods for in Vitro Evaluating Antimicrobial Activity: A Review. *J. Pharm. Anal.* **2016**, *6*, 71–79, doi:10.1016/j.jpha.2015.11.005.

10. Aureus, L.P.S.; Leistner, R.; Hanitsch, L.G.; Krüger, R.; Lindner, A.K.; Stegemann, M.S.; Nurjadi, D. Skin Infections Due to Panton-Valentine. **2022**, *2*, 775–784, doi:10.3238/arztebl.m2022.0308.

11. Bezpalyi, I.F.; Bondarenko, L. V U Krainian Journal of Veterinary and Agricultural Sciences Study of the Microbiological Composition of Sludge during the Cultivation of Chironomus Larvae. **2023**, *6*, 102–106, doi:10.32718/ujvas6-1.16.

12. Manyi-loh, C.E. Listeria Monocytogenes and Listeriosis : The Global Enigma. **2025**, doi:10.3390/foods14071266.

13. Kowalczyk, P.; Beł, G. Plant Growth Promotion Using Bacillus Cereus. **2023**, 1–18, doi:10.3390/ijms24119759.

14. Hanifeh, M.; Spillmann, T.; Huhtinen, M.; Sclivagnotis, Y.S.; Grönthal, T.; Hynönen, U. Ex-Vivo Adhesion of Enterococcus Faecalis and Enterococcus Faecium to the Intestinal Mucosa of Healthy Beagles. **2021**, doi:10.3390/ani11113283.

15. Siniagina, M.N.; Markelova, M.I.; Boulygina, E.A.; Laikov, A. V; Khusnutdinova, D.R.; Abdulkhakov, S.R.; Danilova, N.A.; Odintsova, A.H. Diversity and Adaptations of Escherichia Coli Strains : Exploring the Intestinal Community in Crohn ' s Disease Patients and Healthy Individuals. **2021**, doi:10.3390/microorganisms9061299.

16. Losito, A.R.; Raffaelli, F.; Giacomo, P. Del; Tumbarello, M. New Drugs for the Treatment of Pseudomonas Aeruginosa Infections with Limited Treatment Options : A Narrative Review. **2022**, 1–25, doi:10.3390/ antibiotics11050579 Academic Editors: Evangelos.

17. Awoke, T.; Teka, B.; Seman, A.; Sebre, S.; Yeshitela, B. High Prevalence of Multidrug-Resistant Klebsiella Pneumoniae in a Tertiary Care Hospital in Ethiopia. **2021**, 1–9, doi:10.3390/antibiotics10081007.

18. Jawhara, S. How Gut Bacterial Dysbiosis Can Promote Candida Albicans Overgrowth during Colonic Inflammation. **2022**.

19. Srb, N.; Talapko, J.; Meštrovi, T.; Fureš, R.; Stupnišek, M.; Milosti, A. A Comprehensive Overview of Candida Albicans as the Leading Pathogen in Vulvovaginal Candidiasis. **2025**, 1–20, doi:10.3390/jof11090632.

20. Nariya, P.B.; Bhalodia, N.R.; Shukla, V.J.; Nariya, M.B.; Pankaj B. Nariya, Nayan R.

Bhalodia, V.J.S.; Nariya, M.B. In Vitro Evaluation of Antimicrobial and Antifungal Activity of Cordia Macleodii Bark. *PharmTech* **2010**, *2*, 2522–2526.

21. Rai, N.P.; Narayanaswamy, V.K.; Govender, T.; Manuprasad, B.K.; Shashikanth, S.; Arunachalam, P.N. Design, Synthesis, Characterization, and Antibacterial Activity of {5-Chloro-2-[(3-Substitutedphenyl-1,2,4-Oxadiazol-5-Yl)-Methoxy]-Phenyl} -(Phenyl)-Methanones. *Eur. J. Med. Chem.* **2010**, *45*, 2677–2682, doi:10.1016/j.ejmech.2010.02.021.

22. Sindi, A.; Chawn, M.V.B.; Hernandez, M.E.; Green, K.; Islam, M.K.; Locher, C.; Hammer, K. Anti-Biofilm Effects and Characterisation of the Hydrogen Peroxide Activity of a Range of Western Australian Honeys Compared to Manuka and Multifloral Honeys. *Sci. Rep.* **2019**, *9*, 1–17, doi:10.1038/s41598-019-54217-8.

23. Benzenine, D.; Daoud, I.; Aissaoui, N.; Kibou, Z.; Seijas, J.A.; Vázquez-Tato, M.P.; Ziani-Cherif, C.; Belarbi, L.; Choukchou-Braham, N. Design, Synthesis, Molecular Docking, and ADME-Tox Investigations of Imidazo[1,2-a]Pyrimidines Derivatives as Antimicrobial Agents. *Molecules* **2024**, *29*, 5058, doi:10.3390/molecules29215058.

24. Wasihun, A.G.; Kasa, B.G. Evaluation of Antibacterial Activity of Honey against Multidrug Resistant Bacteria in Ayder Referral and Teaching Hospital, Northern Ethiopia. *Springerplus* **2016**, *5*, doi:10.1186/s40064-016-2493-x.

CHAPTER 3: C-MOLECULAR DOCKING STUDY

C- Molecular Docking Study

1. Introduction

Given the excellent results from the biological activity of imidazo[1,2-a]pyrimidine derivatives, especially **IPM-4OMe, IPM-3,4diMe** and**, IPM-2Naph**, we were motivated and encouraged to perform molecular docking calculations for these heterocycles.

In this chapter, we aim to assess the molecular docking and enzyme kinetics of the chosen imidazo[1,2-a]pyrimidines through *in silico* studies.

2. Definition

Molecular docking is widely used in pharmacology, biology, and medicine, as it aims to predict the mechanisms and interactions involved with a biological target of therapeutic interest. It is a computational simulation process that anticipates the alignment, conformation, orientation, and potential affinity between two molecular structures, particularly the substrate (ligand). This ligand either facilitates or inhibits the biological activity of a target protein (receptor), forming a unique, stable complex in a three-dimensional (3D) space, such as ligand-protein, protein-protein, carbohydrate-protein, or DNA-protein complexes. Most protein structures are available through the Protein Data Bank (PDB) [1].

3. Principle of Molecular Docking

Molecular docking involves analyzing two entities: the ligand (small molecule) and the receptor (target protein). The process is divided into two complementary steps. The first step, known as combinatorial or deterministic, identifies the position and orientation of the ligand within the active site of the selected protein [2]. This involves determining conformations based on degrees of freedom, including rotation and translation, called "scoring", involves calculating the binding energy to evaluate the potential interactions between the ligand and the protein. This scoring process assigns a numerical value to each pose obtained during the docking phase, which helps identify the most stable ligand conformation [3]. A lower energy value indicates a more stable system, guiding the selection of the optimal pose [4].

4. General Docking Protocol

Modern computational methods are used to analyze enzyme-ligand interactions, often with visualization software that identifies co-crystallized components such as water molecules, ligands, or ions. The protocol can be divided into the following successive steps [5,6]:

- Protein Representation: Choose how to represent the proteins, such as pseudo-atoms, individual atoms, or grids.
- Conformational Acquisition: Determine the ligand's configuration, including its rigid or flexible positioning, orientation, and shape.
- Energy Minimization: Minimize the interaction energy by scoring functions to evaluate the conformations derived from the exploration phase.
- Clustering and Ranking: Group similar conformations and rank them based on a more precise score. When the scoring function does not clearly distinguish initial conformations from other generated conformations, a manual visual analysis of the results may be performed.
- Optional Refinement: Refine selected complexes through molecular dynamics or additional minimization steps.
- Search Algorithm: Implement algorithms to explore possible interactions, ligand placement on the binding site, and scoring functions to classify various binding modes.

5. Material and Methods

The three-dimensional structure (3D) of the most active compounds (**IPM-4OMe**, **IPM-3,4diMe** and, **IPM-2Naph**) were optimized with the semi-empirical AM1 method [7] using Hyperchem 8.0.8 software (Version 8.0.8, Hypercube, USA, http://www.hyper.com). These optimized structures were then converted to the format .mdb for use as input in MOE docking. Six crystal structures of target proteins were downloaded from the Protein Data Bank (http://www.rcsb.org/pdb/) and selected as antibacterial targets: gyrase B (PDB ID: 4URM) [8] from *S. aureus* (*Staphylococcus aureus*), the DNA topoisomerase complex (PDB ID: 3FV5) from *E. coli* (*Escherichia coli*), BcOMT2 (PDB ID: 3DUW) [9] from *B. cereus* (*Bacillus cereus*), BsFtsZ (PDB ID: 2RHL) [10] from *B. subtilis* (*Bacillus subtilis*), and *hexaprenyl* diphosphate synthase (PDB ID: 3AQC) [11] from *M. luteus* (*Micrococcus luteus)*. Additionally, secreted aspartic protease (PDB ID: 3Q70) [9] from *C. albicans* (*Candida albicans*) was

selected as an antifungal target to explore the antibacterial and antifungal activities of these compounds. Details about the target structures are provided in Table 1.

This chapter presents results, including Tables 1 to 4, were previously published in [12].

Table 1: Details about the six investigated targets.

Targets PDB	Methods	Organism	Chain	Sequence length	Resolution (Å)	Native-Ligands
4URM	X-ray diffraction	*Staphylococcus aureus*	A, B	123	1.85	9JH
3FV5	X-ray diffraction	*Escherichia coli K-12*	A, B	201	1.80	1EU
3DUW	X-ray diffraction	*Bacillus cereus*	A, B	223	1.20	SAH
2RHL	X-ray diffraction	*Bacillus subtilis*	A, B	325	2.45	GDP
3AQC	X-ray diffraction	*Micrococcus luteus*	A, B, C, D,	325	2.61	2DE
3Q70	X-ray diffraction	*Candida albicans*	A	342	1.40	RIT

a) Procedure and validation of the Docking methodology

Molecular docking simulations were carried out using MOE software [10] to explore and determine the compound's binding interactions with the residues in the active site of six targets. The docking protocol followed and described in previous studies of Daoud et al. [13,14] was applied, using the default parameters: Placement: Triangle Matcher, Rescoring 1: London dG. The scoring function employed was London dG."

Additionally, the method's accuracy was confirmed by re-docking all native ligands to their corresponding targets. The RMSD values of the resulting target-ligand complexes (Targets-Crystallized ligands) were below 2.0 Å [15], indicating that the docking approach is both accurate and effective.

b) ADME-Tox assessment

To validate the drug-likeness rules—specifically those of Lipinski, Veber, and Ghose—various physicochemical parameters, including LogP, nROT, MW, TPSA, the nHA (number of

hydrogen bond acceptors), and the nHD (number of hydrogen bond donors), were calculated using the SwissADME server (http://www.swissadme.ch/) [16].

Conversely, the pkCSM server (http://biosig.unimelb.edu.au/pkcsm/prediction) [17] was employed to analyze ADMET profiles by calculating the subsequent parameters:

- Toxicity (hepatotoxicity, hERG: human Ether-à-go-go-related gene).
- Excretion (total clearance, renal OCT2 substrate: organic cation transporter 2),
- Distribution (BBB: blood-brain barrier permeability, CNS: central nervous system permeability),
- Absorption (HIA: human intestinal absorption, Caco-2: colon adenocarcinoma permeability), and
- Metabolism (CYP2D6, CYP1A2, and CYP2C19 inhibition).

6. Results and Discussion

6.1 Molecular docking analysis

6.1.1. Protein-ligand Interaction

Following the docking of the three active imidazo[1,2-a]pyrimidines (**IPM-4OMe**, **3,4diMe** and, **IPM-2Naph**) using the six X-ray crystal structures of the examined targets, the comprehensive results of the semi-flexible docking simulations are summarized in Table 2.

To assess all possible interactions, the docking outputs produced through MOE software were converted to (.pdb) files and then visualized using the default settings of the BIOVIA DS Visualizer package (Dassault Systèmes BIOVIA, Discovery Studio Modeling Environment, 2020).

Table 2: The docking score energy, the RMSD results, and the interactions between the most active **IPMs**, native ligands, and the active site residues of antifungal and antibacterial targets.

***Staphylococcus aureus* (PDB ID : 4URM)**								
Compounds	**S-Score (kcal/mol)**	**RMSD** (Å)	**Bonds between atoms of compounds and active site residues**					
			Atom of compound	**Involved receptor Atoms**	**Involved receptor Residues**	**Category**	**Type of interaction**	**Distance** (Å)
IPM-4OMe	-5.241	2.016	N	HH21	ARG144(A)	Hydrogen Bond	Conventional H Bond	2.70
			N	OE2	GLU58(A)	Hydrogen Bond	Conventional H-Bond	3.23
			H	OD2	ASP81(A)	Hydrogen Bond	Carbon-H Bond	2.93
			H	OD2	ASP81(A)	Hydrogen Bond	Carbon-H Bond	2.61
			/	NH2	ARG84(A)	Electrostatic	Pi-Cation	3.84
			/	NH2	ARG84(A)	Electrostatic	Pi-Cation	4.46
			/	OE1	GLU58(A)	Electrostatic	Pi-Anion	4.48
			/	OE2	GLU58(A)	Electrostatic	Pi-Anion	3.64
			/	C	ASN54(A)	Hydrophobic	Amide-Pi Stacked	4.94

			/	C	GLY85(A)	Hydrophobic	Amide-Pi Stacked	5.31
			/	/	ARG84(A)	Hydrophobic	Pi-Alkyl	5.11
			/	/	PRO87(A)	Hydrophobic	Pi-Alkyl	4.75
			/	/	ARG84(A)	Hydrophobic	Pi-Alkyl	5.42
			/	/	PRO87(A)	Hydrophobic	Pi-Alkyl	5.13
			/	/	ILE86(A)	Hydrophobic	Pi-Alkyl	4.31
IPM-3,4-di Me	-4.871	1.898	/	NH2	ARG84(A)	Electrostatic	Pi-Cation	4.78
			/	NH2	ARG84(A)	Electrostatic	Pi-Cation	4.49
			/	OE1	GLU58(A)	Electrostatic	Pi-Anion	4.57
			C	/	ILE86(A)	Hydrophobic	Alkyl	4.99
			/	/	PRO87(A)	Hydrophobic	Pi-Alkyl	4.44
			/	/	PRO87(A)	Hydrophobic	Pi-Alkyl	4.42
			/	/	ILE86(A)	Hydrophobic	Pi-Alkyl	4.53
Native ligand (XAM)	-5.813	1.408	OBB	HZ3	LYS93(A)	Hydrogen Bond	Conventional H-Bond	2.19
			OBY	HZ2	LYS11(A)	Hydrogen Bond	Conventional H-Bond	1.99

			CLX	HD3	ARG84(A)	Hydrogen Bond	Carbon-H Bond	3.02
			/	/	ALA108(A)	Hydrophobic	Alkyl	4.86
			CLW	/	PRO87(A)	Hydrophobic	Alkyl	5.09
			CLX	/	ARG84(A)	Hydrophobic	Alkyl	3.98
			CLX	/	PRO87(A)	Hydrophobic	Alkyl	4.70
			CAK	/	MET94(A)	Hydrophobic	Alkyl	5.09
			CAK	/	VAL105(A)	Hydrophobic	Alkyl	4.36
			/	/	PRO87(A)	Hydrophobic	Pi-Alkyl	4.22
***Escherichia coli* (PDB ID: 3FV5)**								
IPM-3,4-di Me	-3.662	0.884	H	OD2	ASP69(A)	Hydrogen Bond	Carbon-H Bond	2.13
			H	OD2	ASP69(A)	Hydrogen Bond	Carbon-H Bond	2.41
			/	OE2	GLU46(A)	Electrostatic	Pi-Anion	3.96
			/	C	ASN42(A)	Hydrophobic	Amide-Pi Stacked	4.27
			/	C	ASN42(A)	Hydrophobic	Amide-Pi Stacked	4.21

			C	/	PRO75(A)	Hydrophobic	Alkyl	4.58
			/	/	MET74(A)	Hydrophobic	Pi-Alkyl	4.78
			/	/	VAL165(A)	Hydrophobic	Pi-Alkyl	5.19
			/	/	MET74(A)	Hydrophobic	Pi-Alkyl	4.03
			/	/	MET74(A)	Hydrophobic	Pi-Alkyl	5.06
Native Ligand (1EU)	-3.552	1.362	N24	HH11	ARG132(A)	Hydrogen Bond	Conventional H-Bond	2.50
			H6	OD2	ASP69(A)	Hydrogen Bond	Conventional H-Bond	1.76
			H7	OD2	ASP69(A)	Hydrogen Bond	Conventional H-Bond	2.35
			H5	OG	SER43(A)	Hydrogen Bond	Carbon-H Bond	2.89
			H17	O	GLY73(A)	Hydrogen Bond	Carbon-H Bond	2.63
			/	NH1	ARG72(A)	Electrostatic	Pi-Cation	3.63
			/	OE2	GLU46(A)	Electrostatic	Pi-Anion	4.09
			/	/	MET74(A)	Hydrophobic	Pi-Alkyl	4.51
			/	/	PRO75(A)	Hydrophobic	Pi-Alkyl	4.91
			/	/	ARG72(A)	Hydrophobic	Pi-Alkyl	5.09

			/	/	PRO75(A)	Hydrophobic	Pi-Alkyl	4.70
***Bacillus Cereus* (PDB ID : 3DUW)**								
IPM-2-Naph	-5.855	1.164	N	HA	GLU90(A)	Hydrogen Bond	Carbon-H Bond	2.76
			/	OE2	GLU90(A)	Electrostatic	Pi-Anion	4.16
			/	OD1	ASP140(A)	Electrostatic	Pi-Anion	4.36
			/	/	HIS40(A)	Hydrophobic	Pi-Pi Stacked	5.95
			/	C	ALA141(A)	Hydrophobic	Amide-Pi Stacked	4.79
			/	C	ALA141(A)	Hydrophobic	Amide-Pi Stacked	4.17
			/	/	ALA91(A)	Hydrophobic	Pi-Alkyl	3.52
			/	/	ALA119(A)	Hydrophobic	Pi-Alkyl	5.01
			/	/	ALA141(A)	Hydrophobic	Pi-Alkyl	4.08
			/	/	ALA91(A)	Hydrophobic	Pi-Alkyl	4.36
			/	/	ALA141(A)	Hydrophobic	Pi-Alkyl	3.69
			/	/	ALA141(A)	Hydrophobic	Pi-Alkyl	4.62

			/	/	LEU68(A)	Hydrophobic	Pi-Alkyl	5.08
Native Ligand (SAH)	-5.616	1.623	N7	H	ALA119(A)	Hydrogen Bond	Conventional H-Bond	2.56
			O	HZ1	LYS143(A)	Hydrogen Bond	Conventional H-Bond	2.19
			HN1	O	ASP140(A)	Hydrogen Bond	Conventional H-Bond	1.88
			HN61	OH	TYR149(A)	Hydrogen Bond	Conventional H-Bond	2.78
			O	HA	ALA141(A)	Hydrogen Bond	Carbon-H Bond	2.93
			/	OD1	ASP142(A)	Electrostatic	Pi-Anion	3.36
			/	OD2	ASP142(A)	Electrostatic	Pi-Anion	3.14
			HN2	OD2	ASP140(A)	Electrostatic	Attractive charge	2.00
			OXT	NZ	LYS143(A)	Electrostatic	Attractive charge	4.31
			SD	/	HIS40(A)	Other	Pi-Sulfur	5.65
			/	/	ALA91(A)	Hydrophobic	Pi-Alkyl	3.80
			/	/	LEU118(A)	Hydrophobic	Pi-Alkyl	5.30
			/	/	ALA119(A)	Hydrophobic	Pi-Alkyl	5.09
			/	/	ALA141(A)	Hydrophobic	Pi-Alkyl	4.75

			/	/	ALA91(A)	Hydrophobic	Pi-Alkyl	4.69
			/	/	LEU118(A)	Hydrophobic	Pi-Alkyl	4.66
***Bacillus Subtilis* (PDB ID : 2RHL)**								
IPM-4OMe	-5.205	1. 634	O	HG1	THR109(A)	Hydrogen Bond	Conventional H-Bond	2.95
			H	O	MET105(A)	Hydrogen Bond	Carbon-H Bond	2.70
			/	NH1	ARG143(A)	Electrostatic	Pi-Cation	4.97
			/	OE1	GLU139(A)	Electrostatic	Pi-Anion	4.72
			/	C	GLY104(A)	Hydrophobic	Amide-Pi Stacked	4.68
			/	C	GLY104(A)	Hydrophobic	Amide-Pi Stacked	4.52
Native Ligand (GDP)	-6.077	1.336	O1A	H	GLY21(A)	Hydrogen Bond	Conventional H-Bond	2.01
			O2	H	GLY22(A)	Hydrogen Bond	Conventional H-Bond	1.82
			O2	H	GLY23(A)	Hydrogen Bond	Conventional H-Bond	2.76
			O3B	H	ALA71(A)	Hydrogen Bond	Conventional H-Bond	2.19
			O3B	H	ALA72(A)	Hydrogen Bond	Conventional H-Bond	2.65

			O3B	H	ALA73(A)	Hydrogen Bond	Conventional H-Bond	2.13
			O2B	H	GLY108(A)	Hydrogen Bond	Conventional H-Bond	2.30
			O2B	H	THR109(A)	Hydrogen Bond	Conventional H-Bond	1.86
			O2B	HG1	THR109(A)	Hydrogen Bond	Conventional H-Bond	2.30
			O6	HD21	ASN166(A)	Hydrogen Bond	Conventional H-Bond	2.19
			HO3	O	GLY104(A)	Hydrogen Bond	Conventional H-Bond	2.90
			O2	HA2	GLY22(A)	Hydrogen Bond	Carbon-H Bond	3.03
			N3	HA2	GLY22(A)	Hydrogen Bond	Carbon-H Bond	2.57
			O1B	HA	ALA73(A)	Hydrogen Bond	Carbon-H Bond	2.65
			O2B	HA2	GLY108(A)	Hydrogen Bond	Carbon-H Bond	2.98
			O6	HA	PRO135(A)	Hydrogen Bond	Carbon-H Bond	2.59
			H2	O	GLY104(A)	Hydrogen Bond	Carbon-H Bond	2.16
			O1B	NH2	ARG143(A)	Electrostatic	Attractive charge	4.10
			/	/	PHE183(A)	Hydrophobic	Pi-Pi Shaped	4.82

***Micrococcus luteus* (PDB ID : 3AQC)**								
IPM-2-Naph	-4. 958	1.424	H	O	LYS170(B)	Hydrogen Bond	Carbon-H Bond	2.61
			/	OE2	GLU146(B)	Electrostatic	Pi-Anion	3.69
			/	OE2	GLU146(B)	Electrostatic	Pi-Anion	4.02
			/	HB2	SER80(B)	Hydrophobic	Pi-Sigma	2.66
			/	/	HIS83(B)	Hydrophobic	Pi-Pi Stacked	5.61
			/	/	HIS83(B)	Hydrophobic	Pi-Pi Stacked	5.72
			/	/	VAL142(B)	Hydrophobic	Pi-Alkyl	5.49
			/	/	VAL142(B)	Hydrophobic	Pi-Alkyl	5.31
			/	/	CYS143(B)	Hydrophobic	Pi-Alkyl	5.11
Native Ligand (2DE)	-7.534	1.144	O1A	HZ2	LYS170(B)	Hydrogen Bond	Conventional H-Bond	1.71
			O1A	HE3	LYS170(B)	Hydrogen Bond	Carbon-H Bond	2.87
			H2	OE2	GLU146(B)	Hydrogen Bond	Carbon-H Bond	2.47

			O3B	HZ1	LYS225(B)	Electrostatic	Attractive charge	2.13
			O3B	NH1	ARG93(B)	Electrostatic	Attractive charge	4.10
			O2B	NZ	LYS170(B)	Electrostatic	Attractive charge	4.96
			O2B	NZ	LYS170(B)	Electrostatic	Attractive charge	4.58
			O2B	NZ	LYS225(B)	Electrostatic	Attractive charge	3.84
			PA	OD2	ASP84(B)	Electrostatic	Attractive charge	3.69
			PA	OD2	ASP88(B)	Electrostatic	Attractive charge	3.87
			PA	OE2	GLU146(B)	Electrostatic	Attractive charge	5.36
			PB	OD2	ASP84(B)	Electrostatic	Attractive charge	4.52
			PB	OD2	ASP88(B)	Electrostatic	Attractive charge	4.40
			PB	OD2	ASP211(B)	Electrostatic	Attractive charge	5.34
			PB	OD1	ASP230(B)	Electrostatic	Attractive charge	5.06
			C10	/	VAL142(B)	Hydrophobic	Alkyl	5.13
			C14	/	ILE87(B)	Hydrophobic	Alkyl	5.25
			C15	/	HIS83(B)	Hydrophobic	Pi-Alkyl	5.30

***Candida albicans* (PDB ID : 3Q70)**								
IPM-3,4-di Me	-5.040	1.501	H	OG1	THR221(A)	Hydrogen Bond	Carbon-H Bond	2.65
			/	/	TYR84(A)	Hydrophobic	Pi-Pi Stacked	5.27
			/	/	TYR225(A)	Hydrophobic	Pi-Pi Stacked	5.02
			C	/	ILE119(A)	Hydrophobic	Alkyl	4.00
			C	/	ILE123(A)	Hydrophobic	Alkyl	5.22
			C	/	ILE123(A)	Hydrophobic	Alkyl	4.97
			C	/	TYR84(A)	Hydrophobic	Pi-Alkyl	4.43
			C	/	TYR84(A)	Hydrophobic	Pi-Alkyl	4.56
Native ligand (RIT)	-5.107	1.464	O24	HN	GLY85(A)	Hydrogen Bond	Conventional H-Bond	2.42
			H5	O	GLY220(A)	Hydrogen Bond	Conventional H-Bond	2.87
			H5	OG1	THR221(A)	Hydrogen Bond	Conventional H-Bond	2.54
			H18	O	GLY220(A)	Hydrogen Bond	Conventional H-Bond	2.38
			H4	OD2	ASP218(A)	Hydrogen Bond	Carbon-H Bond	3.09

			/	/	TYR225(A)	Hydrophobic	Pi-Pi Stacked	4.90
			/	/	TYR51(A)	Hydrophobic	Pi-Pi Stacked	4.40
			C64	/	ILE30(A)	Hydrophobic	Alkyl	5.20
			C68	/	VAL12(A)	Hydrophobic	Alkyl	5.49
			C68	/	ILE30(A)	Hydrophobic	Alkyl	5.29
			C86	/	TYR51(A)	Hydrophobic	Pi-Alkyl	4.03

6.1.2. Orientation and bonding interactions of the IPMs within the receptor's active site

As illustrated in Table 2, compounds **IPM-4OMe** and **IPM-3,4-diMe** were expected to be the strongest binders to the *Staphylococcus aureus* target (PDB ID: 4URM). The stability of the formed complexes was confirmed by the negative binding energies of -5.241 and -4.871 kcal/mol, respectively. In particular, the binding energy of compound **IPM-4OMe** is very close to that of the native ligand (XAM), which has a score of -5.813 kcal/mol (Table 2).

The results indicate that the compound **IPM-4OMe** forms four strong hydrogen bonds [18] with the active site residues of the *Staphylococcus aureus* target (PDB ID: 4URM). These include two carbon-hydrogen bonds: H/ASP81(A)-OD2 (bond distance = 2.93 Å) and H/ASP81(A)-OD2 (bond distance = 2.61 Å), as well as two conventional hydrogen bonds: N/ARG144(A)-HH21 (bond distance = 2.70 Å) and N/GLU58(A)-OE2 (bond distance = 3.23 Å). Additionally, four electrostatic interactions were observed with ARG84(A) and GLU58(A). The compound also formed seven hydrophobic interactions with the enzyme's active site (Table 2 and Figure 1 (a1)).

In the same fashion, compound **IPM-3,4-diMe** formed four hydrophobic interactions within the target pocket (Table 2 + Figure 1 (a2)) and three electrostatic interactions with the active site residue of the *Staphylococcus aureus* target (PDB ID: 4URM). Several studies [19–21] have shown that ARG84(A) plays a crucial role in inhibiting the *Staphylococcus* aureus target (PDB ID: 4URM).

Simultaneously, compound **IPM-4OMe** established seven hydrophobic interactions and one electrostatic interaction with residues in the target's active site. In particular, several studies [22,23] have indicated that GLU46(A), PRO75(A), and ASN42(A) play a crucial role in the inhibition of the *Escherichia coli* receptor (PDB ID: 3FV5).

Especially, the complex formed by compound **IPM-4OMe** achieved the best negative energy score of -3.662 kcal/mol in comparison to the native ligand (1EU) (-3.552 kcal/mol) (Table 2). The docked conformation of compound **IPM-4OMe** with the *Escherichia coli* target (PDB ID: 3FV5) is illustrated in Figure 1 (a3). This compound forms two strong carbon H-bonds: H/ASP69(A)-OD2 with a bond distance of 2.13Å, and H/ASP69(A)-OD2 with a bond distance of 2.41Å (Table 2 + Figure 1 (a3)). Additionally, compound **IPM-4OMe** established one electrostatic interaction and seven hydrophobic interactions with residues in the target's active

site. Particularly, previous studies [22,23] have identified ASN42(A), GLU46(A) and PRO75(A) as key residues in the inhibition of the *Escherichia coli* receptor (PDB ID: 3FV5).

The heterocycle **IPM-2Naph** establishes the most stable complex with the *Bacillus cereus* target (PDB ID: 3DUW) when compared to the native ligand (SAH), as evidenced by the binding energy scores of -5.855 kcal/mol and -5.616 kcal/mol, respectively. This heterocycle forms a strong carbon-hydrogen bond with the residue GLU90(A) (bond distance = 2.76 Å), along with two electrostatic interactions with ASP140(A) and GLU90(A). Additionally, it establishes ten hydrophobic interactions with the active site residues of the *Bacillus cereus* target (PDB ID: 3DUW) (Table 2 + Figure 1 (a4)). The importance of these residues is confirmed by Sokolova et al. [24] in forming various interactions within the active site of this target.

The complex formed by heterocycle **IPM-4OMe** showed the lowest binding energy value of -5.205 kcal/mol, which is very similar to the binding energy of the native ligand GDP 5 (-6.077 kcal/mol) (Table 2). Additionally, compound **IPM-4OMe** formed one strong hydrogen bond (both conventional and carbon types) with the residues THR109(A) in MET105(A), with bond distances of 2.95 Å and 2.70 Å, respectively. Two electrostatic interactions (Pi-Anion and Pi-Cation) were observed with ASP140(A) and GLU90(A), correspondingly. Furthermore, two hydrophobic interactions were established involving this compound and the residue GLY104(A) (Table 2 + Figure 1 (a5)). These findings have been supported by recent studies [11,23–27].

As shown in Table 2, compound **IPM-2Naph** demonstrates a binding affinity very similar to that of the native ligand 2DE for the *Micrococcus luteus* target (PDB ID: 3AQC), with a binding energy of -4.958 kcal/mol compared to -7.534 kcal/mol for the native ligand. This affinity is reflected in the stable complex formed, with a negative energy score and a low RMSD value.

The docked conformation of heterocycle **IPM-2Naph** within the active site pocket of *Micrococcus luteus* (PDB ID: 3AQC) revealed one strong hydrogen bond between compound **IPM-2Naph** and the residue LYS170(B) (bond distance = 2.61 Å). Two electrostatic interactions (Pi-Anion) were also observed between this heterocycle and the residue GLU146(B). In addition, compound **IPM-2Naph** formed six hydrophobic interactions with various residues in the active site of the *Micrococcus luteus* target (PDB ID: 3AQC) (Table 2 + Figure 1 (a6)). These results are consistent with findings from previous studies [28–30].

Finally, the docking findings of compound **IPM-3,4-diMe** with the *Candida albicans* target (PDB ID: 3Q70) show that the complex binding value (S-score) is -5.040 kcal/mol, which is very similar to that of the native ligand (3Q70-RIT), with a score of -5.107 kcal/mol (Table 2). Additionally, compound **IPM-3,4-diMe** forms a strong hydrogen bond with the *Candida albicans* receptor, specifically with the residue THR221(A) with bond distance = 2.65 Å. Furthermore, seven hydrophobic interactions were established between this compound and various residues in the active site of the target (Table 2 + Figure1 (a7)). These findings are supported by Barakat, A. et al. [31].

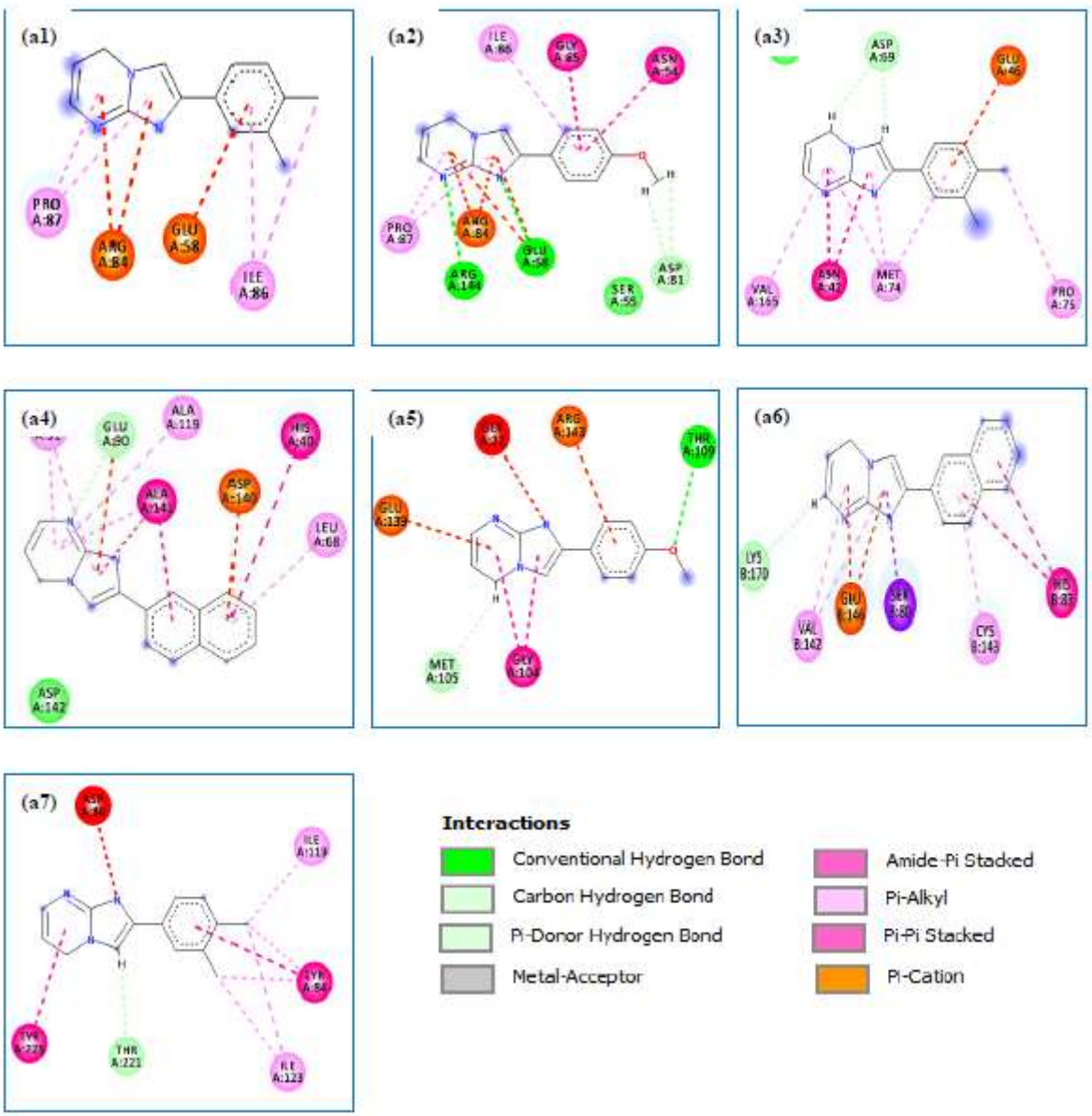

Figure 1: 2D diagrams of the interaction between: **(a1)**: **IPM-4OMe** and *Staphylococcus aureus* (PDB ID:**4URM**), **(a2)**: **IPM-3,4-diMe** and *Staphylococcus aureus* (PDB ID:**4URM**), **(a3)**: **IPM-3,4-diMe** and *Escherichia coli* (PDB ID:**3FV5**), **(a4)**: **IPM-2Naph** and *Bacillus*

cereus (PDB ID:**3DUW**), **(a5)**: **IPM-4OMe** and *Bacillus subtilis* (PDB ID:**2RHL**), **(a6)**: **IPM-2Naph** and *Micrococcus luteus* (PDB ID:**3AQC**), **(a7)**: **IPM-3,4-diMe** and *Candida albicans* (PDB ID:**3Q70**)

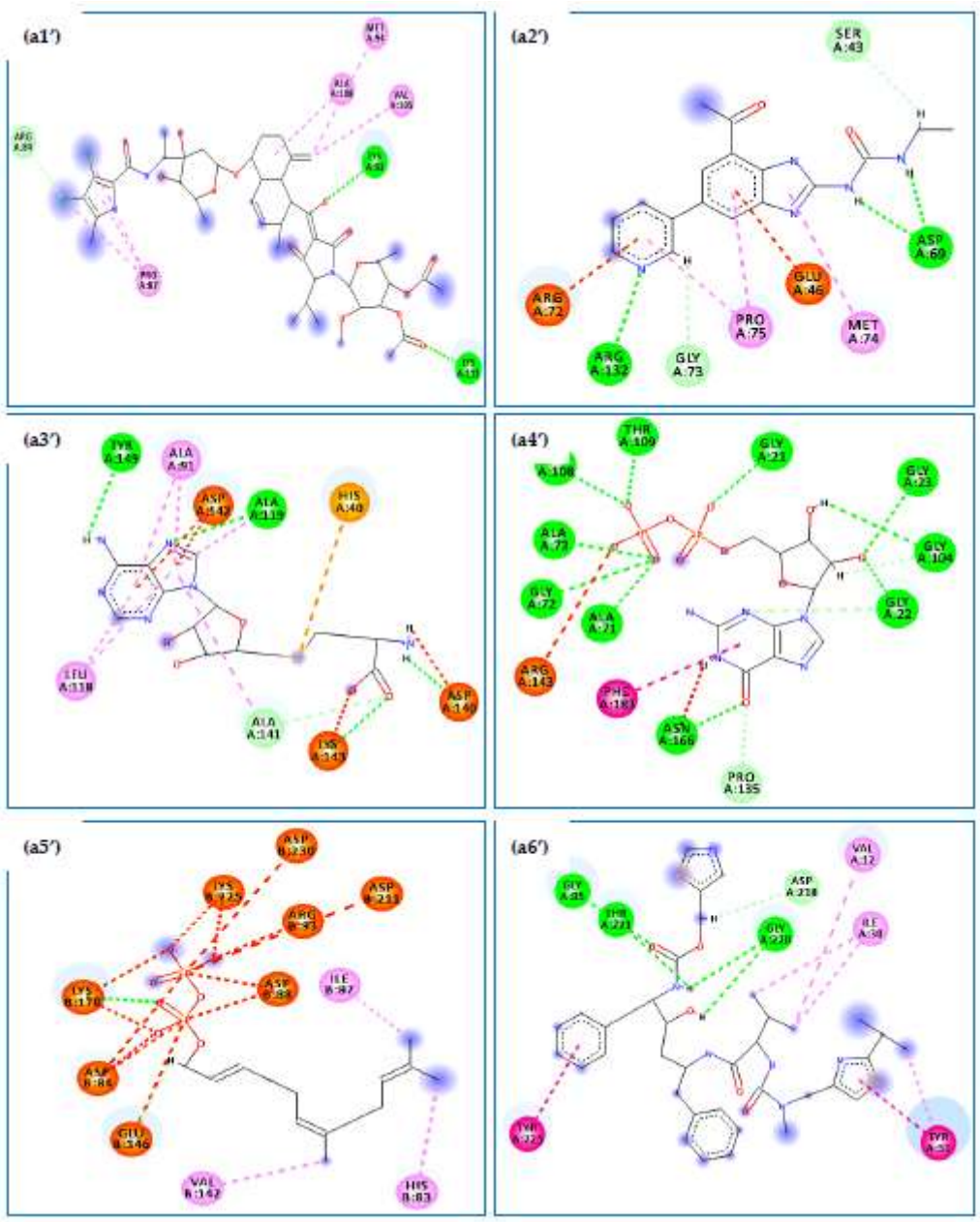

Figure 2: 2D diagrams of the interaction between: **(a1')**: XAM and *Staphylococcus aureus* (PDB ID:**4URM**), **(a2')**: 1EU and *Escherichia coli* (PDB ID:**3FV5**), **(a3')**: SAH and *Bacillus cereus* (PDB ID:**3DUW**), **(a4')**: GDP and *Bacillus subtilis* (PDB ID:**2RHL**), **(a5')**:2DE and *Micrococcus luteus* (PDB ID:**3AQC**), **(a6')**: RIT and *Candida albicans* (PDB ID:**3Q70**).

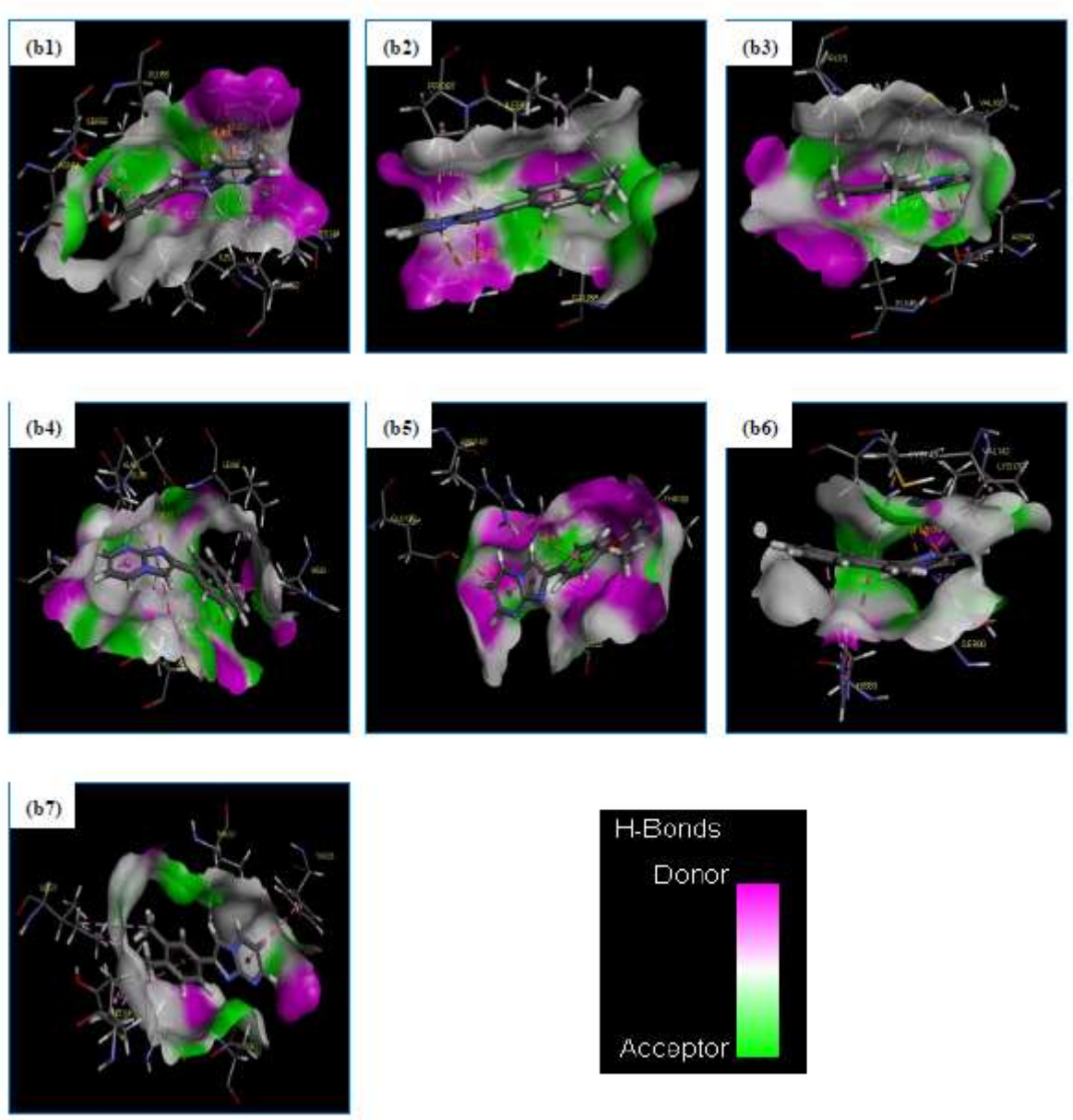

Figure 3: 3D diagrams of the interaction between: **(b1)**: **IPM-4OMe** and *Staphylococcus aureus* (PDB ID:**4URM**), **(b2)**: **IPM-3,4-diMe** and *Staphylococcus aureus* (PDB ID:**4URM**), **(b3)**: **IPM-3,4-diMe** and *Escherichia coli* (PDB ID:**3FV5**), (**b4**): **IPM-2Naph** and *Bacillus cereus* (PDB ID:**3DUW**), (**b5)**: **IPM-4OMe** and *Bacillus subtilis* (PDB ID:**2RHL**), **(b6)**: **IPM-2Naph** and *Micrococcus luteus* (PDB ID:**3AQC**), **(b7): IPM-3,4-diMe** and *Candida albicans* (PDB ID: **3Q70**).

6.2. Assessment of drug-likeness

Various parameters of physicochemical properties were evaluated for the purpose of verifying the drug-likeness rules with the use of SwissADME [16] online servers. All the findings are summarized in Table 3.

Table 3: Physicochemical properties and Drug-likeness predictions of the heterocycles **IPM-4OMe, IPM-3,4-diMe** and **IPM-2Naph.**

Compounds	Physicochemical Property						Medicinal Chemistry Rules drug likeness		
	TPSA (Å^2)	n-ROT	MW (g/mol)	MLog P / WLogP	n-HA	n-HD	Lipinski	Veber	Egan
	(0~140)	(0~11)	(100~500)	(0~5)	(0~12)	(0~7)			
IPM-4OMe	39.42	2	225.25	1.49 / 2.40	3	0	Accepted	Accepted	Accepted
IPM-3,4-diMe	30.19	1	223.27	2.33 / 3.01	2	0	Accepted	Accepted	Accepted
IPM-2Naph	30.19	1	245.28	2.65 / 3.55	2	0	Accepted	Accepted	Accepted

As indicated in Table 3, it is evident that all compounds—**IPM-4OMe, 3,4diMe,** and **IPM-2Naph**—have fewer than five hydrogen bond donors (**n-HD**: 0–7) and fewer than ten hydrogen bond acceptors (**n-HA**: 0–10). Furthermore, the molecular weights (**MW**) of these heterocycles range from 100 to 500 g/mol. Both **MLogP** (Moriguchi LogP) and **WLogP** (Wildman and Crippen LogP) values, representing the Logarithm of the partition coefficient of the compound between n-octanol and water are below 5. The **n-ROTB** (Number of Rotatable Bonds) values are also below 11, indicating the flexibility of these compounds. In addition, all **TPSA (**Topological Polar Surface Area**)** values are under 140 Å. Based on these results, it can be deduced that each compound meets the drug-likeness criteria, without violating Veber, Egan, or Lipinski rules. This suggests that none of the compounds should present issues related to oral bioavailability or pharmacokinetic parameters.

6.3. ADME-T properties

ADMET (Absorption, Distribution, Metabolism, Excretion, and Toxicity) predictions were obtained via the pkCSM online server [17] , and the complete results are compiled in Table 4.

Table 4: Pharmacokinetic and ADMET profiles of the compounds **IPM-4OMe**, **3,4diMe** and, **IPM-2Naph**.

ADME	*Parameters*	IPM-4OMe	3,4diMe	IPM-2Naph
Absorption	Caco2 (10^{-6} cm/s)	1.178	1.417	1.526
	HIA (%)	99.207	97.682	97.629
Distribution	CNS (log PS)	-1.800	-1.692	-1.462
	BBB (log BB)	0.311	0.030	0.123
Metabolism	CYP1A2 inhibitor	Yes	Yes	Yes
	CYP2C19 Inhibitor	No	No	No
	CYP2D6 substrate	No	No	No
	CYP3A4 substrate	No	No	No
Excretion	Renal OCT2 substrate	No	No	No

	Total Clearance (log mL/min/kg)	0.744	0.780	0.737
Toxicity	hERG I and II inhibitors	No	No	No
	Hepatotoxicity	No	No	No

From the analysis in Table 4, it is clear that:

- All compounds have **Caco-2** (colon adenocarcinoma) permeability values greater than -5.15 cm/s, indicating good permeability. Furthermore, all compounds exhibit **HIA** (Human Intestinal Absorption) values exceeding 30%, suggesting that they are effectively absorbed into the bloodstream when administered orally.

- The three heterocycles are also capable of crossing the **CNS** (central nervous system) barrier, the **BBB** (blood-brain barrier), as indicated by their logPS values, which range from -3 to -2 (-3 < logPS < -2). In addition, the logBB values for the studied heterocycles (**IPM-4OMe**, **IPM-3,4diMe** and, **IPM-2Naph**) are 0.311, 0.030, and 0.123, correspondingly. These results suggest that **IPM-4OMe** can easily penetrate the BBB and reach the CNS, while **IPM-3,4diMe** and, **IPM-2Naph** exhibit limited distribution to the brain (Table 4).
- P450 CYP inhibition test is conducted to evaluate whether a drug inhibits or reduces the activity of one or more isoforms of the CYP450 enzyme. The data from this table suggest that the compounds **IPM-4OMe, IPM-3,4diMe,** and **IPM-2Naph** act as inhibitors of the CYP1A2 isoform, but do not inhibit CYP2C19. Furthermore, these compounds are not substrates for CYP2D6 or CYP3A4.
- Additional analysis from the table reveals that none of the candidates are likely to be renal OCT2 substrates **(**Organic Cation Transporter 2**)**. Furthermore, it is evident that these compounds exhibit low excretion clearance (<5 mL/min/kg) (Table 4).
- Finally, the compounds do not act as inhibitors of either **hERG I** or **hERG II (**Human Ether-à-go-go-Related Gene**)**, which are potassium channels associated with cardiac repolarization. As inhibition of these channels can cause dangerous arrhythmias, the absence of such effects suggests a minimal risk of cardiotoxicity. Furthermore, these heterocycles do not demonstrate any hepatotoxicity risk, as they do not appear to cause liver damage or dysfunction, which is crucial for ensuring their safety as drug candidates.

7. Conclusion

This study highlights the promising potential of compounds namely **IPM-4OMe**, **IPM-3,4-diMe**, and **IPM-2Naph** as inhibitors of various bacterial and fungal targets. The results show that these compounds form stable complexes with key active site residues in *Staphylococcus aureus*, *Escherichia coli*, *Bacillus cereus*, *Micrococcus luteus*, and *Candida albicans*. Notably, **IPM-4OMe** demonstrated strong binding affinity with both *Staphylococcus aureus* and *Escherichia coli*, with interactions including hydrogen bonds, electrostatic forces, and hydrophobic contacts. Similarly, **IPM-3,4-diMe** and **IPM-2Naph** also formed significant interactions with their respective targets, indicating their potential as effective inhibitors. These findings suggest that the compounds studied here could serve as promising leads for further drug development aimed at combating bacterial and fungal infections.

Furthermore, and based on key physicochemical parameters, all the studied heterocycles demonstrate favorable drug-likeness properties, including balanced hydrogen bonding capabilities, optimal molecular weight, and suitable lipophilicity. Their flexibility and polar surface area measurements meet Lipinski, Egan, and Veber rules, indicating that these imidazo[1,2-a]pyrimidines show favorable characteristics for oral bioavailability and favorable pharmacokinetic, making them potential efficacy as drug candidates.

The selected heterocycles demonstrated good permeability and were effectively absorbed into the bloodstream when administered orally. They are also capable of crossing the BBB, although their distribution to the CNS varies, with one compound showing better penetration than the others. The imidazo[1,2-a]pyrimidines act as inhibitors of certain enzymes but do not affect others, and they are not likely to interact with key metabolic pathways. Additionally, none of the compounds are expected to be excreted through the kidneys at a high rate, indicating limited renal elimination.

Finally, the studied compounds do not interfere with key heart-related channels, reducing the risk of potential heart-related issues. Additionally, none of these compounds show signs of causing liver damage, indicating a low risk of hepatotoxicity.

References

1. Pinzi, L.; Rastelli, G. Metode Berbasis Struktur Bergantung Pada Informasi Yang Diperoleh Dari Pengetahuan Tentang Struktur 3D Target Yang Menarik, Dan Mereka Memungkinkan Database Peringkat Molekul Sesuai Dengan Struktur Dan Komplementaritas Elektronik Ligan Ke Target Tertentu. *igms drug Discov. InternatInPinzi, L., Rastelli, G. (2019). Mol. docking Shifting Parad. J. Mol. Sci. 20(18). https//doi.org/10.3390/ijms20184331ternational J. Mol. Sci.* **2019**, *20*, 1–23, doi:10.3390/ijms20184331.

2. MAY, A.; EISENHARDT, S.; SCHMIDT-EHRENBERG, J.; CORDES, F. Rigid Body Docking for Virtual Screening. *Konrad-Zuse-Zentrum für Informationstechnik, Berlin* **2003**, *47*, 31.

3. Chase, J. Caring for Frail Older Adults During COVID-19: Integrating Public Health Ethics into Clinical Practice. *J. Am. Geriatr. Soc.* **2020**, *68*, 1666–1670, doi:10.1111/jgs.16666.

4. Kumsa, D.M.; Tucho, G.T. The Impact of Formal and Informal Institutions on ART Drug Adherence. *J. Int. Assoc. Provid. AIDS Care* **2019**, *18*, 1–9, doi:10.1177/2325958219845419.

5. Huang, H.; Sarai, A. Analysis of the Relationships between Evolvability, Thermodynamics, and the Functions of Intrinsically Disordered Proteins/Regions. *Comput. Biol. Chem.* **2012**, *41*, 51–57, doi:10.1016/j.compbiolchem.2012.10.001.

6. Hanafi-Bojd, A.A.; Jafari, S.; Telmadarraiy, Z.; Abbasi-Ghahramanloo, A.; Moradi-Asl, E. Spatial Distribution of Ticks (Arachniada: Argasidae and Ixodidae) and Their Infection Rate to Crimean-Congo Hemorrhagic Fever Virus in Iran. *J. Arthropod. Borne. Dis.* **2021**, *15*, 41–59, doi:10.18502/jad.v15i1.6485.

7. Stewart, J.J.P. Optimization of Parameters for Semiempirical Methods V: Modification of NDDO Approximations and Application to 70 Elements. *J. Mol. Model.* **2007**, *13*, 1173–1213, doi:10.1007/s00894-007-0233-4.

8. Lu, J.; Patel, S.; Sharma, N.; Soisson, S.M.; Kishii, R.; Takei, M.; Fukuda, Y.; Lumb, K.J.; Singh, S.B. Structures of Kibdelomycin Bound to Staphylococcus Aureus GyrB and ParE Showed a Novel U-Shaped Binding Mode. *ACS Chem. Biol.* **2014**, *9*, 2023–2031, doi:10.1021/cb5001197.

9. Cho, J.H.; Park, Y.; Ahn, J.H.; Lim, Y.; Rhee, S. Structural and Functional Insights into O-Methyltransferase from Bacillus Cereus. *J. Mol. Biol.* **2008**, *382*, 987–997, doi:10.1016/j.jmb.2008.07.080.

10. Raymond, A.; Lovell, S.; Lorimer, D.; Walchli, J.; Mixon, M.; Wallace, E.; Thompkins, K.; Archer, K.; Burgin, A.; Stewart, L. Combined Protein Construct and Synthetic Gene Engineering for Heterologous Protein Expression and Crystallization Using Gene Composer. *BMC Biotechnol.* **2009**, *9*, 1–15, doi:10.1186/1472-6750-9-37.

11. Miguel, A.; Hsin, J.; Liu, T.; Tang, G.; Altman, R.B.; Huang, K.C. Variations in the Binding Pocket of an Inhibitor of the Bacterial Division Protein FtsZ across Genotypes and Species. *PLoS Comput. Biol.* **2015**, *11*, 1–17, doi:10.1371/journal.pcbi.1004117.

12. Benzenine, D.; Daoud, I.; Aissaoui, N.; Kibou, Z.; Seijas, J.A.; Vázquez-Tato, M.P.; Ziani-Cherif, C.; Belarbi, L.; Choukchou-Braham, N. Design, Synthesis, Molecular Docking, and ADME-Tox Investigations of Imidazo[1,2-a]Pyrimidines Derivatives as Antimicrobial Agents. *Molecules* **2024**, *29*, 5058, doi:10.3390/molecules29215058.

13. Daoud, I.; Melkemi, N.; Salah, T.; Ghalem, S. *Combined QSAR, Molecular Docking and Molecular Dynamics Study on New Acetylcholinesterase and Butyrylcholinesterase Inhibitors*; Elsevier Ltd, 2018; Vol. 74; ISBN 0000000191.

14. Daoud, I.; Mesli, F.; Melkemi, N.; Ghalem, S.; Salah, T. Discovery of Potential SARS-CoV 3CL Protease Inhibitors from Approved Antiviral Drugs Using: Virtual Screening, Molecular Docking, Pharmacophore Mapping Evaluation and Dynamics Simulation. *J. Biomol. Struct. Dyn.* **2022**, *40*, 12574–12591, doi:10.1080/07391102.2021.1973563.

15. Bajda, M.; Więckowska, A.; Hebda, M.; Guzior, N.; Sotriffer, C.A.; Malawska, B. Structure-Based Search for New Inhibitors of Cholinesterases. *Int. J. Mol. Sci.* **2013**, *14*, 5608–5632, doi:10.3390/ijms14035608.

16. Daina, A.; Michielin, O.; Zoete, V. SwissADME: A Free Web Tool to Evaluate Pharmacokinetics, Drug-Likeness and Medicinal Chemistry Friendliness of Small Molecules. *Sci. Rep.* **2017**, *7*, 1–13, doi:10.1038/srep42717.

17. Pires, D.E.V.; Blundell, T.L.; Ascher, D.B. PkCSM: Predicting Small-Molecule Pharmacokinetic and Toxicity Properties Using Graph-Based Signatures. *J. Med. Chem.* **2015**, *58*, 4066–4072, doi:10.1021/acs.jmedchem.5b00104.

18. Sindi, A.; Chawn, M.V.B.; Hernandez, M.E.; Green, K.; Islam, M.K.; Locher, C.; Hammer, K. Anti-Biofilm Effects and Characterisation of the Hydrogen Peroxide Activity of a Range of Western Australian Honeys Compared to Manuka and Multifloral Honeys. *Sci. Rep.* **2019**, *9*, 1–17, doi:10.1038/s41598-019-54217-8.

19. Wasihun, A.G.; Kasa, B.G. Evaluation of Antibacterial Activity of Honey against Multidrug Resistant Bacteria in Ayder Referral and Teaching Hospital, Northern Ethiopia. *Springerplus* **2016**, *5*, doi:10.1186/s40064-016-2493-x.

20. Imberty, A.; Hardman, K.D.; Carver, J.P.; Perez, S. Molecular Modelling of Protein-Carbohydrate Interactions. Docking of Monosaccharides in the Binding Site of Concanavalin A. *Glycobiology* **1991**, *1*, 631–642, doi:10.1093/glycob/1.6.631.

21. Wade, R.C.; Goodford, P.J. The Role of Hydrogen-Bonds in Drug Binding. *Prog. Clin. Biol. Res.* **1989**, *289*, 433–444.

22. Skok, Ž.; Barančoková, M.; Benek, O.; Cruz, C.D.; Tammela, P.; Tomašič, T.; Zidar, N.; Mašič, L.P.; Zega, A.; Stevenson, C.E.M.; et al. Exploring the Chemical Space of Benzothiazole-Based DNA Gyrase B Inhibitors. *ACS Med. Chem. Lett.* **2020**, *11*, 2433–2440, doi:10.1021/acsmedchemlett.0c00416.

23. Kowalczyk, A.; Paneth, A.; Trojanowski, D.; Paneth, P.; Zakrzewska-Czerwińska, J.; Stączek, P. Thiosemicarbazide Derivatives Decrease the ATPase Activity of Staphylococcus Aureus Topoisomerase IV, Inhibit Mycobacterial Growth, and Affect Replication in Mycobacterium Smegmatis. *Int. J. Mol. Sci.* **2021**, *22*, 3881, doi:10.3390/ijms22083881.

24. Sokolova, N.; Zhang, L.; Deravi, S.; Oerlemans, R.; Groves, M.R.; Haslinger, K. Structural Characterization and Extended Substrate Scope Analysis of Two Mg2+-Dependent O-Methyltransferases from Bacteria**. *ChemBioChem* **2023**, *24*, doi:10.1002/cbic.202300076.

25. Aljohny, B.O.; Rauf, A.; Anwar, Y.; Naz, S.; Wadood, A. Antibacterial, Antifungal, Antioxidant, and Docking Studies of Potential Dinaphthodiospyrols from Diospyros Lotus Linn Roots. *ACS Omega* **2021**, *6*, 5878–5885, doi:10.1021/acsomega.0c06297.

26. Aarjane, M.; Slassi, S.; Tazi, B.; Amine, A. Synthesis and Biological Evaluation of Novel Isoxazole Derivatives from Acridone. *Arch. Pharm. (Weinheim).* **2021**, *354*, doi:10.1002/ardp.202000261.

27. Hosseini, Z.S.; Housaindokht, M.R.; Razzaghi-Asl, N.; Miri, R. Virtual Screening of Some Heterocyclic Structures toward Novel Antibacterial Agents. *J. Iran. Chem. Soc.* **2018**, *15*, 621–628, doi:10.1007/s13738-017-1262-2.

28. Then, A.; Zhang, H.; Ibrahim, B.; Schuster, S. Bioinformatics Analysis of the Periodicity in Proteins with Coiled-Coil Structure—Enumerating All Decompositions of Sequence Periods. *Int. J. Mol. Sci.* **2022**, *23*, doi:10.3390/ijms23158692.

29. Desai, J.; Liu, Y.; Wei, H.; Liu, W.; Ko, T.; Guo, R.; Oldfield, E. Structure, Function, and Inhibition of Staphylococcus Aureus Heptaprenyl Diphosphate Synthase. *ChemMedChem* **2016**, *11*, 1915–1923, doi:10.1002/cmdc.201600311.

30. Sasaki, D.; Fujihashi, M.; Okuyama, N.; Kobayashi, Y.; Noike, M.; Koyama, T.; Miki, K. Crystal Structure of Heterodimeric Hexaprenyl Diphosphate Synthase from Micrococcus Luteus B-P 26 Reveals That the Small Subunit Is Directly Involved in the Product Chain Length Regulation. *J. Biol. Chem.* **2011**, *286*, 3729–3740, doi:10.1074/jbc.M110.147991.

31. Barakat, A.; Al-Majid, A.M.; Al-Qahtany, B.M.; Ali, M.; Teleb, M.; Al-Agamy, M.H.; Naz, S.; Ul-Haq, Z. Synthesis, Antimicrobial Activity, Pharmacophore Modeling and Molecular Docking Studies of New Pyrazole-Dimedone Hybrid Architectures. *Chem. Cent. J.* **2018**, *12*, 1–13, doi:10.1186/s13065-018-0399-0.

CHAPTER 4:
EXPERIMENTAL PART

This chapter describes the experimental procedures employed in the synthesis and characterization of the compounds discussed in the preceding sections. All reactions were carried out under the conditions described, and the products were purified and characterized using standard techniques such as melting point determination, IR spectroscopy, NMR spectroscopy, and mass spectrometry.

I. Materials and Methods

All solvents and reagents were purchased from Aldrich or Merck and used as received without further purification. The compound 2-bromo-1-(4-chlorophenyl)ethenone and the catalyst Al_2O_3 are commercially available and were used without further purification. The progress of the reactions was routinely monitored by thin-layer chromatography (TLC). Melting points were determined using a Bank KoferHrizbank WME apparatus (range: 50–266 °C) and are reported uncorrected. Infrared (IR) spectra were recorded on a Perkin Elmer FTIR spectrometer using KBr pellets, and only the most prominent absorption bands are listed. Electron impact mass spectra (MS) were obtained using a Bruker 320-MS spectrometer. Proton nuclear magnetic resonance (^{1}H NMR) spectra were recorded on a Magritek SPINSOLVE 91 MHz spectrometer using $(CD)_3SO$ as the solvent and tetramethylsilane (TMS) as the internal reference. Chemical shifts are expressed in parts per million (δ, ppm) relative to TMS, and signal multiplicities are abbreviated as follows: s (singlet), d (doublet), dd (doublet of doublets), and m (multiplet). Microwave-assisted reactions were carried out using a domestic microwave oven. Diffuse Reflectance UV-Visible (DRUV-Vis) spectra were recorded at room temperature using a Lambda 800 spectrophotometer in the 200–800 nm wavelength range.

Note on the characterization of intermediates:

The intermediates used in this work, including bromoacetophenones and alkene derivatives were synthesized and characterized using infrared (IR) spectroscopy. Although full structural elucidation techniques such as ^{1}H NMR, ^{13}C NMR, and MS were not performed, their identities were reasonably inferred based on the application of well-established and widely reported synthetic protocols [1–8]. Furthermore, the successful conversion of these intermediates into final products, which were obtained in good yields and fully characterized by spectroscopic and analytical techniques, provides strong indirect evidence supporting the structure and purity of the intermediates. The consistency of reaction outcomes and the reproducibility of these transformations further validate the reliability of the intermediates used.

II. Synthesis of Imidazo-heterocycles

The targeted heterocyclic compounds were synthesized through a multi-step process starting with the bromination of various acetophenone derivatives. This initial transformation was followed by cyclization reactions involving appropriate amine partners under thermal, or microwave-assisted conditions. The resulting products were purified and characterized using standard analytical techniques.

II.1. Bromination of Acetophenones

General procedure for the synthesis of 2-bromoacetophenone derivatives:

To a solution of aryl ketone (10 mmol) and N-bromosuccinimide (NBS, 10 mmol) in chloroform, 10% p-toluenesulfonic acid (PTSA) was added. The reaction mixture was stirred at room temperature overnight. The resulting solid was filtered and washed several times with ethanol and diethyl ether.

➢ 2-bromo-1-phenylethanone (Br-H)

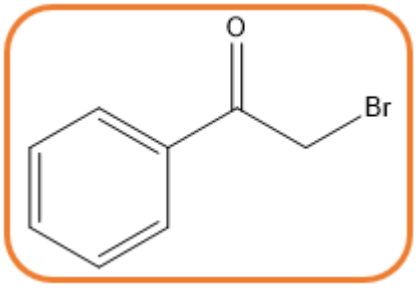

Structure: C_8H_7BrO

Molar mass (g/mol): 199,04

Yield (%): 60

Aspect: white solid

Mp (°C): 50

IR ν_{max} cm^{-1}: 1649 (C=O), 1577 (C=C).

➢ 2-bromo-1-(3-bromophenyl)ethenone (Br-3Br)

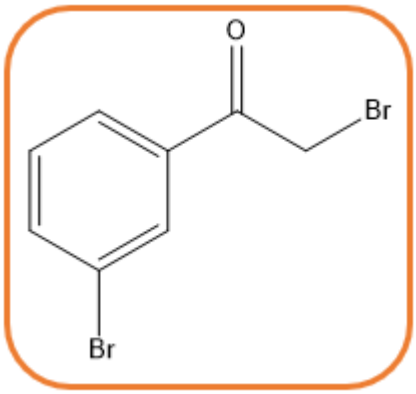

Structure: $C_8H_6Br_2O$

Molar mass (g/mol): 277,94

Yield (%): 88

Aspect: white solid

Mp (°C): 80

IR ν_{max} cm^{-1}: 1652 (C=O), 1518 (C=C).

➢ 2-bromo-1-(4-bromophenyl)ethanone (Br-4Br)

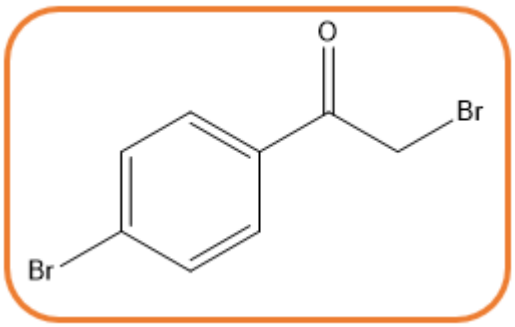

Structure: $C_8H_6Br_2O$

Molar mass (g/mol): 277,94

Yield (%): 91

Aspect: white solid

Mp (°C): 110

IR ν_{max} cm^{-1}: 1645 (C=O), 1522 (C=C).

➢ 2-bromo-1-(p-tolyl)ethanone (Br-4Me)

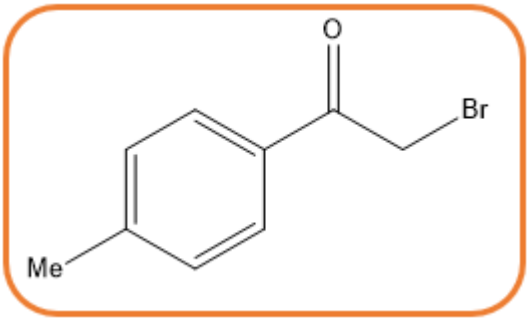

Structure: C_9H_9BrO

Molar mass (g/mol): 213,07

Yield (%): 50

Aspect: white solid

Mp (°C): 60

IR ν_{max} cm^{-1}: 1644 (C=O), 1602 (C=C).

➢ 2-bromo-1-(2-methoxyphenyl)ethanone (Br-2OMe)

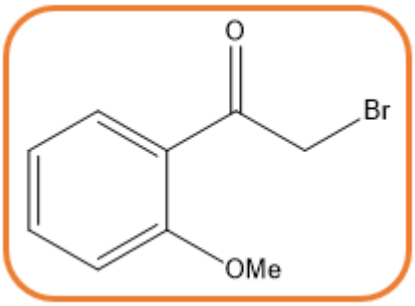

Structure: $C_9H_9BrO_2$

Molar mass (g/mol): 229,07

Yield (%): 82

Aspect: white solid

Mp (°C): 57

IR ν_{max} cm^{-1}: 1657 (C=O), 1578 (C=C).

➢ 2-bromo-1-(3-methoxyphenyl)ethanone (Br-3OMe)

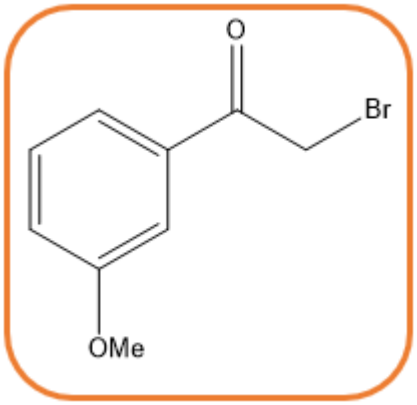

Structure: $C_9H_9BrO_2$

Molar mass (g/mol): 229,07

Yield (%): 66

Aspect: white solid

Mp (°C): 75

IR ν_{max} cm^{-1}: 1694 (C=O), 1573 (C=C).

➢ 2-bromo-1-(4-methoxyphenyl)ethanone (Br-4OMe)

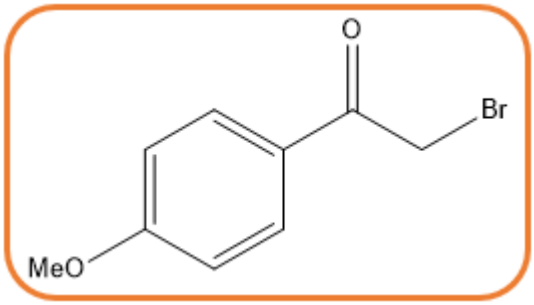

Structure: $C_9H_9BrO_2$

Molar mass (g/mol): 229,07

Yield (%): 70

Aspect: white solid

Mp (°C): 74

IR ν_{max} cm^{-1}: 1632 (C=O), 1549 (C=C).

➢ 2-bromo-1-(4-fluorophenyl)ethanone (Br-4F)

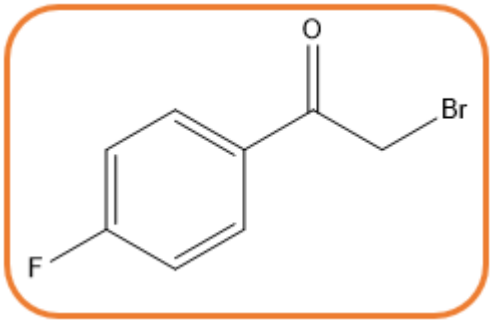

Structure: C_8H_6BrFO

Molar mass (g/mol): 217,04

Yield (%): 88

Aspect: white solid

Mp (°C): 70

IR ν_{max} cm^{-1}: 1650 (C=O), 1588 (C=C).

➢ 2-bromo-1-(naphthalen-2-yl)ethanone (Br-2Naph)

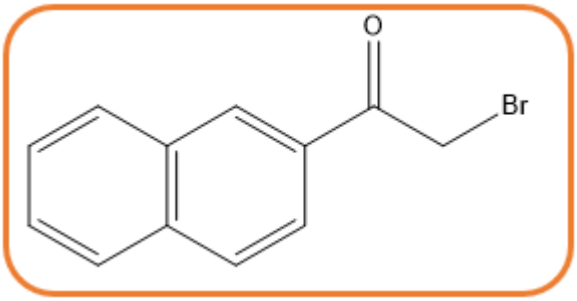

Structure: $C_{12}H_9BrO$

Molar mass (g/mol): 249,10

Yield (%): 68

Aspect: white solid

Mp (°C): 90

IR ν_{max} cm^{-1}: 1614 (C=O), 1572 (C=C).

➢ 2-bromo-1-(3,4-dimethylphenyl)ethanone (Br-3,4-diMe)

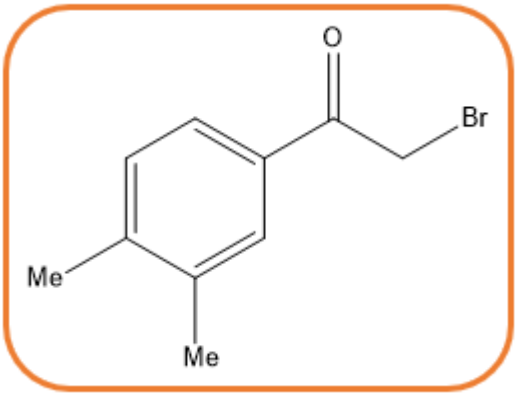

Structure: $C_{10}H_{11}BrO$

Molar mass (g/mol): 227,10

Yield (%): 52

Aspect: white solid

Mp (°C): 68

IR ν_{max} cm^{-1}: 1690 (C=O), 1603 (C=C).

II.2. Synthesis of imidazo[1,2-a]pyridines (IPs)

Imidazo[1,2-a]pyridine derivatives were synthesized using two different methods.

Method (A): In the first approach, bromoacetophenones (10 mmol) were reacted with commercially available 2-aminopyridine (10 mmol) in ethanol (10 mL) under reflux conditions. The progress of the reaction was monitored by TLC. Upon completion, the reaction mixture was allowed to cool to room temperature, then filtered, and the resulting solid was washed several times with a mixture of diethyl ether and ethanol.

Method (B): General procedure for the synthesis of imidazo[1,2-a]pyridine derivatives using 4% Au/TiO_2: In the second method, 2-aminopyridine (10 mmol) was reacted with bromoacetophenones (10 mmol) in ethanol (10 mL) under reflux conditions, in the presence of

a heterogeneous gold-based catalyst (4% Au supported on TiO_2). The catalyst was added in an amount corresponding to 10% w/w relative to the mass of 2-aminopyridine. The progress of the reaction was monitored by TLC. Upon completion, the hot reaction mixture was filtered to recover the catalyst. The filtrate was then cooled to room temperature, and the resulting product successively washed with ethanol and diethyl ether.

➢ 2-phenylimidazo[1,2-a]pyridine (IP-H)

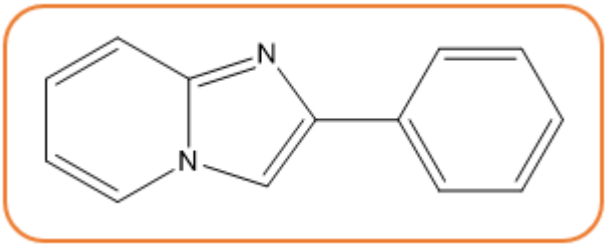

Structure: $C_{13}H_{10}N_2$

Molar mass (g/mol): 194,24

Yield: 47% (A), 82% (B)

Aspect: yellow solid

Mp (°C): 136

^{1}H NMR 91 MHz, $(CD)_3SO$ δ_H: 8.95 (1H, d, J = 7.0 Hz, N–CH, imidazole ring), 7.98–7.55 (9H, m, H_{arom}, pyridine and phenyl rings).

^{13}C NMR 23 MHz, $(CD)_3SO$ δ: 120.58 (C_{arom}, phenyl ring at C2), 115.76 (C_{arom}, pyridine moiety), 106.79 (CH, imidazole moiety).

IR ν_{max} cm^{-1}: 1654 (C=N), 1528 (C=C).

MS *m/z* (% relative abundance): 195

➢ 2-(2-bromophenyl)imidazo[1,2-a]pyridine (IP-3Br)

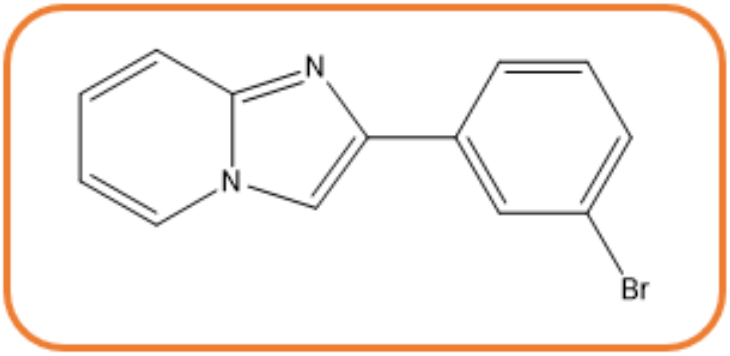

Structure: $C_{13}H_9BrN_2$

Molar mass (g/mol): 273,13

Yield: 40% (A), 50% (B)

Aspect: grice solid

Mp (°C): 130

^{1}H NMR 91 MHz, $(CD)_3SO$ δ_H: 8.62 (1H, d, J = 6.0 Hz, N–CH, imidazole ring), 8.23–6.67 (8H, m, H_{arom}, pyridine and 3-bromophenyl rings).

^{13}C NMR 23 MHz, $(CD)_3SO$ δ: 144.01 (C=N, imidazole ring), 140.64 (C_{arom}, 3-bromophenyl), 134.63 (C_{arom}, pyridine moiety), 122.75 (CH, imidazole ring).

IR ν_{max} cm^{-1}: 1647 (C=N), 1528 (C=C)

MS *m/z* (% relative abundance): 273.1

➢ 2-(4-bromophenyl)imidazo[1,2-a]pyridine (IP-4Br)

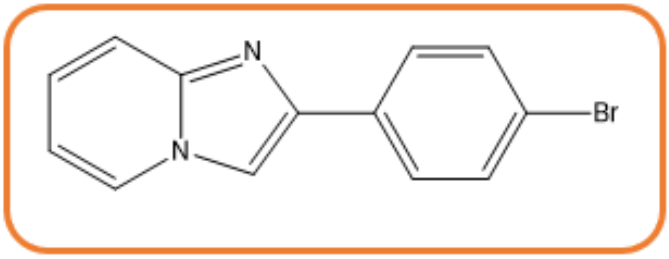

Structure: $C_{13}H_9BrN_2$

Molar mass (g/mol): 273,13

Yield: 57% (A), 96% (B)

Aspect: yellow solid

Mp (°C): 218

^{1}H NMR 91 MHz, (CD)$_3$SO δ_H: 8.74–8.42 (1H, m, N–CH, imidazole ring), 7.86–6.87 (8H, m, H_{arom}, pyridine and 4-bromophenyl rings)

^{13}C NMR 23 MHz, (CD)$_3$SO δ: 132.57 (C_{arom}, 4-bromophenyl ring), 130.56 (C_{arom}, pyridine moiety), 128.34 (C_{arom}, phenyl ring), 115.77 (CH, pyridine ring), 114.55 (CH, imidazole ring).

IR ν_{max} cm^{-1}: 1626 (C=N), 1528 (C=C)

MS *m/z* (% relative abundance): 274.1

- **2-(p-tolyl)imidazo[1,2-a]pyridine (IP-4Me)**

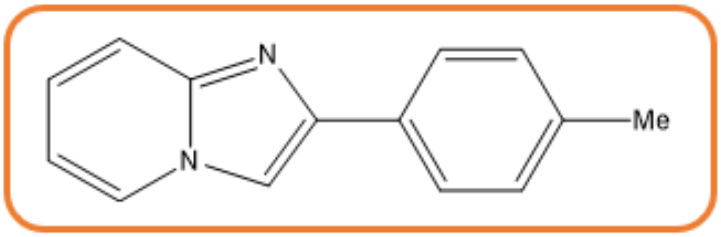

Structure: $C_{14}H_{12}N_2$

Molar mass (g/mol): 208,26

Yield: 39% (A), 66% (B)

Aspect: white solid

Mp (°C): 144

^{1}H NMR 91 MHz, (CD)$_3$SO δ_H: 9.21–8.89 (1H, m, N–CH, imidazole ring), 8.04–7.36 (8H, m, H_{arom}, pyridine and phenyl rings), 2.84 (3H, s, CH_3).

^{13}C NMR 23 MHz, (CD)$_3$SO δ: 133.88 (C_{arom}, tolyl ring), 130.41 (C_{arom}, pyridine moiety), 129.47 (C_{arom}, tolyl ring), 126.50 (CH, imidazole ring), 117.81 (CH, pyridine ring), 112.37 (CH, aromatic ring).

IR ν_{max} cm^{-1}: 1657 (C=N), 1533 (C=C)

MS *m/z* (% relative abundance): 208.3

➢ 2-(2-methoxyphenyl)imidazo[1,2-a]pyridine (IP-2OMe)

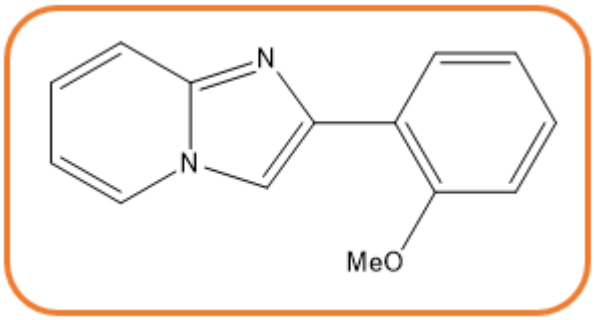

Structure: $C_{14}H_{12}N_2O$

Molar mass (g/mol): 224,26

Yield: 33% (A), 68% (B)

Aspect: pale solid

Mp (°C): 94

^{1}H NMR 91 MHz, $(CD)_3SO$ δ_H: 9.08–8.72 (1H, m, N–CH, imidazole ring), 7.97–7.34 (8H, m, H_{arom}, pyridine and 2-methoxyphenyl rings), 4.02 (3H, s, OCH_3).

^{13}C NMR 23 MHz, $(CD)_3SO$ δ: 133.95 (C_{arom}, 2-methoxyphenyl ring), 132.26 (C_{arom}, pyridine moiety), 129.38 (C_{arom}, phenyl ring), 128.21 (CH, pyridine ring), 121.46 (CH, imidazole ring), 117.67 (C_{arom}, adjacent to OCH_3 group), 112.80 (CH, aromatic ring), 112.24 (CH, aromatic ring), 56.54 (OCH_3, methoxy group).

IR ν_{max} cm^{-1}: 1650 (C=N), 1578 (C=C)

MS *m/z* (% relative abundance): 224.2

➢ 2-(3-methoxyphenyl)imidazo[1,2-a]pyridine (IP-3OMe)

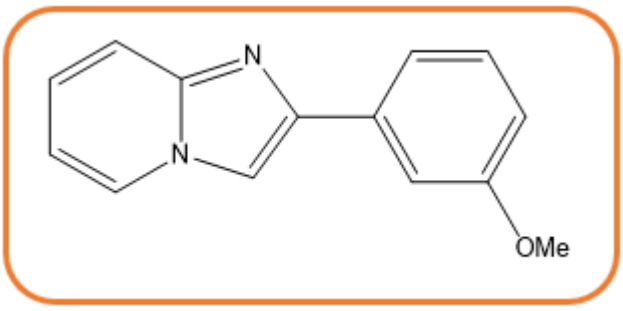

Structure: $C_{14}H_{12}N_2O$

Molar mass (g/mol): 224,26

Yield: 47% (A), 84% (B)

Aspect: pale solid

Mp (°C): 96

^{1}H NMR 91 MHz, (CD)$_3$SO δ_H: 8.89 (1H, t, J = 3.4 Hz, N–CH, imidazole ring), 7.96–7.11 (8H, m, H_{arom}, pyridine and 3-methoxyphenyl rings), 3.87 (3H, s, OCH_3)

^{13}C NMR 23 MHz, (CD)$_3$SO δ: 160.28 (C_{arom}, C–OCH_3 of 3-methoxyphenyl ring), 140.40 (C_{arom}, pyridine moiety), 135.49 (C_{arom}, phenyl ring), 127.92 (CH, imidazole ring).

IR ν_{max} cm^{-1}: 1653 (C=N), 1526 (C=C)

MS *m/z* (% relative abundance): 224.3

➢ 2-(4-methoxyphenyl)imidazo[1,2-a]pyridine (IP-4OMe)

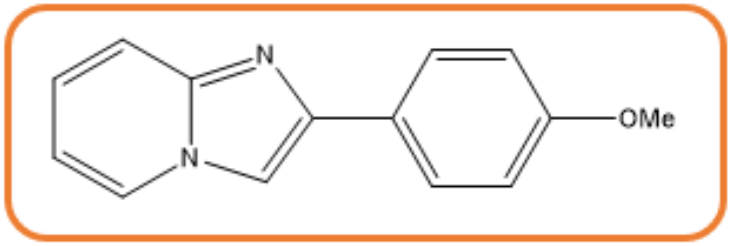

Structure: $C_{14}H_{12}N_2O$

Molar mass (g/mol): 224,26

Yield: 49% (A), 92% (B)

Aspect: pale solid

Mp (°C): 134

^{1}H NMR 91 MHz, (CD)$_3$SO δ_H: 9.02–8.56 (1H, m, N–CH, imidazole ring), 8.06–7.02 (8H, m, H_{arom}, pyridine and 4-methoxyphenyl rings), 3.85 (3H, s, OCH_3)

^{13}C NMR 23 MHz, (CD)$_3$SO δ: 133.65 (C_{arom}, pyridine moiety), 129.30 (C_{arom}, 4-methoxyphenyl ring), 128.17 (CH, imidazole ring), 117.76 (CH, pyridine ring), 115.25 (CH, aromatic ring), 112.16 (CH, aromatic ring), 55.99 (OCH_3, methoxy group).

IR ν_{max} cm^{-1}: 1653 (C=N), 1583 (C=C)

MS *m/z* (% relative abundance): 224.3

➢ 2-(4-fluorophenyl)imidazo[1,2-a]pyridine (IP-4F)

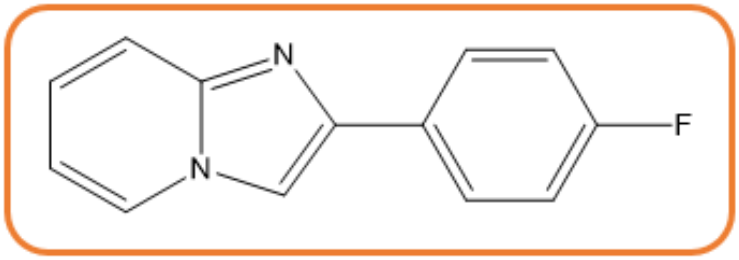

Structure: $C_{13}H_9FN_2$

Molar mass (g/mol): 212,23

Yield: 53% (A), 89% (B)

Aspect: yellow solid

Mp (°C): 158

^{1}H NMR 91 MHz, $(CD)_3SO$ δ_H: 9.04–8.75 (1H, m, N–CH, imidazole ring), 8.80 (1H, s, H_{arom}, pyridine ring), 8.20–7.29 (7H, m, H_{arom}, pyridine and 4-fluorophenyl rings)

^{13}C NMR 23 MHz, $(CD)_3SO$ δ: 133.91 (C_{arom}, pyridine moiety), 129.22 (C_{arom}, 4-fluorophenyl ring), 128.84 (CH, imidazole ring), 117.73 (CH, pyridine ring), 117.45 (CH, aromatic ring), 116.47 (CH, aromatic ring), 112.37 (CH, aromatic ring).

IR ν_{max} cm^{-1}: 1654 (C=N), 1529 (C=C)

MS *m/z* (% relative abundance): 213

➢ 2-(4-chlorophenyl)imidazo[1,2-a]pyridine (IP-4Cl)

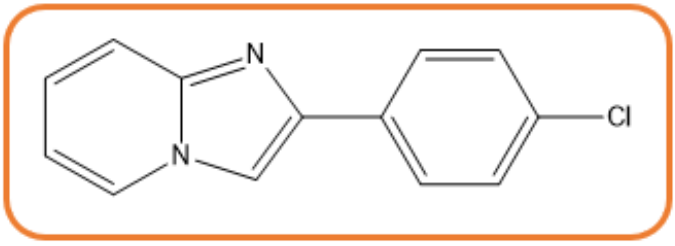

Structure: $C_{13}H_9ClN_2$

Molar mass (g/mol): 228,68

Yield: 46% (A), 83% (B)

Aspect: yellow solid

Mp (°C): 204

^{1}H NMR 91 MHz, (CD)$_3$SO δ_H: 8.87 (1H, d, J = 7.4 Hz, N–CH, imidazole ring), 7.99–7.46 (8H, m, H_{arom}, pyridine and 4-chlorophenyl rings).

^{13}C NMR 23 MHz, (CD)$_3$SO δ: Not interpretable due to low signal quality.

IR ν_{max} cm^{-1}: 1656 (C=N), 1527 (C=C)

MS *m/z* (% relative abundance): 228

➢ 2-(naphthalen-2-yl)imidazo[1,2-a]pyridine (IP-2Naph)

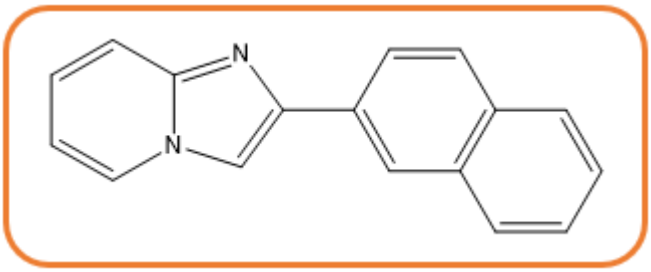

Structure: $C_{17}H_{12}N_2$

Molar mass (g/mol): 244,30

Yield: 41% (A), 85% (B)

Aspect: white solid

Mp (°C): 152

^{1}H NMR 91 MHz, (CD)$_3$SO δ_H: 8.92 (1H, d, J = 5.2 Hz, N–CH, imidazole ring), 8.31–7.33 (11H, m, H_{arom}, pyridine and naphthyl rings)

^{13}C NMR 23 MHz, (CD)$_3$SO δ: 136.09 (C_{arom}, pyridine moiety), 133.62 (C_{arom}, naphthyl ring), 132.97 (C_{arom}, naphthyl ring), 129.56 (CH, naphthyl ring), 129.37 (CH, aromatic ring), 128.60 (CH, naphthyl ring), 128.17 (CH, aromatic ring), 127.88 (CH, aromatic ring), 127.67 (CH,

naphthyl ring), 125.86 (CH, imidazole ring), 124.43 (CH, pyridine ring), 123.60 (CH, naphthyl ring), 117.48 (CH, aromatic ring).

IR ν_{max} cm^{-1}: 1656 (C=N), 1530 (C=C)

MS *m/z* (% relative abundance): 245

➢ 2-(3,4-dimethylphenyl)imidazo[1,2-a]pyridine (IP-3,4-diMe)

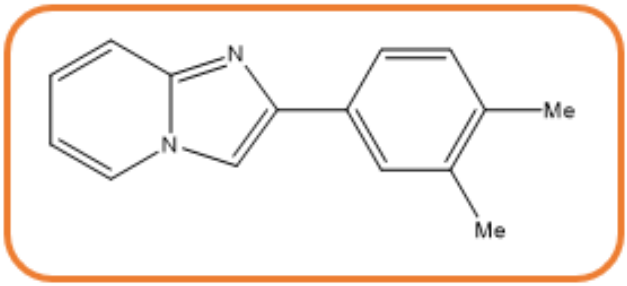

Structure: $C_{15}H_{14}N_2$

Molar mass (g/mol): 222,29

Yield: 33% (A), 60% (B)

Aspect: pale solid

Mp (°C): 144

^{1}H NMR 91 MHz, $(CD)_3SO$ δ_H: 9.03–8.67 (1H, m, N–CH, imidazole ring), 8.07–7.22 (7H, m, H_{arom}, pyridine and 3,4-dimethylphenyl rings), 2.64–2.21 (6H, m, 2 × CH_3)

^{13}C NMR 23 MHz, $(CD)_3SO$ δ:135.65 (C_{arom}, pyridine moiety), 123.89 (CH, imidazole ring), 20.1 (2xCH_3, 3,4-dimethyl group).

IR ν_{max} cm^{-1}: 1657 (C=N), 1529 (C=C)

MS *m/z* (% relative abundance): 223

II.3. Synthesis of imidazo[1,2-a]pyrimidines (IPMs)

Imidazo[1,2-a]pyrimidine derivatives were prepared using three distinct synthetic approaches, each based on the reaction of 2-aminopyrimidine with various bromoacetophenones under different conditions.

General procedure for the synthesis of imidazo[1,2-a]pyrimidine derivatives:

Equimolar amounts of 2-aminopyrimidine (10 mmol) and the appropriate bromoacetophenone derivative (10 mmol) were used in each method, as described below:

Method A: Thermal Reflux: The reaction was carried out in ethanol (10 mL) under reflux for 5 to 6 hours. After completion of the reaction (monitored by TLC), the mixture was allowed to cool to room temperature. The resulting solid was collected by filtration, then washed repeatedly with ethanol and diethyl ether, and dried under vacuum.

Method B: Gold Catalyst-Assisted Reflux: A heterogeneous catalytic system based on gold nanoparticles supported on titanium dioxide (1% Au/TiO_2) was used. The catalyst was added at 10% w/w relative to the amount of 2-aminopyrimidine. The reaction mixture containing 2-aminopyrimidine (10 mmol), bromoacetophenone (10 mmol), and the catalyst was refluxed in ethanol (10 mL) for 2 to 3 hours. After completion (checked by TLC), the hot mixture was filtered to remove the catalyst. The filtrate was cooled, and the crude product was purified by washing several times with ethanol and diethyl ether, then dried under reduced pressure.

Method C: Solvent-Free Microwave Irradiation: A mixture of 2-aminopyrimidine (10 mmol), bromoacetophenone (10 mmol), and aluminum oxide (Al_2O_3, 30% w/w) was homogenized under solvent-free conditions prior to microwave irradiation. The mixture was then placed in a domestic microwave and irradiated for 90 to 300 seconds (depending on the substitution pattern). Upon completion of the reaction, the mixture was cooled then washed with ethanol and diethyl ether.

➢ 2-phenylimidazo[1,2-a]pyrimidine (IPM-H)

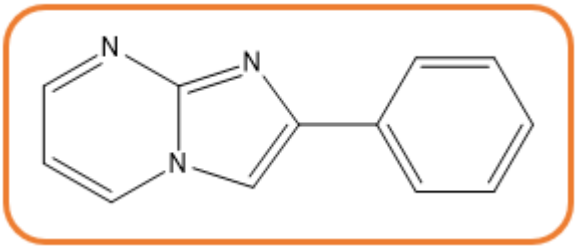

Structure: $C_{12}H_9N_3$

Molar mass (g/mol): 195,23

Yield: 37 (A); 73 (B); 70 (C)

Aspect: solid light brown

Mp (°C): 196

^{1}H NMR 91 MHz, (CD)$_3$SO δ_H: 9.30 (1H, dd, J = 6.7, 1.9 Hz, N–CH, imidazole ring), 8.98–7.44 (8H, m, H_{arom}, pyrimidine and phenyl rings)

^{13}C NMR 23 MHz, (CD)$_3$SO δ: 157.29 (C_{arom}, pyrimidine moiety), 138.22 (C_{arom}, phenyl ring), 131.07 (CH, pyrimidine ring), 130.02 (CH, aromatic ring), 126.81 (CH, phenyl ring), 114.31 (CH, aromatic ring).

IR ν_{max} cm^{-1}: 1644 (C=N), 1528 (C=C)

MS *m/z* (% relative abundance): 196

- **2-(3-bromophenyl)imidazo[1,2-a]pyrimidine 1 (IPM-3Br)**

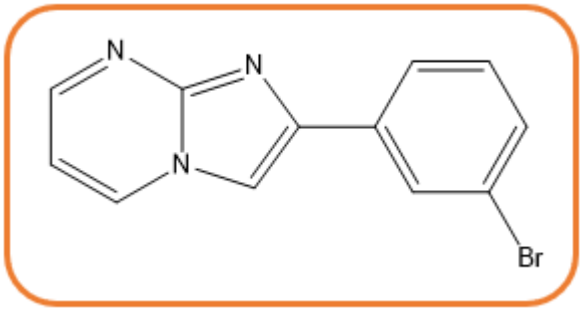

Structure: $C_{12}H_8BrN_3$

Molar mass (g/mol): 274,12

Yield: 44 (A) ; 60 (B) ; 56 (C)

Aspect: solid light brown

Mp (°C): 192

^{1}H NMR 91 MHz, (CD)$_3$SO δ_H: 9.02 (1H, dd, J = 6.7, 1.9 Hz, N–CH, imidazole ring), 8.59 (2H, d, J = 9.6 Hz, H_{arom}, pyrimidine ring), 8.31–7.17 (5H, m, H_{arom}, 3-bromophenyl and imidazopyrimidine rings)

^{13}C NMR 23 MHz, (CD)$_3$SO δ: Not interpretable due to low signal quality.

IR ν_{max} cm^{-1}: 1616 (C=N), 1597 (C=C)

MS *m/z* (% relative abundance): 274

➢ 2-(4-bromophenyl)imidazo[1,2-a]pyrimidine (IPM-4Br)

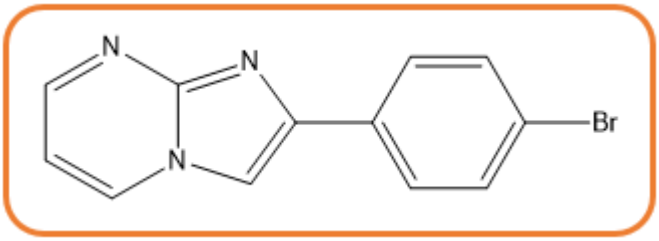

Structure: $C_{12}H_8BrN_3$

Molar mass (g/mol): 274,12

Yield: 61 (A) ; 72 (B) ; 63 (C)

Aspect: white solid

Mp (°C): 210

^{1}H NMR 91 MHz, $(CD)_3SO$ δ_H: 9.21 (1H, dd, J = 6.6, 1.9 Hz, N–CH, imidazole ring), 8.86–7.45 (7H, m, H_{arom}, pyrimidine and 4-bromophenyl rings).

^{13}C NMR 23 MHz, $(CD)_3SO$ δ: Not interpretable due to low signal quality.

IR ν_{max} cm^{-1}: 1644 (C=N), 1528 (C=C)

MS *m/z* (% relative abundance): 276

➢ 2-(p-tolyl)imidazo[1,2-a]pyrimidine (IPM-4Me)

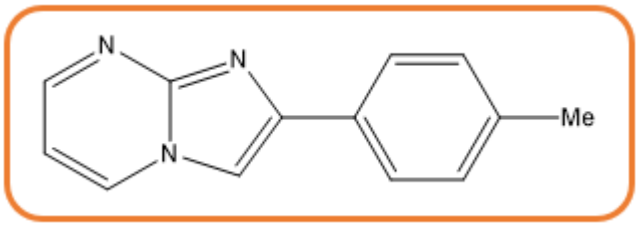

Structure: $C_{13}H_{11}N_3$

Molar mass (g/mol): 209,25

Yield: 62 (A); 76 (B); 68 (C)

Aspect: pale solid

Mp (°C): 230

^{1}H NMR 91 MHz, (CD)$_3$SO δ: 9.48 (1H, dd, J = 6.9, 1.7 Hz, N–CH, imidazole ring), 9.13–7.37 (7H, m, H_{arom}, pyrimidine and p-tolyl rings), 2.74–2.55 (3H, m, CH_3, methyl group)

^{13}C NMR 23 MHz, (CD)$_3$SO δ: 156.90 (C_{arom}, pyrimidine ring), 144.71 (C_{arom}, p-tolyl ring), 140.87 (C_{arom}, imidazole ring), 137.96 (C_{arom}, pyrimidine moiety), 136.74 (C_{arom}, point of substitution), 130.35 (CH, aromatic ring), 126.51 (CH, imidazole ring), 124.12 (CH, pyrimidine ring), 114.14 (CH, aromatic ring), 109.40 (CH, aromatic ring), 19.40 (CH_3, methyl group)

IR ν_{max} cm^{-1}: 1643 (C=N), 1535 (C=C)

MS *m/z* (% relative abundance): 210

➢ 2-(2-methoxyphenyl)imidazo[1,2-a]pyrimidine (IPM-2OMe)

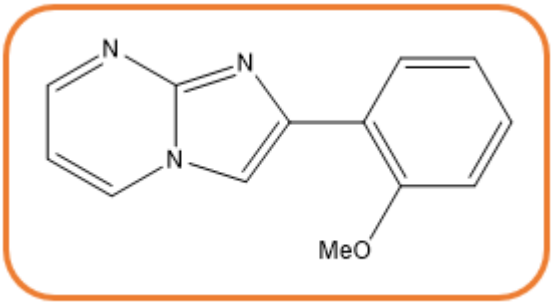

Structure: $C_{13}H_{11}N_3O$

Molar mass (g/mol): 225,25

Yield: 42 (A); 76 (B); 57 (C)

Aspect: yellow solide

Mp (°C): 266

^{1}H NMR 91 MHz, (CD)$_3$SO δ$_H$: 9.09–8.73 (1H, m, N–CH, imidazole ring), 8.12–7.00 (7H, m, H_{arom}, pyrimidine and 2-methoxyphenyl rings), 4.02 (3H, s, OCH_3, methoxy group).

^{13}C NMR 23 MHz, (CD)$_3$SO δ: 157.00 (C_{arom}, pyrimidine ring), 139.61 (C_{arom}, imidazo core), 133.97 (C_{arom}, 2-methoxyphenyl ring), 132.23 (CH, aromatic ring), 131.69 (CH, pyrimidine ring), 129.37 (CH, phenyl ring), 128.17 (CH, aromatic ring), 121.40 (CH, imidazole ring),

114.77 (CH, aromatic rings), 114.18 (CH, aromatic rings), 112.72 (CH, aromatic rings), 112.17 (CH, aromatic rings), 56.53 (OCH_3, methoxy group).

IR ν_{max} cm^{-1}: 1638 (C=N), 1527 (C=C)

MS *m/z* (% relative abundance): 226

➢ 2-(3-methoxyphenyl)imidazo[1,2-a]pyrimidine (IPM-3OMe)

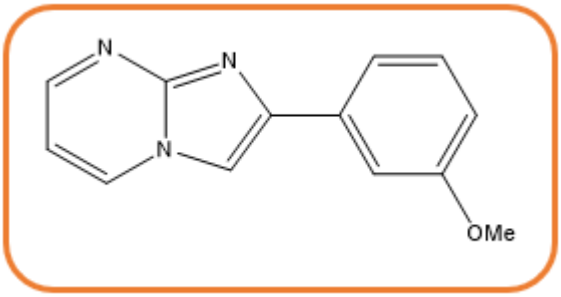

Structure: $C_{13}H_{11}N_3O$

Molar mass (g/mol): 225,25

Yield: 49 (A); 71 (B); 53 (C)

Aspect: brown solid

Mp (°C): 220

^{1}H NMR 91 MHz, $(CD)_3SO$ δ_H: 9.31 (1H, dd, J = 6.7, 1.8 Hz, N–CH, imidazole ring), 9.13–6.86 (7H, m, H_{arom}, pyrimidine and 3-methoxyphenyl rings), 3.85 (3H, d, J = 1.7 Hz, OCH_3, methoxy group).

^{13}C NMR 23 MHz, $(CD)_3SO$ δ: 160.25 (C_{arom}, carbon linked to the methoxy group), 157.27 (C_{arom}, pyrimidine ring), 144.80 (C_{arom}, imidazo core), 138.09 (C_{arom}, substituted phenyl), 136.54 (C_{arom}, pyrimidine ring), 131.11 (CH, pyrimidine ring), 128.26 (CH, aromatic ring), 118.91 (CH, imidazole ring), 116.77 (CH, aromatic rings), 114.26 (CH, aromatic rings), 111.90 (CH, aromatic rings), 110.38 (CH, aromatic rings), 56.03 (OCH_3, methoxy group).

IR ν_{max} cm^{-1}: 1647 (C=N), 1530 (C=C)

MS *m/z* (% relative abundance): 226

➢ 2-(4-methoxyphenyl)imidazo[1,2-a]pyrimidine (IPM-4OMe)

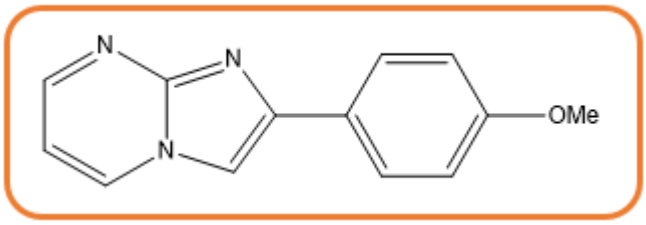

Structure: $C_{13}H_{11}N_3O$

Molar mass (g/mol): 225,25

Yield: 32 (A); 65 (B); 52 (C)

Aspect: yellow solid

Mp (°C): 190

^{1}H NMR 91 MHz, $(CD)_3SO$ δ_H: 9.52 (1H, s, N–CH, imidazole ring), 8.15–7.04 (7H, m, H_{arom}, pyrimidine and 4-methoxyphenyl rings), 3.87 (3H, d, J = 2.2 Hz, OCH_3, methoxy group). **^{13}C NMR 23 MHz, $(CD)_3SO$ δ:** 169.47 (C_{arom}, carbon linked to the methoxy group), 164.43 (C_{arom}, pyrimidine ring), 131.19 (CH, aromatic ring), 127.30 (CH, aromatic ring), 114.66 (CH, aromatic ring), 107.81 (CH, aromatic ring), 56.27 (OCH_3, methoxy group).

IR ν_{max} cm^{-1}: 1642 (C=N), 1535 (C=C)

MS *m/z* (% relative abundance): 226

➢ 2-(4-fluorophenyl)imidazo[1,2-a]pyrimidine (IPM-4F)

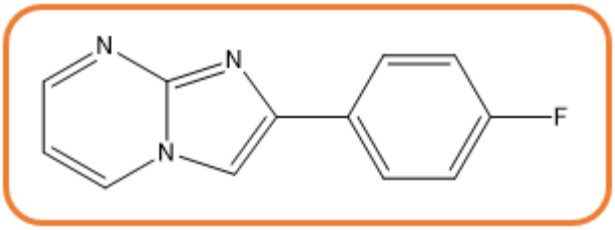

Structure: $C_{12}H_8FN_3$

Molar mass (g/mol): 213,22

Yield: 50 (A); 68 (B); 63 (C)

Aspect: solid light brown

Mp (°C): 230

^{1}H NMR 91 MHz, (CD)$_3$SO δ_H: 9.29 (1H, dd, J = 6.7, 1.9 Hz, N–CH, imidazole ring), 8.96–7.26 (7H, m, H_{arom}, pyrimidine and 4-fluorophenyl rings).

^{13}C NMR 23 MHz, (CD)$_3$SO δ: 157.01 (C_{arom}, C-F), 144.81 (C_{arom}, pyrimidine ring), 137.99 (C_{arom}, imidazole core), 135.90 (C_{arom}, phenyl ring linked to pyrimidine core), 129.26 (CH, aromatic ring), 128.89 (CH, aromatic ring), 123.79 (CH, imidazole ring), 117.39 (CH, aromatic ring), 116.44 (CH, aromatic ring), 114.06 (CH, aromatic ring), 109.88 (CH, aromatic ring).

IR ν_{max} cm^{-1}: 1644 (C=N), 1547 (C=C)

MS *m/z* (% relative abundance): 214

➢ 2-(4-chlororophenyl)imidazo[1,2-a]pyrimidine (IPM-4Cl)

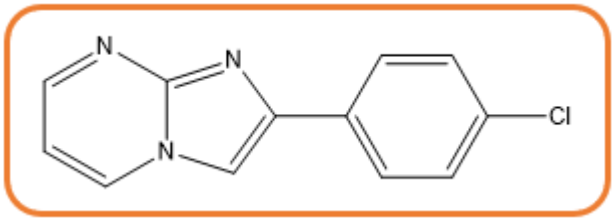

Structure: $C_{12}H_8ClN_3$

Molar mass (g/mol): 229,67

Yield: 60 (A); 73 (B); 65 (C)

Aspect: solid light brown

Mp (°C): 274

^{1}H NMR 91 MHz, (CD)$_3$SO δ_H: 9.25 (1H, d, J = 6.9 Hz, N–CH, imidazole ring), 8.92–7.26 (7H, m, H_{arom}, pyrimidine and 4-chlorophenyl rings).

^{13}C NMR 23 MHz, (CD)$_3$SO δ: 156.80 (C_{arom}, C–Cl), 145.13 (C_{arom}, pyrimidine ring), 137.97 (C_{arom}, imidazole core), 136.45 (C_{arom}, phenyl ring), 129.32 (CH, aromatic ring), 128.94 (CH, aromatic ring), 124.24 (CH, imidazole ring), 117.46 (CH, aromatic ring), 116.50 (CH, aromatic ring), 113.87 (CH, aromatic ring), 109.74 (CH, aromatic ring).

IR ν_{max} cm^{-1}: 1646 (C=N), 1533 (C=C)

MS *m/z* (% relative abundance): 230

➢ 2-(naphthalen-2-yl)imidazo[1,2-a]pyrimidine (IPM-2Naph)

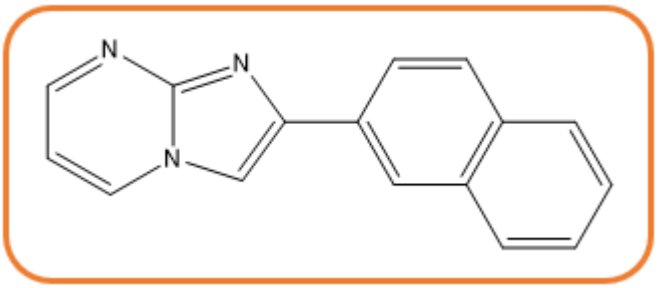

Structure: $C_{16}H_{11}N_3$

Molar mass (g/mol): 245,29

Yield: 53 (A); 79 (B); 67 (C)

Aspect: pale solid

Mp (°C): 250

^{1}H NMR 91 MHz, $(CD)_3SO$ δ_H: 9.25 (1H, dd, J = 6.8, 1.9 Hz, N–CH, imidazole ring), 8.96–7.46 (10H, m, H_{arom}, pyrimidine and naphthyl rings).

^{13}C NMR 23 MHz, $(CD)_3SO$ δ: 156.03 (C_{arom}, pyrimidine ring), 145.74 (C_{arom}, pyrimidine ring), 138.58 (C_{arom}, imidazole ring), 137.64 (C_{arom}, naphthyl ring), 133.77 (C_{arom}, naphthyl ring), 133.21 (C_{arom}, naphthyl ring), 129.49 (CH, aromatic ring), 128.84 (CH, aromatic ring), 128.29 (CH, aromatic ring), 127.85 (CH, aromatic ring), 123.79 (CH, imidazole ring), 113.27 (CH, aromatic ring), 110.08 (CH, aromatic ring).

IR ν_{max} cm^{-1}: 1657 (C=N), 1532 (C=C)

MS *m/z* (% relative abundance): 246

➢ 2-(3,4-dimethylphenyl)imidazo[1,2-a]pyrimidine (IPM-3,4-diMe)

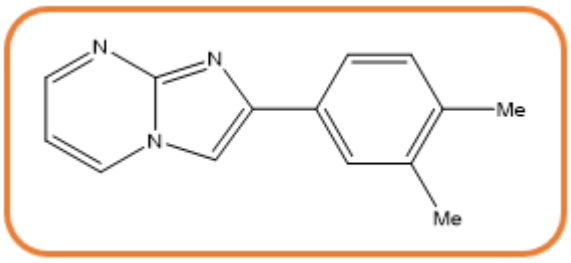

Structure: $C_{14}H_{13}N_3$

Molar mass (g/mol): 223,28

Yield: 41 (A); 81 (B); 64 (C)

Aspect: solid light brown

Mp (°C): 232

^{1}H NMR 91 MHz, $(CD)_3SO$ δ_H: 9.27 (dd, J = 6.8, 1.9 Hz, 1H), 8.95 - 7.35 (m, 6H), 2.64 – 2.20 (m, 6H)

^{13}C NMR 23 MHz, $(CD)_3SO$ δ: 156.77 (C_{arom}, pyrimidine ring), 144.58 (C_{arom}, imidazo core), 139.63 (C_{arom}, 3,4-dimethylphenyl ring), 137.82 (C_{arom}, pyrimidine ring), 136.73 (C_{arom}, aromatic ring), 130.70 (CH, aromatic ring), 127.36 (CH, aromatic ring), 124.29 (CH, imidazole ring), 123.94 (CH, pyrimidine ring), 114.00 (CH, aromatic ring), 109.19 (CH, aromatic ring), 19.72 (CH_3, methyl group), 19.63 (CH_3, methyl group).

IR ν_{max} cm^{-1}: 1644 (C=N), 1531 (C=C)

MS *m/z* (% relative abundance): 224

II.4. Synthesis of imidazo[2,1-b]thiazoles (IMThs)

Imidazo[2,1-b]thiazole derivatives were synthesized through two different procedures involving the condensation of 2-aminothiazole with bromoacetophenone derivatives in ethanol under reflux conditions.

General procedure for the synthesis of imidazo[2,1-b]thiazoles:

Method A: A mixture of 2-aminothiazole (10 mmol) and the appropriate bromoacetophenone (10 mmol) was dissolved in ethanol (10 mL) and heated under reflux for 8–12 hours. Upon completion of the reaction, monitored by TLC, the reaction mixture was cooled to room temperature. The precipitated solid was washed thoroughly with ethanol and diethyl ether, then dried under vacuum.

Method B: The same procedure was followed as in Method A, but aluminum oxide (Al_2O_3, 30% w/w relative to 2-aminothiazole) was added as a catalyst to the reaction mixture. The mixture was refluxed in ethanol for 6–8 hours. After completion, the hot mixture was filtered

to remove Al_2O_3. The filtrate was cooled, and the resulting solid was collected by filtration, washed with ethanol and diethyl ether, and dried under reduced pressure.

➢ 6-phenylimidazo[2,1-b]thiazole (IMTh-H)

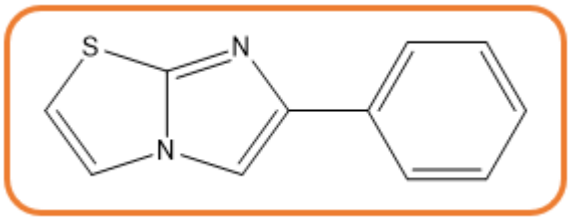

Structure: $C_{11}H_8N_2S$

Molar mass (g/mol): 200,26

Yield: 67% (A), 80% (B)

Aspect: white solid

Mp (°C): 252

^{1}H NMR 91 MHz, $(CD)_3SO$ δ_H: 9.53 (1H, s, N–CH, imidazole ring), 8.47–7.01 (7H, m, H_{arom}, phenyl and imidazole-thiazole rings).

^{13}C NMR 23 MHz, $(CD)_3SO$ δ: 128.86 (CH, aromatic ring), 128.08 (CH, aromatic ring), 126.82 (CH, aromatic ring), 118.83 (CH, imidazole ring), 80.80 (C_{arom}, thiazole ring), 79.36 (C_{arom}, thiazole ring), 77.91 (C_{arom}, imidazole core).

IR ν_{max} cm^{-1}: 1636 (C=N), 1558 (C=C), 683 (C-S)

MS *m/z* (% relative abundance): 201.

➢ 6-(p-tolyl)imidazo[2,1-b]thiazole (IMTh-4Me)

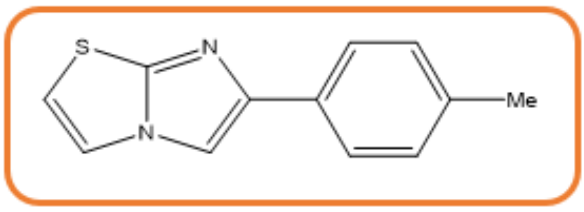

Structure: $C_{11}H_{10}N_2S$

Molar mass (g/mol): 214,29

Yield: 76% (A), 91% (B)

Aspect: white solid

Mp (°C): 240

^{1}H NMR 91 MHz, (CD)$_3$SO δ_H: 9.68 (1H, s, N–CH, imidazole ring), 8.51–7.14 (6H, m, H_{arom}, p-tolyl and imidazole-thiazole rings), 2.63–2.42 (3H, m, CH_3, methyl group).

^{13}C NMR 23 MHz, (CD)$_3$SO δ:169.31 (C_{arom}, thiazole ring), 145.20 (C_{arom}, imidazole core), 142.64 (C_{arom}, tolyl ring), 130.25 (CH, aromatic ring), 129.37 (CH, aromatic ring), 128.65 (CH, aromatic ring), 126.54 (CH, aromatic ring), 118.82 (CH, imidazole ring), 21.12 (CH_3, methyl group).

IR ν_{max} cm^{-1}: 1681 (C=N), 1560 (C=C), 619 (C-S)

MS *m/z* (% relative abundance): 215.

➢ 6-(naphthalen-2-yl)imidazo[2,1-b]thiazole (IMTh-2Naph)

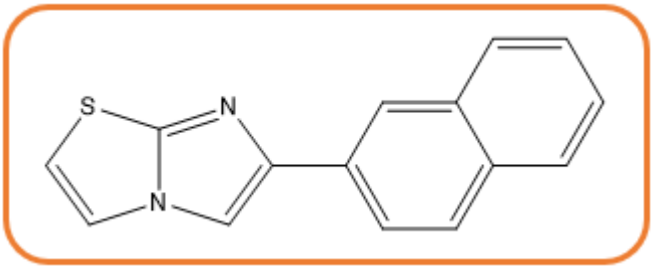

Structure: $C_{15}H_{10}N_2S$

Molar mass (g/mol): 250,32

Yield: 72% (A), 79% (B)

Aspect: white solid

Mp (°C): 254

^{1}H NMR 91 MHz, (CD)$_3$SO δ_H: 9.61 (1H, s, N–CH, imidazole ring), 8.79–7.08 (9H, m, H_{arom}, naphthyl and imidazole-thiazole rings).

^{13}C NMR 23 MHz, (CD)$_3$SO δ: 169.38 (C_{arom}, thiazole ring), 135.68 (C_{arom}, imidazole core), 131.07 (CH, aromatic ring), 129.89 (CH, aromatic ring), 128.15 (CH, aromatic ring), 123.64 (CH, imidazole ring), 107.70 (CH, aromatic ring).

IR ν_{max} cm^{-1}: 1627 (C=N), 1553 (C=C), 671 (C-S)

MS *m/z* (% relative abundance): 251

➢ 6-(2-methoxyphenyl)imidazo[2,1-b]thiazole (IMTh-2OMe)

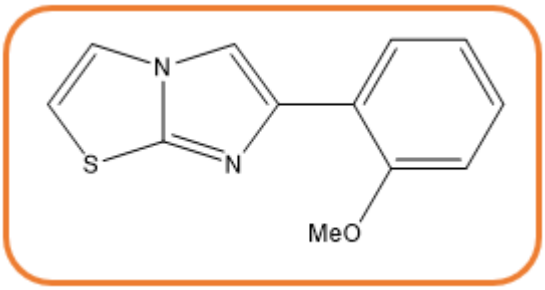

Structure: $C_{12}H_{10}N_2OS$

Molar mass (g/mol): 230,29

Yield: 62% (A), 66% (B)

Aspect: white solid

Mp (°C): 266

^{1}H NMR 91 MHz, $(CD)_3SO$ δ_H: 9.55 (1H, s, N–CH, imidazole ring), 8.52–7.03 (6H, m, H_{arom}, 2-methoxyphenyl and imidazole-thiazole rings), 4.00 (3H, s, OCH_3, methoxy group).

^{13}C NMR 23 MHz, $(CD)_3SO$ δ: 169.36 (C_{arom}, thiazole ring), 160.62 (C_{arom}, carbon linked to the methoxy group), 136.58 (C_{arom}, imidazole core), 131.39 (CH, aromatic ring), 130.89 (CH, aromatic ring), 123.75 (CH, imidazole ring), 121.31 (CH, aromatic ring), 113.57 (CH, aromatic ring), 107.60 (CH, aromatic ring), 59.16 (OCH_3, methoxy group).

IR ν_{max} cm^{-1}: 1677 (C=N), 1562 (C=C), 774 (C-S)

MS *m/z* (% relative abundance): 231

➢ 6-(3-methoxyphenyl)imidazo[2,1-b]thiazole (IMTh-3OMe)

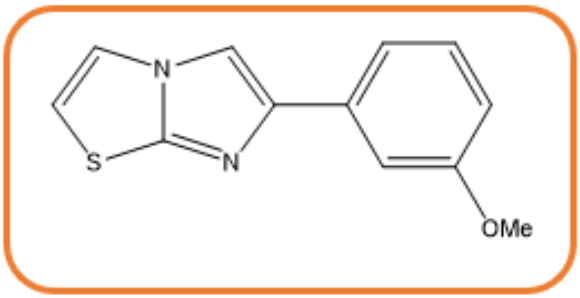

Structure: $C_{12}H_{10}N_2OS$

Molar mass (g/mol): 230,29

Yield: 82% (A), 93% (B)

Aspect: white solid

Mp (°C): 256

^{1}H NMR 91 MHz, $(CD)_3SO$ δ_H: 9.60 (1H, s, N–CH, imidazole ring), 7.61–7.06 (6H, m, H_{arom}, 3-methoxyphenyl and imidazole-thiazole rings), 3.87 (3H, s, OCH_3, methoxy group).

^{13}C NMR 23 MHz, $(CD)_3SO$ δ: 169.37 (C_{arom}, thiazole ring), 159.80 (C_{arom} carbon linked to the methoxy group), 135.56 (C_{arom}, imidazole core), 131.00 (CH, aromatic ring), 130.51 (CH, aromatic ring), 121.09 (CH, aromatic ring), 120.48 (CH, aromatic ring), 113.27 (CH, aromatic ring), 107.74 (CH, aromatic ring), 55.92 (OCH_3, methoxy group).

IR ν_{max} cm^{-1}: 1634 (C=N), 1570 (C=C), 698 (C-S)

MS *m/z* (% relative abundance): 231

➢ 6-(4-methoxyphenyl)imidazo[2,1-b]thiazole (IMTh-4OMe)

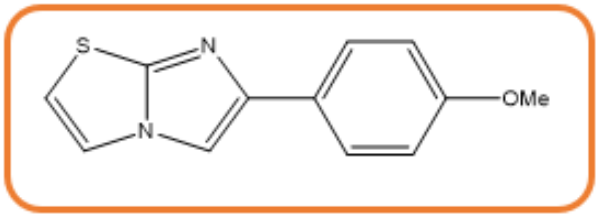

Structure: $C_{12}H_{10}N_2OS$

Molar mass (g/mol): 230,29

Yield: 80% (A), 88% (B)

Aspect: white solid

Mp (°C): 262

^{1}H NMR 91 MHz, (CD)$_3$SO δ_H: 9.62 (1H, s, N–CH, imidazole ring), 8.04–7.06 (6H, m, H_{arom}, 4-methoxyphenyl and imidazole-thiazole rings), 3.88 (3H, s, OCH_3, methoxy group).

^{13}C NMR 23 MHz, (CD)$_3$SO δ: 169.38 (C_{arom}, thiazole ring), 164.34 (C_{arom}, carbon linked to the methoxy group), 131.12 (CH, aromatic ring), 127.22 (CH, aromatic ring), 114.58 (CH, aromatic ring), 107.75 (CH, aromatic ring), 56.21 (OCH_3, methoxy group).

IR ν_{max} cm^{-1}: 1635 (C=N), 1561 (C=C), 719 (C-S)

MS *m/z* (% relative abundance): 231.

➢ 6-(4-chlorophenyl)imidazo[2,1-b]thiazole (IMTh-4Cl)

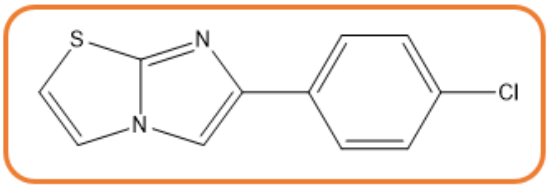

Structure: $C_{11}H_7ClN_2S$

Molar mass (g/mol): 234,70

Yield: 83% (A), 93% (B)

Aspect: white solid

Mp (°C): 232.

^{1}H NMR 91 MHz, (CD)$_3$SO δ_H: 9.67 (1H, s, N–CH, imidazole ring), 8.62–7.07 (6H, m, H_{arom}, 4-chlorophenyl and imidazole-thiazole rings).

^{13}C NMR 23 MHz, (CD)$_3$SO δ: 169.51 (C_{arom}, thiazole ring), 148.76 (C_{arom}, C–Cl), 139.60 (C_{arom}, imidazole core), 139.13 (C_{arom}, aromatic ring), 129.54 (CH, aromatic ring), 127.52 (CH, aromatic ring), 121.83 (CH, aromatic ring), 108.10 (CH, aromatic ring).

IR ν_{max} cm^{-1}: 1605 (C=N), 1556 (C=C), 613 (C-S)

MS *m/z* (% relative abundance): 234,9

➢ 6-(4-fluorophenyl)imidazo[2,1-b]thiazole (IMTh-F)

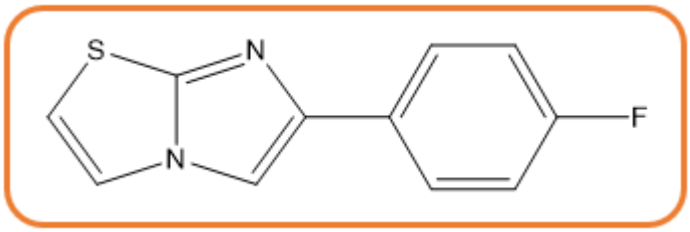

Structure: $C_{11}H_7FN_2S$

Molar mass (g/mol): 218,25

Yield: 50% (A), 87% (B)

Aspect: white solid

Mp (°C): 234

^{1}H NMR 91 MHz, $(CD)_3SO$ δ_H: 9.06 (1H, s, N–CH, imidazole ring), 7.63–7.00 (6H, m, H_{arom}, 4-fluorophenyl and imidazole-thiazole rings).

^{13}C NMR 23 MHz, $(CD)_3SO$ δ: 169.31 (C_{arom}, thiazole ring), 131.89 (C_{arom}, phenyl ring), 131.47 (CH, aromatic ring), 131.09 (CH, aromatic ring), 130.91 (CH, aromatic ring), 116.82 (CH, aromatic ring), 115.86 (C_{arom}, C–F), 107.74 (CH, aromatic ring).

IR ν_{max} cm^{-1}: 1638 (C=N), 1560 (C=C), 672 (C-S)

MS *m/z* (% relative abundance): 219.

III. Synthesis of 2-pyridone derivatives

The aimed heterocyclic derivatives (2-pyridones) were synthesized via a multi-step procedure beginning with the preparation of various alkenes. These intermediates were subsequently reacted with arylacetophenones and ammonium acetate under either thermal or ultrasonic conditions. The resulting products were then purified and characterized using standard analytical techniques.

III.1. Synthesis of alkenes (Alks)

Alkene derivatives were synthesized via a condensation reaction involving aromatic aldehydes, ethyl 2-cyanoacetate, and ammonium acetate in distilled water at room temperature under magnetic stirring.

General procedure for the synthesis of alkenes: A mixture of aromatic aldehyde (10 mmol), ethyl 2-cyanoacetate (10 mmol), and ammonium acetate (10 mmol) was stirred in distilled water (10 mL) at room temperature overnight. Upon completion of the reaction, as confirmed by TLC, the resulting solid was collected by filtration, washed with water to remove any unreacted materials, and dried under vacuum.

➢ Ethyl 2-cyano-3-phenylacrylate (Alk-H)

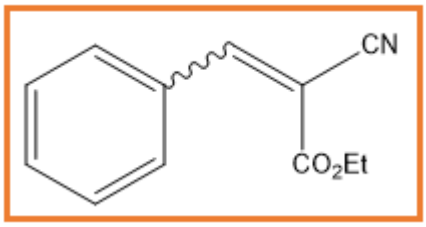

Structure: $C_{12}H_{11}NO_2$

Molar mass (g/mol): 201,08

Yield (%): 82

Aspect: white solid

Mp (°C): 224

IR ν_{max} cm^{-1}: 1637 (C=O), 1572 (C=C), 2223 (CN)

➢ Ethyl 2-cyano-3-(4-fluorophenyl)acrylate (Alk-4F)

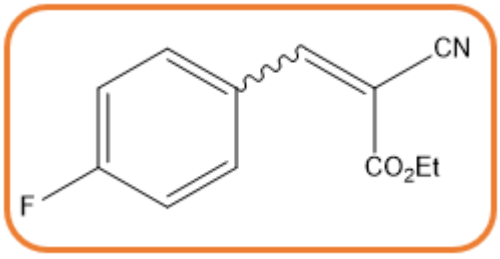

Structure: $C_{12}H_{10}FNO_2$

Molar mass (g/mol): 219,21

Yield (%): 92

Aspect : white solid

Mp (°C): 102

IR ν_{max} cm^{-1}: 1644 (C=O), 1580 (C=C), 2220 (CN)

➢ Ethyl 3-(2-chlorophenyl)-2-cyanoacrylate (Alk-2Cl)

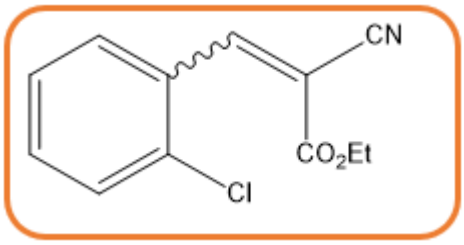

Structure: $C_{12}H_{10}ClNO_2$

Molar mass (g/mol): 235,67

Yield (%): 90

Aspect: white solid

Mp (°C): 60

IR ν_{max} cm^{-1}: 1647 (C=O), 1582 (C=C),2225 (CN)

➢ Ethyl 3-(3-chlorophenyl)-2-cyanoacrylate (Alk-3Cl)

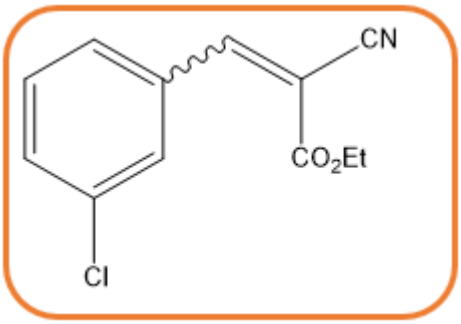

Structure: $C_{12}H_{10}ClNO_2$

Molar mass (g/mol): 235,67

Yield (%): 81

Aspect: white solid

Mp (°C): 212

IR ν_{max} cm^{-1}: 1633 (C=O), 1575 (C=C), 2224 (CN)

➢ Ethyl 3-(4-chlorophenyl)-2-cyanoacrylate (Alk-4Cl)

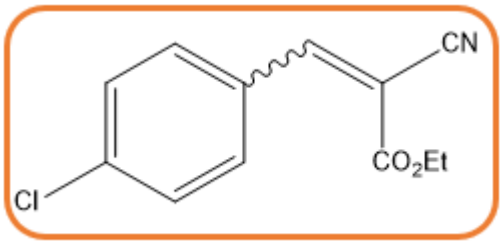

Structure: $C_{12}H_{10}ClNO_2$

Molar mass (g/mol): 235,67

Yield (%): 86

Aspect: white solid

Mp (°C): 98

IR ν_{max} cm^{-1}: 1636 (C=O), 1573 (C=C), 2222 (CN)

➢ Ethyl 3-(2,4-dichlorophenyl)-2-cyanoacrylate (Alk-2,4-diCl)

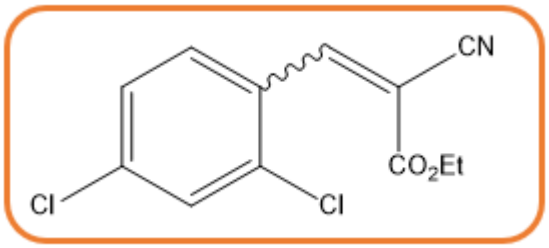

Structure: $C_{12}H_{11}NO_2$

Molar mass (g/mol): 208,26

Yield (%): 80

Aspect: white solid

Mp (°C): 224

IR ν_{max} cm^{-1}: 1639 (C=O), 1580 (C=C), 2224 (CN)

III.2. Synthesis of 2-pyridones (2-PyOs)

Two methods were employed for the cyclization of the alkene intermediates into 2-pyridone derivatives:

Method A (Classical heating): The alkene intermediate (10 mmol), an aromatic ketone (10 mmol), and ammonium acetate (10 mmol) were refluxed in ethanol (10 mL) at 80 °C for 10 hours. Upon completion, the reaction mixture was cooled to room temperature. The precipitate was collected by filtration, washed with ethanol/diethyl ether, and dried.

Method B (Ultrasound-assisted synthesis): The same reactants and proportions as in Method A were used. The reaction mixture was sonicated using an ultrasonic bath operating in ultrasound mode at 80 °C for 3 to 6 hours. After completion, the mixture was allowed to cool, and the precipitated product was isolated by filtration, washed, and dried.

➢ 4,6-bis(4-fluorophenyl)-2-oxo-1,2-dihydropyridine-3-carbonitrile: 2-PyO-(4F, 4F)

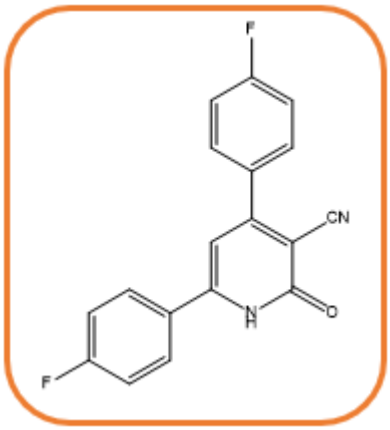

Structure: $C_{18}H_{10}F_2N_2O$

Molar mass (g/mol): 308,28

Yield (%): 70 (A); 83 (B)

Aspect: yellow solid

Mp (°C): 194

^{1}H and ^{13}C NMR: Not recorded due to limited sample purity and quantity.

IR ν_{max} cm^{-1}: 3245 (N-H), 2217 (CN), 1608 (C=O), 1524 (C=C)

MS *m/z* (% relative abundance) : 309.

➢ 6-(2,4-dichlorophenyl)-4-(4-fluorophenyl)-2-oxo-1,2-dihydropyridine-3-carbonitrile : 2-PyO-(4F, 2.4-diCl)

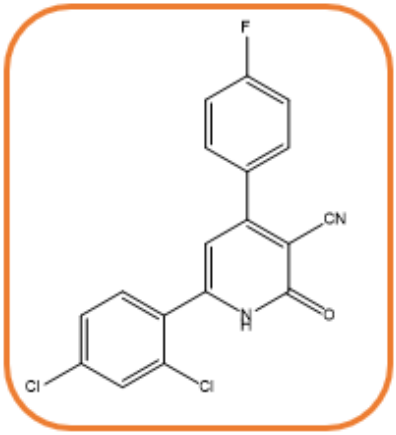

Structure: $C_{18}H_9Cl_2FN_2O$

Molar mass (g/mol): 359,18

Yield (%): 79 (A); 90 (B)

Aspect: yellow solid

Mp (°C): 264

^{1}H NMR 91 MHz, $(CD)_3SO$ δ: 7.50–6.68 (7H, m, H_{arom}, 2,4-dichlorophenyl and 4-fluorophenyl rings), 6.13 (1H, s, C=CH, pyridone ring).

^{13}C NMR 23 MHz, $(CD)_3SO$ δ: 162.28 (C_{arom}, carbonyl group of pyridone ring), 159.49 (C_{arom}, C–F), 149.46 (C_{arom}, pyridone ring), 136.76 (C_{arom}, dichlorophenyl ring), 133.80 (C_{arom}, dichlorophenyl ring), 133.56 (C_{arom}, aromatic ring), 132.36 (CH, aromatic ring), 131.98 (CH, aromatic ring), 131.59 (CH, aromatic ring), 130.39 (CH, aromatic ring), 128.61 (CH, aromatic ring), 117.38 (CH, aromatic ring), 116.42 (CN, nitrile group), 109.62 (CH, pyridone ring).

IR ν_{max} cm^{-1}: 3544 (N-H), 2220 (CN), 1646 (C=O), 1580 (C=C)

MS *m/z* (% relative abundance): 360

➢ 4-(4-fluorophenyl)-2-oxo-6-(p-tolyl)-1,2-dihydropyridine-3-carbonitrile : 2-PyO-(4F, 4Me)

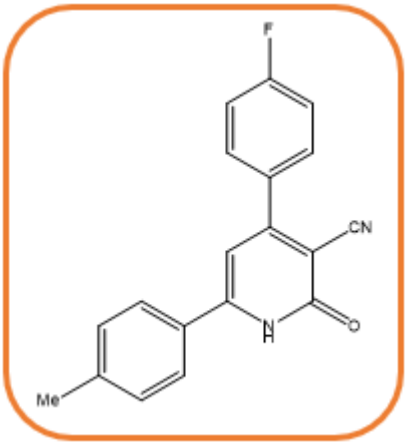

Structure: $C_{19}H_{13}FN_2O$

Molar mass (g/mol): 304,32

Yield (%): 22 (A); 62 (B)

Aspect: yellow solid

Mp (°C): > 266

^{1}H NMR 91 MHz, $(CD)_3SO$: not recorded due to limited sample purity and quantity.

^{13}C NMR 23 MHz, $(CD)_3SO$: 130.08 (CH, aromatic ring), 129.70 (CH, aromatic ring), 128.59 (CH, aromatic ring), 126.74 (CH, aromatic ring), 115.36 (CH, aromatic ring), 114.42 (CN, nitrile group), 104.78 (CH, pyridone ring), 19.99 (CH_3, methyl group).

IR ν_{max} cm^{-1}: 3845 (N-H), 2212 (CN), 1643 (C=O), 1578 (C=C)

MS *m/z* (% relative abundance): 305

➢ 6-(3,4-dimethylphenyl)-4-(4-fluorophenyl)-2-oxo-1,2-dihydropyridine-3-carbonitrile: 2-PyO-(4F, 3.4-diMe)

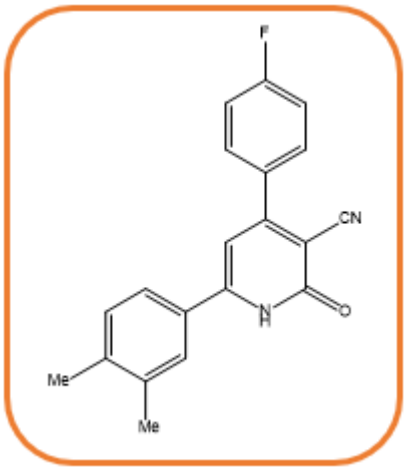

Structure: $C_{20}H_{15}FNO_2$

Molar mass (g/mol): 318,34

Yield (%): 47 (A), 60 (B)

Aspect: yellow solid

Mp (°C): 264

^{1}H NMR 91 MHz, $(CD)_3SO$ δ: 7.92–6.80 (7H, m, H_{arom}, 3,4-dimethylphenyl and 4-fluorophenyl rings), 6.59 (1H, d, J = 8.8 Hz, C=CH, pyridone ring), 2.28 (6H, s, 2×CH_3, methyl groups).

^{13}C NMR 23 MHz, $(CD)_3SO$ δ: 162.25 (C_{arom}, carbonyl group of pyridone ring), 156.88 (C_{arom}, C–F), 151.97 (C_{arom}, pyridone ring), 135.48 (C_{arom}, substituted phenyl ring), 134.63 (C_{arom}, substituted phenyl ring), 132.37 (CH, aromatic ring), 131.89 (CH, aromatic ring), 130.82 (CH, aromatic ring), 130.43 (CH, aromatic ring), 129.69 (CH, aromatic ring), 128.18 (CH, aromatic ring), 116.78 (CH, aromatic ring), 115.86 (CN, nitrile group), 107.35 (CH, pyridone ring), 19.02 (CH_3, methyl groups).

IR ν_{max} cm^{-1}: 3144 (N-H), 2220 (CN), 1651 (C=O), 1509 (C=C)

MS *m/z* (% relative abundance): 319.

➢ 4-(4-fluorophenyl)-6-(naphthalen-2-yl)-2-oxo-1,2-dihydropyridine-3-carbonitrile : 2-PyO-(4F, 2-Naph)

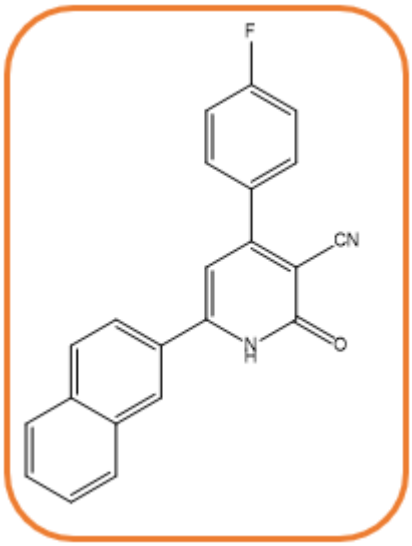

Structure: $C_{22}H_{13}FN_2O$

Molar mass (g/mol): 340,35

Yield (%): 80 (A), 81 (B)

Aspect: yellow solid

Mp (°C): > 266

^{1}H and ^{13}C NMR: Not recorded due to limited sample purity and quantity.

IR ν_{max} cm^{-1}: 3496(N-H), 3067, 2213(CN), 1737 (C=O), 1568 (C=C)

MS *m/z* (% relative abundance): 341

➢ 4-(4-fluorophenyl)-6-(4-methoxyphenyl)-2-oxo-1,2-dihydropyridine-3-carbonitrile: 2-PyO-(4F, 4OMe)

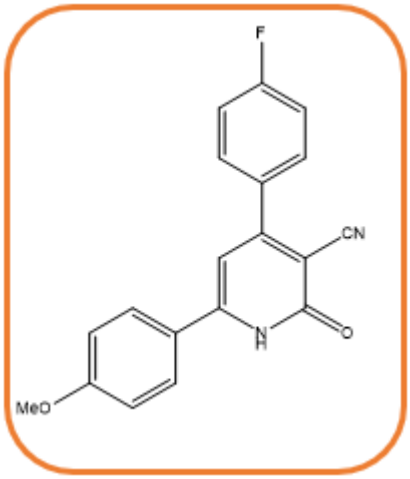

Structure: $C_{19}H_{13}FN_2O_2$

Molar mass (g/mol): 320,32

Yield (%): 12 (A), 35 (B)

Aspect: yellow solid

Mp (°C): 232

^{1}H and ^{13}C NMR: Not recorded due to limited sample purity and quantity.

IR ν_{max} cm^{-1}: 2989 (N-H), 2221 (CN), 1609 (C=O), 1511 (C=C)

MS *m/z* (% relative abundance): 321

➢ 4-(2-chlorophenyl)-6-(4-fluorophenyl)-2-oxo-1,2-dihydropyridine-3-carbonitrile: 2-PyO-(2-Cl, 4F)

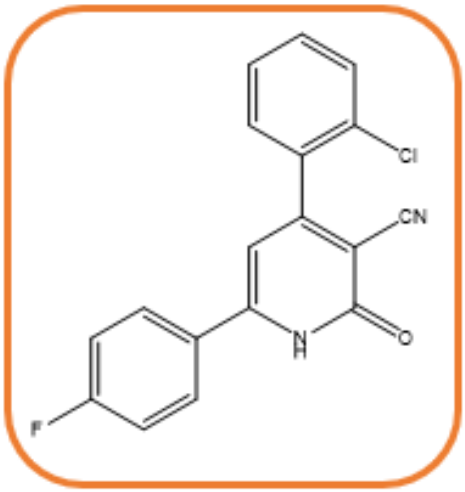

Structure: $C_{18}H_{10}ClFN_2O$

Molar mass (g/mol): 324,74

Yield (%): 30 (A), 90 (B)

Aspect: yellow solid

Mp (°C): > 266

^{1}H and ^{13}C NMR: Not recorded due to limited sample purity and quantity.

IR ν_{max} cm^{-1}: 3467(N-H), 2226 (CN),1745 (C=O), 1580 (C=C)

- **4-(2-chlorophenyl)-6-(2,4-dichlorophenyl)-2-oxo-1,2-dihydropyridine-3-carbonitrile: 2-PyO-(2Cl, 2.4-diCl)**

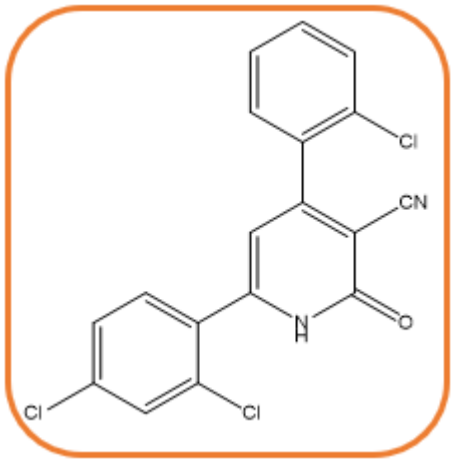

Structure: $C_{18}H_9Cl_3N_2O$

Molar mass (g/mol): 375,64

Yield (%): 38 (A), 85 (B)

Aspect: yellow solid

Mp (°C): > 266

^{1}H and ^{13}C NMR: Not recorded due to limited sample purity and quantity.

IR ν_{max} cm^{-1}: 3462 (N-H), 2215 (CN), 1747 (C=O), 1569 (C=C)

MS *m/z* (% relative abundance): 376

➢ 4-(2-chlorophenyl)-2-oxo-6-(p-tolyl)-1,2-dihydropyridine-3-carbonitrile: 2-PyO-(2Cl, 4Me)

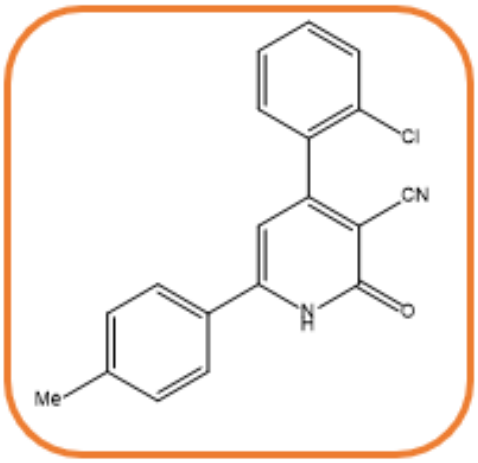

Structure: $C_{19}H_{13}ClN_2O$

Molar mass (g/mol): 320,77

Yield (%): 17 (A), 41 (B)

Aspect: yellow solid

Mp (°C): 260

^{1}H NMR 91 MHz, $(CD)_3SO$ δ_H: 12.51 (1H, s, NH, pyridone ring), 7.61–6.87 (8H, m, H_{arom}, 2-chlorophenyl and p-tolyl rings), 6.45 (1H, s, C=CH, pyridone ring), 2.05 (3H, s, CH_3, methyl group).

^{13}C NMR 23 MHz, $(CD)_3SO$ δ: 161.88 (C_{arom}, carbonyl group of pyridone ring), 158.45 (C_{arom}, C–Cl), 141.96 (C_{arom}, pyridone ring), 135.77 (C_{arom}, tolyl ring), 131.72 (CH, aromatic ring), 131.12 (CH, aromatic ring), 130.52 (CH, aromatic ring), 130.23 (CH, aromatic ring), 129.98 (CH, aromatic ring), 129.53 (CH, aromatic ring), 128.02 (CH, aromatic ring), 115.91 (CN, nitrile group), 106.85 (CH, pyridone ring), 21.09 (CH_3, methyl group).

IR ν_{max} cm^{-1}: 3494 (N-H), 2221(CN), 1654 (C=O), 1590 (C=C)

MS *m/z* (% relative abundance): 321

➢ 4-(2-chlorophenyl)-6-(3,4-dimethylphenyl)-2-oxo-1,2-dihydropyridine-3-carbonitrile: 2-PyO-(2Cl, 3.4diMe)

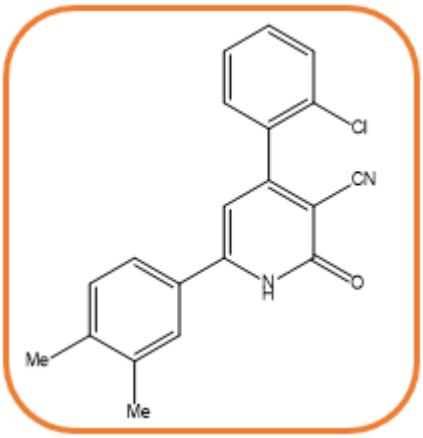

Structure: $C_{20}H_{15}ClFN_2O$

Molar mass (g/mol): 334,80

Yield (%): 91 (B)

Aspect: yellow solid

Mp (°C): 224

^{1}H and ^{13}C NMR: Not recorded due to limited sample purity and quantity.

IR ν_{max} cm^{-1}: 33153(N-H), 2221 (CN), 1654 (C=O), 1610 (C=C)

MS *m/z* (% relative abundance): 335

➢ 4-(2-chlorophenyl)-6-(naphthalen-2-yl)-2-oxo-1,2-dihydropyridine-3-carbonitrile: 2-PyO-(2Cl, 2Naph)

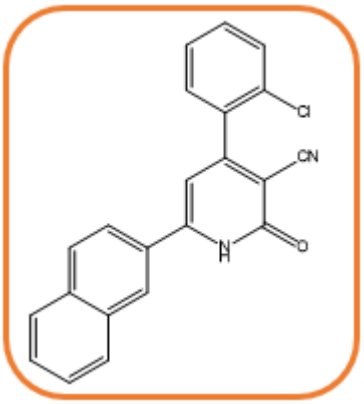

Structure: $C_{22}H_{13}ClN_2O$

Molar mass (g/mol): 356,80

Yield (%): 20 (A), 36 (B)

Aspect: yellow solid

Mp (°C): > 266

^{1}H and ^{13}C NMR: Not recorded due to limited sample purity and quantity.

IR ν_{max} cm^{-1}: 3405 (N-H), 2215(C=O), 1745(C=O), 1612 (C=C)

MS *m/z* (% relative abundance): 357

- **4-(2-chlorophenyl)-6-(4-methoxyphenyl)-2-oxo-1,2-dihydropyridine-3-carbonitrile : 2-PyO-(2Cl, 4OMe)**

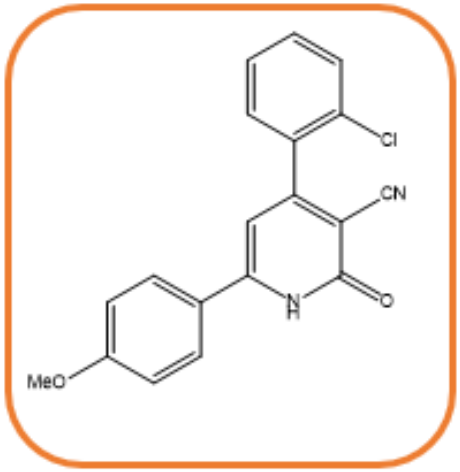

Structure: $C_{19}H_{13}ClN_2O_2$

Molar mass (g/mol): 336,77

Yield (%): 12 (A), 46 (B)

Aspect: yellow solid

Mp (°C): 224

^{1}H NMR 91 MHz, $(CD)_3SO$ δ_H: 7.48–6.60 (8H, m, H_{arom}, 2-chlorophenyl and 4-methoxyphenyl rings), 6.30 (1H, s, C=CH, pyridone ring), 3.37 (3H, s, OCH_3, methoxy group).

^{13}C NMR 23 MHz, $(CD)_3SO$ δ: 162.24 (C_{arom}, carbonyl group of pyridone ring), 158.27 (C_{arom}, carbon linked to methoxy group), 152.20 (C_{arom}, pyridone ring), 135.99 (C_{arom}, C–Cl), 131.17 (CH, aromatic ring), 130.55 (CH, aromatic ring), 130.23 (CH, aromatic ring), 129.88 (CH, aromatic ring), 128.87 (CH, aromatic ring), 128.01 (CH, aromatic ring), 127.60 (CH, aromatic ring), 124.66 (CH, aromatic ring), 116.25 (CN, nitrile group), 106.25 (CH, pyridone ring), 55.94 (OCH_3, methoxy group).

IR ν_{max} cm^{-1}: 3150 (N-H), 2221 (CN), 1638 (C=O), 1511 (C=C)

MS *m/z* (% relative abundance): 337

- **6-(naphthalen-2-yl)-2-oxo-4-phenyl-1,2-dihydropyridine-3-carbonitrile : 2-PyO-(H, 2-Naph)**

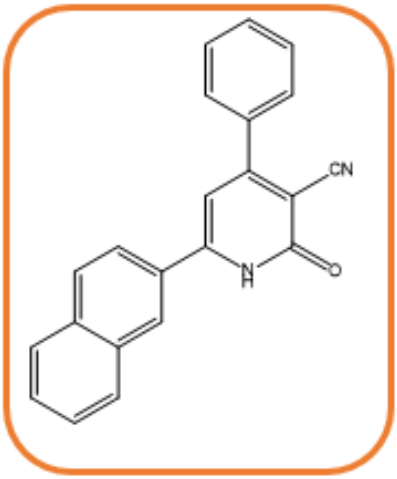

Structure: $C_{22}H_{14}N_2O$

Molar mass (g/mol): 322,36

Yield (%): 59 (B)

Aspect: yellow solid

Mp (°C): 260

^{1}H NMR 91 MHz, $(CD)_3SO$ δ_H: 12.10 (1H, s, NH, pyridone ring), 7.53–7.42 (5H, m, H_{arom}, phenyl ring), 7.24–7.18 (2H, m, H_{arom}, naphthyl ring), 7.12–7.01 (5H, m, H_{arom}, naphthyl and phenyl rings), 6.46 (1H, s, C=CH, pyridone ring).

^{13}C NMR 23 MHz, $(CD)_3SO$ δ: 162.69 (C_{arom}, carbonyl group of pyridone ring), 151.96 (C_{arom}, pyridone ring), 136.57 (C_{arom}, naphthyl ring), 134.29 (C_{arom}, phenyl ring), 132.88 (CH, naphthyl ring), 130.84 (CH, phenyl ring), 130.10 (CH, phenyl ring), 129.27 (CH, naphthyl ring), 128.95 (CH, phenyl ring), 128.72 (CH, naphthyl ring), 128.08 (CH, phenyl ring), 127.49 (CH, naphthyl ring), 124.80 (CH, naphthyl ring), 107.16 (CH, pyridone ring).

IR ν_{max} cm^{-1}: 3051 (N-H), 2220 (CN), 1659 (C=O), 1568 (C=C)

MS *m/z* (% relative abundance): 323

- **6-(4-fluorophenyl)-2-oxo-4-phenyl-1,2-dihydropyridine-3-carbonitrile: 2-PyO-(H, 4F)**

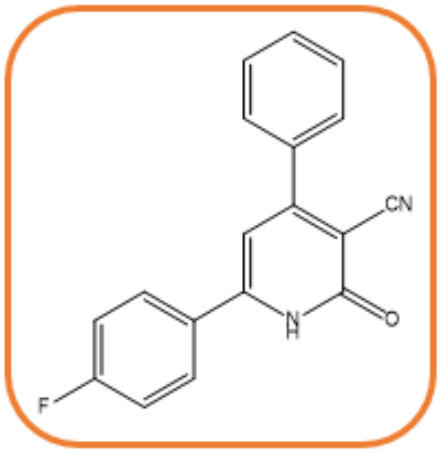

Structure: $C_{18}H_{11}FN_2O$

Molar mass (g/mol): 290,29

Yield (%): 89 (B)

Aspect: yellow solid

Mp (°C): 210

^{1}H NMR 91 MHz, $(CD)_3SO$ δ_H: 7.99 – 7.94 (3H, m, H_{arom}, 4-fluorophenyl and phenyl rings), 7.87 – 7.84 (1H, m, H_{arom}, phenyl ring), 7.72 – 7.70 (2H, m, H_{arom}, phenyl ring), 7.55 – 7.54 (1H, t, H_{arom}, phenyl ring), 7.47 – 7.46 (1H, m, H_{arom}, 4-fluorophenyl ring), 7.36 – 7.32 (2H, m, H_{arom}, 4-fluorophenyl ring).

^{13}C NMR 23 MHz, $(CD)_3SO$ δ: Not recorded due to insufficient sample purity.

IR ν_{max} cm^{-1}: 3051 (N-H), 2220 (CN), 1657 (C=O), 1510 (C=C)

MS *m/z* (% relative abundance): 291

Remarks on Analytical Data

Note on NMR data: Due to the use of a low-field NMR instrument (91 MHz for ^{1}H and 23 MHz for ^{13}C), some spectra recorded during this work were of limited resolution or sensitivity, which may have resulted in missing or overlapping signals. Nevertheless, the available data, in combination with IR and MS support the proposed structures.

Clarification: Some final 2-pyridone derivatives, though successfully synthesized and confirmed by IR and mass spectrometry, could not be analyzed by NMR due to limited purity and material availability. Nevertheless, the mass spectra displayed clean molecular ion peaks, and the synthetic pathways are consistent with related, fully characterized compounds.

References:

1. Vekariya, R.; Panchal, S.; Patel, K.; Patel, H. Solvent and Catalyst Free, Regioselective .α-Bromination of Aralkyl Ketones Using N-Bromosuccinimide (NBS) Under Microwave Irradiation: An Efficient Protocol. *Curr. Microw. Chem.* **2015**, *2*, 61–68, doi:10.2174/2213335602011502121115O6.

2. Adhikari, M. V.; Samant, S.D. Sonochemical Bromination of Acetophenones Using P-Toluenesulfonic Acid-N-Bromosuccinimide. *Ultrason. Sonochem.* **2002**, *9*, 107–111, doi:10.1016/S1350-4177(01)00108-0.

3. Pravst, I.; Zupan, M.; Stavber, S. Halogenation of Ketones with N-Halosuccinimides under Solvent-Free Reaction Conditions. *Tetrahedron* **2008**, *64*, 5191–5199, doi:10.1016/j.tet.2008.03.048.

4. Grjol, B.; Jereb, M. Reactivity of Substrates with Multiple Competitive Reactive Sites toward NBS under Neat Reaction Conditions Promoted by Visible Light. *Chem. Pap.* **2021**, *75*, 5235–5248, doi:10.1007/s11696-021-01711-x.

5. Appaturi, J.N.; Ratti, R.; Phoon, B.L.; Batagarawa, S.M.; Din, I.U.; Selvaraj, M.;

Ramalingam, R.J. A Review of the Recent Progress on Heterogeneous Catalysts for Knoevenagel Condensation. *Dalt. Trans.* **2021**, *50*, 4445–4469, doi:10.1039/d1dt00456e.

6. Gawande, M.B.; Jayaram, R. V. A Novel Catalyst for the Knoevenagel Condensation of Aldehydes with Malononitrile and Ethyl Cyanoacetate under Solvent Free Conditions. *Catal. Commun.* **2006**, *7*, 931–935, doi:10.1016/j.catcom.2006.03.008.

7. Zhao, S.; Fan, Y.; Wang, Z.; Qiao, Y.; Jia, X. Knoevenagel Reaction Promoted by Functional Ionic Liquids with Primary and Tertiary Amines. *Green Chem. Lett. Rev.* **2024**, *17*, 1–14, doi:10.1080/17518253.2024.2337743.

8. Merugu, S.K.; Bollikolla, H.B. Improved Knoevenagel Condensation Protocol for the Synthesis of Cyanoacrylates and Their Anticancer Activity. *J. Mex. Chem. Soc.* **2023**, *67*, 60–69, doi:10.29356/jmcs.v67i1.1835.

GENERAL CONCLUSION

GENERAL CONCLUSION

This work focused on the synthesis and application of four major families of nitrogen-containing heterocycles: imidazo[1,2-a]pyridines, imidazo[1,2-a]pyrimidines, imidazo[2,1-b]thiazoles, and 2-pyridone derivatives. These structures are of considerable interest due to their broad range of biological activities and relevant industrial applications, particularly in the fields of pharmaceutical chemistry and corrosion protection.

In the first part of the thesis, a variety of eco-friendly and efficient synthetic strategies were developed. The synthesis of imidazo-heterocycles was based on the reaction of 2-aminoheterocycles (pyridine, pyrimidine, or thiazole) with α-bromoarylketones, which were prepared in a prior step from acetophenone derivatives using N-bromosuccinimide (NBS). Several methods were explored and compared, including:

- Classical thermal conditions in ethanol,
- Catalysis using Au/TiO_2, which provided enhanced yields and reduced reaction times,
- Microwave-assisted synthesis, offering solvent-free and rapid access to the desired compounds,
- Al_2O_3-assisted synthesis, particularly effective for the formation of imidazo[2,1-b]thiazoles.

The second synthetic strategy was dedicated to 2-pyridone derivatives, obtained through a two-step multicomponent strategy. Initially, alkenes were prepared by Knoevenagel condensation of aldehydes with ethyl cyanoacetate in water. These intermediates were then reacted with acetophenones and ammonium acetate to yield 2-pyridones via a cyclocondensation process. Two approaches were investigated:

- Conventional heating in ethanol (10 h),
- Ultrasound-assisted synthesis, which significantly shortened reaction times by more than half (3–6 hours vs. 10 hours) and enhanced yields up to nearly fourfold, confirming the effectiveness of cavitation in accelerating multicomponent reactions.

In the second part of the thesis, the synthesized compounds were assessed for their functional and biological properties:

1. **Corrosion Inhibition:** Several **IP** and **IPM** derivatives were evaluated as corrosion inhibitors for mild steel in 1 M HCl using the gravimetric method. The results demonstrated high inhibition efficiencies, in some cases exceeding 97,51% and 96,55% for **IP-4Br** and **IPM-4Br**, respectively. The efficiency was found to increase with concentration and temperature, suggesting a chemisorption mechanism. Thermodynamic studies (activation energy, ΔH, ΔS) confirmed the spontaneity and endothermic nature for **IP** and exothermic nature for **IPM** of adsorption, while fitting to the Langmuir adsorption isotherm indicated the formation of a monolayer on the metal surface. These results underline the potential of these heterocycles as eco-friendly corrosion inhibitors.

2. **Biological Activity:** A selection of **IP** and **IPM** compounds was screened for antibacterial and antifungal activities. Using the agar diffusion method, MIC and MBC determination, several compounds exhibited significant inhibition against *Staphylococcus aureus*, *Micrococcus luteus*, *Bacillus subtilis*, *Bacillus cereus* and *Candida albicans*. The activity varied depending on the nature and position of the substituents, with compounds such as **IPM-4OMe**, **IPM-3,4diMe**, and **IPM-2Naph** particularly exhibiting higher potency. These findings support the potential of imidazo[1,2-a]pyridines/pyrimidines as broad-spectrum antimicrobial agents.

3. **Molecular Docking and ADME-Tox Prediction:** To better understand how the most active compounds might act at the molecular level, we carried out computer-based simulations to predict how these molecules bind to bacterial proteins involved in essential biological functions. These docking studies showed that the compounds fit well into the active sites of the target proteins and formed specific interactions, such as hydrogen bonds and hydrophobic contacts, which are often essential for biological activity. In addition, the calculated binding strengths were consistent with the biological results obtained *in vitro*, supporting the idea that these compounds exert their effects by directly interacting with the bacterial targets. We also evaluated the pharmacokinetic profiles of the compounds using theoretical models (ADME-Tox), which help predict how the molecules behave in the body (Absorption, Distribution, Metabolism, Excretion, and Toxicity). The results were encouraging, indicating that the compounds

follow the main criteria for drug-likeness (such as Lipinski's rule of five) and do not present risks of general or cardiac toxicity.

Together, these results illustrate the versatility of the synthesized compounds and the interdisciplinary nature of this research, combining synthetic organic chemistry, materials science, biological evaluation, and computational modeling. The methods developed are not only effective and reproducible, but also aligned with the principles of green and sustainable chemistry.

As future perspectives, several promising directions can be considered:

- Structural optimization of the most active compounds by introducing new substituents or functional groups in order to improve their selectivity, potency, and pharmacokinetic properties.
- Mechanistic investigations using surface analysis techniques (such as SEM) to better understand the interaction between the inhibitors and the metal surface at the microscopic level.
- *In vivo* biological evaluation to confirm the antimicrobial activity of the most promising molecules and assess their toxicity in biological systems.
- Advanced molecular modeling could be used to explore new targets and support rational drug design based on the synthesized heterocycles.

الملخص
تقدم هذه الرسالة تطوير طرق تحضير صديقة للبيئة لإنتاج الهتيروسايكلات الإيميدازو و 2-بيريدونات، باستخدام تقنيات مثل التحضير بدون مذيبات، الحفز، إشعاع الميكروويف، والموجات فوق الصوتية. بعد النجاح في تحضير هذه المركبات، تم التحقيق في تطبيقاتها العملية. تم تقييم فعالية المثبطات للمشتقات الهتيروسايكلية الإيميدازو المختارة ضد تآكل الفولاذ اللين، مما يبرز إمكانياتها كمثبطات للتآكل. بالإضافة إلى ذلك، تم اختبار النشاط البيولوجي للإيميدازو[a -2,]بيريدينات/بيريميدينات المُصَنعة، مما كشف عن خصائص صيدلانية واعدة. تم إجراء دراسات الربط الجزيئي لنمذجة التفاعلات بين المركبات الفعالة والأهداف البيولوجية المحددة، مما يوفر رؤى حول إمكانياتها العلاجية. تعزز هذه الدراسة تحضير وتطبيق الهتيروسايكلات في السياقات الصناعية والطبية الحيوية.
الكلمات المفتاحية: التحضير الأخضر، إيميدازو-الحلقات غير المتجانسة العطرية، 2-بيريدونات، تثبيط التآكل، النشاط البيولوجي، الربط الجزيئي.

Abstract

This thesis presents the development of eco-friendly synthetic methods for producing imidazo-heterocycles and 2-pyridones, utilizing techniques such as solvent-free synthesis, catalysis, microwave irradiation, and ultrasound. Following the successful synthesis of these compounds, their practical applications were investigated. The inhibitory effectiveness of selected imidazo-heterocyclic derivatives on mild steel corrosion was evaluated, highlighting their potential as corrosion inhibitors. Additionally, the biological activity of the synthesized imidazo[1,2-a]pyridines/pyrimidines was tested, revealing promising pharmacological properties. Molecular docking studies were performed to model the interactions of potent compounds with specific biological targets, providing insights into their therapeutic potential. This research advances the synthesis and application of heterocycles in industrial and biomedical contexts.

Keywords: green synthesis, imidazo-heterocycles, 2-pyridones, corrosion inhibition, biological activity, molecular docking.

Résumé

Cette thèse présente le développement de méthodes de synthèse écologiques pour la production d'imidazo-hétérocycles et de 2-pyridones, en utilisant des techniques telles que la synthèse sans solvant, la catalyse, l'irradiation micro-ondes et les ultrasons. Après la réussite de la synthèse de ces composés, leurs applications pratiques ont été étudiées. L'efficacité inhibitrice de certains dérivés imidazo-hétérocycliques sur la corrosion de l'acier doux a été évaluée, mettant en évidence leur potentiel en tant qu'inhibiteurs de corrosion. De plus, l'activité biologique des imidazo[1,2-a]pyridines/pyrimidines synthétisées a été testée, révélant des propriétés pharmacologiques prometteuses. Des études de docking moléculaire ont été réalisées pour modéliser les interactions des composés puissants avec des cibles biologiques spécifiques, fournissant des informations sur leur potentiel thérapeutique. Cette recherche fait progresser la synthèse et l'application des hétérocycles dans les contextes industriels et biomédicaux.

Mots-clés : synthèse verte, imidazo-hétérocycles, 2-pyridones, inhibition de la corrosion, activité biologique, docking moléculaire.